Modelling the influence of fines on liquefaction behaviour

Author:
Rahman, Md. Mizanur

Publication Date:
2009

DOI:
https://doi.org/10.26190/unsworks/22259

Modelling the influence of fines on liquefaction behaviour

By
Md. Mizanur Rahman

Thesis submitted to
School of Engineering and Information Technology
The University of New South Wales at Australian Defence Force Academy

For fulfillment of the degree of
Doctor of Philosophy

2009

STATEMENT OF ORIGINALITY

I hereby declare that this submission is my own work and to the best of my knowledge it contains no material previously published or written by another person, nor material which to a substantial extent has been accepted for the award of any other degree or diploma at UNSW or any other educational institution, except where due acknowledgement is made in the thesis. Any contribution made to the research by colleagues, with whom I have worked at UNSW or elsewhere, during my candidature, is fully acknowledged.

I also declare that the intellectual content of this thesis is the product of my own work, except to the extent that assistance from others in the project's design and conception or in style, presentation and linguistic expression is acknowledged.

Md. Mizanur Rahman

Dedicated to my wife Tamanna

ACKNOWLEDGEMENT

I wish to express my sincere gratitude to my supervisor Associate Professor Robert Lo who has been a constant source of ideas, guidance and support throughout this research. I especially appreciate his stimulating discussions, which were essential in the development of this study. I am also grateful for his careful reading of the draft of this dissertation. I would like to extend my appreciation to my co-supervisor Dr. Rajah Gnanendran for his helpful suggestions.

Special appreciation is extended to the technical officer, Mr. Jimmy Baxter for his warm support and continuous assistance during the experimental works undertaken for this study. I also like to thank Mr. David Sharp, Mr. Wayne Jealous, Mr. Ian Leves for their technical supports. Special thanks go to the all workshop staffs: especially to Michael Jones, Douglas Collier, Mark Dumbrell, Rick Waring, Marcus De Almeida, Stuart Gay and electronic staffs: Andrew Roberts, Evan Hawke, Geno Ewyk for their invaluable assistance in the setting up of the triaxial apparatus.

I also like to thanks my friends: Kamal, Dejin, Rongan, Ovidiu, Vinod, Khin, Adnan, Kamrul, Barkat, Rajibul, Shahidul, Dalim, and Baki for their continuous support and encouragements during the study.

I also like to acknowledge the supports and education leave provided by Rajshahi University of Engineering & Technology (RUET), Bangladesh to continue this research. I like to acknowledge the stimulating encouragement from Professor Sayed

Abdul Mofiz to continue my higher study in geotechnical engineering. I also acknowledge the supports from my teachers from Bangladesh. I also like to thank Denise for careful reading of the draft.

I like to acknowledge the supports and scarifies made by my beloved wife Tamanna. Without her warm and continuous supports, it would not be possible to submit this thesis. I also like to acknowledge continuous encouragement from my family in Bangladesh.

Finally, I would also like to acknowledge the Endeavour International Postgraduate Research Scholarship (EIPRS) and NSW Global Scholarship and the support from the School of Engineering and Information Technology, SEIT (former ACME) for the study.

TABLE OF CONTENTS

ACKNOWLEDGEMANT i
ABSTRACT x
NOTATIONS xiv
LIST OF TABLES xvii
LIST OF FIGURES xix
CHAPTER 1. INTRODUCTION
1.1 GENERAL 1
1.2 THESIS ORGANIZATION 4
CHAPTER 2. LITERATURE REVIEW
2.1 INTRODUCTION 7
2.2 STATIC LIQUEFACTION PHENOMENON 7
2.2.1 *Undrained Behaviours* 8
2.2.2 *Instability Line/Collapse Line* 14
2.2.3 *Phase Transformation, PT* 18
2.2.4 *Critical/Steady State Line (CSL/SSL)* 20
2.2.5 *Quasi-Steady State, QSS* 22
2.3 STATE PARAMETERS 23
2.3.1 *State Parameter* 23
2.3.2 *State Index* 25
2.3.3 *Pressure Index* 27
2.3.4 *Modified State Parameter* 27
2.4 EFFET OF FINES IN SAND 30
2.4.1 *Effects of Fines on Undrained Behaviour* 31
2.4.2 *Effects of Fines on Steady State Line, SSL* 33

2.4.3 *Effects of Fines on Quasi Steady State Line, QSSL* 35
2.4.4 *Effect of Fines on Peak Stress Ratio/Instability Stress Ratio* 35
2.4.5 *Challenges with the Presences of Fines* 36
2.4.6 *Inter-granular Void Ratio, e_g* 37
2.4.7 *Equivalent Granular Void Ratio, e** 44
2.5 MODELLING OF UNDRAINED BEHAVIOUR 50
2.6 EFFECT OF FINES TYPE 51
2.6.1 *Effects of Plasticity of Fines* 52
2.6.2 *Effects of Sphericity and Angularity of Fines* 53
2.7 EFFECT OF CYCLIC LOADING ON SAND WITH FINES 54
2.9 SUMMARY AND RESEARCH OBJECTIVES 56

CHAPTER 3. EXPERIMENTAL METHODOLOGY

3.1 INTRODUCTION 58
3.2 TRIAXIAL TESTING SYSTEM 59
3.2.1 *Axial Force* 63
3.2.2 *Cell Pressure* 63
3.2.3 *Pore Water Pressure and Volume Change* 65
3.2.4 *Axial deformation* 65
3.3 MATERIALS TESTED 67
3.3.1 *Sydney sand* 67
3.3.2 *MI fines* 68
3.3.3 *MII fines* 69
3.3.4 *SI fines* 70
3.3.5 *SII fines* 71
3.4 HOMOGENEITY OF SPECIMEN 72
3.4.1 *Enlarge Platen with Free Ends* 72
3.4.2 *Specimen Preparation* 73
3.5 SATURATION 76
3.5.1 *Carbon Dioxide Percolation* 76
3.5.2 *Vacuum Flushing* 77
3.5.3 *Back Pressure Saturation* 78

3.6 VOID RATIO MEASUREMENT 78
3.6.1 *Mass of the Specimen* 78
3.6.2 *Volume of the Specimen* 79
3.6.3 *Errors in Assessment* 80
3.7 MEMBRANE PENETRATION 82
3.8 MICRO EXPERIMENTATION 86
3.8.1 *Light Microscopy* 86
3.8.2 *Scanning Electron Microscope, SEM* 88
3.9 SUMMARY 93

CHAPTER 4. BINARY PACKING AND THE PARAMETER "*b*"

4.1 INTRODUCTION 95
4.2 DETERMINATION OF *b*-VALUE 96
4.2.1 *Finding "b"* 96
4.2.2 *Characteristic of Reported b- values* 97
4.3 BINARY PACKING AND *b*-VALUE 98
4.3.1 *Binary Packing* 99
4.3.2 *Factors Affecting "b"* 103
4.4 PREDICTION OF "*b*" 105
4.4.1 *Prediction of TFC* 105
4.4.2 *General Equation of "b"* 110
4.4.3 *Determination of "m"* 111
4.4.4 *Attributes of Prediction Equation* 112
4.5 VERIFICATION 114
4.5.1 *Steady State Behaviour from Monotonic Undrained Shearing* 119
4.5.2 *Cyclic Mobility Behaviour* 127
4.5.3 *Discussion* 133
4.5.4 *Variation of m Among Different Data Sets* 134
4.6 SUMMARY 135

CHAPTER 5. EQUIVALENT GRANULAR STEADY STATE LINE

5.1 INTRODUCTION 137

5.2 CONCEPTUAL FRAMEWORK OF EG-SSL 137

5.3 EXPERIMENTAL INVESTIGATION 139

5.4 EVALUATION OF EG-SSL CONCEPT 143

5.4.1 *EG-SSL for Sydney Sand with Fines* 143

5.4.2 *Overall Evaluation of EG-SSL within CSSM framework* 147

5.4.2.1 Preliminary Investigation 147

5.4.2.2 Prediction of F, NF and LF behaviour for all tests 148

5.4.3 *Concept of Equivalent Granular State Parameter,* $\psi^*_{(0)}$ 151

5.4.4 *Relationship between Undrained Behaviour and* $\psi^*_{(0)}$ 153

5.4.4.1 Influence of $\psi^*_{(0)}$ on ESP Responses of Clean Sand: a Consistency Check 153

5.4.4.2 Influence of $\psi^*_{(0)}$ with ESP and Deviator Stress-Strain Responses of Specimen with 15% Fines Content 156

5.4.4.3 Influence of $\psi^*_{(0)}$ on the ESP and Deviator Stress-Strain Responses for Specimens with Different Fines Content 158

5.4.4.4 ESP and Deviator Stress-Strain Responses of Specimen with Different Fines Content but Same $\psi^*_{(0)}$ 160

5.5 VERIFICATION WITH PUBLISHED DATA SETS 163

5.5.1 *Evaluation of the EG-SSL concept* 164

5.5.2 *EG-SSL for Host sand with two different types of fines* 164

5.5.3 *Over all evaluation of EG-SSL with in CSSM framework* 167

5.5.4 *Undrained Behaviours with respect to EG-SSL* 170

5.5.4.1 Influence of $\psi^*_{(0)}$ on the ESP Spectrum at Same GS Fines Content 170

5.5.4.2 Sand with KS-10 materials 173

5.5.4.3 Sand with Different Fines Content and Types 175

5.5.4.4 Sand at Similar $\psi^*_{(0)}$ but Different Fines Content and Type 177

5.6 SUMMARY 179

CHAPTER 6. MODELLING OF SAND WITH FINES

6.1 INTRODUCTION 180

6.2 MODEL SELECTION 180

6.2.1 *Elastic Components* 182

6.2.2 *Plastic Components* 182

6.3 THE MODIFIED COSTITUTIVE MODEL 184

6.3.1 *Elastic Components* 184

6.3.2 *Plastic Components* 185

6.4 CRITICAL STATE PARAMETERS 186

6.5 DETERMINATION OTHER MODEL PARAMETERS 188

6.5.1 *Elastic Parameter* 189

6.5.2 *Dilatancy parameters* 191

6.5.3 *Hardening parameter* 193

6.5.3.1 Determination of "*n*" 193

6.5.3.2 Determination of "*h*" 193

6.6 PREDICTION OF FLOW RULE OF DRAINED TESTS 196

6.7 PREDICTION OF UNDRAINED TESTS 200

6.7.1 *Prediction of Flow Behaviour* 202

6.7.2 *Prediction of Limited Flow Behaviour* 212

6.7.3 *Prediction of Non Flow Behaviour* 212

6.8 PREDICTION FOR OTHER INDEPENDENT RESEARCH 215

6.9 SUMMARY 219

CHAPTER 7. EFFECT OF FINES TYPE IN SAND FINES MIX

7.1 INTRODUCTION 221

7.2 THE EFFECT OF FINES TYPE AND METHODOLOGY 221

7.3 TESTING PROGRAM 229

7.4 RESULTS AND DISCUSSION 232

7.4.1 *The Effect of Fines Types on Prediction Equation of 'b'* 232

7.4.2 *The Effect of Angularity of Fines* 236

7.4.2.1 Comparison between SI and MI 236
7.4.2.2 Comparison between SII and MII 239
7.4.3 *Effect of Plasticity of Fines* 241
7.4.3.1 Comparison between MI and MII 241
7.4.3.2 Comparison between SI and SII 244
7.5 SYNTHESIS OF RESULTS 246
7.6 SUMMARY 247

CHAPTER 8. EFFECTS OF FINES ON CYCLIC LOADING

8.1 INTRODUCTION 249
8.2 THE CONCEPTUAL FRAMEWORK 249
8.3 TESTING PROGRAM 252
8.4 COMPARISON BETWEEN CYCLIC AND MONOTONIC LOADING BEHAVIOUR 255
8.4.1 *Type A: significant strain softening to QSS followed by slight strain hardening* 255
8.4.2 *Type A: Test pair M-15-05 for monotonic loading and C-15-21 for cyclic loading* 255
8.4.3 *Type A: Test pair M-15-04 for monotonic loading and C-15-20 for cyclic loading* 258
8.4.4 *Type A: Test pair M-20-02 for monotonic loading and C-20-20 for cyclic loading* 261
8.4.5 *Type B: significant strain softening to QSS followed by significant strain hardening* 264
8.4.6 *Type B: Test pair M-00-08 for monotonic loading and C-00-20 for cyclic lading* 264
8.4.7 *Type B: Test pair M-00-07 for monotonic loading and C-00-21 for cyclic loading* 267
8.4.8 *Type B: Test pair M-15-05 for monotonic loading and C-15-22 for cyclic loading* 270
8.4.9 *Type C: slight strain softening to QSS followed by significant strain hardening* 273

8.4.10 *Type C: Test pair M-00-05 for monotonic loading and C-00-22 for cyclic loading* 273
8.4.11 *Type C: Test pair M-15-07 for monotonic loading and C-15-23 for cyclic loading* 274
8.4.12 *Synthesis of the Tests Results* 277
8.5 EFFECT OF η RELATIVE TO η_{IS} ON CYCLIC INSTABILITY 277
8.5.1 *Effect of η relative to η_{IS} on Cyclic Instability for clean sand* 278
8.5.2 *Effect of η relative to η_{IS} on Cyclic Instability for sand with 15% Fines* 278
8.5.3 *Effect of η relative to η_{IS} on Cyclic Instability for sand with 20% Fines* 279
8.5.4 *Synthesis of the Results* 281
8.6 SUMMARY 282

CHAPTER 9 CONCLUSIONS AND RECOMMENDATIONS FOR FURTHER RESEARCH
9.1 GENERAL 284
9.2 CONCLUSIONS 285
9.3 RECOMMENDATIONS FOR FUTURE RESEARCH 288

APPENDIX A DEFINITIONS A1
REFERENCES R1

ABSTRACT

Traditionally, void ratio, e has been used as a state variable for predicting the liquefaction behaviour of soils under the Critical State (Steady State) framework. Recent publications show that void ratio, e may not be a good parameter for characterizing sand with fines as the steady state, SS data points move downward in e-log(p') space up to certain fines content termed as threshold fines content, TFC. Thus, it was difficult to apply SS concept on sand with fines as a small variation of fines content may lead to different SS line. Many researchers proposed to used equivalent granular void ratio, e^* as an alternative state variable (i.e. in lieu of void ratio, e) in attempt to obtain a narrow trend line for SS data points irrespective of f_c provided $f_c \leq$ TFC. The e^* is obtained from e. For the conversion from e to e^*, one need a parameter b which presents the active fraction of fines in overall force structure of sand. However, predicting the b is problematic. Most, if not all, of the b reported were determined by case-specific back-analysis, that is, the b-value was selected so that the test results for a given sand-fines type could be correlated with the equivalent granular void ratio, e^* irrespective of fines content. This thesis examines the factors that affecting the b value by examining published work on binary packing. This leads to a simple semi-empirical equation for predicting the value of b based on

particle size ratio, χ and fines content, f_c. Published data and experimental results on Sydney sand appears to be in support of the proposed equation. The single relation of SS data points in e^*-log(p') space for sand with fines is referred as Equivalent Granular Steady State Line, EG-SSL. The EG-SSL is then used to define the equivalent granular state parameter, ψ^*. A good correlation observed between ψ^* and q-p', q-ε_q responses in undrained shearing. The e^* and ψ^* are also used to modified a state dependent constitutive model. Seven model input parameters are needed in addition four to critical state input parameters. These parameters are obtained from drained test. The model is used to predict q-$p'$and q-ε_q responses for flow, non-flow and limited flow behaviour for 0% to 30% fines contents. The model predictions are in good agreement with experimental results. The effect of fines types (in terms of plasticity and angularity) on the prediction equation of b are also examined with four different types of fines. A negligible effect of fines type on the prediction equation of b is observed. The link between monotonic and cyclic loading behaviour for sand with fines are also examined with emphasis on cyclic instability and strain hardening behaviour after quasi steady state, QSS for a range of fines contents (provided that f_c < TFC). It is found that a single set of rules could be used to correlate monotonic and cyclic behaviour for a range of fines contents at same ψ^*.

List of publications from this thesis

1. **Rahman, M. M.** and Lo, S. R. (2009). “On equivalent granular SSL for sand with fines”. *In proc. 17th International Conference on Soil Mechanics & Geotechnical Engineering*, Alexandria, Egypt, 205-208.
2. **Rahman, M. M.,** Lo, S. R. & Gnanendran, C. T. (2009). “Reply to discussion by Wanatowski, D. and Chu, J. on- On equivalent granular void ratio and steady state behaviour of loose sand with fines”. *Canadian Geotechnical Journal*, **46** (4), 483-486.
3. Lo, S.R., **Rahman, M.M.,** and Bobei, D.C. (2009). “Limited flow characteristics of sand with fines under cyclic loading” *Geomechanics and Geoengineering,* **In Press.**
4. Bobei, D.C., Lo, S.R., Wanatowski, D., Gnanendran, C.T., and **Rahman, M.M.** (2009). "A modified state parameter for characterizing static liquefaction of sand with fines." *Canadian Geotechnical Journal*, **46** (3), 281-295.
5. **Rahman, M. M.,** S. R. Lo, et al. (2008). "On equivalent granular void ratio and steady state behaviour of loose sand with fines." *Canadian Geotechnical Journal* **45**(10): 1439-1455.
6. **Rahman, M. M.** and S. R. Lo (2008). "The prediction of equivalent granular steady state line of loose sand with fines." *Geomechanics and Geoengineering*, **3**(3): 179 - 190.
7. **Rahman, M.M.,** and Lo, S.R. (2008). Effect of sand gradation and fines type on the liquefaction behaviour of sand-fines mixtures. In *4th decennial Geotechnical Earthquake Engineering and Soil Dynamics Conference*, **GSP-181**, ASCE. Sacramento, California, USA.
8. Lo, S. R., **Rahman, M. M.** & Bobei, D. C. (2008). Limited flow behaviour of sand with fines under monotonic and cyclic loading. *Proceedings of the 2nd International*

Conference on Geotechnical Engineering for Disaster Mitigation & Rehabilitation (GEDMAR08), Nanjing, China, 201-209.

9. **Rahman, M.M.,** and Lo, S.R. (2007a). On intergranular void ratio of loose sand with small amount of fines. In *16th South East Asian Geotechnical Conference*. Kuala Lumpur, Malaysia. 8-11 May, 2007, pp. 255-260.

10. **Rahman, M.M.,** and Lo, S.R. (2007b). Equivalent granular void ratio and state parameters for loose clean sand with small amount of fines. In *10th Australia New Zealand Conference on Geomechanics*. Brisbane, Australia, Vol.**2**, pp. 674-679.

NOTATIONS

σ'_1	Effective axial stress
σ'_3	Effective radial stress
p	Confining stress
p'	Effective confining stress
$p'_{(0)}$	Initial effective confining stress (end of consolidation)
p'_{SS}	Confining effective stress at SS
p_a	Atmospheric pressure
q	Total/effective deviatoric stress
q_{peak}	Peak deviatoric stress
η	Effective stress ratio, q / p'
η_{IS}	Instability stress ratio
M	Effective stress ratio, η at CS/SS
ψ	State parameter
ψ^*	Equivalent granular state parameter
$\psi^*_{(0)}$	Equivalent granular state parameter after isotropic consolidation
e	Void ratio
$e_{(0)}$	Initial void ratio (end of consolidation)
e_{SS}	Void ratio at SS
e^*_Γ	Threshold void ratio, obtained by exploration of EG-SSL towards zero effective stress in e^*-p' space
e_g	Inter-granular void ratio
e^*	Equivalent granular void ratio
b	Active fraction of fines in sand force structure
f_c	fines content (in decimal)
u	Pore water pressure
ε_1	Axial strain

ε_v	Volumetric strain
ε_q	Deviatoric strain
χ_T	Diameter ratio of coarse and fines grain as denoted ($D_{50,\ sand}/d_{50,\ silt}$)
χ	Diameter ratio, $D_{10,\ sand}/d_{50,\ silt}$
G	Elastic shear modulus
G_0	Material constant for elastic shear modulus
K	Elastic bulk modulus
Kp	Plastic hardening modulus
h	Plastic model parameter
h_1,h_2	Two parameter for h
n	Plastic model parameter
ν	Poisson's ratio
λ	Constant in EG-SSL equation
ξ	Constant in EG-SSL equation
Δ	Dilatancy
Δ_0	Modelling parameter for dilatancy
m_d	Modelling parameter of dilatancy
A	Parameter for determination of G_0
A_{TFC}	Constant in TFC prediction equation

Note: Following prefixes are used in front of u, p', q, ε_1, ε_v and ε_q according to their meaning.

d	increment (infinitesimal)
δ	small finite increment/step

Superscript

$'$	indicates effective stress
*	indicates equivalent granular
^{p}	indicates plastic part
^{e}	indicates elastic part

Subscript

$_{(0)}$	indicates initial state (at the end of consolidation)
$_{(SS)}$	indicates at steady state
$_{(q)}$	indicates deviatoric
$_{(v)}$	indicates volumetric
$_{(ij)}$	indicates tensor notation

ABBREVIATIONS

SS	Steady sate
CS	Critical state
SSL	Steady state line
CSL	Critical state line
EG-SSL	Equivalent granular steady state line
TFC	Threshold fines content
PT	Phase transformation
PTL	Phase transformation line
QSS	Quasi steady state
QSSL	Quasi steady state line

LIST of TABLES

Table No.	Description	Page No.
Table 2. 1:	The variation of b with e^* and χ after Ni et al. (2004)	49
Table 3. 1:	Physical properties of Sydney sand	67
Table 3. 2:	Physical properties of MI fines	68
Table 3. 3:	Physical properties of MII fines	69
Table 3. 4:	Physical properties of SII fines	71
Table 3. 5:	Atomic weight of different element of S-I fines	92
Table 3. 6:	Atomic weight of different element of M-I fines	93
Table 3. 7:	Atomic weight of different element of Kaolin	93
Table 4. 1:	Summary of steady state behaviour from previous study and the respective b values	117
Table 4. 2:	Summary of cyclic mobility behaviour from previous study and the respective b value	118
Table 4. 3:	Variation of the calibrated m for different data sets	134
Table 4. 4:	Sensitivity of m over all data sets	135
Table 5. 1:	Summary of triaxial tests	141
Table 5. 2:	The details of material tested	163
Table 5. 3:	Summary of tests data after Thevanayagam and Mohan (2000)	169
Table 6. 1:	Critical/ Steady state parameters of constitutive model	187
Table 6. 2:	The other parameters required for the proposed model	188
Table 6. 3:	Details of drained tests used in determination of model parameters	189
Table 6. 4:	Dilatancy parameters for sand and sand with fines	191

Table 6. 5:	Dilatancy parameters for Sydney sand with 10% M-II fines	192
Table 6. 6:	All parameters for the model from drained test	195
Table 6. 7:	Summary of the tests used for flow rule prediction	196
Table 6. 8:	The details testing condition for Sydney sand with 10% M-II fines (Bobei 2004)	215
Table 7. 1:	Summary of the testing program: (a) for MI and MII fines	230
Table 7. 1:	Summary of the testing program: (b) for SI and SII fines	231
Table 7. 2:	The required parameters for equivalent granular void ratio for different types of fines	233
Table 8. 1:	The summary of triaxial testing	254

LIST of FIGURES

Figure No.	Description	Page No.
Figure 2.1	Schematic diagram of undrained triaxial tests at same confining pressure; (a) Effective stress path, (b) Stress-strain response in q-ε_q space	11
Figure 2. 2	Effective stress path for Banding sand in CIU test (data from Castro (1969)); (a) same e, different p', (b) different e, same p' after Mohamad and Dobry (1986)	12
Figure 2. 3	Stress-strain response of Banding sand in CIU test (data from Castro (1969)); (a) same e, different p', (b) different e, same p' after Mohamad and Dobry (1986).	13
Figure 2. 4	Collapse line in normalize stress space; (a) for Banding NO. 6 sand after Sladen et al. (1985), (b) for Toyoura sand after Ishihara (1993)	16
Figure 2. 5	Instability line, IL for marine-dredged sand; (a) single IL for sample with same void ratio but different mean effective stress, (b) multiple ILs for different void ratio but same mean effective stress after Chu and Leong (2002)	17
Figure 2. 6	Relation between instability stress ratio and void ratio after Chu and Leong (2002)	18
Figure 2. 7	Definition of state parameter by Been and Jefferies (1985), slightly modified notations	25
Figure 2. 8	Definition of state index, I_S according to Ishihara (1993)	27
Figure 2. 9	Definition of state pressure index, I_p according to Li et al. (1999)	29
Figure 2. 10	Definition of modified state parameter, ψ_m according to Bobei and Lo (2005)	29
Figure 2. 11	Reverse behaviour for Nevada 50/200 sand with 7% fines; (a) q-p'	32

space, (b) q-ε_1 space

Figure 2. 12 SS data points for sand with fines; (a) Toyoura sand with non-plastic fines, modified from Zlatovic and Ishihara (1995), (b) F55, Foundry sand with non-plastic crushed silica, modified from Thevanayagam et al. (2002b) 34

Figure 2. 13 Quasi steady state data points for Toyoura sand with fines, modified from Zlatovic and Ishihara (1995) 35

Figure 2. 14 Effect of fines content on instability stress ratio line for Hokksund sand with Chengbei non-plastic fines, modified after Yang et al. (2006b) 36

Figure 2. 15 Undrained monotonic triaxial test results for silty 20/200 sand after Kuerbis et al. (1988) 40

Figure 2. 16 Stress path response at similar inter-granular void ratio for Ham river sand with Speswhite kaolin after Georgiannou et al. (1990) 41

Figure 2. 17 Schematic diagrams; (a) particle arrangement for clean sand and sand with small amount of fines, (b) definition of inter-granular and inter-fine void ratio after Thevanayagam (1998) 43

Figure 2. 18 Schematic diagram of particle arrangement for sand with higher amount of fines 44

Figure 2. 19 Steady state line in e^*-log(p') space; (a) for F55, Foundry sand with non-plastic crushed silica by selecting b = 0.25 after Thevanayagam et al. (2002b), (b) for Hokksund sand with Chengbei fines when b = 0.25 after Yang et al. (2006c) 46

Figure 2. 20 (a) Single trend for F55, Foundry sand with 0-25% non-plastic fines in e^*-E_L space at b = 0.40, slightly modified after Thevanayagam et al. (2002a), (b) Single trend for Hokksund sand with 0% - 20% Chengbei fines at b = 0.25, slightly modified after Yang et al. (2006b) 47

Figure 2. 21 Cyclic liquefaction resistance increases with increasing in plasticity of fines 53

Figure 2. 22 Particle shape determination-sphericity, S and roundness, R chart (after Cho et al. (2006)) 54

Figure 3. 1	Schematic diagram of the triaxial testing system	61
Figure 3. 2	Overall view of triaxial loading system	62
Figure 3. 3	Schematic diagram of Digital Pressure Volume Controller (DPVC)	64
Figure 3. 4	Grain size distribution curve for Sydney sand	68
Figure 3. 5	Grain size distribution curve of MI fines (Majura silt)	69
Figure 3. 6	Grain size distribution curve of MII fines	70
Figure 3. 7	Grain size distribution curve of SI fines (Crushed Sydney sand)	71
Figure 3. 8	Grain size distribution curve of SII fines	72
Figure 3. 9	Cross section of sample preparation mould	76
Figure 3. 10	Details diagram of water flushing through the sample	77
Figure 3. 11	Membrane penetration mechanism for undrained test; (a) mechanism for contractive soil, (b) mechanism for dilative soil	83
Figure 3. 12	Microscope used in the study; (a) Light microscope, (b) Scanning Electron Microscope, SEM	87
Figure 3. 13	Sand with fines; (a) Clean sand, (b) Sand with 15% fines, (c) Sand with 20% fines, (d) Sand with 30% fines	88
Figure 3. 14	Sample preparation of SEM; (a) Gold coating on sample, (b) Sample prepared on carbon tape	90
Figure 3. 15:	Analytical spectrum for S-I fines	92
Figure 3. 16	Analytical spectrum of M-I fines	92
Figure 3. 17	Analytical spectrum of Kaolin	93
Figure 4. 1	Effect of diameter ratio of binary packing density after McGeary (1961), slightly modified	100
Figure 4. 2	Geometric calculation of a small sphere fitting inside of three large spheres, modified from Lade et al. (1998)	100
Figure 4. 3	Effect of fines content on minimum void ratio of binary mix after Lade et al. (1998) (slightly modified)	102
Figure 4. 4	Effect of diameter ratio on minimum void ratio of binary mix after Lade et al. (1998)	103
Figure 4. 5	Effects of fines content on SS data points for sand with fines after Thevanayagam et al. (2002b)	106
Figure 4. 6	Variation of steady state void ratio at mean effective stress, p' = 100kPa with fines content after Thevanayagam et al. (2002b)	107

Figure 4. 7	Sensitivity of steady state void ratio for sand-fines mix with steady state confining pressure after Thevanayagam et al. (2002b)	108
Figure 4. 8	Relation between TFC and particle diameter ratio	110
Figure 4. 9	Factors affecting *b*; (a) Influence of χ on *b* (TFC=35%), (b) Influence of χ on the first factor of Equation 4.2a (c) Influence of fines content on *b* (TFC=35%)	114
Figure 4. 10	Steady state lines for Hokksund sand with Chengbei non-plastic fines; (a) source data after Yang et al. (2006a), (b) interpreted based on *e** using Equation. 4.2a and 2.14, (c) interpreted based on eg using Equation 2.12	120
Figure 4. 11	Steady state lines for Mai Liao sand with fines; (a) source data after Huang et al. (2004), (b) interpreted based on *e** using Equation 4.2a and 2.6	122
Figure 4. 12	Steady state lines for Old Alluvium sand with fines; (a) source data after Ni et al. (2004), (b) interpreted based on *e** using Equation 4.2a and 2.14	123
Figure 4. 13	Steady state lines for Toyoura sand with fines; (a) source data after Zlatovic and Ishihara (1995), (b) interpreted based on *e** using Equation 4.2a and 2.14	125
Figure 4. 14	Steady state lines for Foundry sand with non-plastic fines; (a) source data after Thevanayagam et al. (2002), (b) interpreted based on *e** using Equation 4.2a and 2.14	126
Figure 4. 15	Cyclic Resistance for 20/200 Brenda sand with silty fines; (a) source data after Vaid (1994), (b) interpreted based on *e** using Equation 4.2a and 2.14	128
Figure 4. 16	Cyclic resistance for Monterey sand and Yatesville fines; (a) source data after Polito and Martin (2001), (b) interpreted based on *e** using Equation 4.2a and 2.14	129
Figure 4. 17	Cyclic resistance for Yatesville sand with fines; (a) source data after Polito (1999), (b) interpreted based on *e** using Equation 4.2a and 2.14	130
Figure 4. 18	No. of cycles (N_L) required to trigger cyclic liquefaction for Ottawa sand with non-plastic fines at cyclic stress ratio of 0.20; (a) source data after Thevanayagam and Martin (2002), (b) interpreted based	

	on e^* using Equation 4.2a and 2.14	132
Figure 5. 1	Threshold fines content, TFC for Sydney sand with fines	144
Figure 5. 2	Effect of fines on SS data points for sand with fines, (a) Effect of fines on SSL in e-log(p') space, (b) A single EG-SSL for sand with fines in e^*-log(p') space	146
Figure 5. 3	SSL for Sydney sand with 15% M-II fines and consolidation curve of two special tests in e-log(p') space	149
Figure 5. 4	EG-SSL for Sydney sand with 15% M-II fines and consolidation curve for two special tests in e^*-log(p') space	149
Figure 5. 5	Non-flow and limited flow behaviour for special tests; (a) stress path behaviour, (b) stress-strain behaviours	150
Figure 5. 6	Initial state of all tests for sand and sand with fines (up to 30%) relative to EG-SSL	151
Figure 5. 7	Definition of equivalent state parameter, ψ^*	152
Figure 5. 8	Different equivalent granular state parameter for different undrained behaviour for clean sand; (a) $q/p'_{(0)}$- $p'/p'_{(0)}$ space, (b) $q/p'_{(0)}$- ε_q space	155
Figure 5. 9	Different equivalent granular state parameter for different undrained behaviour for same fines content, (a) $q/p'_{(0)}$- $p'/p'_{(0)}$ space, (b) $q/p'_{(0)}$- ε_q space	157
Figure 5. 10	Different undrained behaviours for different $\psi^*_{(0)}$ for different fines content; (a) $q/p'_{(0)}$- $p'/p'_{(0)}$ space, (b) $q/p'_{(0)}$-ε_q space	159
Figure 5. 11	Comparison at same equivalent granular state parameter, $\psi^*_{(0)}$ = 0.97 for different fines content; (a) in $q/p'_{(0)}$- $p'/p'_{(0)}$ space, (b) in $q/p'_{(0)}$ -ε_q space	161
Figure 5. 12	Comparison at same equivalent state parameter, $\psi^*_{(0)}$ = 0.81 for different fines content ; (a) in $q/p'_{(0)}$- $p'/p'_{(0)}$ space, (b) in $q/p'_{(0)}$ -ε_q space	162
Figure 5. 13	Grain size distribution curve of Host sand with fines	164
Figure 5. 14	Effect of fines on SS data points for Host sand with fines; (a) Effect of fines in e-log(p') space, (b) A single EG-SSL e^*-log(p') space	166
Figure 5. 15	EG-SSL and initial state of tests with flow/non-flow behaviours for	168

	0% - 27% fines	
Figure 5. 16	Equivalent granular state parameter and different ESP behaviour for host sand with GS-10 fines; (a) q-p' space, (b) q-ε_1 space, reproduced from Thevanayagam and Mohan (2000)	172
Figure 5. 17	Influence of $\psi^*_{(0)}$ on the ESP Spectrum of same KS-10 fines; (a) in q-p' space, (b) in q-ε_1 space, reproduced from Thevanayagam and Mohan (2000)	174
Figure 5. 18	Influence of $\psi^*_{(0)}$ on the ESP Spectrum of different fines content; (a) in q-p' space, (b) in q-ε_1 space, reproduced from Thevanayagam and Mohan (2000)	176
Figure 5. 19	ESP spectrum at different fines content but same $\psi^*_{(0)}$; (a) in q-p' space, (b) in q-ε_1 space, reproduced from Thevanayagam and Mohan (2000)	178
Figure 6. 1	The slope of Critical or Steady State Line, M in q-p' space	187
Figure 6. 2	Determination of A to obtain G_0	191
Figure 6. 3	Determination of dilatancy parameter from Test A2	192
Figure 6. 4:	Determination of hardening parameter from test S-MII-10-01	194
Figure 6. 5	Relation between hardening parameter and equivalent granular void ratio, e^*	195
Figure 6. 6	The conventional stress-strain and volume change diagram for the tests ised in the flow rule prediction	197
Figure 6. 7	Prediction of flow rule; (a) Sydney sand, (b) Sydney sand with 10% M-II fines	198
Figure 6. 8	Prediction of flow rule; (a) Sydney sand with 15% M-II fines, (b) Sydney sand with 25% M-II fines	199
Figure 6. 9	Comparison between undrained triaxial compression tests results and model prediction for different fines content, f_c and different initial mean effective stress, $p'_{(0)}$	204
Figure 6. 10	Comparison between undrained triaxial compression tests results and model prediction for different fines content, f_c and different initial mean effective stress, $p'_{(0)}$	205
Figure 6. 11	Comparison between undrained triaxial compression tests results and model prediction for different fines content, f_c at same initial	206

	mean effective stress, $p'_{(0)}$ = 850kPa	
Figure 6. 12	Comparison between undrained triaxial compression tests results and model prediction for different fines content, f_c at same initial mean effective stress, $p'_{(0)}$ =850kPa	207
Figure 6. 13	Comparison between undrained triaxial compression tests results and model prediction for different fines content, f_c at same initial mean effective stress, $p'_{(0)}$ =850kPa	208
Figure 6. 14	Comparison between undrained triaxial compression tests results and model prediction for different fines content, f_c but same equivalent granular sate parameter, $\psi^*_{(0)} \approx 0.09$	209
Figure 6. 15	Comparison between undrained triaxial compression tests results and model prediction for different fines content, f_c but same equivalent granular sate parameter, $\psi^*_{(0)} \approx 0.08$	210
Figure 6. 16	Comparison between undrained triaxial compression tests results and model prediction for different fines content, f_c and same equivalent granular sate parameter, $\psi^*_{(0)} \approx 0.08$	210
Figure 6. 17	Comparison of limited flow between undrained triaxial compression tests results and model prediction for different fines content, f_c	213
Figure 6. 18	Comparison of non flow behaviour between undrained triaxial compression tests results and model prediction for different fines content, f_c	214
Figure 6. 19	Comparison between undrained triaxial compression tests results and model prediction for 10% fines content, f_c at a initial mean effective stress, $p'_{(0)}$ = 100kPa, after Bobei (2004)	216
Figure 6. 20	Comparison between undrained triaxial compression tests results and model prediction for 10% fines content, fc at initial mean effective stress, $p'_{(0)}$ of 300kPa and 400kPa, after Bobei (2004)	217
Figure 6. 21	Comparison between undrained triaxial compression tests results and model prediction for 10% fines content, fc at initial mean effective stress, $p'_{(0)}$ of 600kPa and 1115kPa, after Bobei (2004)	218
Figure 7. 1	SEM photograph of MI fines (500x magnification)	224
Figure 7. 2	SEM photograph of SI fines (500 x magnification)	225
Figure 7. 3	SEM photograph of kaolin (1000x magnification)	226

Figure 7. 4	SEM photograph of MII fines (500x magnification)	227
Figure 7. 5	SEM photograph of SII fines (500 x magnification)	228
Figure 7. 6:	Effect of different types of fines; (a) SSL in e-log(p') space, (b) EG-SSL in e*-log(p') space	235
Figure 7. 7	The effect of increasing plasticity on "I" fines to; (a) in q-p' space, (b) in q-ε_q space	238
Figure 7. 8:	The effect of increasing plasticity on "II" fines to; (a) in q-p′ space, (b) in q-ε_q space	240
Figure 7. 9	The effect of increasing plasticity on "*M*" fines to; (a) in q-p' space, (b) in q-ε_q space	243
Figure 7. 10	The effect of increasing plasticity on "S" fines to; (a) in q-p' space, (b) in q-ε_q space	245
Figure 8. 1	Relation between cyclic and monotonic behaviour for strain softening type triaxial tests; (a) in q-p' space, (b) in q-ε_q space	251
Figure 8. 2	Limited understanding for strain hardening type behaviour	251
Figure 8. 3	Test pair M-15-05 and C-15-21 for 15% fines: a) ESP; b) q-ε_q response; c) stress-time plot	257
Figure 8. 4	Test pair M-15-04 and C-15-20 for 15% fines: (a) ESP; (b) q-ε_q response; (c) stress-time plot	260
Figure 8. 5:	Test pair M-20-02 and C-20-20 for 20% fines; (a) ESP; (b) q-ε_q response; (c) stress-time plot	262
Figure 8. 6:	Test pair M-00-08 and C-00-20 for host sand: a) ESP; b) q-ε_q response; c) stress-time plot	265
Figure 8. 7:	Test pair T-00-07 and C-00-21 for host sand: a) ESP; b) q-ε_q response; c) stress-time plot	269
Figure 8. 8:	Test pair M-15-05 and C-15-22 for 15% fines: (a) ESP; (b) q-ε_q response; (c) stress-time plot	272
Figure 8. 9:	Test pair M-00-05 and C-00-22 for clean sand: a) ESP; b) q-ε_q response; c) stress-time plot	275
Figure 8. 10:	Test pair M-15-07 and C-15-23 for 15% fines: a) ESP; b) q-ε_q response; c) stress-time plot	276
Figure 8. 11:	The effect of parameter, ϖ on cyclic instability for clean sand	279

Figure 8. 12: The effect of parameter, ϖ on cyclic instability for sand with 15% Fines 280

Figure 8. 13: The effect of parameter, ϖ on cyclic instability for sand with 20% Fines 280

Figure 8. 14: The effect of parameter, ϖ on cyclic instability for sand and sand with fines (f_c < TFC) 281

CHAPTER 1

Introduction

1.1 GENERAL

The phenomenon of liquefaction/instability was recognized in early stage of soil mechanics development. The term “spontaneous liquefaction” was first used by Terzhagi and Peck (1948) to explain the phenomenon of sudden loss of strength in loose sand deposit. It was recognized as the main cause of slope failure in saturated sandy deposit. But soon, it was realized from Fukui earthquake (1948) that it can be observed in widespread ground condition in plan areas (Ishihara 1993). Later, it was more thoroughly brought to the attention of engineers and seismologists by several natural hazards around the world; Niigata and Alaska (1964), San Fernando Dam failure (1971), Loma Prieta (1989), Kobe (1995) and Chi-Chi (1999) earthquakes. Since then, a numerous investigation on filed and laboratory revealed that pore water pressure generation due rapid loading is the reason of “liquefaction”.

Alone this line, numerous experimental investigations was done on undrained condition in laboratory due to the limitations in field investigation such as instrumentations and uncertainty associated with the occurrence of earthquake. However, these laboratory studies were initially focused on undrained cyclic loading as it was believed that liquefaction mainly occurs due to earthquake loading. But sooner, it was clear to the greater audience that liquefaction can also be occurs due to

static loading and the key factor driving cyclic liquefaction/instability can also be analyzed from the static loading condition.

A clear understanding on liquefaction/instability behaviour of clean sand was achieved over last few decades. But, the understandings for sand with fines are not clear although sand with fines are common. Probably experimental difficulties associated with the investigation on sand with fines behaviour are the main reason of less number of investigations and understanding. The progressive experimental developments over decades make it possible of conducting investigations on this challenging area. Thus, systematic studies on sand with fines are seen only from 1980's.

Three different findings were observed for sand with fines. The first finding was from early studies showed that liquefaction resistance decreases with the increase in fines content (Troncoso 1986). The second finding showed that liquefaction resistance increased with the increase in fines content (Amini and Qi 2000; Kuerbis et al. 1988; Pitman et al. 1994). The third finding was from relatively recent studies showed that liquefaction resistance decreases with increase in fines contents up to a threshold fines content and then liquefaction resistance decreases with increase in fines content beyond the threshold fines content (Altun et al. 2005; Thevanayagam 1998; Xenaki and Athanasopoulos 2003; Yang et al. 2006a; Zlatovic and Ishihara 1995). Some publications revealed that these apparently contradictory outcomes are due to the inconsistent interpretation /comparison basis (Polito and Martin 2001; Sadek and Saleh 2007; Xenaki and Athanasopoulos 2003). If void ratio is used as a comparison basis, a consistent outcome as third group is found. However, this observation did not

help to overcome the challenges for sand with fines. One can not analyzed sand with fines in a single framework within Critical State Soil Mechanics, CSSM as different Critical/Steady State lines are achieved for sand with different fines content in e-log(p') space. Many researcher suggested void ratio, e is not a good state variable for sand with fines.

The equivalent granular void ratio, e^* instead of void ratio, e was proposed to use for sand with fines to overcome this problem. As most of the fines particles are non-active in sand force structure due to their size ratio, the non-active fines are considered as void space in equivalent granular void ratio. When e^* is used instead of e, the steady state data points are come to a single trend in e^*-log(p') space for sand with fines. This trend/line is called equivalent granular steady state line, EG-SSL. That gives a prospect of analyzing sand with fines in a single framework and it can even be extended to a single constitutive model irrespective to fines contents. However, this hypothetical conceptual framework based on e^* which requires a parameter, b (represents the fraction of fines active in sand force structure). In literature, b was achieved by back analysis. But, the conceptual framework can not be used as predictive tools without a proper prediction formula for b.

From the above discussion, it is apparent that the concept of equivalent granular void ratio, e^* and b parameter for sand with fines requires additional attention and it is vigorously investigated in the present study. This will provide valuable information on the single framework for sand with fines toward the development of a single constitutive model irrespective of fines contents.

1.2 THESIS ORGANIZATION

This thesis is organized in nine chapters and the contents of each chapter are briefly summarized below.

In Chapter 1, it is emphasized on the importance of conducting experimental study on sand with fines and the challenges with analytical approach within CSSM. The emphasis is also placed on equivalent granular void ratio, e^* and the prospect of achieving a single trend of Critical/Steady data points and a single state dependent constitutive model irrespective of fines contents. The emphasis is also placed on the effect of fines types and cyclic loading on the hypothetical framework.

Chapter 2 presents a review of the liquefaction phenomenon of clean sand and sand with fines under static and cyclic loading. It discusses about the common framework used to describe undrained behaviour and the state parameters. Then, it discusses on the effect of fines on the liquefaction phenomenon, challenges and analytical approaches in attempt to over come the problems encountered with the presence of fines. An approach of developing a single constitutive model irrespective of fines content is also discussed in this Chapter. It also discusses on the effects fines types and cyclic loading on sand-fines mix.

Chapter 3 discusses in details about experimentation on macro and micro level behaviour of sand-fines mix. The macro experimentation discusses about triaxial testing system, control program, error minimization etc. The micro experimentation discusses about microscopic investigation of sand-fines size, shape and mineralogy. It includes light microcopy and scanning electron microscopy (SEM). Mineralogical analyses of fines by SEM are also presented in this Chapter.

Chapter 4 discusses about the concept of equivalent granular void ratio, e^* and the b parameter. It presents a physically reasonable semi-empirical equation for predicting the b parameter. The prediction formula for b is evaluated by a single equivalent granular steady state line, EG-SSL with nine published data sets from six different countries.

Chapter 5 presents an experimental program for sand with fines to evaluate the prediction formula for b, hence e^* and the EG-SSL. The experimental SS data sets showed a single trend in e^*-log(p') space irrespective fines content i.e. EG-SSL was obtained. Then the concept of EG-SSL was verified by equivalent granular state parameter, $\psi^*_{(0)}$ (at the end of consolidation) to their corresponding effective stress path. A good predictive capability of $\psi^*_{(0)}$ is observed. The same exercise is repeated with published data set by Thevanayagam and Mohan (2000). A good predictive capability of $\psi^*_{(0)}$ is also observed for the published data set.

In Chapter 6, the implement of the above concepts in an existing constitutive model and the prediction of undrained behaviour of sand with fines independent of fines contents are discussed. It gives emphasis on the selection of an appropriate model, determination of model parameter and discusses on the success in predicting undrained behaviour irrespective of fines contents. It also compares model prediction and undrained behaviour for sand with 10% fines published by Bobei (2004).

Chapter 7 presents an experimental program on sand with different types of fines. It discusses the effect of fines types on b parameter and hence, the EG-SSL. It also discusses the effect of fines angularity and plasticity on their effective stress path. It

emphasizes that the EG-SSL is not enough for sand with different fines types to describe their effective stress path.

Chapter 8 presents a short literature review on the link between monotonic and cyclic loading behaviour. It also presents exclusive experimental evidence that over all key feature of cyclic loading behaviour (e.g. cyclic instability) of sand and sand with fines are linked with monotonic behaviour. It also introduces a new index referred to as "instability index" which can be used to predict whether a cyclic loading path will exhibit instability or not.

Chapter 9 includes the main conclusion and recommendations for future works.

CHAPTER 2

Literature Review

2.1 INTRODUCTION

This Chapter presents a review of the liquefaction phenomenon of clean sand and sand-fines mix under static and cyclic loading. All these literatures are presented in six different parts. Part one focuses on the liquefaction phenomenon of clean sand and the corresponding terminology used in literature, particularly for undrained behaviour. Part two discusses about the various state parameters; state parameter (Been and Jefferies 1985), state index (Ishihara 1993), pressure index (Wang et al. 2002), modified state parameter (Bobei and Lo 2005). Part three focuses on the effect of fines on the liquefaction phenomenon, challenges and analytical approaches in attempt to over come the problems encountered with the presence of fines. Part four discusses about the modelling of sand with fines irrespective of fines contents. Part five discusses on the effects fines types on liquefaction analysis and Part six focuses on the effect of cyclic loading on the liquefaction phenomenon.

2.2 STATIC LIQUEFACTION PHENOMENON

Although, liquefaction have been long recognized, it was more thoroughly brought to the attention of engineers and seismologists by several natural hazards around the world; Niigata and Alaska (1964), San Fernando Dam failure (1971), Loma Prieta (1989), Kobe (1995) and Chi-Chi (1999) earthquakes (Baziar and Jafarian 2007). And

a considerable amount of controversy has been develop over time about the liquefaction phenomenon (Morris 1983; Sladen et al. 1985). However, from the on going understanding, it may be better describe as a catastrophic failure phenomenon in which a saturated/near-saturated cohesionless soil losses strength due to increase in pore water pressure under rapid loading and the failed soil acquires a degree of mobility sufficient to permit movement from meters to kilometer. This includes: major landslides, lateral movement of bridge supports, settling and tilting of buildings, failure of water front structure etc. Liquefaction is associated with pore water pressure generation due to undrained condition occurred in soil. Thus, undrained triaxial tests are widely used in liquefaction study although some researchers claimed to observed liquefaction instability in non-undrained conditions (Bobei and Lo 2007; Chu and Leong 2001; Lo et al. 2008). However, the literature in this chapter is mainly concentrated on undrained triaxial tests on clean sand and sand with fines under static and cyclic loading following to the intention of this study. Before going to detail literature, typical undrained clean sand behaviours and related terminologies are discussed in next subsections.

2.2.1 *Undrained Behaviours*

There are three types of undrained behaviour typically observed for clean sand. These behaviours are highly dependent on initial state of undrained shearing i.e. initial mean effective stress, $p'_{(0)}$ and initial void ratio, $e_{(0)}$ (at the end of isotropic consolidation). They are discussed below.

At the high confining stress/very loose state, the specimen shows strong contractive tendency. Thus, a continuous increase in pore water pressure develops with in the

specimen and effective stress path reaches a peak, q_{peak} in q-p' space. Further shearing cause a continuous decrease in mean effective stress and deviatoric stress until the stress path reaches to the steady state, SS point at steady state line, SSL. At steady state, sand deform at constant volume and under constant stress ($dp' = 0$ and $dq = 0$) and the shear strength at SS is called residual strength (Ishihara 1993). This type of soil shows strain softening in q-ε_q space until the shearing may eventually reach the steady state point without any tendency for dilation. The schematic diagram of test-1 in Figure 2. 1a&b is an example of such behaviour. This behaviour of sand is called "flow" behaviour. However, different researchers called this behaviour in different names: "flow deformation" (Alarcon-Guzman et al. 1988), "static liquefaction" (Bobei and Lo 2001), "unstable" (Yamamuro and Lade 1998). "Instability" is a common terminology that is used to describe this type of behaviour and it is discussed in details in sub-section 2.2.2.

At low confining stress/very dense state, sand possesses initially little contractive tendency and then shows dilative tendency in q-p' stress path. Negative pore pressure develops due to dilation tendency and the stress path traced towards high mean effective stress and ultimately it reached to the steady state line (SS line). Furthermore, this type of soil shows strain hardening in q-ε_q space until the shearing may eventually reach to the steady state, SS point. The schematic diagram of test-2 in Figure 2. 1a&b is an example of such behaviour. This behaviour is called "stable behaviour" by Yamamura and Lade (1998). Other researcher called it "non-flow" behaviour (Alarcon-Guzman et al. 1988).

At moderate high confining stress/medium loose state, the specimen initially shows contractive tendency. Thus, initially, greater pore water pressures develop with in the specimen which cause effective stress path "warp around" the top of the plastic yield surface and exhibit an initial increase of maximum deviatoric stress, q_{peak}. Further increase in pore water pressure causes decrease in mean effective stress, p' and deviatoric stress, q. However, the reduction of p' and q is temporary. The effective stress path bends sharply upward and to the right at a transition state in q-p' space and ultimately reach to the steady state. This transition state is a point called "phase transformation point" by Ishihara et al. (1975) and it is discussed in coming subsection 2.2.3. However, this type of soil shows a temporary drop of shear stress followed by strain hardening in q-ε_q space until the shearing may eventually reach to the steady state (SS) point. The schematic diagram of test-3 in Figure 2. 1a&b is an example of such behaviour. As the stress path shows temporary flow in q-p' space, some researcher called this behaviour as "limited flow" behaviour (Alarcon-Guzman et al. 1988; Bobei and Lo 2003; Bobei and Lo 2005; Lo et al. 2008). However, different researchers called this behaviour at different names: "temporary instability" (Yamamuro and Lade 1998), "limited liquefaction" (Ibsen 1998; Mohamad and Dobry 1986).

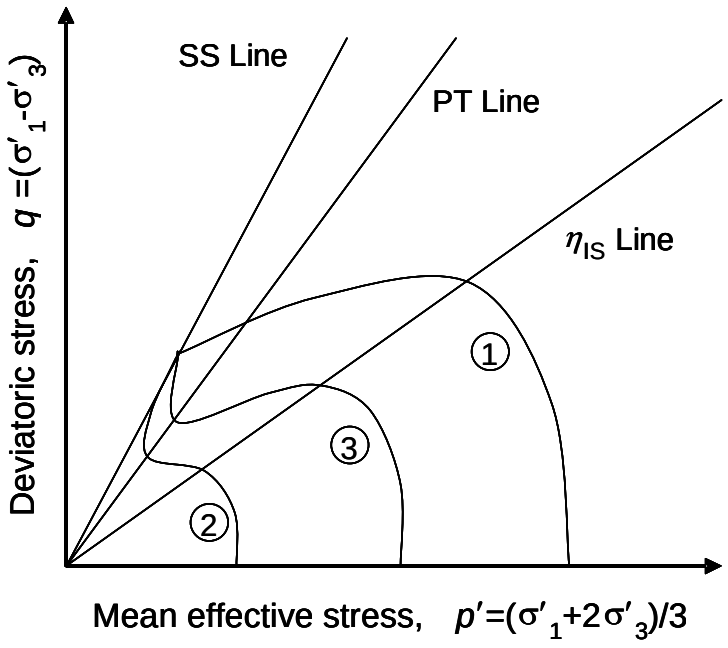

(a)

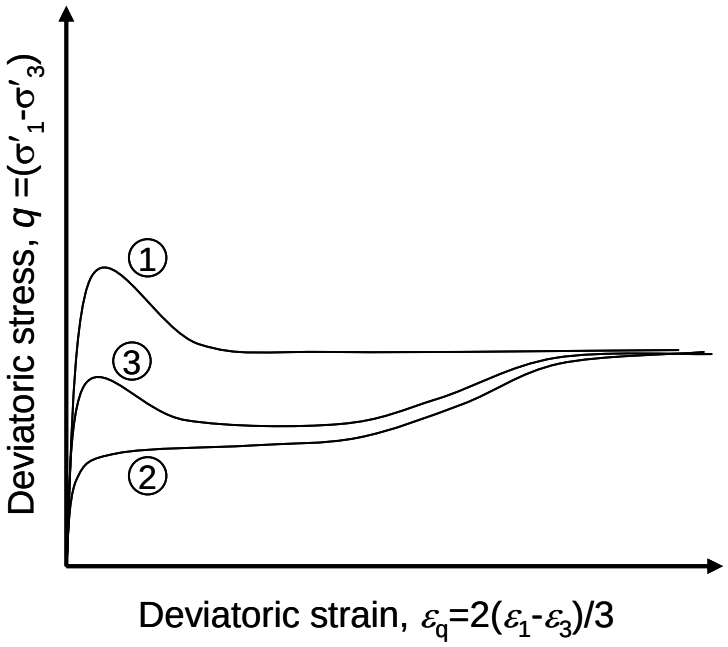

(b)

Figure 2. 1 **Schematic diagram of undrained triaxial tests at same confining pressure; (a) Effective stress path, (b) Stress-strain response in q-ε_q space**

Though these three behaviours are presented with schematic diagram, they are also well documented in literature. One such example is presented in Figure 2. 2a and Figure 2. 3a from Mohamad and Dobry (1986). Figure 2. 2a shows that at same void

ratio after consolidation ($e_{(0)} \approx 0.70$), clean sand behaviour changed from "non-flow" to "flow" behaviour with increase in mean effective stress. This sequence of soil behaviours, with mean effective stress, is a well documented for clean sand. However, Yamamura and Lade (1998) named it as "normal" behaviour after they found a "reversed" trend for sand with fines and these are discussed in details in section 2.6.

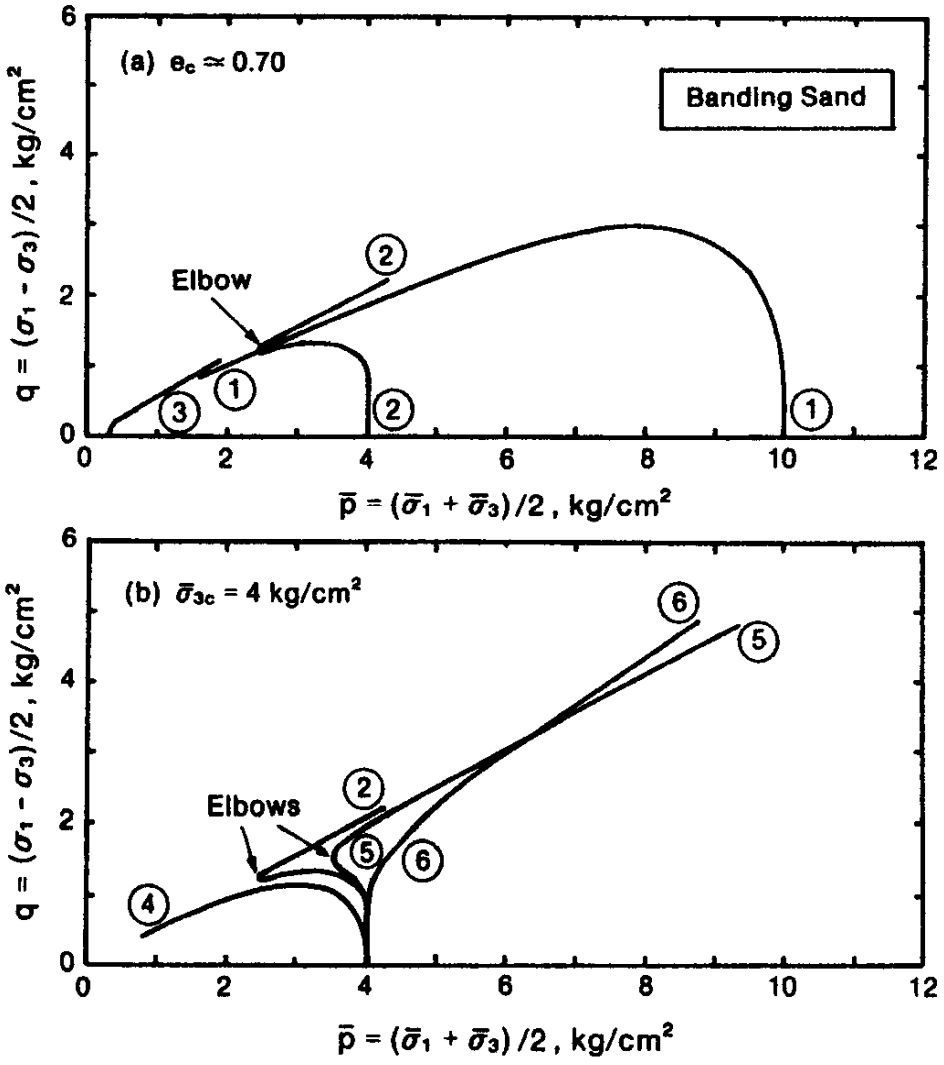

Figure 2. 2 **Effective stress path for Banding sand in CIU test (data from Castro (1969)); (a) same *e*, different *p′*, (b) different *e*, same *p′* after Mohamad and Dobry (1986).**

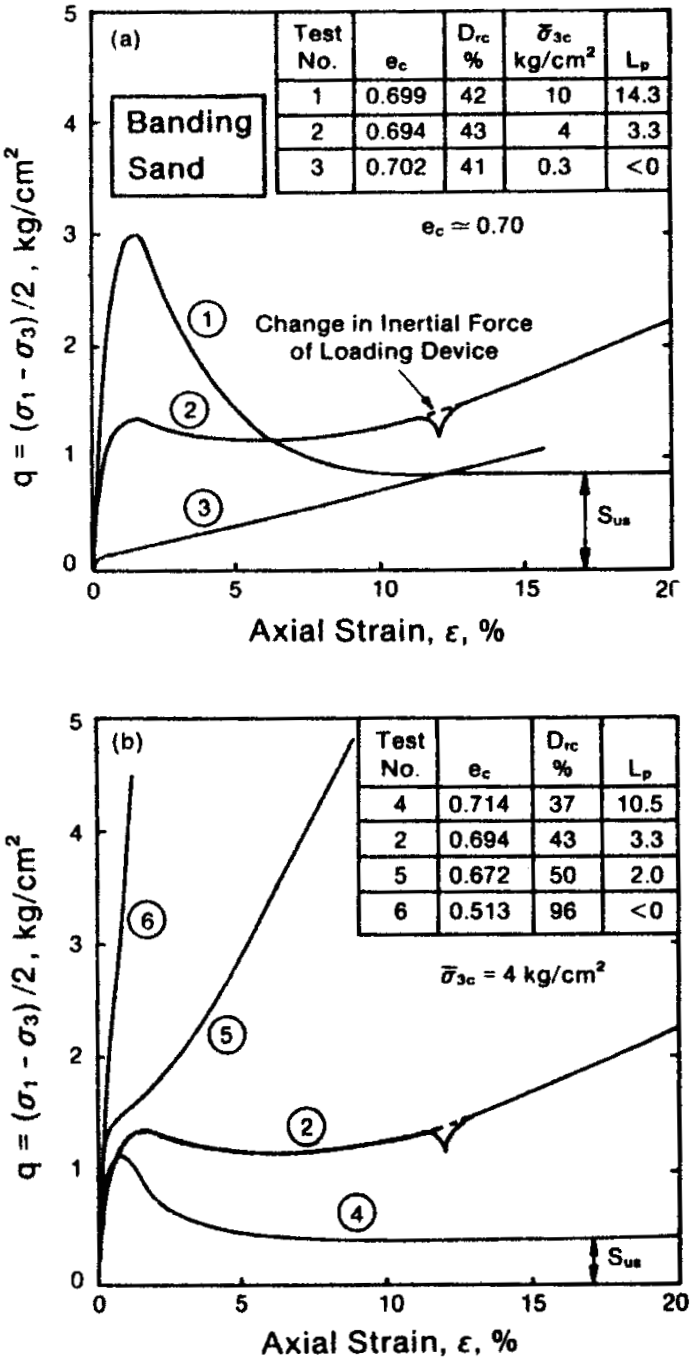

Figure 2. 3 **Stress-strain response of Banding sand in CIU test (data from Castro (1969)), (a) same *e*, different *p′*, (b) different *e*, same *p′* after Mohamad and Dobry (1986).**

The above discussion shows that at same void ratio after consolidation, sand behaviours are changed from dilative to contractive with increasing mean effective stress. However, these three distinct behaviours are also observed at same mean effective stress but with different void ratios in q-p' space (Ishihara 1993; Mohamad and Dobry 1986; Thevanayagam and Mohan 2000). Mohamad and Dobry (1986) found that sand behaviours are changed from stable to unstable with increasing void ratio after consolidation $e_{(0)}$ at same initial mean effective stress $p'_{(0)}$ (at the end of consolidation) as shown in Figure 2. 2 and Figure 2. 3. Thus, it is evident that initial void ratio, $e_{(0)}$ and mean effective stress, $p'_{(0)}$ are the initial state parameters that have very strong influence on soil ultimate behaviour. However, there are few common terminologies used to explain undrained behaviour of sand. They are explained in details in coming subsections.

2.2.2 *Instability Line/Collapse Line*

The typical stress path of "flow" and "limited flow" shows a temporary peak deviatoric stress, q_{peak} in q-p' space. This is the stress state where strain softening initiates and leads to the concept of collapse surface. Sladen et al. (1985) showed that the peak points of the stress paths tend to fall close to a straight line in q/p'_{SS}-p'/p'_{SS} space (normalized with respect to mean effective stress, p' at steady state, SS) and that this line passes through the steady state point as shown in Figure 2. 4a. This straight line is called collapse line, CL (Sladen et al. 1985). They mentioned that in normalized q-p' space, the position of the collapse line shifts with changes in void ratio while the slope remains constant. Thus, there are potentially an infinite number of these lines, which in three-dimensional q-p'-e space to form a surface that passes

through the steady state line, SSL. This surface is called collapse surface (Sladen et al. 1985). Ishihara (1993) reported slightly different finding on Toyoura sand. He reported that that normalized peak deviatoric stress (normalized by mean effective stress at quasi steady state (QSS) fall in a straight line which passes through the quasi steady state, QSS point as shown in Figure 2. 4b. Alarcon-Guzman et al. (1988) also reported similar finding except they called it critical stress ratio, CSR line.

Apart from the normalized stress path, a simple observation on the points where strain softening initiate was reported in literature. These points can be connected by a straight line in q-p' space and that also passes through the origin of q-p' space as shown in Figure 2. 5a. This is different from collapse line, CL which passes through either SS or QSS points in normalized q-p' space. Some researchers called it instability line, IL (Chu and Leong 2002; Lade 1992) and Leong at al. (2000) also called it as peak stress line, PSL. Yamamuro and Lade (1997) and Lade and Yamamuro (1997) reported that instability line, IL may not be a straight line, little concave upward at low mean effective stress though it passing through the origin in q-p' space. However, the instability line, IL is not a unique line as shown in Figure 2. 5b (Chu and Leong 2002). It varies with void ratio. However, they showed that instability stress ratio versus void ratio after consolidation posses a trend as shown in Figure 2. 6. Yamamuro and Lade (1997) also reported that instability friction angle versus void ratio after consolidation posses a certain relationship.

Form the above discussion, it is clear that CL and IL are slightly different line where CL passes through SS or QSS points in a normalized stress space and IL passes through the origin of q-p' space. Despite the arguments on CL and IL, by definition

the peak stress ratio in *q-p′* space is the triggering points of deviatoric strain softening and can be used to define instability. This point is called as instability stress ratio, η_{IS} and used to define the triggering of instability in this thesis. It is only the stress ratio in *q-p′* space; not presenting any lines either straight or concave upward.

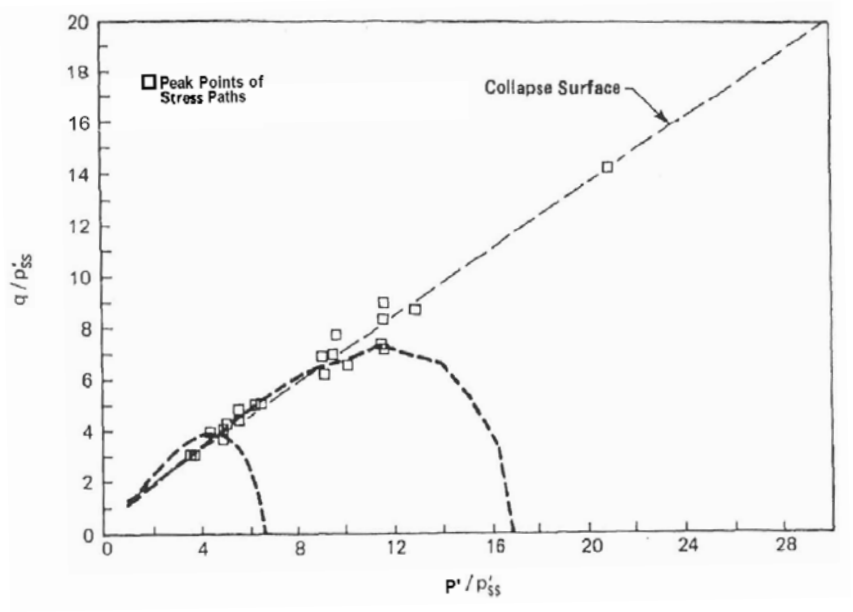

(a)

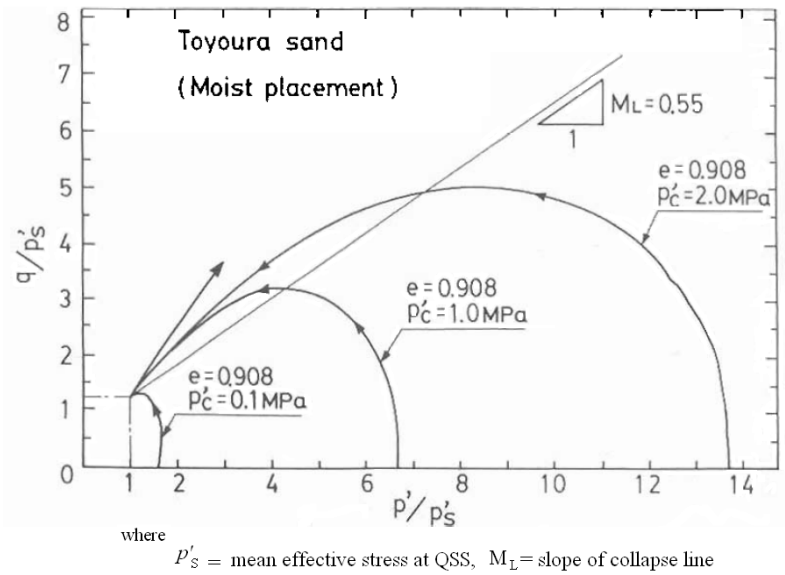

(b)

Figure 2. 4 Collapse line in normalized stress space; (a) for Banding NO. 6 sand after Sladen et al. (1985), (b) for Toyoura sand after Ishihara (1993)

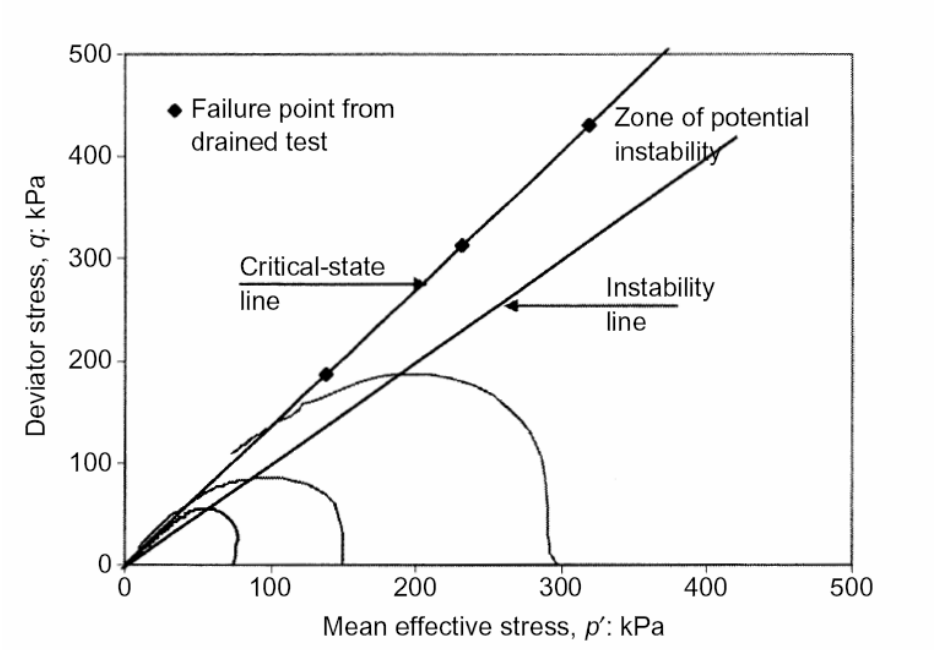

(a)

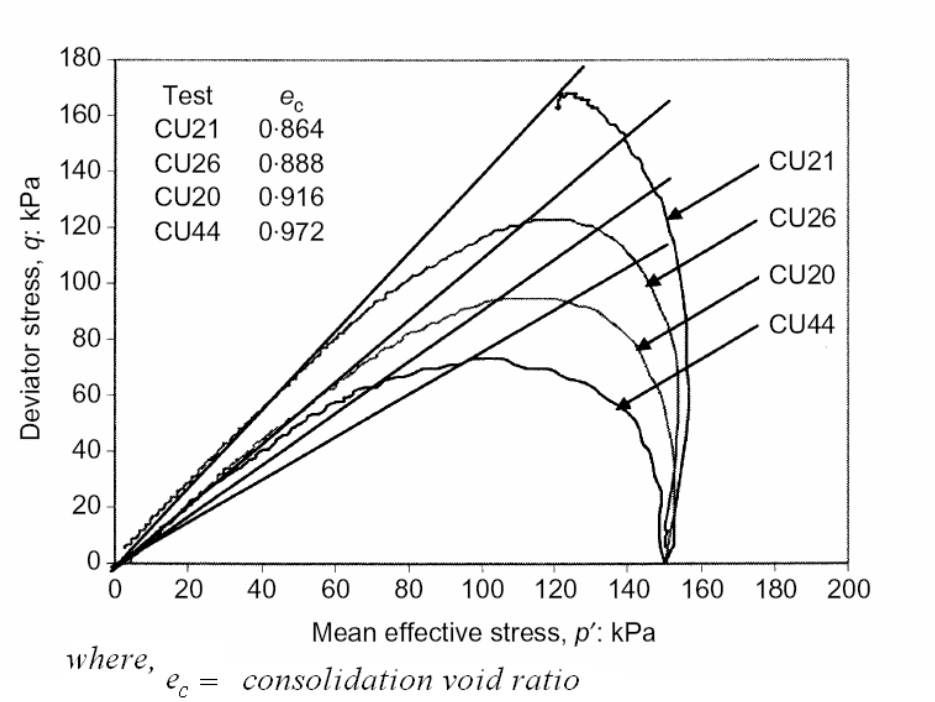

(b)

Figure 2. 5 **Instability line, IL for marine-dredged sand, (a) single IL for sample with same void ratio but different mean effective stress, (b) multiple ILs for different void ratio but same mean effective stress after Chu and Leong (2002)**

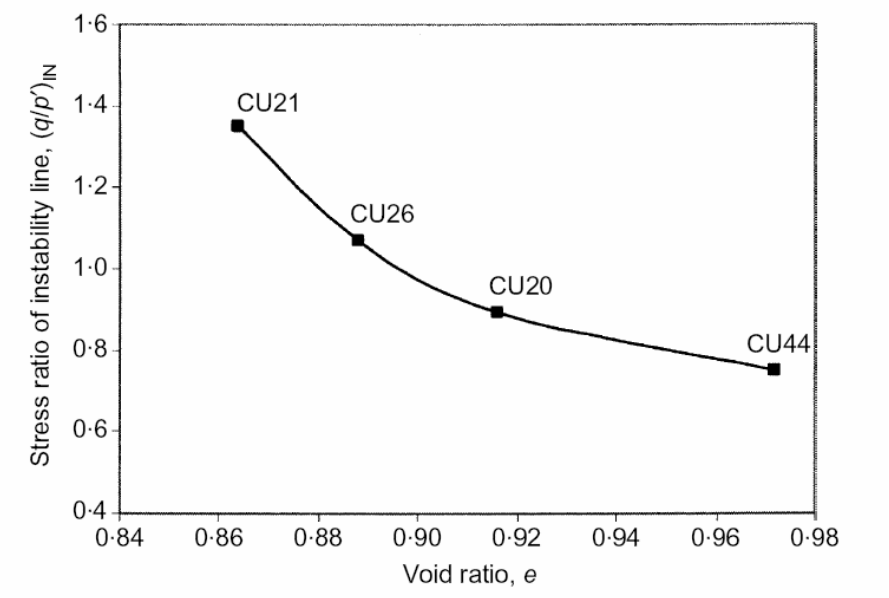

Figure 2. 6 Relation between instability stress ratio and void ratio after Chu and Leong (2002)

Though the concept of instability stress ratio, η_{IS} originally developed for strain softening behaviour of undrained static loading in triaxial tests, it could be successfully extended to provide a unified frame work both for static and cyclic loading (Gennaro et al. 2004; Lo et al. 2008; Mohamad and Dobry 1986; Vaid and Sivathayalan 2000; Yamamuro and Covert 2001). However, it is addressed in details in Chapter 8.

2.2.3 *Phase Transformation, PT*

It is seen in Figure 2. 1a that the stress paths of test-3 bend sharply upward to the right at a threshold stress ratio in q-p' space. This threshold stress ratio can be considered as a threshold point which separates two different phases (contraction and dilation) of soil behaviour. As this point separates two different phases of soil, Ishihara et al. (1975) named it as the point of phase transformation. Thus, at this point $d\varepsilon_v = 0$ and can be easily identified from a drained test. However, in undrained test, $d\varepsilon_v = 0$ is

maintain all through the shearing. Thus, the interpretation of phase transformation for undrained test was done in different ways by different researchers. According to Lade and Ibsen (1997), it is a point where the effective stress path has a "knee" and the mean effective stress reaches to a minimum i.e. dp'=0 in q-p' space. But according to Sukumaran et al. (1996) phase transformation can be defined unambiously as the peak point in the plot of pore water pressure versus strain i.e. PT point is the u_{max} (du = 0) point in u-ε space. These two interpretations of PT for undrained test were based on two different criteria. Thus it should be clarified whether this two interpretations for PT are same and justified related to dε_v = 0.

In a triaxial undrained test, one can have-

$$\mathrm{d}p = \mathrm{d}p' + \mathrm{d}u = \mathrm{d}\sigma_3 + \mathrm{d}q/3 \qquad \textbf{2. 1}$$

As dσ_3 = 0 for conventional undrained test, the above equation can be rewrite as

$$\mathrm{d}q/3 = \mathrm{d}p' + \mathrm{d}u \qquad \textbf{2. 1a}$$

We know that, $\mathrm{d}q = \mathrm{d}\eta.p' + \mathrm{d}p'.u$ then

$$(\mathrm{d}\eta)\,p' = (3-\eta)\mathrm{d}p' + 3\mathrm{d}u \qquad \textbf{2. 1b}$$

According to Lade and Ibsen (1997), dp' = 0, then d$u \neq 0$. Again, when du = 0 then d$p' \neq 0$. Thus these interpretations give slightly, but distinctly different PT points. The choice of using one of these interpretations needs further justification.

According to Ishihara et al. (1975), the phase transformation is a state corresponds to dε_v = 0, thus

$$\mathrm{d}\varepsilon_v = \mathrm{d}\varepsilon_v^e + \mathrm{d}\varepsilon_v^p = 0 \qquad \textbf{2. 2}$$

According to Lade and Ibsen (1997), $dp' = 0$ at PT, then $d\varepsilon_v^e = 0$ for isotropic condition. Thus, $d\varepsilon_v^p$ must be zero which corresponds to characteristic state of drained test. Even for non-isotropic elastic condition, $dp' = 0$ leads to approximately $d\varepsilon_v^p = 0$ condition. Thus, $dp' = 0$ is a better interpretation of PT for undrained tests. For consistency, $dp' = 0$ is used in this thesis.

According to Ishihara et al. (1975) the locus of phase transformation points is a straight line in q-p' space and this straight line is termed as phase transformation line, PTL.

2.2.4 *Critical/Steady State Line (CSL/SSL)*

Critical state, CS or steady state, SS is an important anchor concept for modelling of soil behaviours with in Critical State Soil Mechanics, CSSM frame work. Probably, Roscoe et al. (1958) first defined critical state as a state where "*soils continue to deform at constant stress and constant void ratio*". Mathematically it can be expressed as

$$dq = 0, dp' = 0, d\varepsilon_v = 0 \quad \text{while} \left| d\varepsilon_q \right| \neq 0 \qquad \textbf{2. 3}$$

Where, $q = (\sigma_1' - \sigma_3')$ is the deviatoric stress, $p' = (\sigma_1' + 2\sigma_3')/3$ is the mean effective stress, ε_v is the volumetric strain, and ε_q is the deviatoric strain. Traditionally, critical states are measured from a drained test.

Later, Poulos (1981) proposed the concept of steady state, SS. It is the "*state in which the mass is continuously deforming at constant volume, constant normal stress, constant shear stress and constant velocity*". Mathematically it can be expressed as

$$\mathrm{d}q = 0, \mathrm{d}p' = 0, \mathrm{d}\varepsilon_v = 0, \mathrm{d}u = 0 \quad \text{while} \left|\mathrm{d}\varepsilon_q\right| \neq 0 \qquad \textbf{2. 4}$$

Where, u is the pore water pressure. Traditionally, steady states are measured from an undrained test. The pore water pressure generation is maintained constant during drained test and therefore the condition of du = 0 is also satisfied for critical state. Thus, there is no theoretical difference between mathematical formulation of critical state and steady state. Despite of no theoretical difference, there are many arguments in literature whether the critical state or steady state is the same state or different states. A number of researchers reported that critical state and steady state are different states (Alarcon-Guzman et al. 1988; Konrad 1990a; Konrad 1990b; Konrad 1993). On the other hand, lot of literature showed that critical state or steady state may be the same state (Been and Jefferies 1986; Been and Jefferies 1985; Been et al. 1991; Bobei 2004; Bobei and Lo 2001; Bobei and Lo 2005; Casagrande 1975; Chu 1995; Chu and Lo 1992; Chu and Lo 1993; Poulos 1981; Sladen et al. 1985; Sladen et al. 1986; Verdugo 1992; Verdugo and Ishihara 1996; Yamamuro and Lade 1998; Yoshimine and Ishihara 1998).

However, on critical review of literature and extreme experimental evidence, it can be concluded that there is no theoretical distinction between these two states, other than wording and the test method used to obtain them (Bobei and Lo 2001; Bobei and Lo 2005; Chu and Lo 1992; Chu and Lo 1993). As critical states are measured from a drained test and steady states are measured from an undrained test, therefore, they have different intrinsic errors. Lo and coworkers (Bobei and Lo 2001; Bobei and Lo 2005; Bobei et al. 2009; Chu and Lo 1992; Chu and Lo 1993) highlighted that strictly controlled experiments are needed to determine (reliably) CS or SS data points in the

e-log(*p*′) space, otherwise different intrinsic errors between drained and undrained tests may lead to an apparent difference between CSL and SSL. However, following the arguments of Lo and co-workers CS and SS are considered as equivalent in this thesis.

2.2.5 *Quasi-Steady State, QSS*

Test-3 in Figure 2. 1a&b shows that a minimum deviatoric stress takes place after the initial peak deviatoric stress within a limited range of deviatoric strain and then deviatoric stress increase with deviatoric strain. According to Ishihara (1993), this minimum deviatoric stress was termed as "the quasi steady state" by Alarcon-Guzman et al (1988) and Been et al. (1991). The QSS behaviour are also observed by many other researchers (Been et al. 1991; Georgiannou et al. 1991; Konrad 1990a; Konrad 1990b; Mohamad and Dobry 1986; Vaid et al. 1990). In spite of large number of experimental evidences, Zhang and Garga (1997) doubt whether limited flow behaviour is due to experimental errors. Two main reasons inspired to doubt on QSS behaviour are: first, difficulty in explaining the rapid decrease in deviatoric stress followed by a continuous increase in deviatoric resistance with further strain and second, there is no published field evidence of the existence of limited flow behaviour. There are number of discussions on literature to answer the first issue (Chu 1999; Vaid et al. 1999a; Yoshimine 1999). However, answering the second issue is more difficult, Lo and coworkers showed that void ratio redistribution mechanism may be one of the reason of not observing limited flow behaviour in field (Bobei and Lo 2007; Lo et al. 2008). Thus, QSS and limited flow behaviour are considered as real experimental observation in this thesis.

2.3 STATE PARAMETERS

Sand behaviours are highly depending on the state of soil, which is in tri-axial condition usually defined by void ratio, e and effective stress, p'. However, initially the effect of mean effective stress was not recognized as clearly as density. Schofield and Wroth (1968) took critical states as a reference base to compare with current state to predict soil behaviour in effective stress versus specific volume space. If the soil state is looser than the critical state (above CSL), it will be contractive and if the soil state denser than critical state (below CSL), it will be dilative. Been and Jefferies (1985) gave a mathematical formulation to this factor and introduced the first-order state parameter for soil. They called this parameter as "state parameter". However, several state parameters were introduced by alternate resembles to improve parameter's ability to explain soil behaviours. They are: state parameter, state index, pressure index, modified state parameter. Though only state parameter is used in coming Chapters, a details discussion of all parameters are given in next sub-sections for better understanding. These discussions inherently assumes critical state and steady state are equivalent.

2.3.1 *State Parameter*

Been and Jefferies (1985) choose SSL as reference line to predict undrained behaviours of soil. They combined the influence of void ratio and the stress level with the SSL and proposed "state parameter" which is defined as the void ratio difference between the current state and the steady state, SS at the same mean effective stress. It is usually denoted by

$$\psi = e - e_{SS} \qquad \textbf{2. 5}$$

where, ψ = state parameter, e = current void ratio of the sample, e_{SS} = void ratio at SS for same mean effective stress. The state parameter at the end of consolidation is used in many discussions in this thesis and it is denoted by $\psi_{(0)}$ here after. In general, positive value of ψ indicates contractive (limited flow to flow) tendency of soil and negative value indicates dilative tendency during undrained shearing (non-flow). The definition of the state parameter is shown in Figure 2. 7.

Numerous tests have been done on Kogyuk sand by Been and Jefferies (1985) to prove the applicability of state parameter. It has been demonstrated that there is a correlation between both drained/undrained strength properties and the state parameter at the end of consolidation, $\psi_{(0)}$ for Kogyuk sand, at four silt contents covering a wide range of states. It has been also demonstrated that there is a correlation between friction angle and state parameter at the end of consolidation, $\psi_{(0)}$ for several sands reported in the literature. The state parameter, ψ were also used to uniquely characterize various responses of different sand such as peak strength, cone penetration resistance (Been et al. 1986; Been et al. 1987). The state parameter was also used to develop state dependent constitutive model (Li 2002; Li and Dafalias 2000). It was appeared that state parameter, ψ is very good first-order parameter until, Ishihara (1993) reported that though state parameter at the end of consolidation, $\psi_{(0)}$ is useful for quantifying the behaviour of medium dense sand under relatively high mean effective stress and it become less tenable for loose sand under low mean effective stress.

However, along this line, the ratio of current void ratio and the void ratio at steady state, e/e_{SS} was used as another from of state parameter (Bauer 1996; Wan and Guo

1998). Wan and Guo (1998) introduced the ratio of e/e_{SS} on Rowe's classical dilatancy equation in order to impose void ratio dependency on dilatancy.

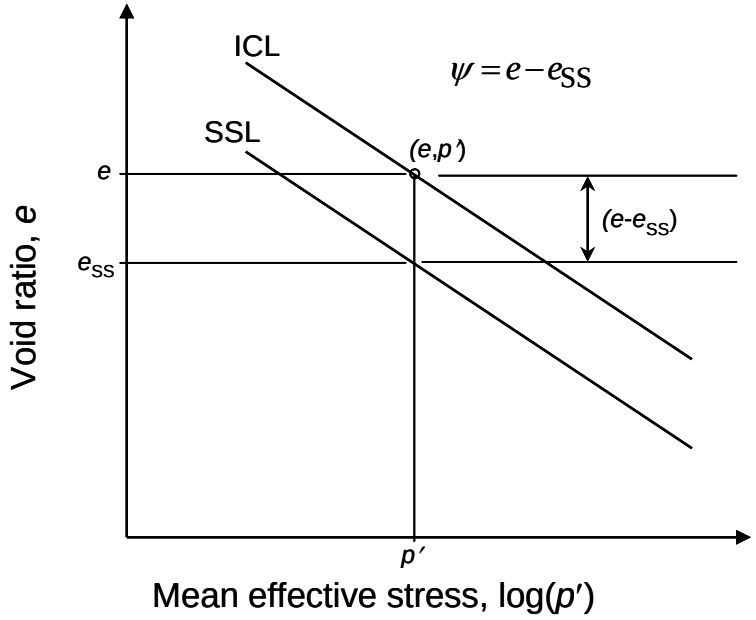

Figure 2. 7 Definition of state parameter by Been and Jefferies (1985), slightly modified notations

2.3.2 *State Index*

According to the "state parameter" definition, if the difference in void ratio at current and steady state at same mean effective stress are identical then the soil behaviours will be the same. After analyzing a numerous test data, Ishihara (1993) concluded that it is not the case at low mean effective stress. He reported that at low mean effective stress, there is a threshold void ratio, e_Γ which is the extrapolation point of SSL/QSSL towards zero mean effective stress in e-p' space. If sample sheared at low mean effective stress with any void ratio greater than that threshold, then sample will come up with zero residual strength, though their state parameter is not identical. To resolve this problem, he proposed an upper reference line which is a combination of the threshold void ratio line and the segment of isotropically consolidated line, ICL below

the threshold void ratio line. He also proposed QSSL as a base reference to capture soil behaviours at medium range strain near QSS and defined state index, I_s as

$$I_s = \frac{e_{UR} - e}{e_{UR} - e_{QSS}} \qquad \textbf{2. 6}$$

where, e_{UR} = void ratio at corresponding upper reference line for a given mean effective stress, e_{QSS} = void ratio at quasi steady state, QSS at the same mean effective stress. The definition of state index is shown in Figure 2. 8.

Physical implications of state index, I_S are given below:

$I_S < 0$	Zero residual strength
$I_S = 0$	Zero residual strength for an initial mean effective stress less than p'_{CR}, or non-zero residual strength for an initial mean effective stress greater than p'_{CR}.
I_S = 0-0.72	occurrence of the QSS, with minimum deviatoric stress coupled with moderately large strains
$I_S \geq 0.72$	occurrence of the steady state at large strains

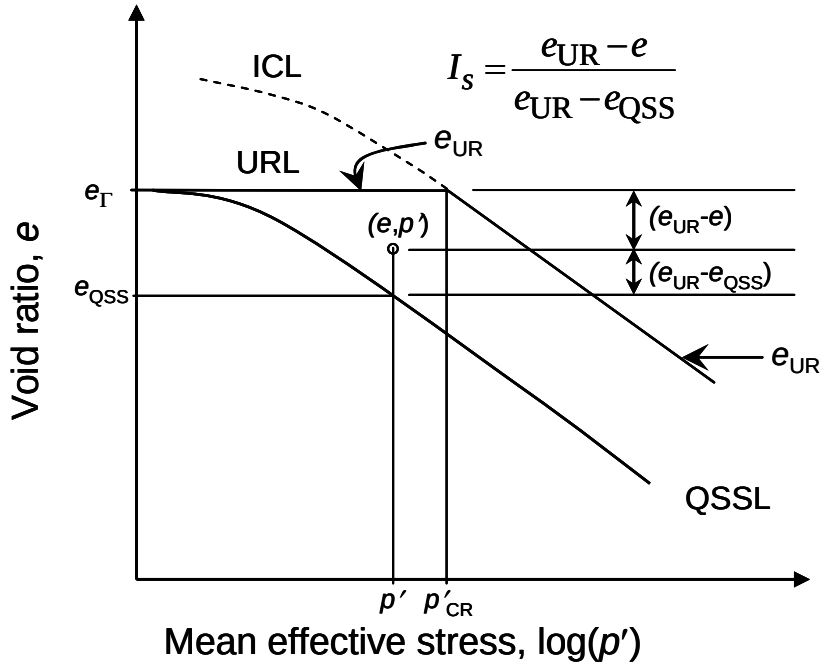

Figure 2. 8 Definition of state index, I_S according to Ishihara (1993)

2.3.3 *Pressure Index*

Along the similar line, Wang et al. (2002) reported that the ratio of current mean effective stress, p' to the mean effective stress at critical state/steady state, p'_{SS} is an appropriate state variable for the constitutive modelling of sand. Thus, they introduced the concept of state pressure index, Ip as

$$I_p = \frac{p'}{p'_{SS}} \qquad \textbf{2. 7}$$

where, p' = current mean effective stress and p'_{SS} = mean effective stress at critical state at current void ratio, e. The definition of the state index is shown in Figure 2. 9.

2.3.4 *Modified State Parameter*

The steady/critical state line, CSL/SSL is not necessarily linear in e-log(p') space. Recent literature shows that SSL/CSL is curved (Bobei and Lo 2005; Li et al. 1999; Verdugo and Ishihara 1996). Thus, possible curvature needs to borne in mind, despite

the word “line” used for SSL/CSL. Bobei and Lo (2005) and Bobei et al. (2009) realized that due to curve shape of SSL, state parameter related to only void ratio or effective stress is not enough to capture the observed behaviour of undrained shear test for sand with fines.

Thus, they proposed modified state parameter, ψ_m. The definition of modified state parameter is given in Figure 2. 10 and it can be expressed as

$$\psi_m = \psi \left| \frac{\Delta p'}{p'} \right| e \qquad \textbf{2. 8}$$

where, ψ_m = modified state parameter, $\Delta p'$=the difference in mean effective stress at current and steady state. By combining “state parameter” (Been and Jefferies 1985) and “state pressure index” (Wang et al. 2002), it can be rewritten as

$$\psi_m = \psi \left| 1 - {}^{1}\!/_{I_p} \right| e \qquad \textbf{2. 8a}$$

Bobei et al. (2009) reported that ψ_m has better prediction capability for sand with fines under CSSM framework.

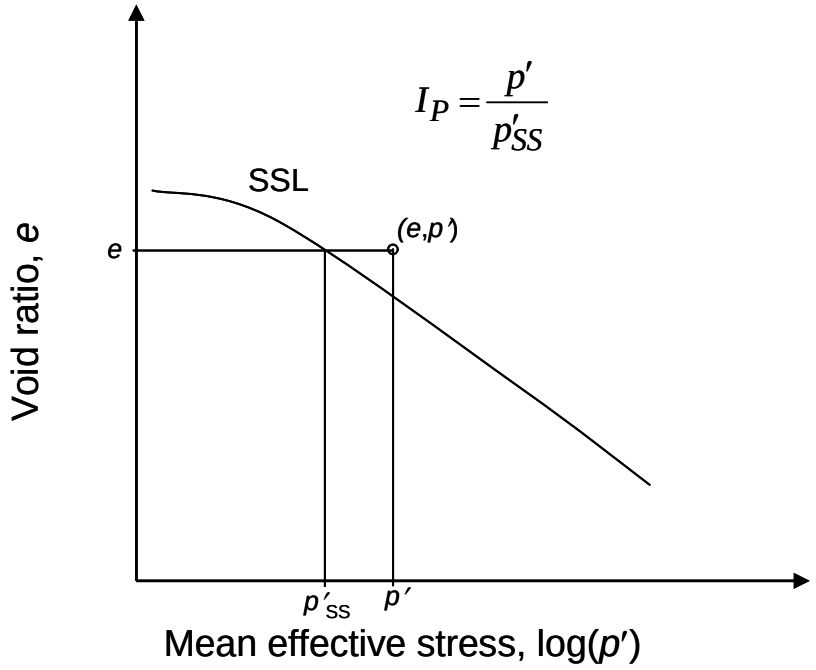

Figure 2. 9 **Definition of state pressure index, *I*p according to Li et al. (1999)**

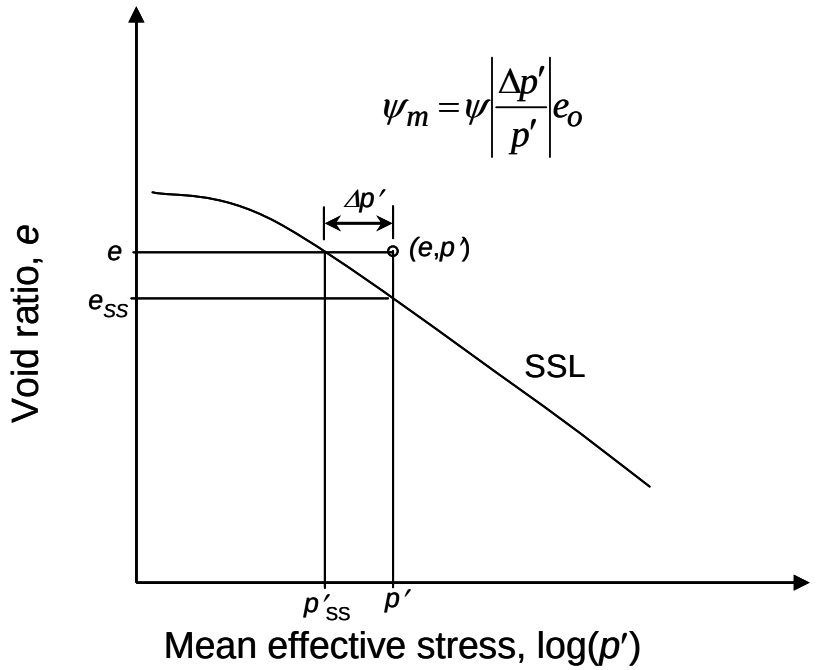

Figure 2. 10 **Definition of modified state parameter, ψ_m according to Bobei and Lo (2005)**

2.4 EFFET OF FINES IN SAND

Early studies on liquefaction were mainly concentrated on clean sand although the occurrence of loose sand with fines (particle diameter ≤ 0.075mm) is not uncommon. Since the 1960's, It has been understood that the presence of fines in some manner affects the resistance to liquefaction. But systematic studies on sand with fines are relatively limited. Careful study on the literature has revealed contradictory out come on the effect of fines. Three different findings have been reported on literature.

- One: liquefaction resistance increased with the increase in fines content (Amini and Qi 2000; Kuerbis et al. 1988; Pitman et al. 1994).

- Two: liquefaction resistance decreases with the increase in fines content (Troncoso 1986).

- Three: liquefaction resistance decreases with increase in fines contents up to a threshold fines content and then liquefaction resistance decreases with increase in fines content beyond the threshold fines content (Altun et al. 2005; Thevanayagam 1998; Xenaki and Athanasopoulos 2003; Yang et al. 2006a; Zlatovic and Ishihara 1995).

Third finding might be first reported by Zlatovic and Ishihara in 1995 on Toyoura sand with non-plastic fines. Relatively recent studies also confirmed the third finding on several other sand with fines (Altun et al. 2005; Thevanayagam and Martin 2002; Xenaki and Athanasopoulos 2003). However, there are also some research efforts have been found to investigate the reasons of contradictory out come about the effects of fines. Those studies revealed that these apparently contradictory outcomes are due

to the inconsistent interpretation/comparison basis (Polito and Martin 2001; Sadek and Saleh 2007; Xenaki and Athanasopoulos 2003). If void ratio is used as a comparison basis, many researchers reported a consistent outcome as third group. However, they also reported, void ratio may not be good parameter for sand with fines. The details of these aspects are discussed in coming subsections.

2.4.1 *Effects of Fines on Undrained Behaviour*

The undrained behaviours of clean sand are already discussed in section 2.2.1. Clean sand behaviour changes form dilative tendency to contractive tendency with increasing in mean effective stress for same void ratio as shown in Figure 2. 2a. However, Yamamura and Lade (1998) reported a reversed trend for sand with fines. They found that Nevada sand with 7% fines liquefied at low mean effective stress (25kPa) and become stable with increasing mean effective stress (200kPa) at same void ratio after consolidation ($e \approx 0.779$). This behaviour appears to be opposite to the clean sand behaviour. Considering clean sand behaviour as “normal behaviour”, they named sand with fines behaviour as “reversed behaviour” as shown in Figure 2. 11a&b. They also found the “reverse behaviour” on Nevada sand at several relative density (Dr = 12%, 22%, 31%, 42%) (Yamamuro and Lade 1997). Bobei and Lo (2005) also reported “normal behaviour” for Sydney sand and “reverse behaviour” for Sydney sand with 10% Majura fines (MII fines).

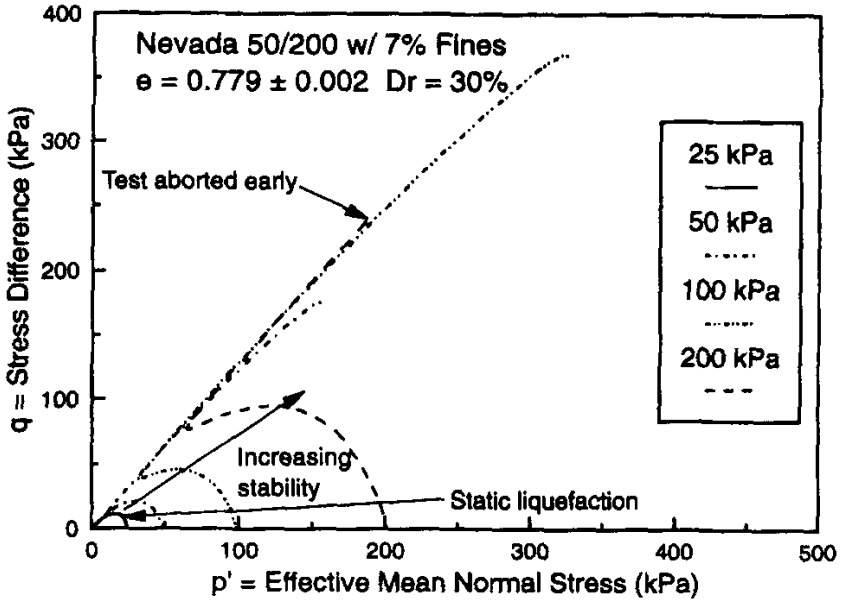

(a)

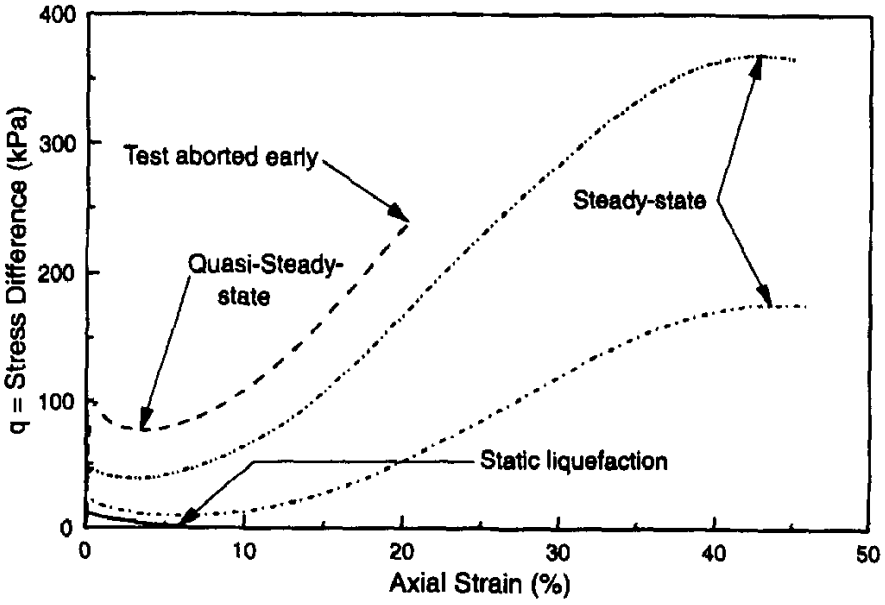

(b)

Figure 2. 11 Reverse behaviour for Nevada 50/200 sand with % fines; (a) q-p' space, (b) q-ε_1 space.

The microstructure of sand-fines mix is responsible for "normal" to "reverse" behaviour. A details microstructure study of sand-fines mix are needed for further understanding of reverse behaviour. Apart form reverse behaviour, fines significantly

affect the location of SSL, QSS and η_{IS} of sand-fines mix with changing fines content. This leads some practical difficulties in applying these concepts in practice. They are discussed in coming sections.

2.4.2 *Effects of Fines on Steady State Line, SSL*

After extensive tests on Toyoura sand with non-plastic fines (milled Toyoura sand), Zlatovic and Ishihara (1995) reported that the SSLs for Toyoura sand with fines move downwards with increase in fines content in e-log(p') space up to a fines content around 30%, but moves upwards for fines content >30% (Figure 2. 12a). Similar behaviour has also been reported for F55, Foundry sand with non-plastic crushed silica fines by Thevanayagam et al. (2002b) as shown in Figure 2. 12b. This lead to the concept of threshold fines content, TFC. Since TFC defines the transition from a "fines-in-sand" to a "sand-in-fines" soil fabric, it can be defined by a reversal of the influence of f_c on the SS data points. Thus, the fines content defining this reversal in the movement of the location of SSL with f_c is TFC. For data sets on the effect of fines content on cyclic resistance, TFC can also be defined by the fines content where the cyclic resistance reverses in direction. The TFC for Toyoura sand is reported around 30% and for F55, Foundry sand is around 40%. Similar finding has been reported in literature by Yang et al. (2006a) for Hokksund sand with Chengbei fines. They reported that the threshold fines for Hokksund sand is around 30%.

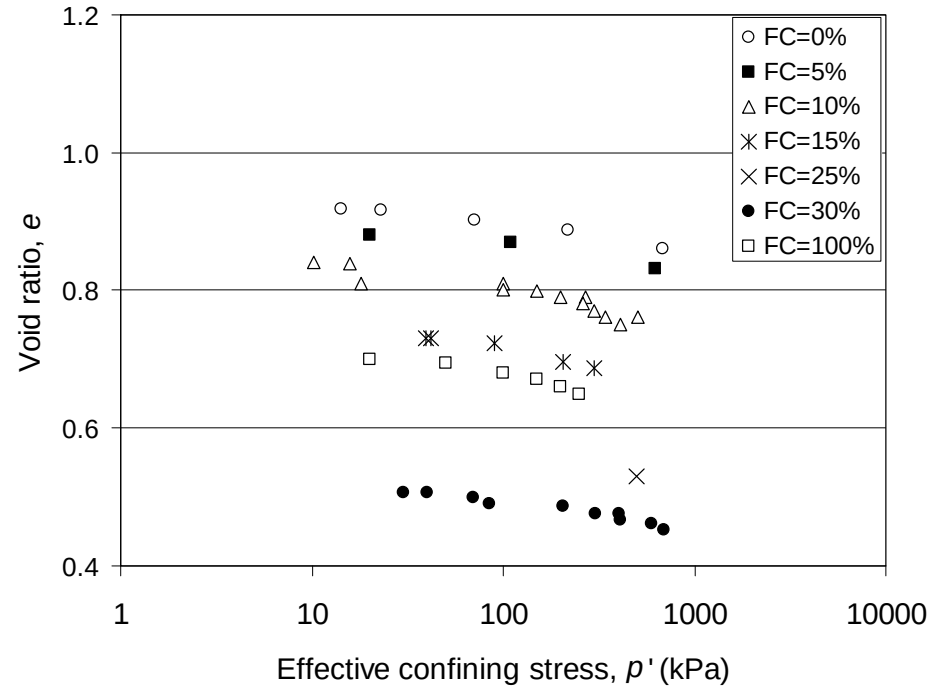

(a)

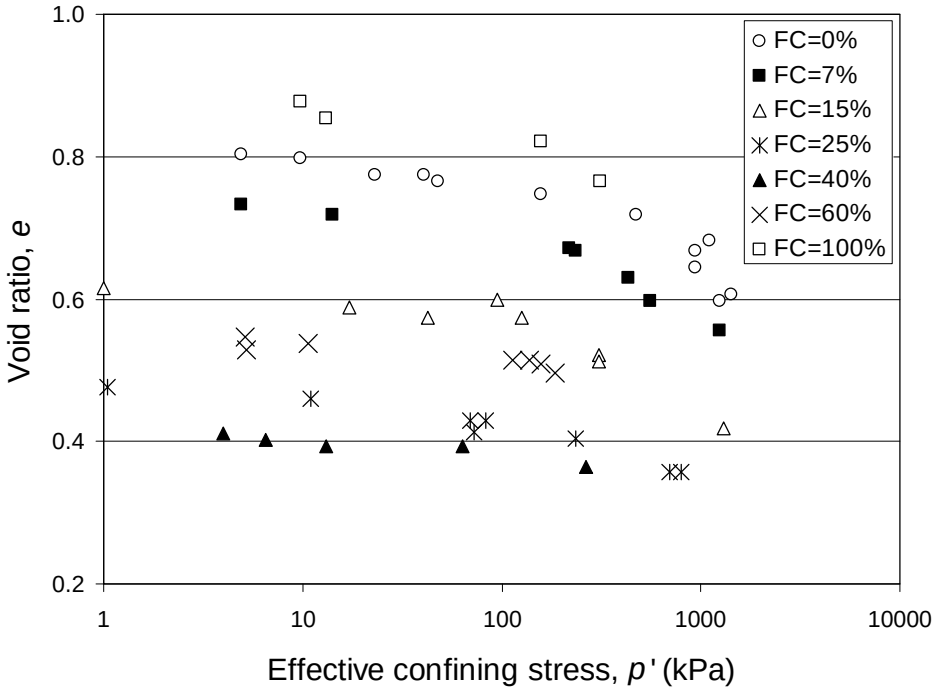

(b)

Figure 2. 12 **SS data points for sand with fines; (a) Toyoura sand with non-plastic fines, modified from Zlatovic and Ishihara (1995), (b) F55, Foundry sand with non-plastic crushed silica, modified from Thevanayagam et al. (2002b)**

2.4.3 *Effects of Fines on Quasi Steady State Line, QSSL*

The location of quasi steady state lines, QSSLs are also affected by the presence of fines in e-log(p') space. Zlatovic and Ishihara (1995) reported that QSSLs moved downwards with fines content up to the threshold fines content, TFC = 30%, and then moved upwards with increase in fines content as shown in Figure 2. 13. The movement of quasi steady state line, QSSLs are also similar as steady state line, SSLs in e-log(p') space.

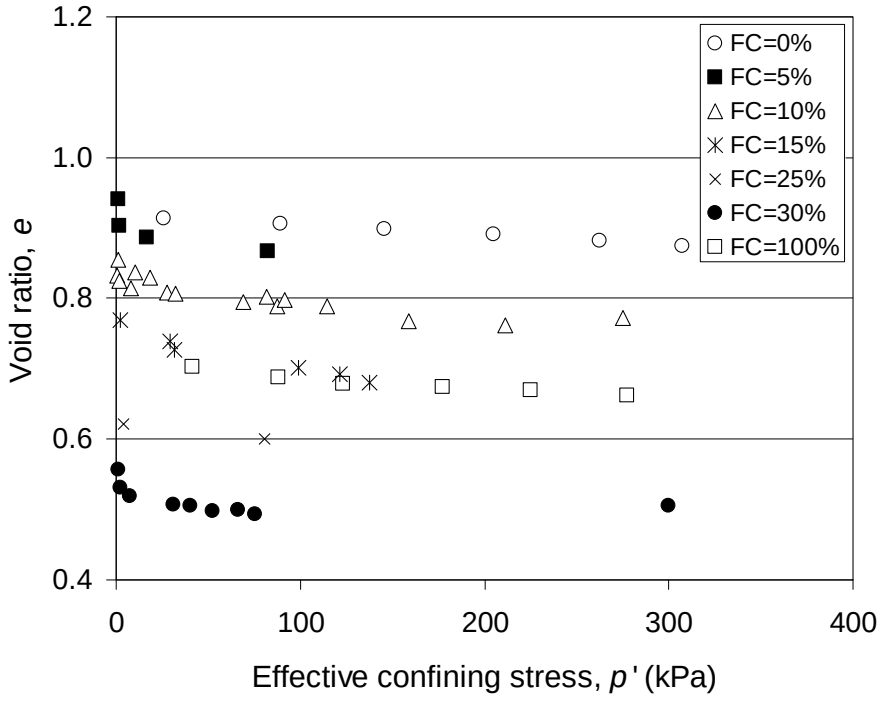

Figure 2. 13 Quasi steady state data points for Toyoura sand with fines, modified from Zlatovic and Ishihara (1995)

2.4.4 *Effect of Fines on Peak Stress Ratio/Instability Stress Ratio*

Chu and Leong (2002) reported that instability stress ratio line is not a unique line, It varies with void ratio at the beginning of shearing. They also reported that instability stress ratio and void ratio at the end of consolidation posses a relation in η_{IS}-e space and it can be presented by a line. This line is called as instability stress ratio lines.

However, the position of instability stress ratio lines in η_{IS}-e space is strongly influence by fines. After numerous tests on Hokksund sand with Chengbei fines, Yang et al. (2006b) reported that the instability stress ratio lines, in η_{IS}-e space (with e in x-axis), moved leftwards with increasing fines content up to 30% and then moved rightwards with further increasing in fines content as shown in Figure 2. 14. The fines content at which the instability stress ratio line reverse its movement with fines content is consistent with the threshold fines content, TFC = 30% as reported by Yang et al (2006a).

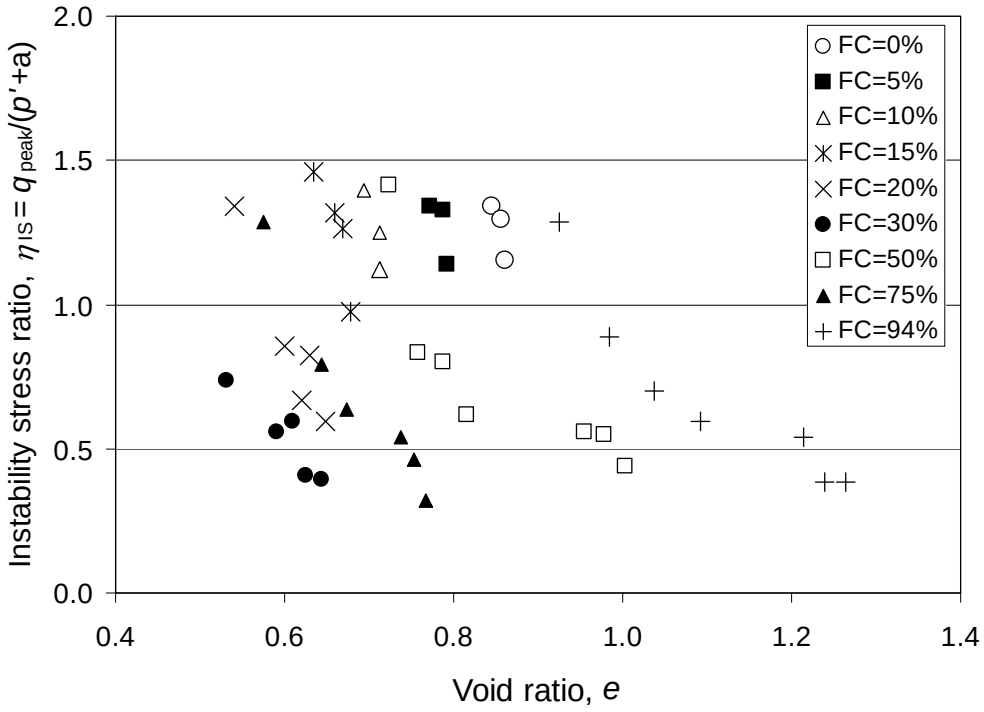

Figure 2. 14 Effect of fines content on instability stress ratio line for Hokksund sand with Chengbei non-plastic fines, modified after Yang et al. (2006b)

2.4.5 *Challenges with the Presences of Fines*

The steady state, SS or critical state, CS line/curve which is essential in interpreting static liquefaction was found to be dependent on fines content. This leads to some practical difficulties in applying the CSSM framework to sand with fines because

each fines content requires its own SS line/curve. One of the possible reasons that lead to the lack of single SS line/curve independent of fines content may be due to the use of void ratio as a state variable. Void ratio is not a good state variable for sand with fines; because some of the fines may simply located in the void space between the sand particles due to their size difference and thus, fines may provide only secondary contribution to the force chain of the solid skeleton. This leads to the concept of "equivalent" void ratio that is consistent with some observed behaviour. Two approaches have been found in literature to get equivalent void ratio from void ratio.

- First, inter-granular void ratio, IVR which considers no contribution of fines in force chain of solid skeleton and thus, the volume of fines is considered as zero in inter-granular void ratio calculation.

- Second, equivalent granular void ratio, EVR which consider partial contribution of fines in force chain of solid skeleton and thus, the volume of fines may not be considered as zero in equivalent granular void ratio calculation.

The detailed development of the concept of inter-granular void ratio and equivalent granular void ratio are discussed in coming sub-sections.

2.4.6 *Inter-granular Void Ratio, e_g*

The concept of an inter-granular void ratio has been investigated by a number of researchers and it is pertinent to note that inter-granular void ratio has also been referred to by different names in the literature: void ratio at granular phase (Mitchell

1976), skeleton void ratio (Kuerbis et al. 1988), granular void ratio (Georgiannou et al. 1990), inter-granular void ratio (Thevanayagam 1998). For consistency, the term "inter-granular void ratio" is used in this thesis.

Mitchell (1976), arguably, may be the first publication that unambiguously pointed out that the clay particles may not play any active role in the force chain of a granular phase structure and introduced the concept of inter-granular void ratio. Considering clay contents are not actively participating on soil structure, Mitchell developed a relation between clay content and void ratio of granular phase i.e. inter-granular void ratio as following:

$$\frac{w}{100}+\frac{C}{100G_{SC}}=\left(1-\frac{C}{100}\right)\frac{e_G}{G_{SG}} \qquad \textbf{2. 9}$$

where w = Water content, C = percent clay by weight, G_{SC} = specific gravity of clay particles, G_{SG} = specific gravity of granular particles and e_G = void ratio of granular phase. He showed that at least one-third of solid needed to be clay to dominate the soil behaviour by clay which is also consistent with the threshold fines, TFC.

This is confirmed by other researchers that fines has an inactive role in terms of soil strength if they are less than a certain amount (Kenney 1977; Troncoso and Verdugo 1985). After experimental study on mineral mixtures composed of a coarse minerals (quartz) and clay minerals (montmorillonite, hydrous mica or kaolinite), Kenney (1977) reported that the mixtures which containing clay minerals and water less than 40% to 50% of the total volume, the residual strength of the mixtures is equal to that of the coarse mineral (quartz) constituents only. That means, if the volume of fines and water is up to 40% to 50% total volume of soil, then fines has an inactive role in

coarse mineral structure and the residual strength of the mixture become equal to the residual strength of coarse material only. Troncoso and Verdugo (1985) also reported similar finding. These experimental results are also in the line of inactive contribution of clay mineral and thus, strengthen the concept of inter-granular void ratio.

However, Kuerbis et al. (1988) may be the first who used inter-granular void ratio as comparison basis for soil strength behaviour. They suggested that fines particle may simply be occupying void in the sand skeleton and therefore, the measured behaviour is controlled by the force chain in sand skeleton. Thus, by neglecting the volume of fines they defined skeleton void ratio, e_{skeleton} and defined by the following expression:

$$e_{skeleton} = \frac{V_T G_S \rho_W - (M_T - M_{silt})}{(M_T - M_{silt})} \qquad \textbf{2. 10}$$

where V_T = total volume of specimen, G_S = specific gravity of sand, ρ_w = density of water, M_T = total mass of specimen and M_{silt} = mass of silt in specimen. The skeleton void ratio, e_{skeleton} is in fact inter-granular void ratio, e^*. They observed almost similar soil strength behaviour at constant skeleton void ratio as shown in Figure 2. 15.

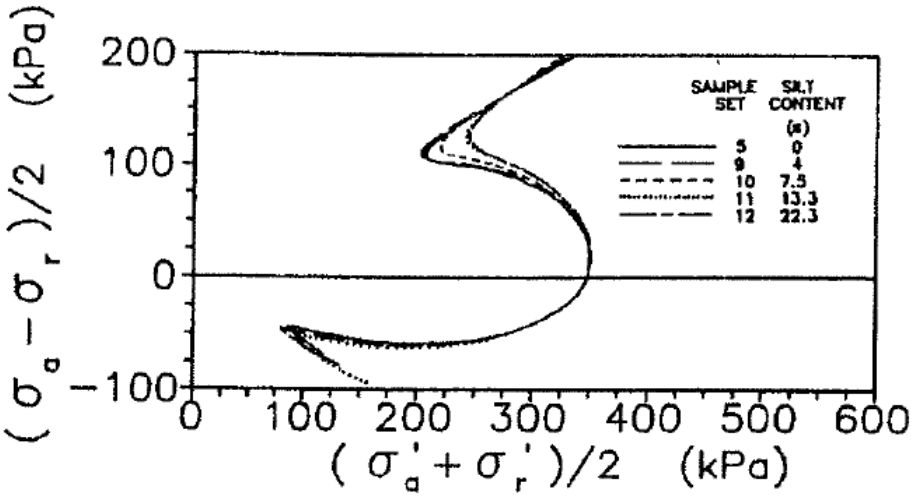

SAMPLE SET	SILT CONTENT (%)	TOTAL e_c	TOTAL Dr_c (%)	SAND SKELETON e_c	SAND SKELETON Dr_c (%)
5	0	0.764	29	0.764	29
9	4	0.728	31	0.802	18
10	7.5	0.669	44	0.805	17
11	13.3	0.547	69	0.784	23
12	22.3	0.446	98	0.863	0

Figure 2. 15 Undrained monotonic triaxial test results for silty 20/200 sand after Kuerbis et al. (1988).

Georgiannou et al. (1990) also calculated inter-granular void ratio by considering the volume of clay equal to zero, and they called it as "granular void ratio, e_{gr}". They expressed granular void ratio as

$$e_{gr} = \frac{\text{Volume of voids} + \text{volume of clay}}{\text{volume of granular phase}} \qquad \textbf{2. 11}$$

They observed effective stress paths in triaxial compression were almost identical for a constant inter-granular void ratio as shown in Figure 2. 16 and undrained brittleness increased with increasing inter-granular void ratio for Ham river sand with Speswhite kaolin. Later, following the work of Georgiannou et al. (1990), Ovando-Shelley and Pérez (1997) found that inter-granular void ratio is also a very significant parameter for Coatzacoalcos River sand with fines.

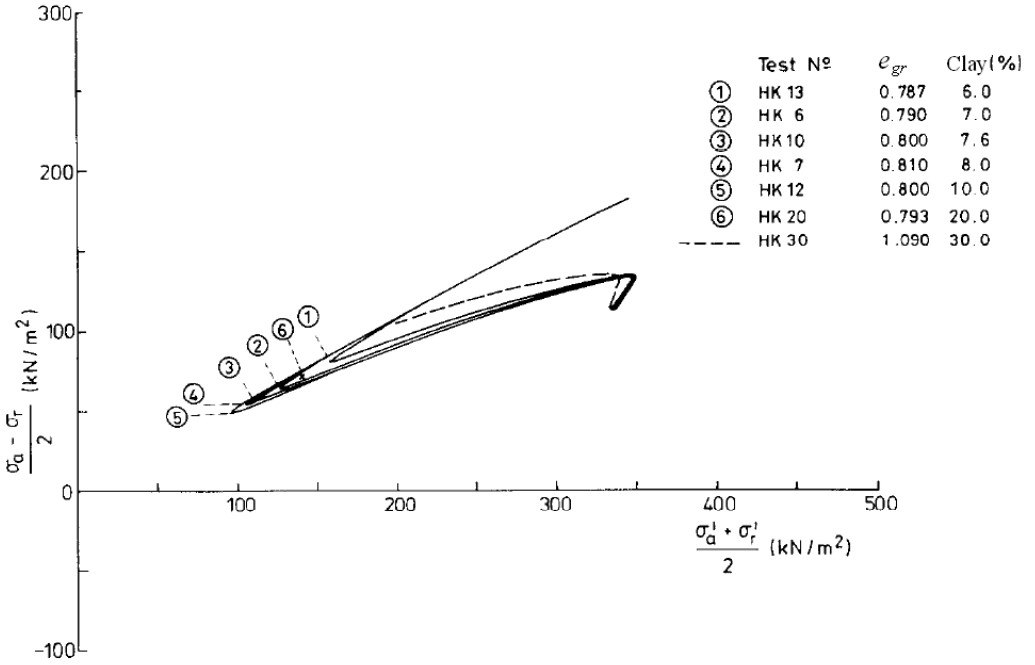

Figure 2. 16 Stress path response at similar inter-granular void ratio for Ham river sand with Speswhite kaolin after Georgiannou et al. (1990)

However, Thevanayagam (1998) simplified the concept of inter-granular void ratio significantly by considering silty sand consists of two sub-components: coarse particles and fines particles as shown in Figure 2. 17. When coarse particle to coarse particle contacts dominate soil behaviours, he defined inter-granular void ratio as

$$e_g = \frac{e + f_c}{1 - f_c} \qquad \textbf{2. 12}$$

And when fines particle to fines particle contacts dominate the soil behaviour, he defined inter-fine void ratio as

$$e_f = \frac{e}{f_c} \qquad \textbf{2. 13}$$

where e_g = inter-granular void ratio, e_f = inter-fine void ratio, e = global void ratio and f_c = fines content (in decimal) with respect to total dry weight of solid. Chu and Leong

(2002) also showed that all definitions of inter-granular void ratio are essentially the same.

The inter-granular and inert-fines void ratio was proposed for “fines in sand” and “sand in fines” matrix. However, there is a transition fines content i.e. TFC where inter-granular and inert-fines void ratio should be same for same global void ratio. It should be noted that the Equation 2. 12 and Equation 2. 13 do not satisfy the transition condition.

However, the applicability of inter-granular void ratio as an alternative void ratio for higher fines content was also investigated by different researchers. Pitman et al. (1994) conducted a systematic study on Ottawa sand C-109 with varying plastic and non-plastic fines content from 0% to 40% to observed effects of fines. Using the same equation as Kuerbis et al. (1988), they found the inter-granular void ratio was increasing with increasing non-plastic fines. But they found that measured soil response showed more dilative tendency instead of contractive tendency as e_g increases with increase in fines content which is contradictory to normal behaviour. Thus, it was realized that the inter-granular void ratio calculated from above formula is not applicable for entire range (0% to 40%) of fines content. They observed from SEM photograph that both fines and sand has grain to grain contact up to 20% fines and soil behave as a composite during undrained loading i.e. fines are active in force structure. More clear observation was reported on Toyoura sand with 0% to 100% non-plastic fines by Zlatovic and Ishihara (1995). They reported that non-plastic fines started to come in between sand grains contact from 5% fines and sand grains contact vanished completely at 30% fines. Thevanayagam (1999; 2000) also reported that SS

data points in e_g-log(p') space come to a narrow trend for small amount of fines; but not for SS data points for higher fines content. Thus, it was realized that inter-granular void ratio is no longer a good state variable as fines started to come in between sand particles at higher fines content.

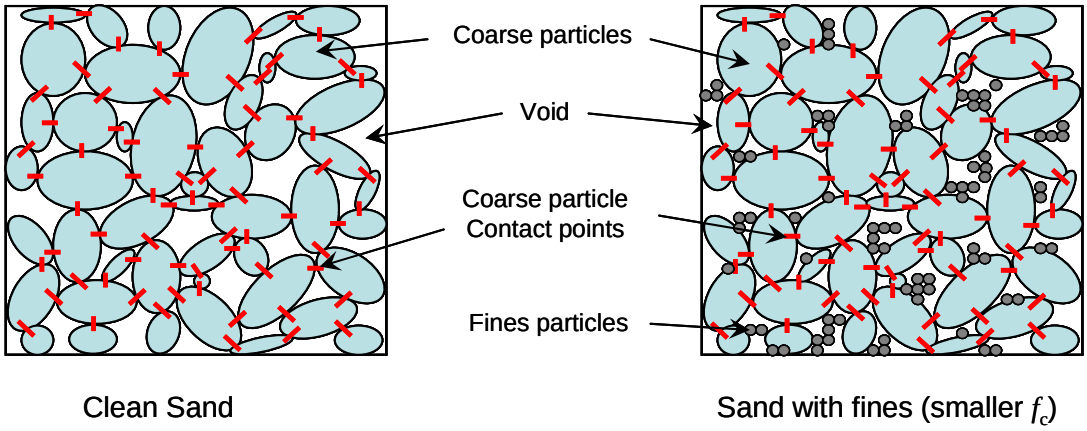

(a)

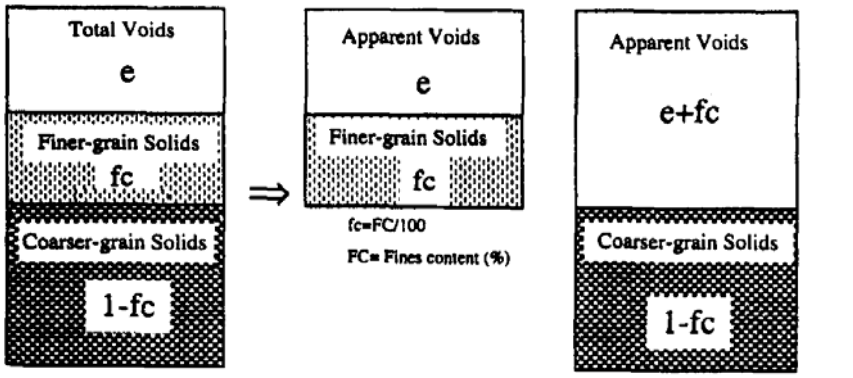

e = global void ratio e_f = inter-fine void ratio e_g = inter-granular void ratio

$$e_f = \frac{e}{fc} \qquad e_g = \frac{e+fc}{1-fc}$$

(b)

Figure 2. 17 Schematic diagrams; (a) particle arrangement for clean sand and sand with small amount of fines, (b) definition of inter-granular and inter fine void ratio after Thevanayagam (1998).

2.4.7 *Equivalent Granular Void Ratio*

The concept of an equivalent granular void ratio has been investigated by a number of researchers and it is pertinent to note that equivalent granular void ratio has also been referred to by different names in the literature: granular void ratio equivalent, equivalent inter-granular contact index void ratio, equivalent inter-granular contact index, corrected intergranular void ratio and equivalent granular void ratio. For simplicity, the last term "equivalent granular void ratio" is used in this thesis.

Thevanayagam (1999; 2000) defined equivalent granular void ratio by introducing a parameter b which represents the fraction of fines that actively take part in the force structure of mixed sand as shown in Figure 2. 18. The equivalent granular void ratio is presented as following

$$e^* = \frac{e + (1-b) f_c}{1-(1-b) f_c} \qquad \textbf{2. 14}$$

where, e^* is equivalent granular void ratio and b is the fraction of particle that are in active contact between sand grain. The b ranges from 0 to 1.

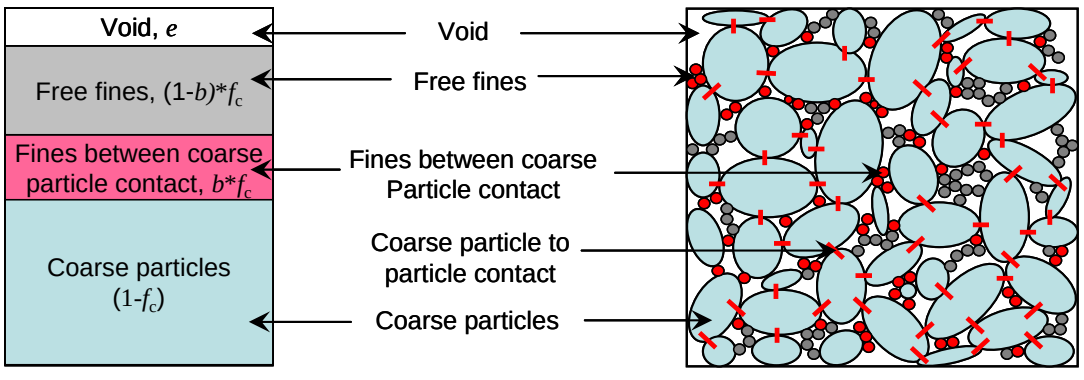

Figure 2. 18 **Schematic diagram of particle arrangement for sand with higher amount of fines.**

This equation further extends the applicability of equivalent granular void ratio as:

- When $b = 0$, the equivalent granular void ratio become the inter-granular void ratio and;
- When $b > 0$, equivalent granular void ratio allows partial contribution of fines in granular force structure.

The concept of equivalent granular void ratio is inherently assumed that the SS data points for sand with fines will come to a single trend even for higher fines content (< TFC) when they are plotted in e^*-log(p') space. For example, Thevanayagam et al. (2002b) found an approximately single relationship of data points (e^*, p') in e^*-log(p') space can be obtained for F55, Foundry sand with up to 25% of non-plastic crushed silica by selecting $b = 0.25$ as shown in Figure 2. 19a. Similar finding are reported by Ni et al. (2004) for Old Alluvium sand from Singapore. Yang et al. (2006c) reported that steady state points both from drained and undrained tests came to a single trend for Hokksund sand with Chengbei fines by selecting $b = 0.25$ as shown in Figure 2. 19b. Thevanayagam et al. (2002a) also reported that the energy required to cause cyclic mobility, E_L (for F55, Foundry sand with different percentage of non-plastic fines) come to a single trend with e^* versus E_L plot, if $b = 0.40$ is used as shown in Figure 2. 20a. Yang et al. (2006b) also got similar finding that at $b = 0.25$, instability stress ratios merged in a single trend for Hokksund sand with 0% to 25% Chengbei fines as shown in Figure 2. 20b.

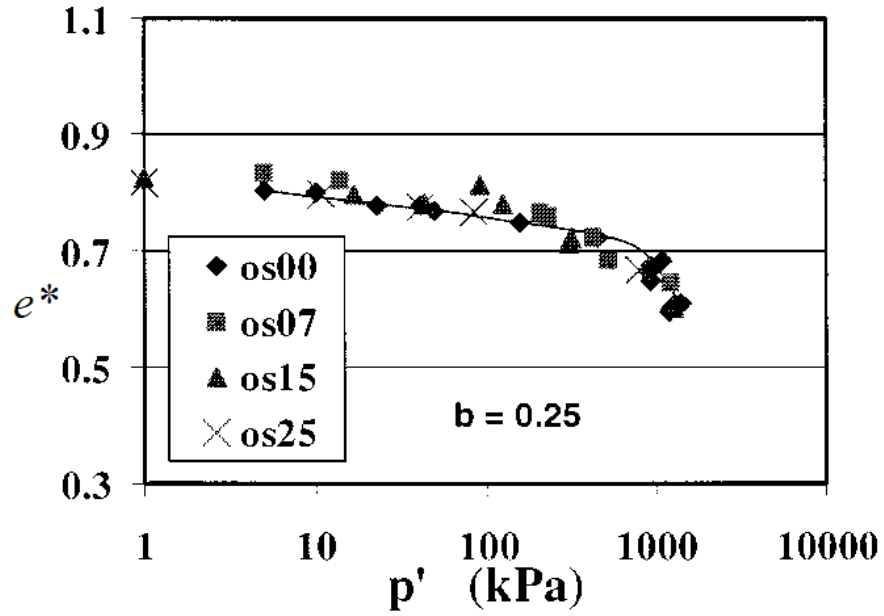

(a)

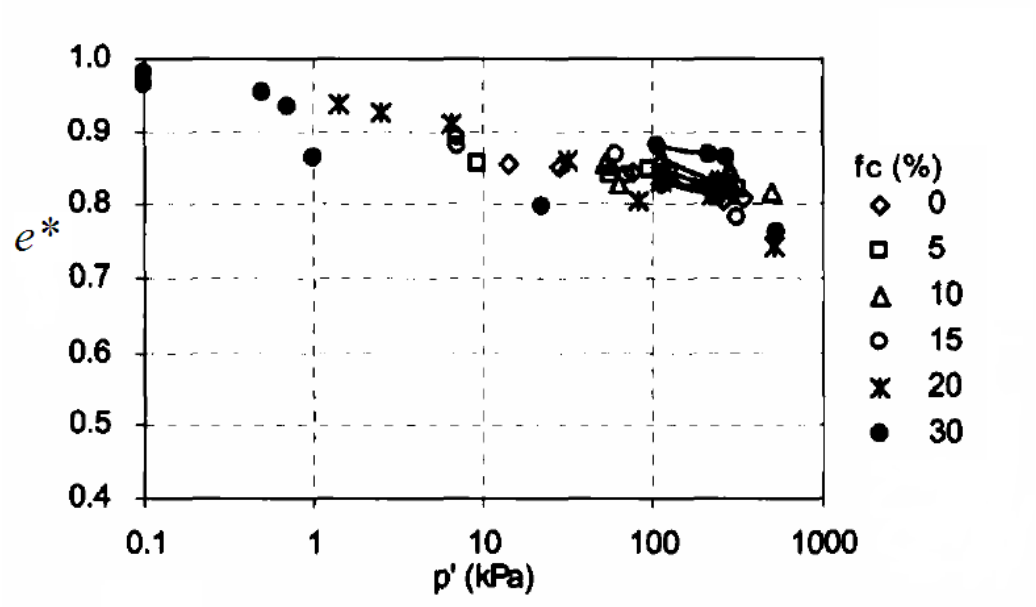

(b)

Figure 2. 19 **Steady state line in *e**-log(*p*′) space; (a) for F55, Foundry sand with non-plastic crushed silica by selecting *b* = 0.25 after Thevanayagam et al. (2002b), (b) for Hokksund sand with Chengbei fines when *b* = 0.25 after Yang et al. (2006c)**

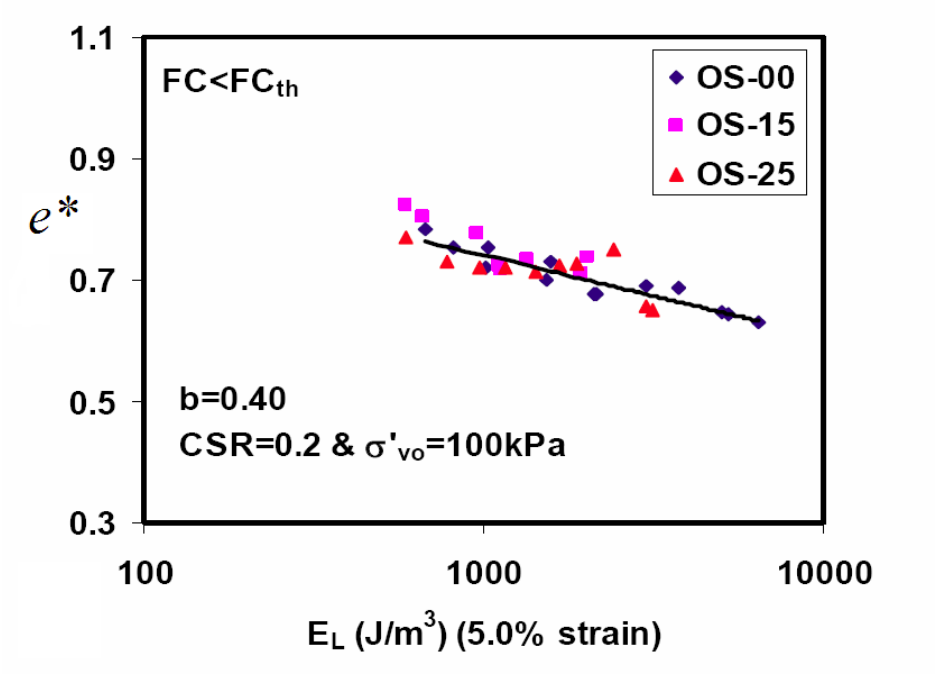

(a)

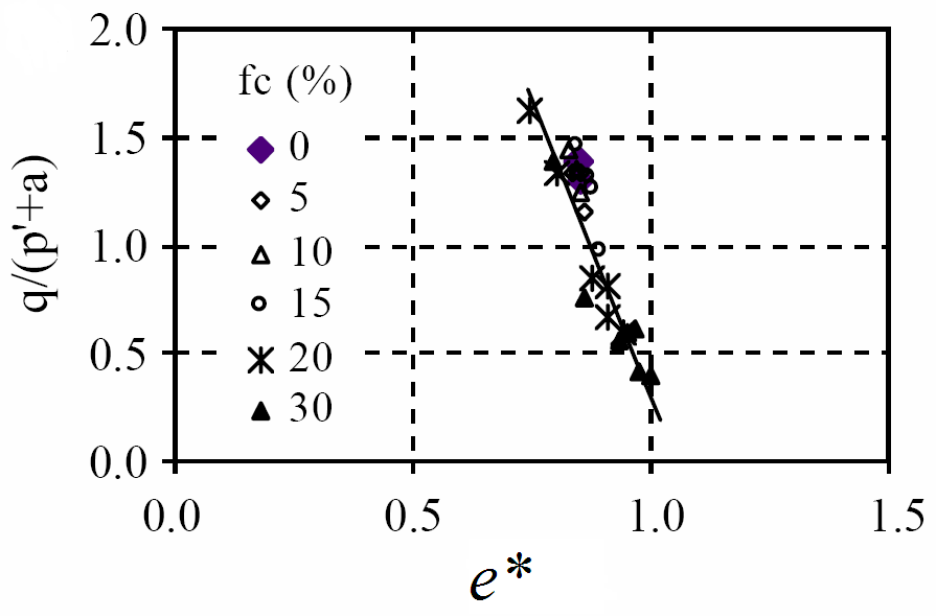

(b)

Figure 2. 20 **(a) Single trend for F55, Foundry sand with 0-25% non-plastic fines in e^*-E_L space at b=0.40, slightly modified after Thevanayagam et al. (2002a), (b) Single trend for Hokksund sand with 0%-20% Chengbei fines at b=0.25, slightly modified after Yang et al. (2006b)**

The parameter *b* reported in literature was selected/back analyzed values so that a single correlation can be achieved irrespective of fines contents among the responses studied. The responses studied may be steady state or cyclic resistance (for cyclic mobility studies), energy for liquefaction, instability stress ratio. However, the most notable point is that there was no prediction formula for *b* though it was very extensively reported. There were only limited studies reported that correlation of the selected *b* with physical parameters of soil (Ni et al. 2004; Thevanayagam 2001). For example, Thevanayagam (2001) suggested that *b* depends on $C_{uc}C_{uf}^2/\chi_T$, provided that $\chi_T > 6$. Where C_{uc} = uniformity coefficient of coarse grain, C_{uf} = uniformity coefficient of fines grain and χ_T = diameter ratio of coarse and fines grain ($D_{50, sand}/d_{50, silt}$), D_{50} = diameter of sand at 50% finer, d_{50} = diameter of fines at 50% finer. However, careful observation revealed the following limitations of the proposed correlation for a selected *b* value:

- It is only a correlation, not a predict formula of *b*.
- The selected *b* is a constant value for entire range of fines and this is not consistent with "fines in sand" model (Thevanayagam 1999). Further the equivalent granular void ratio formula can not merge with inter-granular void ratio formula for a constant *b*.
- The correlation is only applicable when $\chi_T > 6$. It is not applicable for entire range of diameter ratio.

However, Ni et al. (2004) suggested that *b* depends upon sand-fines size ratio, χ ($D_{10,\ sand}/d_{50,\ silt}$). They showed that *b* value increases with smaller χ and the results are shown in Table 2. 1.

Table 2. 1 The variation of *b* with *e and χ after Ni et al. (2004)**

Soil	Reference	*b*	*e**	$\chi=D_{10}/d_{50}$
Old Alluvium	Ni et al. (2004)	0.7, 0.75	0.62–0.75	4.4
Toyoura Sand	Zlatovic and Ishihara (1995)	0.25	0.85–1.15	11
Host sand	Thevanayagam and Mohan (2000)	0	0.69–1.06	15.71

Thus, if we want to use equivalent granular void ratio, *e** to predict behaviour of sand with fines, then we must be able to predict *b* parameter form a formulation which is physically reasonable and mathematically consistent with “fines in sand” model. One of the objectives of this thesis is to develop such a predictive formulation for *b* parameter.

2.5 MODELLING OF UNDRAINED BEHAVIOUR

To model sand with fines behaviour, Thevanayagam and Mohan (2000) modified an existing model in terms inter-granular void ratio, e_g and inter-granular state parameter, ψ_g in order to predict $\frac{d\varepsilon_v^p}{d\varepsilon_q^p}$. Thus, they choose to modify the equation of following flow rule:

$$\frac{d\varepsilon_v^p}{d\varepsilon_q^p} = \frac{\left(M^2 - \eta^2\right)}{2\eta} \qquad \textbf{2. 15}$$

where, $M = \frac{6\sin\phi}{3-\sin\phi}$ and $\eta = \frac{q}{p'}$. ϕ is the mobilized angle of shearing resistance at SS. The above flow rule was rewritten in terms of critical state parameters and state parameter (Thevanayagam and Mohan 2000) as following:

$$\frac{d\varepsilon_v^p}{d\varepsilon_q^p} = \frac{M\left(2 - R_c^{\left(1(\psi/\psi_{(0)})\right)}\right)}{2\left(R_c^{\left(1(\psi/\psi_{(0)})\right)} - 1\right)^{1/2}} \qquad \textbf{2. 16}$$

where, ψ is state parameter at any stage during triaxial compression, $\psi_{(0)}$ is the initial state parameter at isotropic consolidated state, and R_c = 2 according to work assumption (Roscoe and Burland 1968). Thevanayagam and Mohan (2000) proposed to use inter-granular state parameter instead of state parameter in Equation 2. 16 as following:

$$\frac{d\varepsilon_v^p}{d\varepsilon_q^p} = \frac{M\left(2 - R_c^{\left(1(\psi_g/\psi_{g(0)})\right)}\right)}{2\left(R_c^{\left(1(\psi_g/\psi_{g(0)})\right)} - 1\right)^{1/2}} = f\left(\psi_g, \psi_{g(0)}, M, R\right) \qquad \textbf{2. 16a}$$

Where, $\psi_g = e_g - e_{gSS}$ is inter-granular state parameter and $\psi_{g(0)}$ is the initial inter-granular state parameter at the end of isotropic consolidation. Thus, the inter-granular

state parameter, ψ_g defines the direction of the plastic volumetric strain increment, $d\varepsilon_v^p$ in the proposed model. In an undrained test elastic volumetric strain increment, $d\varepsilon_v^e$ is simply the reverse of $d\varepsilon_v^p$. Also note that $d\varepsilon_v^e$ defines the direction of mean effective stress increment, dp'. Thus, the Equation 2. 16a only can tell us whether the effective stress path (irrespective of fines content) will move "left" or "right". The modified flow rule has also some other limitations and they are out lined below:

- The original Cam-clay flow rule was chosen to modify, but it has some inherent limitations in predicting sand behaviour. In particular, it assumed a unique isotropic consolidation line, ICL which is not true for sand with fines.
- The investigation was based on inter-granular void ratio which in only applicable for sand with small amount of fines content.
- The model can only predict "left" or "right" ward movement of effective stress path.

2.6 EFFECT OF FINES TYPE

The conceptual framework for equivalent granular steady state line, EG-SSL is established depending on the study mostly for one host sand and one type of fines (mostly non-plastic fines). The effect of fines mineralogy (plasticity) or shape factor (sphericity, roundness) on sand-fines mix was not investigated from the point of equivalent granular void ratio concept. Thus the effect of fines type on *b* parameter is unknown. Even, a good understanding on the effect of fines types on undrained

response of sand-fines mix yet to be reached as there is very few literature available. Literature review on these aspects are given below.

2.6.1 *Effects of Plasticity of Fines*

The effect of fines plasticity on the over all undrained responses of sand-fines mix are discussed in this section (Chang 1990; Ghahremani and Ghalandarzadeh 2006; Koester 1994). The influence of fines plasticity on liquefaction resistance and pore water pressure generation were analyzed by Koester (1994) using the data from Chang (1990) on reconstitute samples of sand fines mixture. The sand-fines mixture was prepared from a uniform fine sand and pre-selected proportion of a uniform low plasticity silt (Vicksburg) and plastic clay (Vicksburg, Mississippi "buckshot"). The plasticity of fines was controlled by adding plastic clay. It was reported that for same void ratio, the plasticity of fines has less influence on cyclic strength than the presence of fines. A systematic study has been done by Ghahremani and coworkers (Ghahremani and Ghalandarzadeh 2006; Ghahremani et al. 2006). The sand used in the testing program was with Firouzkooh sand which is a medium fine sand with sub-angular particles. The fines were kaolin and bentonite. The plasticity of fines was varied by adjusting relative amount of these two fines. Ghahremani and Ghalandarzadeh (2006) reported, cyclic resistance increased with increase in plasticity of fines (from PI=20 to PI=40) in sand with 16% fines mix at same void ratio after consolidation. Ghahremani et al. (2006) also reported if plasticity of fines increases in sand with 30% fines mix, the steady state strength of sand-fines mix increases at nearly same void ratio after consolidation as shown in Figure 2. 21. Thus, most of the literature reported that cyclic resistance or steady state strength increases with increasing in fines plasticity for fines (Ghahremani and Ghalandarzadeh 2006;

Ghahremani et al. 2006). However, theses studies only discussed about fines plasticity; did not discussed about fines shape and angularity.

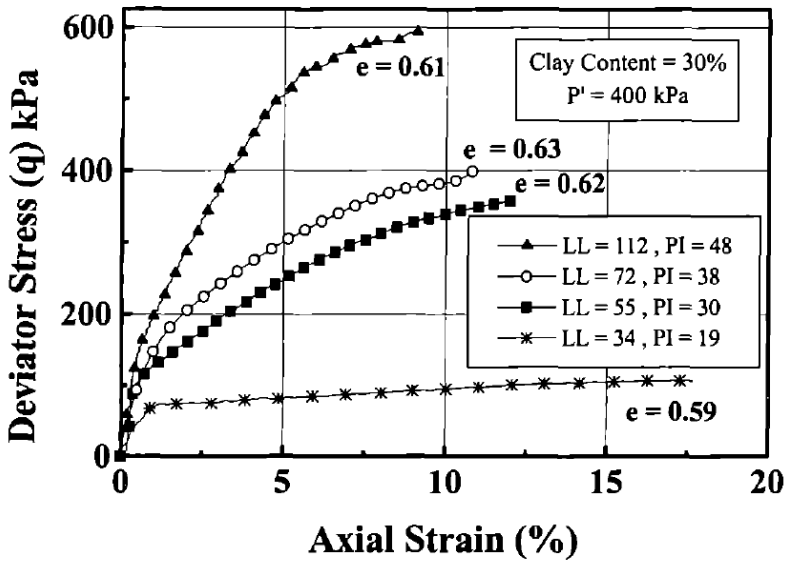

Figure 2. 21: Cyclic liquefaction resistance increases with increasing in plasticity of fines after Ghahremani et al. (2006).

2.6.2 *Effects of Sphericity and Angularit of Fines*

To the best of author knowledge, there is no literature available on the influence of fines angularity on a sand fines mix. However, "fines in sand" model indicates that angularity of fines should have a significant influence on relative arrangement and interaction of fines in a sand-fines mix. Thus, a study on the effect of angularity of fines on a sand-fines mix is done in this thesis.

Angularity is an opposite measure of roundness. Thus, angularity can be defined as

$$Angularity = 1 - \frac{\sum_{i}^{N} r_i / N}{r_{\max}} \qquad \textbf{2. 17}$$

where, r_i is the average radius of curvature of surface feature, r_{max} is the radius of largest inscribe circle as shown in Figure 2. 22. The more details can be found in

literature (Cho et al. 2006; Rouse´ et al. 2008; Wadell 1932). However, only a visual comparison is used as a measure of angularity in the present study.

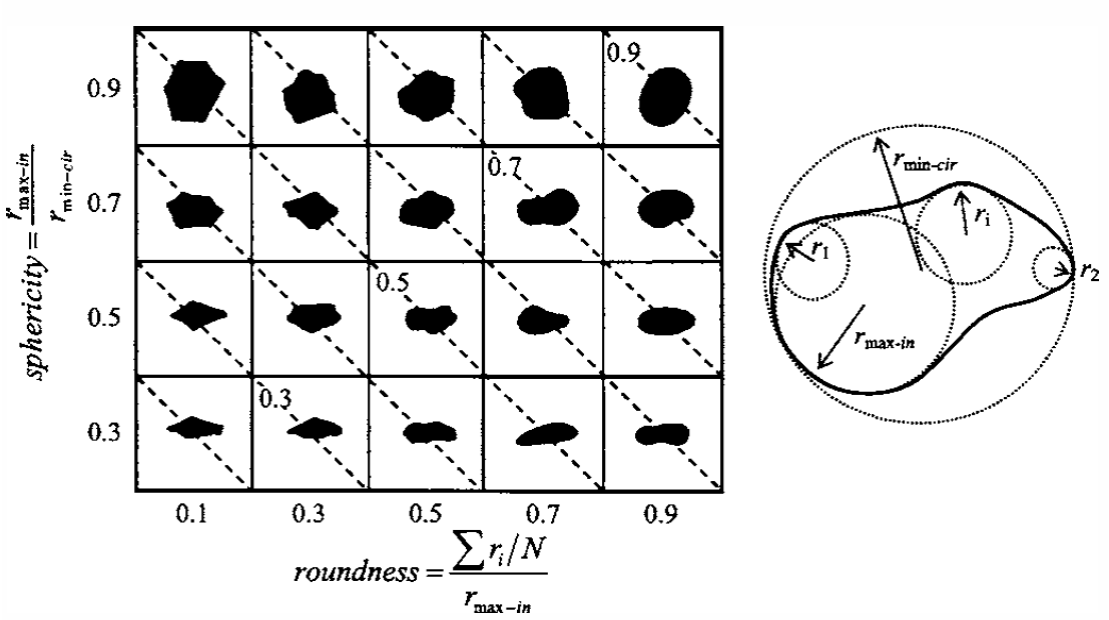

Figure 2. 22: Particle shape determination, sphericity and roundness chart after Cho et al. (2006).

2.7 EFFECT OF CYCLIC LOADING ON SAND WITH FINES

The investigation of cyclic loading behaviour on saturated sand was initiated in 1960's. At the beginning, stress controlled cyclic triaxial tests were done on undrained saturated sample (Seed and Lee 1966). It was found that, in loose sand, zero effective stress (100% pore water pressure) and "state of softening" (i.e. sudden large deformation) was occurred at about 5% double amplitude (DA) axial strain. This condition was defined as 'cyclic liquefaction', later referred to as 'cyclic mobility'. The 5% DA axial strain was found as a bench mark (Ishihara 1993). Thus, it was customary to define cyclic resistance (CR), some time to refer as cyclic strength as the magnitude of cyclic stress ratio required to produce 5% double amplitude axial strain

in 20 cycles of constant amplitude stress application. Cyclic resistance was the measure of cyclic liquefaction.

As triaxial test results are published on isotropic and anisotropic consolidated samples, different outcomes on cyclic resistance were observed. Some publication showed that larger cyclic resistance was observed for higher static shear stress after consolidation (Lee and Seed 1967; Seed 1968; Seed and Lee 1969), on the other hand opposite tendency was presented by Yoshimi and Oh-oka (1975). In 1980s Vaid and coworkers showed that the contradictory out come was due to the difference in relative density, initial static loading and even for the definition of cyclic resistance (Vaid and Chern 1983; Vaid and Chern 1985; Vaid and Finn 1978). They reported cyclic strength can either be increase or decrease due to the presence of initial static loading.

At the same time Mohamad and Dobry (1986) introduced the concept of critical stress ratio line (similar to η_{IS}, detail was explained in section 2.2.2) from monotonic triaxial test to explain the cyclic loading behaviour. According to Mohamad and Dobry (1986) when a cyclic loading path reaches instability stress ratio, instability in cyclic loading begins and cyclic path has no other choice but follow the monotonic loading boundary. However, the conceptual framework was not widely verified with experimental evidence. Further investigation is needed as also the understanding on instability changed over time. However, cyclic loading behaviour can be investigated both in stress “reversal” and “non-reversal” path. For simpler case, the link between monotonic and cyclic loading under non-reversal path are investigated in Chapter 8. The related literatures on non-reversal path are also discussed on that Chapter.

2.8 SUMARRY AND RESEARCH OBJECTIVE

The objective of the thesis is to develop an understanding on the role/influence of fines on undrained behaviour under static and cyclic loading. The main summary and objective of the thesis are given below:

1. There was not prediction formula for the *b* parameter (represents the active fraction of fines in sand force structure) which is used in equivalent granular void ratio formula, *e**.

   The objective is to develop a prediction formula for *b* which mathematically consistent and reasonable with *e**.

2. The concept of inter-granular void ratio, e_g and inter-granular state parameter, ψ_g was introduced and a flow rule was modified which only can predict "left" or "right" movement of effective stress path for sand with fines (applicable for small fines content).

   The objective is develop the concept of equivalent granular void ratio, *e** and equivalent granular state parameter, ψ^*. Then, a state dependent constitutive model is to modified in terms of *e** and ψ^* so that ESP and q-ε_q responses can be predicted irrespective of fines contents (≤ TFC) from a single set of model parameter.

3. There is a lack of detail study on the effect of fines plasticity and angularity on the prediction formula of *b* and equivalent granular void ratio, *e**.

The objective is to evaluate the effect of fines angularity and plasticity on the prediction formula of b and equivalent granular void ratio, e^*.

4. The experimental evidence to support the link between monotonic and cyclic loading is limited, particularly on the limited flow behaviour.

   The objective is to verify the link between monotonic and cyclic loading behaviour, particularly on the limited flow behaviour and to present exclusive experimental evidence on their relation.

CHAPTER 3

Experimental Methodology

3.1 INTRODUCTION

This chapter discuses in details the development of laboratory testing system to study the manner in which fines content affect the liquefaction susceptibility of sand-fines mix. Due to the complexity at micro level on grain to grain contact between sand and fines, the experimentations were designed to study both macro level behaviour and micro fabric of sand-fines mix. The macro experimentation was based on triaxial testing system, both monotonic and cyclic. The micro experimentation focused on microscopic investigation of size, shape, relative distribution and mineralogy of sand-fines mix in order to facilitate better interpretation of triaxial test results. It includes two different experimental techniques due to the size difference of sand and fines: light microscopy for sand and scanning electron microscopy (SEM) for fines.

It should be noted that the knowledge on the experimental mythology is not only a prerequisite for the experiment techniques used in this study, but also it is required for proper and consistent interpretation of data from the literature. In Chapter 3, a large data base is developed for theoretical development of equivalent granular void ratio and *b* parameter. Those data collected from literature and interpreted based on the knowledge of current experimental mythology.

3.2 TRIAXIAL TESTING SYSTEM

In research purpose the general requirements of a triaxial testing system are:

1. The stress and strain distributions inside the sample are sufficiently uniform so that the sample response represents "element" behaviour and
2. Accuracies of the measured quantities are adequate to satisfy research requirements.

Meeting the above requirements in a conventional triaxial testing machine is a challenge. However, the deficiencies of a conventional triaxial testing machine and the ongoing developments are well reported in literature (Bobei 2004; Chu 1991; Lo 1985; Lo et al. 1989). To meet the research requirements of this project and overcoming the critics, a number of additional improvements were also introduced.

The triaxial testing system employed for this study is schematically shown in Figure 3. 1. A perspex cylinder with top and bottom plate was used as the cell, so that a cylindrical sample (100mm in diameter and 100mm in height) and transducers as discussed in section 3.2.4 can be placed inside the cell. The cell was filled with de-aired, de-ionized water. Confining stress on specimen was applied by water pressure. A large capacity Digital Pressure Volume Controller (DPVC) was used to apply/control cell pressure. The top and bottom platens of the specimen were connected to a second DPVC to control pore water pressure/volume inside the sample.

A force actuator controlled by GDS digital controller was used to apply load form the bottom of the specimen. Therefore, the bottom platen was the moving platen and "free" movement was facilitated by a linear roller bearing. The top platen was restrained against movement by a shaft supported by an X-beam. A submersible load cell located just

above the top platen, i.e. between the top platen and the shaft, was used to record the axial force. A swinging arrangement for the X-beam allowed easy access during preparation and dismounting. A photo of the overall view of the triaxial loading system is also shown in Figure 3. 2.

An in-house developed control software was used to have full control on stress/force application with fully automatic data logging facilities. It allowed a smooth switching from displacement control to load control which was very important for some special cyclic loading tests with incremental shear stress.

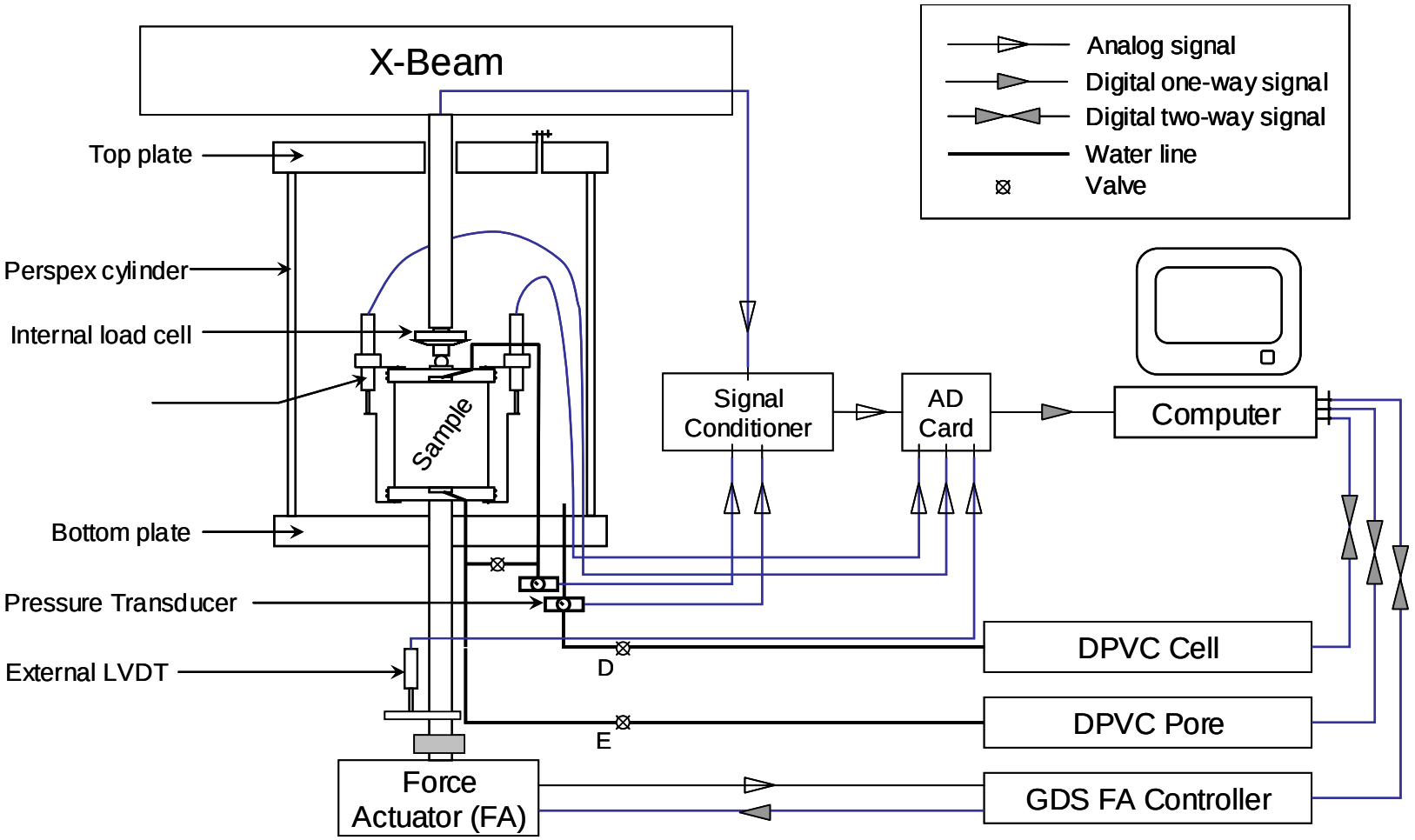

Figure 3. 1 Schematic diagram of the triaxial testing system

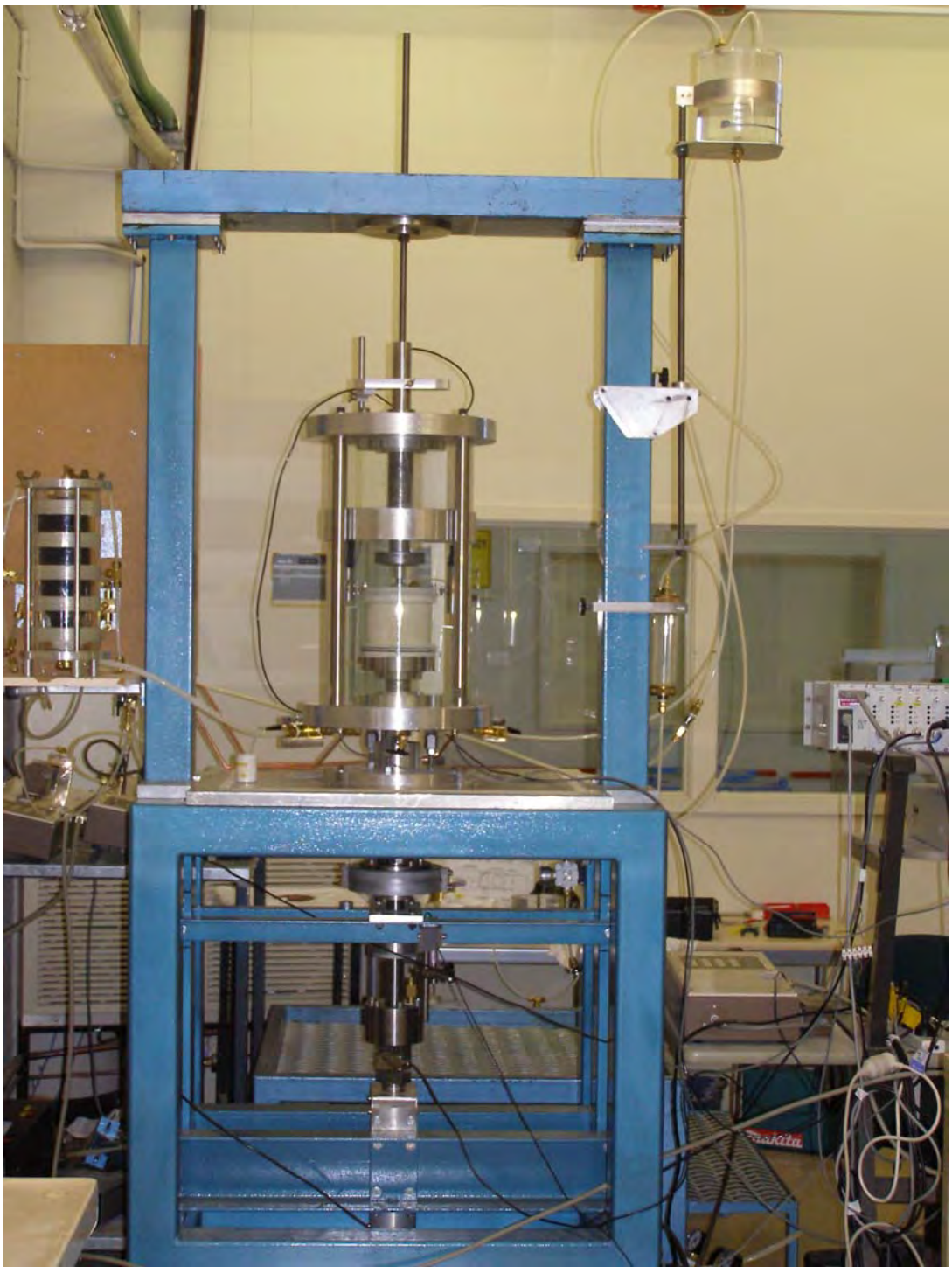

Figure 3. 2 Overall view of triaxial loading system

3.2.1. *Axial Force*

A maximum capacity of 25kN force actuator was used to apply axial force on the specimen. The applied load on the sample was recorded by two individual load cells. One was internal submergible load cell positioned above the top platen of the specimen inside the perspex cylinder so that the recorded data is unaffected by any inevitable frictional forces. However, to increase the accuracy of the measured axial load, five different capacity internal load cells (5kN, 10kN, 16kN, 20kN, 25kN) were used depending on the expected maximum force to be encountered during a test. All load cells are manufactured by GDS with an accuracy of ±0.1% of total capacity. The other load cell was an external load cell integral with the force actuator. Though the data from external load cell was affected by shaft friction, the reason for such arrangement was to have an alternate and independent data logging if in any case internal load cell fails during testing. Furthermore, the shaft friction is expected to be small because of the use of linear roller bearing. However, the need to use the external load cell data in the calculation of deviator stress did not arise during the experimental testing.

However, the stability and calibration of the internal load cell was an important issue for reliability of the data. Therefore, the internal load cells were calibrated at least in every three month against a Shimadzu UDH-100 compression machine and the stability was checked by loading the load cell to its 25% and 75% of capacity and monitoring the reading over a period of 24hours.

3.2.2. *Cell Pressure*

The cell pressure was applied by water pressure using de-aired water by a GDS Digital Pressure Volume Controller (DPVC). A DPVC is a microprocessor controlled linear actuator for precise regulation and measurement of liquid pressure and liquid volume

change. It can be directly connected to a computer for computer control via a HPIB interface.

The principle of DPVC in soil testing is illustrated in Figure 3. 3 and detail description is given in ADVDPC Handbook (2000). The DPVC consists of a pressure cylinder which is filled with de-aired water. De-aired water is pressurized by a piston moving inside the cylinder and the applied pressure is displayed in Liquid Crystal Display (LCD). The piston is activated by a ball screw turned in a captive ball nut by a stepping motor and gearbox that move rectilinearly on a ball slide. The pressure inside the cylinder is detected by means of an integral pressure transducer. Control algorithms are built into the programmable memory to cause the motor to seek to a target pressure or step to a target volume change. The latter is achieved by counting the steps of the stepping motor.

The DPVC used for cell pressure had a maximum operational loading capacity of 2000kPa and a volume change capacity is 1000 cc. Though the resolution of DPVC was 1 kPa for pressure and 1 cu mm for volume change, the accuracy is ≤ 0.1% of maximum capacity of load and volume change.

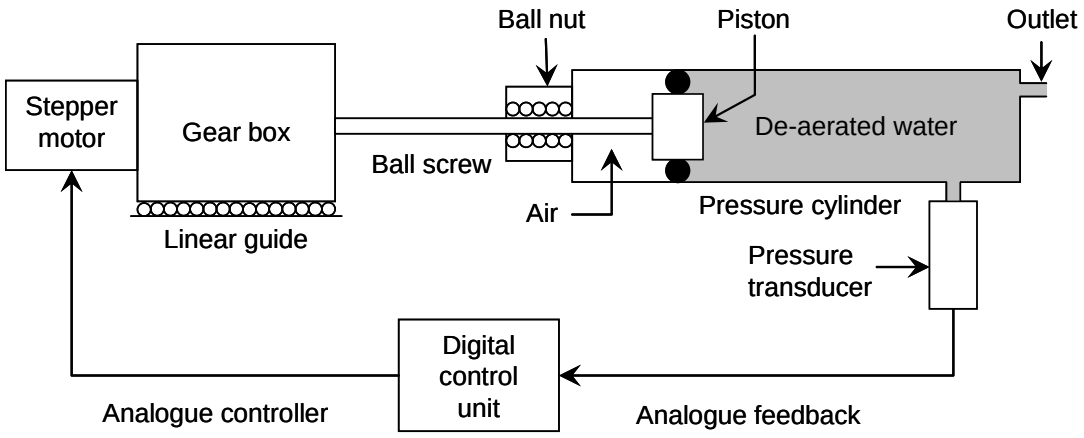

Figure 3. 3 Schematic diagram of Digital Pressure Volume Controller (DPVC)

Another pressure transducer was connected to the cell to cross check that data from DPVC and also to have alternate data source if in any case data logging form DPVC was interrupted. Maximum capacity of the pressure transducer was 2000kPa. However, the data from pressure transducer was only used to cross check the data from DPVC, there was no situation arise to use them for data analysis in the entire study.

3.2.3. *Pore Water Pressure and Volume Change*

The pore water pressure and the volume change of the soil specimen was monitored and controlled by another small capacity DPVC connected to both top and bottom drainage lines. The role of this DPVC was also depending on the testing conditions. Thus, in drained test the DPVC was used to measure the volume change and controlled (kept constant) the pore water pressure. In undrained test, it controlled (kept constant) the volume change and measured the pore water pressure. It can switch from one mode to another via computer control and therefore enable the shearing condition can switch smoothly from a drained condition to undrained condition during testing.

A pressure transducer was connected to the top platen of the specimen to have an alternative data source to cross check data from DPVC and to check pore water pressure uniformity (equilibrium) inside the sample. It was make sure that all tests were running under uniform pore water pressure i.e. pore water pressure equilibrium.

3.2.4. *Axial deformation*

The axial deformation of the sample was monitored by two digital gauges and three LVDTs (Linear Variable Differential Transformer). The digital gauges were used to monitor sample deformation from just after sample preparation to the end of vacuum flushing. The LVDTs were used to monitor deformation from back pressure saturation to the end of shearing.

After sample preparation, two digital dial gauges were placed in diametrically opposite location on the top platen of the specimen so that any disturbance during dismounting the split mould can be monitored. They were also used to keep track of axial deformation during vacuum flushing.

The axial deformation of the specimen after vacuum flushing was measured by three LVDTs. Two submergible internal LVDTs were also placed in diametrically opposite location on the top platen of the specimen so that any deformation of the specimen can be monitor directly. The internal LVDTs had an accuracy of 0.005 mm and were used to monitor deformation at early stage of shearing. An external LVDT was placed on the lower moving shaft outside the perspex cylinder. The accuracy of the external LVDT was 0.05mm and used to monitor deformation at larger strain stage.

The algorithm for calculating deformation is:

IF total displacement is small THEN
δz = displacement increment = (δz_1 + δz_2)/2
where δz_1 and δz_2 are displacement changes calculated from signal changes of internal LVDTs
ELSE
$\delta z = \delta z_e$ where δz_e is calculated from external LVDT
ENDIF

Axial deformation = z = z + δz
Current height H = H - z
Strain increment = $\delta\varepsilon_1 = \delta z/H$
Axial strain = $\varepsilon_1 = \varepsilon_1 + d\varepsilon_1$

Incremental calculation algorithm enable a smooth switch from internal to external LVDT.

However, stable and reliable data from internal LVDT was an important issue of this study. The calibrations of LVDTs were carried out against a Shimadzu Micrometer. Noise and stability of LVDT was checked by monitoring disturbance and irregularity of the data taken from a fixed LVDT over a period of usual test time (5 days). The checking operation was done whenever it was necessary or at lest once in three month.

3.3 MATERIALS TESTED

Sand-fines mixtures were formed by mixing coarse material (>75μm) with a controlled amount of fines (<75μm). The coarse material is Sydney sand. Four types of fines were used for the experimental study. The four types of fines are: MI, MII, SI and SII. The notation "II" denotes that the fines was synthesized from two types of materials. The details description of sand and fines are given below:

3.3.1. *Sydney Sand*

Sydney sand was the major testing material for the study and it was collected in sufficient quantity from the same source so that quality of the sand remains consistent throughout the study. The properties of the sand are summarize in Table 3.1 and the grain size distribution curve of Sydney sand in Figure 3. 4.

Table 3. 1 Physical properties of Sydney sand

Specific Gravity, G_{silt}	2.63
Particle size, D_{50} (mm)	0.27
Particle size, D_{10} (mm)	0.22
Uniformity Coefficient, U_c	1.26
Maximum void ratio, e_{max}	0. 855
Minimum void ratio, e_{min}	0. 565

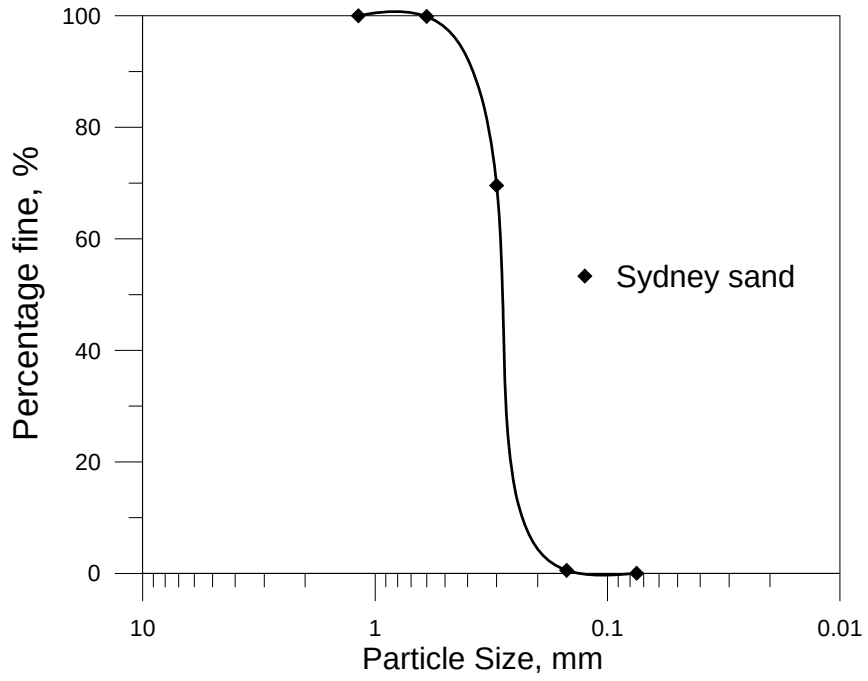

Figure 3. 4 Grain size distribution curve for Sydney sand

3.3.2. *MI fines*

MI was obtained by sieving and collecting the particle smaller that 0.075mm of naturally occurring river deposit called Majura. It was referred to as Majura silt (Bobei 2004). It is a low plasticity fines with a median particles size of 0.025mm. The shapes of the particles are round and smooth. The physical properties of MI is given in Table 3. 2 and grain size distribution curve is given in Figure 3. 5.

Table 3. 2 Index properties of MI fines

Specific Gravity, G_{silt}	2.49
Liquid Limit, LL (%)	41
Plastic Limit, PL (%)	23
Plasticity Index, PI (%)	18
Particle size, d_{50}	0.025

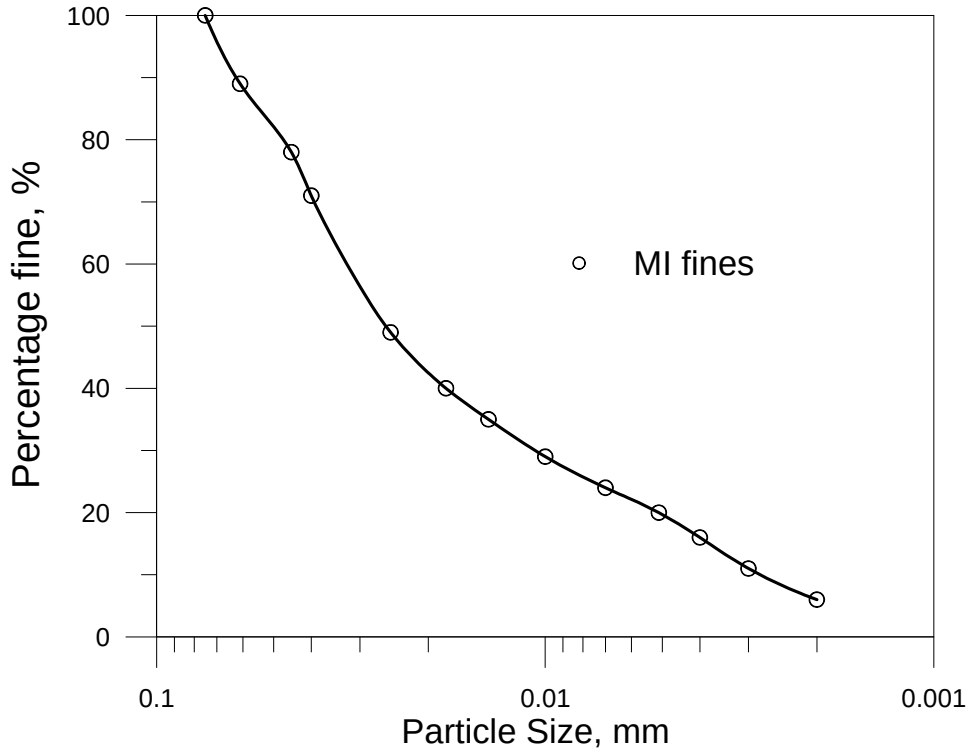

Figure 3. 5 Grain size distribution curve of MI fines (Majura silt)

3.3.3. *MII fines*

MII was designed to introduce extra amount of plasticity into fines. It was obtained by mixing 2/3 of MI with 1/3 of commercial kaolin (by weight). The median size of fines is 0.0055mm. The physical properties of MII are given in Table 3. 3 and grain size distribution curve is given in Figure 3. 6.

Table 3. 3 Index properties of MII fines

Specific Gravity, G_{silt}	2.46
Liquid Limit, LL (%)	54
Plastic Limit, PL (%)	27
Plasticity Index, PI (%)	27
Particle size, d_{50} (mm)	0.0055

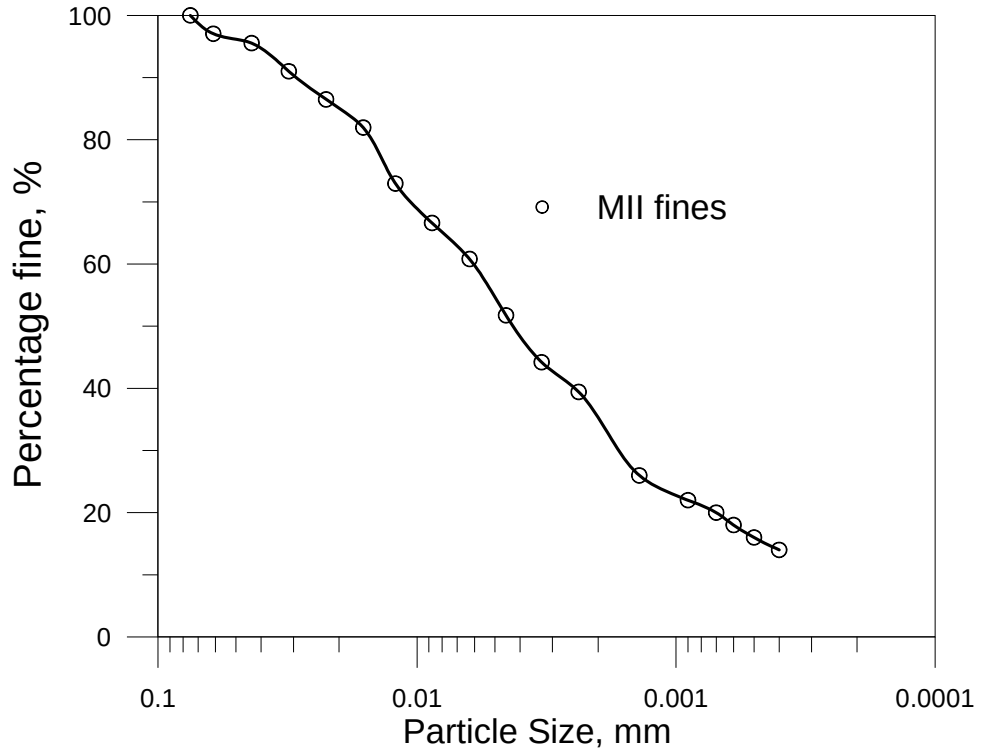

Figure 3. 6 Grain size distribution curve of MII fines

3.3.4. *SI fines*

SI fines was obtained by milling of Sydney sand. It is highly angular non-plastic fines. It designed to observed effect of fines angularity in liquefaction phenomenon. The median particle size is about 0.02mm. It has a specific gravity of 2.63. The grain size distribution curve is given in Figure 3. 7.

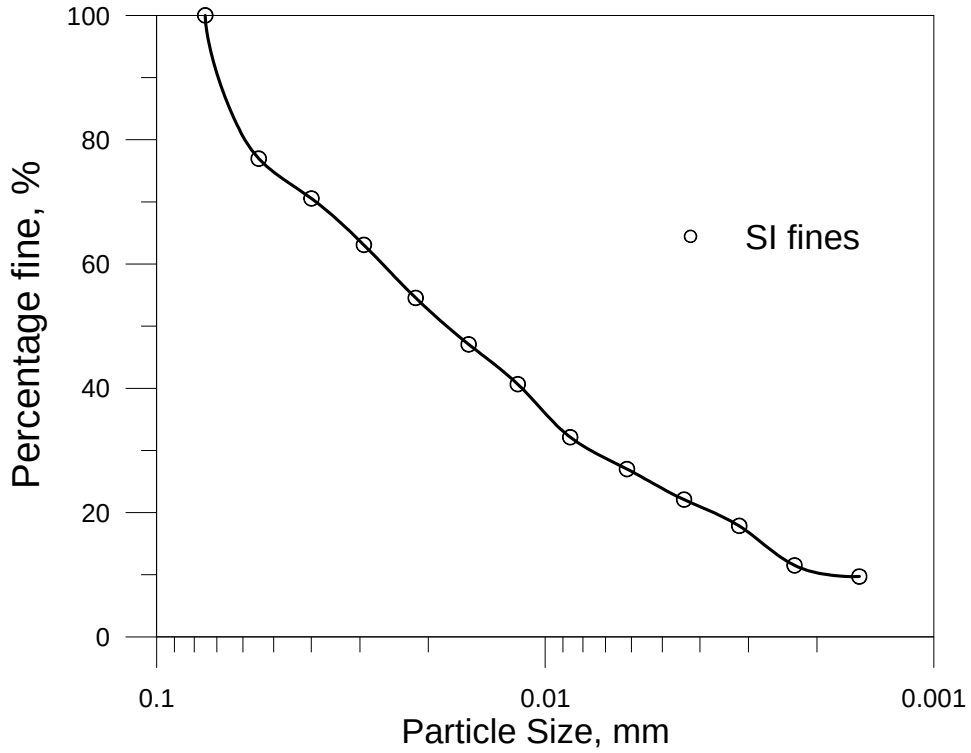

Figure 3. 7 Grain size distribution curve of SI fines (Crushed Sydney sand)

3.3.5. *SII fines*

SII fines was designed to observe the effect of increase in plasticity of highly angular fines on liquefaction susceptibility. It was obtained by mixing 2/3 of SI fines with 1/3 of commercial kaolin (by weight). Thus, it has plasticity index of 16. The median size of fines is 0.0025mm. The physical properties of SII fines is given in Table 3. 4 and grain size distribution curve is given in Figure 3. 8.

Table 3. 4 Index properties of SII fines

Specific Gravity, G_{silt}	2.56
Liquid Limit, LL (%)	36
Plastic Limit, PL (%)	20
Plasticity Index, PI (%)	16
Particle size, d_{50}	0.0025

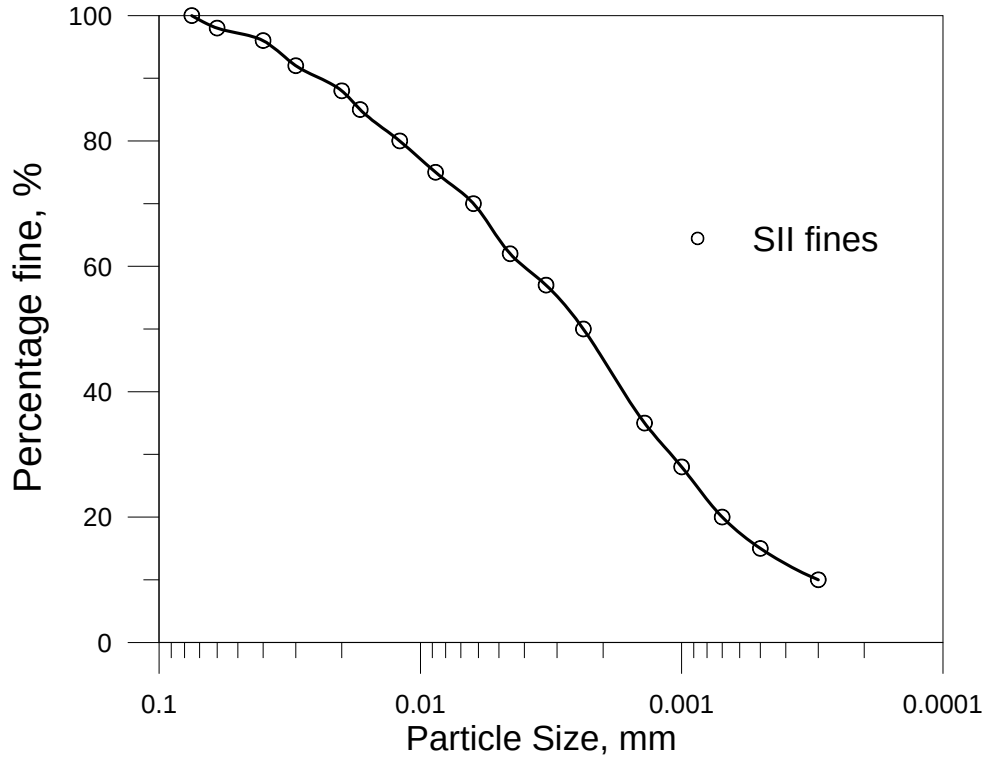

Figure 3. 8 Grain size distribution curve of SII fines

3.4 HOMOGENEITY OF SPECIMEN

Sample homogeneity is an important issue for the study of steady state behaviour of soil. The techniques used for this study were closely based on the procedures and recommendations by Lo et al.(1989), Chu (1991), Bobei (2004). In order to avoid premature development of non-homogeneous deformation of the sample, some special technique was employed such as enlarge platen, free ends, liquid rubber together with moist temping sample preparation method. The details descriptions of these techniques are given in subsequent sub-sections.

3.4.1 *Enlarge Platen with Free Ends*

The frictional force at the contact between the end platen and the soil specimen is one of the reasons of premature development of non-homogeneous deformation during shearing.

Therefore, Rowe and Barden (1964), Lo (1985) proposed to use enlarge platen with free ends to reduce frictional force and to delay the onset non-homogeneous deformation significantly. The free end preparation technique developed by Lo (1985) was used in this study and a brief description of this technique is given below.

Initially, a dice for latex membrane (at platens) was prepared by cutting a transparency sheet with a diameter slightly bigger than the sample diameter so that every time the latex cut from this dice would prepare slightly larger end membrane than sample diameter. It was done to ensure that soil particle would not come in contact with platen at the periphery of the sample. One side of the membrane was lubricated with a thin film of high vacuum grease and placed on the enlarge platen. Enlarge platen was used to allow lateral expansion of soil during shearing. Air trapped between the membrane and platens, if any, were removed carefully. Then the platens with free end were preloaded to a maximum stress likely to encounter during testing to obtain a uniform grease film. Note that the uniformity of this grease film is needed to ensure uniform contact (axial stiffness) between the sample and the platen. It is important to note that non-uniformity in contact stiffness can also lead to non-uniformity in sample deformation even if the contact between the sample and platen is perfectly friction free. The thickness of the membrane was (0.30mm) so as to prevent larger sand grain from penetrating the membrane into the grease film and eventually come in contact with the platen

3.4.2 *Specimen Preparation*

It was very difficult to mix fines with fines thoroughly at natural moisture content because fines forms lumps even at a little moisture content. The fines were first dried in oven at 105°c for 24 hours. The materials were then cool down to room temperature in a tightly sealed dessicator. For fines that were consisted of 2

components, the resultant fines were first prepared in a dried form by mixing predetermined amount of the components. Finally sand with fines were obtained by mixing the sand and fines in a dry state. Then, predetermined amount of water was added to control the moisture content. The moist materials were then cured for several hours before sample preparation.

Several methods for preparing reconstitute sample in laboratory have been reported in literatures. The choice of the sample preparation method depends on the objective of the study and achievability of testing requirements. The variation in achievable ranges of density based upon the sample preparation method greatly affects the potential of soil behavior. It is reported in literature that different undrained stress-strain responses can be found from different sample preparation methods, even at the same density (Ishihara 1993; Vaid et al. 1999b). Therefore, the most appropriate to compare soil behaviour based on the same sample preparation method (Yamamuro and Covert 2001). Considering the achievable range of void ratio required for the study of liquefaction susceptibility of sand-fines mix, moist tamping method was used.

However, moist tamping method was strongly criticized for non-uniform distribution of void ratio along the height of the specimen (Vaid 1994; Vaid et al. 1999b). Vaid et al. (1999b) reported that local relative density difference can be by as much as ±10% from the average value of the entire specimen. On the other hand, different opinion was also presented by Ladd (1978). He mentioned two significant advantages of moist tamping method over water pluviation method which are very important concerns of the present study:

- Firstly, there is no particle segregation during sample preparation which is an important concern for sand with fines mix.

- Secondly, it is easier to achieve a prescribed dry unit weight, particularly for very loose sample.

Therefore, a modified moist tamping method adopted to achieve sample uniformity. The modification aimed at reducing the short comings of moist tamping method but mainyain its advantages. The details description of a specimen preparation by modified moist tamping method is given below:

Specimen was prepared in 10 layers to increase the homogeneity of sand with fines and to reduce the effect of working on the upper surface of each layer to overcome the discrepancy as mentioned by Vaid et al. (1999b). The membrane and a split mould was first installed on the platen as shown in Figure 3. 9. A predetermined amount of sample was placed in each layer by a spoon from predetermined height in small quantities and the surface of each layer was then leveled. Then, the layer was worked to the target thickness by a plastic strip that had a tamping area of 8.5 by 20 mm. As shown in Figure 3. 9 this plastic strip was attached to a horizontal strip so that the working depth can be controlled.

After preparing the sample as described as above, the top platen was carefully seated over the level surface of the top layer. Then, the membrane was stretched around the top platen and secured on it by two O' rings. At this stage, a small amount of vacuum was applied and CO_2 percolated before dismounting the split mould. The details are discussed in next section.

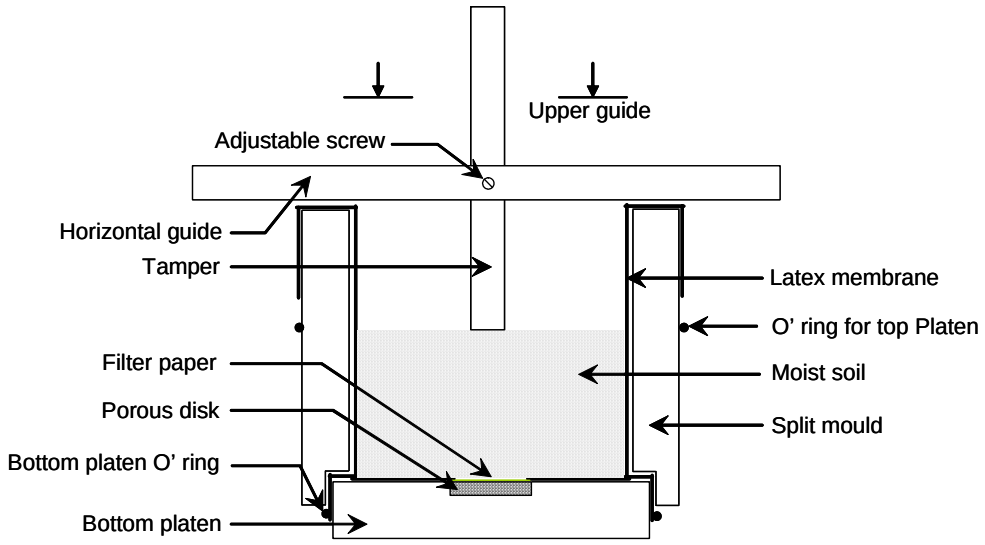

Figure 3. 9: Cross section of sample preparation mould

3.5 SATURATION

Saturation of the specimen was done by three stages: carbon dioxide percolation, vacuum flushing and back-pressure. The details description of these two stages is given below:

3.5.1 *Carbon Dioxide Percolation*

First, a vacuum pressure of ≤ 10kPa was applied from the top platen and carbon dioxide, CO_2 percolated through the bottom platen for about 20 minutes. The flow of CO_2 was monitored in a bubble chamber to make sure that the amount of CO_2 percolated through the specimen was approximately twice the volume of specimen. This can be done by counting the number of bubbles. The objective of CO_2 percolation was to replace air by CO_2 from the specimen as the latter easily dissolves in water under pressure. Then, vacuum pressure increased to 20kPa and at the same time split mould was removed from the specimen. Extreme care was taken during removal of split mould as any disturbance can cause substantial problem at later stage, specially the alignment of the top platen which connect the sample and the load cell during triaxial tests.

3.5.2 *Vacuum Flushing*

At this stage specimen was under a vacuum pressure of 20kpa applied from top platen e.g. valve "C" was open as shown in Figure 3. 10. To percolate fresh de-aired water from the bottom platen valve "A" was opened. Water from the tank flowed through the bottom platen of the specimen and replaced air bubble inside the specimen and came out from the top platen. Air bubble movement was monitored at bubble chamber. The head of water tank was kept small so that it didn't have any effect on fines movement and excessive settlement of specimen during flushing. Before sample preparation, filter papers were placed over the porous disks. At the end of each test filter papers were examined to track fines movement. Any significant change in colour and smoothness of filter paper was an indication of fines movement. The details of this technique can be found in Bobei (2004). It was found that a 0.5 meter constant water head was suitable. All tests presented in this thesis were almost free from fines movement. Water flushing was done for several hours (usually over night) until water flowing through the specimen was continuous and free from air bubble.

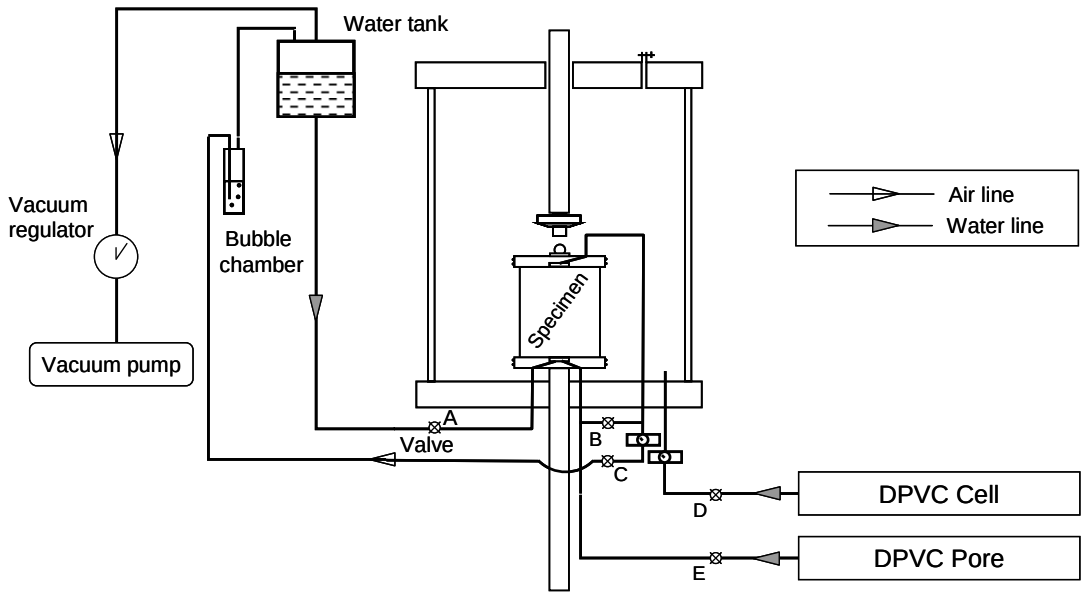

Figure 3. 10: Details diagram of water flushing through the sample

3.5.3 *Back Pressure Saturation*

At first, the cell was assembled carefully so that disturbance in the sample was minimum. Then the cell was filled with de-ionized and de-aired water. The cell pressure was gradually increased to +20kPa while the vacuum pressure was reduced to 0kPa. The valve "D" and "E" were kept open and the valves "A", "B", "C" were kept close to control cell and pore water pressure by DPVC as shown in Figure 3. 10. By using DPVC pore pressure was increasing with increasing cell pressure such that specimen was at 20kPa constant effective stress until the B-value of the specimen was exceeded 0.98 to ensure a high degree of saturation.

3.6 VOID RATIO MEASUREMENT

Correct void ratio measurement is a very important issue for steady state behaviour under critical state soil mechanics, CSSM as void ratio is one of the parameters that define the state of soil. Thus, error involved in void ratio measurement need to be assessed. The void ratio of the specimen was calculated by the following non-dimensional equation.

$$e = \frac{\gamma_w}{\gamma_d} \times G_S - 1 = \frac{\rho_w G_s V_s}{M_d} - 1 \qquad \textbf{3. 1}$$

where γ_w = unit weight of water and γ_d = the dry unit weight of soil, G_S = specific gravity of solid, Vs = volume of solid and M_d = dry mass of solid. Therefore, the uncertainties associated with the dry mass and volume of the solid contributes to the errors in void ratio.

3.6.1 *Mass of the Specimen*

A predetermined amount of moist soil was used to prepare the sample. Since the dry mass was determined indirectly from the moist soil, the error in M_d had two sources of errors;

error of balance and error due to moisture content loss during specimen preparation. The error assessment in dry mass calculation is discussed in subsequent section.

3.6.2 *Volume of the Specimen*

The volume of the specimen was calculated with the measurement of height and the perimeter of the sample. Note that measurement of sample perimeter leads to smaller error in void ratio than that of diameter. Thus, a good track of sample perimeter and height had to record, from sample preparation to the saturation in order to keep track of void ratio change prior to volume measurement by GDS-pore took over.

After sample preparation, two electrical dial gauges with high resolution were place diametrically at the top platen of the specimen to monitor vertical settlement of the specimen during dismounting the split mould. A linear tape was used to measure the perimeter of the sample at three different places. The average perimeter was taken to work out diameter of the sample. The void ratio calculated at this stage is called void ratio after vacuum.

During vacuum flushing, the void ratio of the specimen was also calculated by the same procedure. This void ratio is called void ratio after vacuum flushing. The change in void ratio after vacuum to void ratio after vacuum flashing was monitored. At this stage, the digital dial gauges were replaced by submergible internal LVDTs and their reading were recorded. Then, Perspex cylinder and loading arrangement were placed very carefully. The internal LVDT readings were monitored again; any jump of readings due to disturbance during placing the cell was adjusted.

During back pressure saturation, the change in specimen height was traced by the change in internal LVDT reading. However, there was no direct measurement of specimen

diameter/perimeter change at this stage. It can be approximately corrected by the relation, $d\varepsilon_V \approx 3.0 d\varepsilon_1$. However, It was found that for sand with wide range of fines this relation varies $d\varepsilon_V \approx 2.5 d\varepsilon_1$ to $d\varepsilon_V \approx 3.5 d\varepsilon_1$. Thus, the maximum error associated with the correction was about 0.5 $d\varepsilon_1$.

3.6.3 *Errors in Assessment*

According to first order second moment approximation, the error in independent random measurements can be presented as

$$Err(y) = \sqrt{\sum \frac{\partial f}{\partial X_i} Err(X_i)} \qquad \textbf{3. 2}$$

where, X_i is independent random measurements and $Err(y)$ = error in the measurements. The void ratio of the sample is a function of independent random measurements. Thus, the Equation 3. 1 can re-written with independent measurements as

$$e = G_S \rho_w \pi \frac{(h_{sam} - 2.m_t)(p_{sam}/\pi - 2m_t)^2}{4M_d} - 1 \qquad \textbf{3. 3}$$

where, G_s specific gravity of sample, ρ_w unit weight of water, P_{sam} = perimeter of sample, h_{sam} = height of sample, M_d = dry mass of solid and m_t membrane thickness. Thus the error in void ratio calculation can be presented as

$$Err(e) = \sqrt{\left(\frac{\partial e}{\partial P_{sam}} Err(P_{sam})\right)^2 + \left(\frac{\partial e}{\partial h_{sam}} Err(h_{sam})\right)^2 + \left(\frac{\partial e}{\partial M_d} Err(M_d)\right)^2 + \left(\frac{\partial e}{\partial Mm} Err(m_t)\right)^2} \qquad \textbf{3. 4}$$

where, $Err(e)$ = error in void ratio calculation, $Err(P_{sam})$ = error in perimeter measurement, $Err(h_{sam})$ = error in sample height measurement, $Err(M_d)$ = error in dry mass measurements and $Err(m_t)$ = error in membrane thickness.

The measurements of independent variable were taken from sample preparation to vacuum flushing. The perimeter of the sample was about P_{sam} = 31.3cm and the maximum error involve in the measurement was estimated as Err(P_{sam}) = 0.02cm. The height of the sample was h_{sam} = 10cm and error was $Err(h_{sam})$ = 0.01cm. The membrane thickness was m_t = 0.03cm and error was estimated of about 5% of average thickness i.e. $Err(m_t)$ = 0.0015cm. However, the dry mass of the sample did not obtain from independent direct measurement. It was obtain from direct measurement of bulk mass and the moisture content measurement.

Part A: Error in Dry Mass M_d

The dry mass of the sample was obtained from the following equation

$$M_d = \frac{M}{1+w} \qquad \textbf{3. 5}$$

where, M_d = dry mass of sample, M = bulk mass of sample and w = moisture content. Thus, the error in dry mass calculation is

$$Err(M_d) = \sqrt{\left(\frac{\partial M_d}{\partial M} Err(M)\right)^2 + \left(\frac{\partial M_d}{\partial w} Err(w)\right)^2} \qquad \textbf{3. 6}$$

where, the maximum mass of the sample was M =1250gm and the error in the measurement was $Err(M)$ = 0.05gm. The moisture content of the sample was w = 7.5% i.e. 0.075 and the error of about $Err(w)$ = 0.001. Thus, the error in dry mass calculation $Err(M_d)$ = 1.04gm

Part B: Error in Void Ratio after Vacuum Flushing

The error in void ratio before back pressure saturation can be calculated from the Equation 3. 4. Thus, the error in void ratio is 0.00294 ≈ 0.003.

Part C: Error in Void Ratio after Back Pressure Saturation

The Equation 3. 4 enable us to calculate *Err*(*e*) after vacuum flushing. However, the Equation 3. 4 cannot be used to calculate *Err*(*e*) after back pressure saturation.

The error in void ratio after back pressure is combination of error at end of flushing and error in δe during back pressure. These two steps are independent. Thus, *Err*(*e*) after saturation can be calculated by root-mean-square method as $= \sqrt{(0.003)^2 + (\delta e)^2}$. The error during back pressure saturation, δe was estimated to 0.0015. Thus, the error in void ratio calculation is 0.0034 at the end of saturation. At this point on ward, the void ratio change was kept track by the GDS-pore volume change. Thus, the error in void ratio is very small and suitable for this study.

3.7 MEMBRANE PENETRATION

Soil sample is confined inside of a latex membrane in triaxial testing system. When pressure is applied on soil sample via the latex membrane, the membrane deforms and is forced into the pores between the grains. This occurs whether the membrane is loaded by changes of cell pressure (Newland and Allely 1957) or pore pressure (Newland and Allely 1959) or via rigid platens (Sarsby et al. 1980). This global displacement of the membrane at the circumference of the soil sample by the change in fluid pressure (cell or pore) is known as membrane penetration. At the top and bottom platen of the sample, the membrane is loaded via rigid lubricated platens, the global displacement of membrane at top and bottom platen is known as bedding error. Molenkamp and Luger (1981) reported that two different mechanism involve behind these errors:

- **Flexing Mechanism:** the flexing of elastic membrane into the peripheral voids between the points of contacts with the grains

- **Indentation Mechanism:** indentation of grains into the membrane.

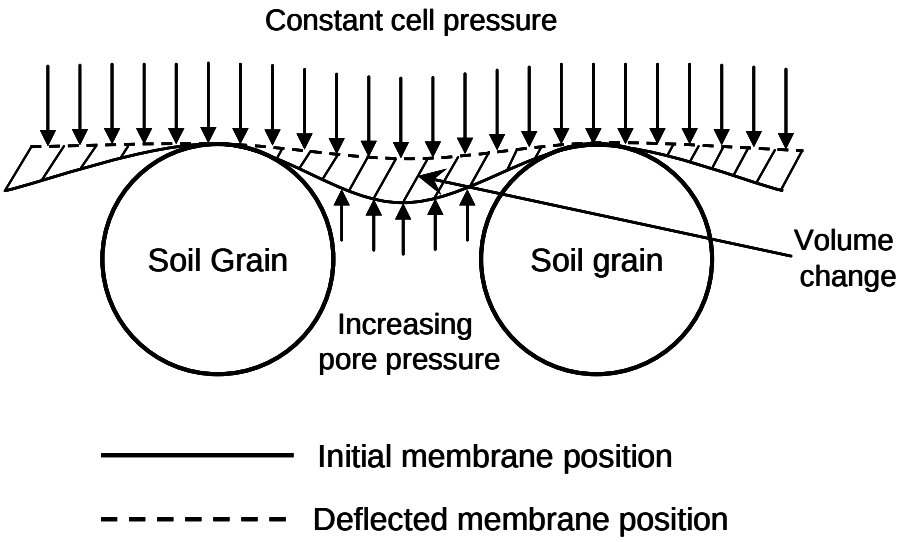

(a)

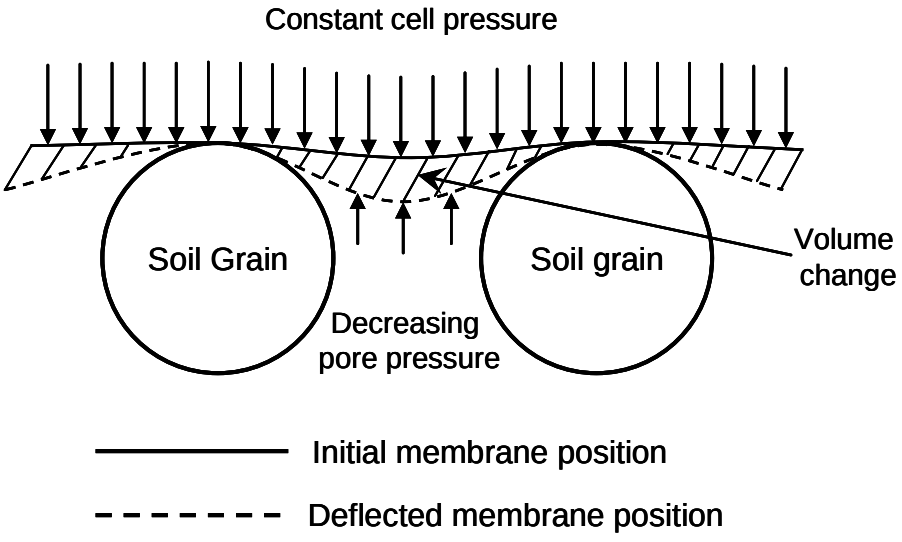

(b)

Figure 3. 11 Membrane penetration mechanism for undrained test; (a) mechanism for contractive soil, (b) mechanism for dilative soil.

The condition of zero volume change has to be satisfied all the time in undrained shearing. However, this condition may no be satisfied due to membrane penetration even though drainage valves are completely turn off. Loose sandy soil shows contractive

tendency with increase in pore water pressure. Thus the increases in pore pressure push the membrane out side which eventually allows extra volume for drainage as shown in Figure 3. 11a. On the other hand, dense sandy soil shows dilative tendency with decrease in pore water pressure. The cell pressure pushes the membrane further in to the peripheral voids as shown in Figure 3. 11b.

Considering the extent of error involve in membrane penetration, a number of investigation have been done on membrane penetration and remedial methods. These methods can be broadly classified as the following groups:

- **Experimental correction method**: these researches mainly concentrated on the experimental technique of the estimation of error involve due to membrane penetration (Frydman et al. 1973; Newland and Allely 1957; Newland and Allely 1959; Raju and Venkataramana 1980; Roscoe et al. 1963; Sarsby et al. 1980; Seed and Anwar 1986).

- **Analytical methods**: These studies develop analytical approach to get an estimation of error involve due to membrane penetration (Baldi and Nova 1984; Molenkamp and Luger 1981; Raines et al. 1988).

- **Error minimization technique**: these studies discussed about the technique to minimization error due to membrane penetration (Kiekbusch and Schuppener 1977; Lade and Hernandez 1977; Lo et al. 1989).

The error minimization technique developed by Lo et al. (1989) is followed in the thesis for clean sand. This technique has been successfully used in many research approaches (Bobei 2004; Chu 1991). A thin film of liquid rubber is applied inside the elastic membrane to effectively reduce membrane penetration effects. The liquid

rubber is a combination of 2/3 of non-shrink liquid rubber and 1/3 of hardening agent. Harden liquid rubber has elasticity same as membrane and a little shrinkage. The liquid rubber fills the void between the soil grains in contact with the rubber membrane, thus reduce error due to the flexing mechanism. Liquid rubber also increase soil grains contact with the membrane and thus reduce the error due to indentation.

Lo et al. (1989) pointed out that apart from the flexing and indentation mechanism, there are two other mechanisms involve in bedding error. They are

- Global deformation of the latex disk under distributed load (free end)
- Squeezing out of grease film under axial stress

Liquid rubber increase the thickness of the latex disk and also increase the contact area of soil grains with the membrane, thus this error is very small and can be neglected (Bobei 2004; Lo et al. 1989). The other error due to squeeze out of grease film is minimize by preloading of the free end.

3.8 MICRO EXPERIMENTATION

The micro experimentation is mainly focused on particles size, shape, mineralogy and relative arrangement. Particle size and their relative arrangements are very important criteria for the development of the concept of equivalent granular void ratio, e^* and the successive development of the conceptual model for sand with fines. These are discussed in Chapter 4 to 6. Particle shape and mineralogy are also important issue in justifying the effect of types of fines. This is also discussed in Chapter 7. Two different set of microscopes have been used for experimentation due to the size difference of sand and fines. They are: light microscope and scanning electron microscope. Light microscope is used to get image of sand and sand-fines mixes. SEM is used to get image of fines and their mineralogical analysis. They are discussed in details in coming subsections.

3.8.1 *Light Microscope*

The optical microscope is often referred to as the "light microscope". It is a type of microscope which uses visible light and a system of lenses to magnify images of small samples. An optical microscope named Wild M400 (photo microscope with SPOT FLEX CCD camera, 14bit, 50Mb) at EMU in Australian National University (ANU) was used for light microscopy (Figure 3. 12a). It was used to get photographs for sand and sand with fines mixture as shown in Figure 3. 13. These photographs show how overall arrangement of sand-fines mixture changes with increase in fines.

(a)

(b)

Figure 3. 12: Microscope used in the study; (a) Light microscope, (b) Scanning Electron Microscope, SEM

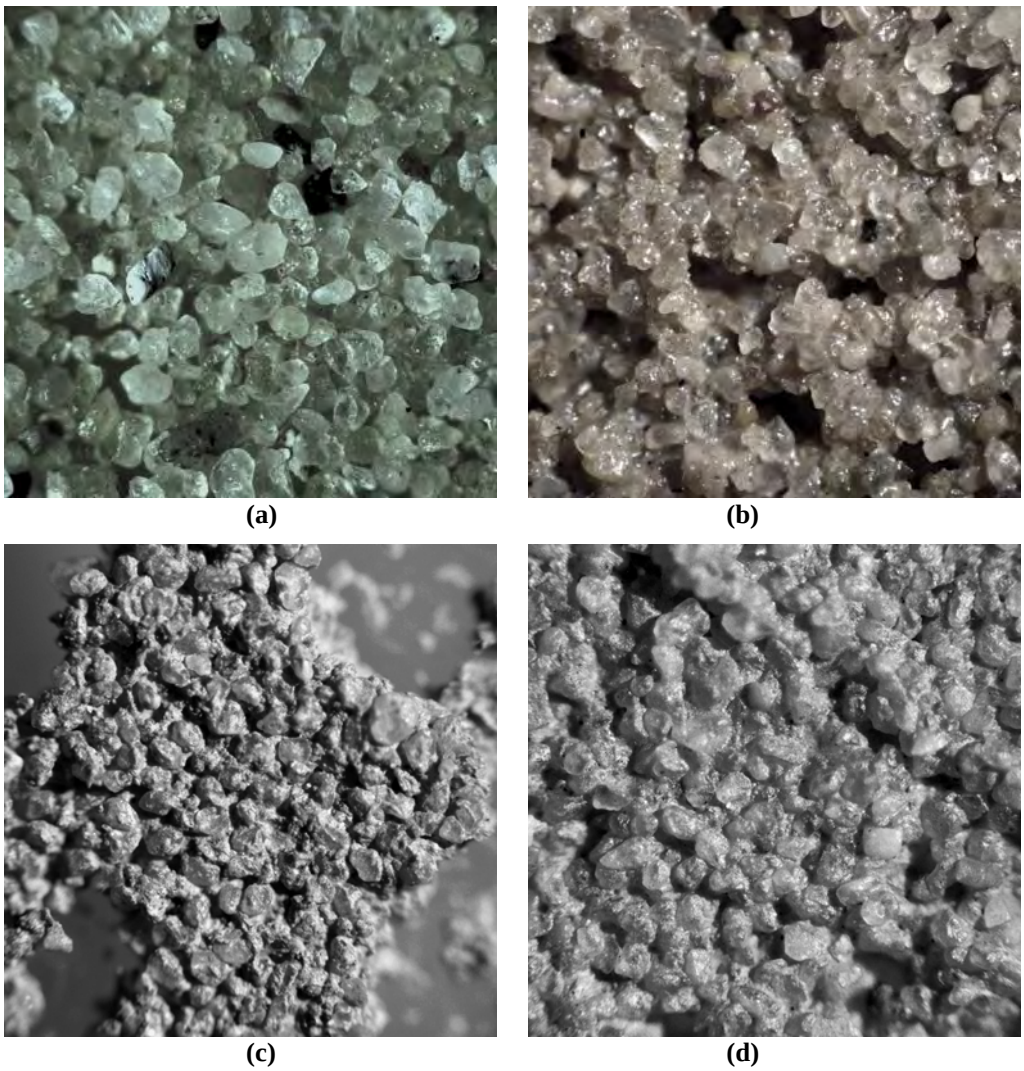

(a) **(b)**

(c) **(d)**

Figure 3. 13: Sand with fines; (a) Clean sand, (b) Sand with 15% fines, (c) Sand with 20% fines, (d) Sand with 30% fines.

3.8.2 *Scanning Electron Microscope, SEM*

The scanning electron microscope (SEM) is an electron microscope that images the sample surface by scanning it with a high-energy beam of electrons in a raster scan pattern. The electrons interact with the atoms that make up the sample producing signals that contain information about the sample's surface topography, composition and other properties such as electrical conductivity. Figure 3. 12b shows the Hitachi 4300 SE/N (Schottky Field Emission SEM, 2006) scanning electron microscope in EMU at ANU which is used for getting SEM image of different types of fines and analyzing their

mineralogy. It has a wide range of magnifications, ranging from about x25 (about equivalent to that of a powerful hand-lens) to about x250,000, about 250 times of the magnification limit of the best light microscopes though it requires special sampling techniques. The sampling technique, SEM photograph and mineralogical analysis are discussed in coming sub-sections.

Sampling

For conventional imaging, the SEM requires that specimens to be conductive for the electron beam to scan the surface and that the electrons have a path to ground. Thus, nonconductive solid specimens are coated with a layer of an ultra thin coating of electrically-conducting material such as, gold, gold/palladium alloy, platinum, tungsten or graphite as shown in Figure 3. 14a. They are deposited on the sample either by low vacuum sputter coating or by high vacuum evaporation. This is done due to two reasons:

- To prevent the accumulation of static electric charge on the specimen during electron irradiation.
- To improve contrast and resolution of samples with low atomic number.

Four different types of fines have been used in the study and it is found that gold coating is not equally good for all types of fines. “Charging effect” was found for some sample which causes white spot on the image. Sample placed on carbon tape is found well enough for sampling in these cases as shown in Figure 3. 14b.

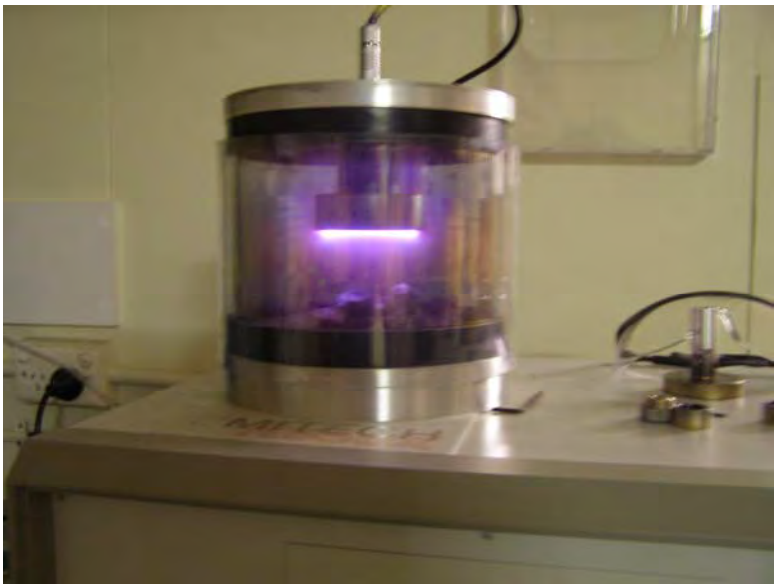

(a)

(b)

Figure 3. 14: Sample preparation of SEM; (a) Gold coating on sample, (b) Sample prepared on carbon tape.

SEM photograph

SEM photographs for four different fines have been taken and their shape and angularity have been analyzed from SEM image. Thus, the effect of shape and angularity of fines on the mechanical behaviour of sand with fines mixture can be analyzed. The details are discussed in Chapter 7.

SEM mineralogical Analysis

Scanning electron microscope (SEM) analysis is another important aspect of micro-experimentation. In this method, the macroscopic surface of a material is analyzed. Thus the analysis is sensitive to representative surface. However, in SEM analysis, the surface to be analyzed can be photographed and analyzed simultaneously. Mitchell (1993) reported that this coupled feature made SEM popular and reliable. During investigation, several representative surfaces were chosen first and then analytical spectrums as shown in Figure 3. 15 were taken on those surfaces. The atomic weight of the elements was obtained by percentage atomic weight as shown in Table 3. 5. It is found that the individual data for several spectrums had a small variability. The average of those data was taken as representative data of the material. The four different fines of this study were achieved by combination of three different types of fines. Thus, the mineralogical analysis of these three materials was done instead of four types of fines. This also reduces the chance of interference by other material. Their spectrums of these three materials are shown in Figure 3. 15 to Figure 3. 17 and their respective materials properties are given in Table 3. 5 to Table 3. 7.

The mineralogical analysis shows that these three fines do not contain any organic matter (C, carbon based materials). Thus, no chemical reaction expected during

sample preparation and testing. The mechanical behaviours of the materials are the reflection of material physical properties; they are not affected by chemical force.

- **SI fines**

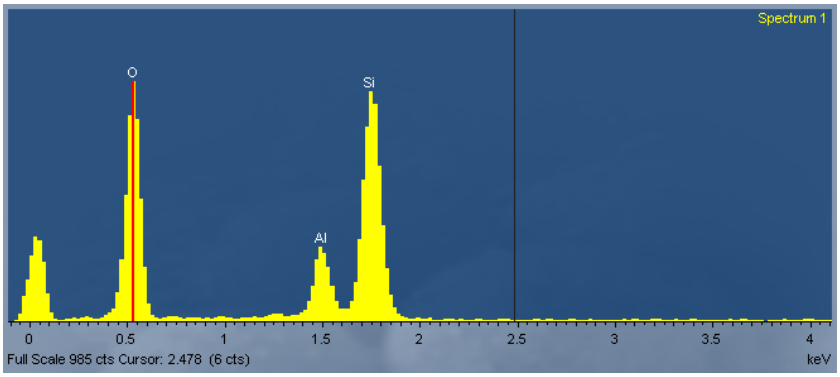

Figure 3. 15: Analytical spectrum for SI fines

Table 3. 5: Atomic weight of different element of SI fines

Spectrums	Atomic of O (%)	Atomic of Fe (%)	Atomic of Al (%)	Atomic of Si (%)
Spectrum-1	75.20	0.32	6.55	22.46
Spectrum-2	65.96	0.90	6.33	12.29
Spectrum-3	69.39	0.90	13.01	16.94
Spectrum-4	66.08	0.99	8.30	16.54
Average	69.14	0.78	8.55	17.06

- **MI fines**

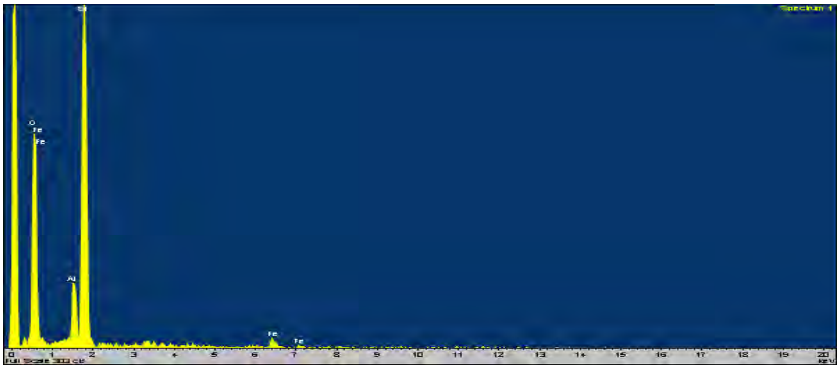

Figure 3. 16: Analytical spectrum of MI fines

Table 3. 6: Atomic weight of different element of MI fines

Atomic of O (%)	Atomic of Fe (%)	Atomic of Al (%)	Atomic of Si (%)
65.07	2.27	5.02	27.64

- **Kaolin**

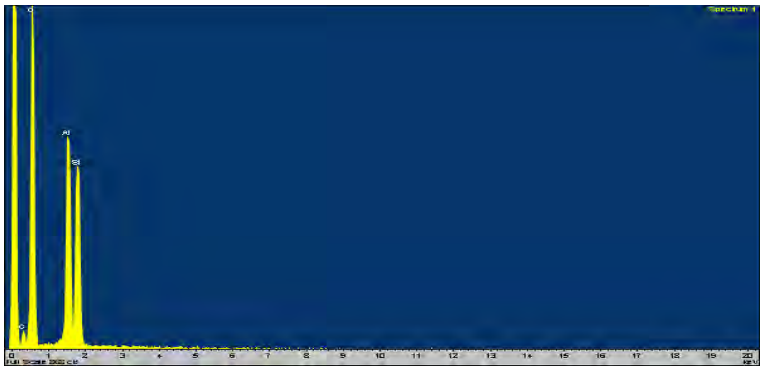

Figure 3. 17: Analytical spectrum of Kaolin

Table 3. 7: Atomic weight of different element of Kaolin

Atomic of O (%)	Atomic of Fe (%)	Atomic of Al (%)	Atomic of Si (%)
63.78	0.00	17.40	18.83

3.9 SUMMARY

A fully automated triaxial testing system was established and it was equipped with adequate instruments to provide sufficient accuracy of the measured quantities such as void ratio, pore water pressure, stress, strain etc. The control software was modified for conducting some special cyclic loading tests. Special effort was given to sample preparation to ensure the uniformity of the sample so that the stress-strain distributions inside represents “element” behaviour.

Sydney sand and four different types of fines were used as testing materials for study the steady state behaviour. Thus, a good track of change in void ratio was kept from the sample preparation to the end of shearing. The maximum error in void ratio was estimated to 0.018. The error due to membrane penetration and bedding were minimized by liquid rubber technique as proposed by Lo et al. (1989).

The angularity and plasticity of fines might have significant effect of steady state behaviour. Thus, micro-experimentation was done with light and scanning electron microscope to study their shape factor and their relative arrangement in sand fines mix. It is discussed in detail in Chapter 7. The mineralogical study by SEM also confirmed that these materials did not have any organic matter and thus, their mechanical behaviour was unlikely affected by chemical forces. Thus, one could investigate the effect of fines angularity which made this study distinct with other previous studies.

CHAPTER 4

Binary Packing and the Parameter "*b*"

4.1 INTRODUCTION

It has been discussed in Chapter 2 that the concept of equivalent granular void ratio, *e** was introduced by considering a silty sand consists of two components: coarse particles (sand) and fines particles (fines) i.e. sand with fines is a binary mix. It is not a new idea to considering soil as a binary mix as indicated by published literatures (Furnas 1928; Kuerbis et al. 1988; Lade et al. 1998; Lupini et al. 1981; Pitman et al. 1994; Tan et al. 1994; Wickland et al. 2006). The idealization as binary mix significantly simplified the derivation of equivalent granular void ratio as explained in Chapter 2. However, a parameter *b* is used in the equation of equivalent granular void ratio, where *b* represents the fraction of fines particles which have the active contacts between coarse particles. It has been discussed earlier that there was no prediction formula for *b*, thus there is a need for the development of prediction formula for *b*.

Therefore, the primary objective of this chapter is to develop a physically reasonable semi-empirical equation for predicting the value of *b* so that equivalent granular void ratio, *e** can be predicted from void ratio, *e* or vice versa. Then, this equivalent granular void ratio, *e** will lead to a single relationship in the *e**-log(*p*′) space that is independent of fines contents.

4.2 DETERMINATION OF *b*-VALUE

It is discussed in Chapter 2 that the equivalent granular void ratio, e^* was determined by using selected *b*-value/values for particular sand with fines. The selected *b*-value has been successfully applied by many researchers. For example, Thevanayagam et al. (2002b) found that, despite the SS data points in e-log(p') space is highly dependent on the fines contents, an approximately single relationship in e^*-log(p') space can be obtained for F55, Foundry sand with non-plastic crushed silica. Similar finding are reported in literature (Ni et al. 2004; Yang et al. 2006c). However, *b* was determined mainly by back analysis process and it is discussed in details in next sub-sections.

4.2.1 *Finding b*

From the available published papers, it can be inferred that the selection of appropriate *b* was done by back analysis process. The key feature of back analysis was the assumption that all SS data points for sand with fines will come to a single trend in e^*-log(p') space. Thus, by trial and error a *b* value has to be found until all SS data points for sand with different fines content come to a single trend. Alone the same line, it was assumed that cyclic liquefaction resistance will also come to a single trend in e^*- CR relationship and *b* can also be found by trial and error.

A number research have been found on back analyzed *b*-value such as Thevanayagam et al. (2002b) reported $b = 0.25$ for F55, Foundry sand with non-plastic crushed silica, Ni (2004) reported $b = 0.75$ for Old Alluvium sand from Singapore. Yang et al. (2006c) reported $b = 0.25$ for Hokksund sand with Chengbei fines when fines content less that TFC.

However, this back analysis procedure has some serious limitations:

- It needs large amount of tests data as input and thus, intrinsically it is a very expensive process and sometimes not practical because of time limitations
- It can not be use as a predictive tool as the results have to be known first.
- This process may yield unreasonable *b*-values. For example, a very high *b* of 0.70 was reported for small amount of fines (9%) as discussed in Ni et al. (2004). They also reported negative *b*-value which is contradictory to the physical meaning of *b*.

4.2.2 *Characteristics of Reported b-values*

The concept of equivalent granular void ratio, e^* and the parameter *b* have been investigated by many researchers (Ni et al. 2004; Thevanayagam 2003; Thevanayagam and Martin 2002; Thevanayagam et al. 2002b; Yang et al. 2006a; Yang et al. 2006c). The followings are the important characteristics of *b* observed in literature:

- The *b*-values reported in literature are back-analyzed values.
- The concept of equivalent granular void ratio implies when the overall matrix of soil is formed by sand, i.e. it is a "fines in sand" material. There is a fines content where the overall matrix ceases to be formed by sand is called threshold fines content, TFC, (Thevanayagam 1998; Xenaki and Athanasopoulos 2003; Yang et al. 2006b). When the fines content exceeds the threshold value, the overall matrix is formed by fines and the concept of equivalent granular void ratio ceases to be meaningful.

- A constant *b* value (for a given sand-fines mixtures) irrespective of the fines content is reported in most literatures. An exception is Yang et al. (2006b; 2006c), which suggested $b = 0.25$ could be used for fines content less than or equal to 20%, but $b = 0.40$ at a fines content of 30%. However, the "fines in sand" model of Thevanayagam (1999) implied that fines content can affect the value of *b*. Physical consideration suggested that, for large size ratio, $b \rightarrow 0$ at adequately low fines content.
- Although the work of both Thevanayagam (2001) and Ni et al. (2004) suggested that *b* depends upon size ratio, the factors that may influence the value of *b* still need to be clarified.

To further characterize the parameter *b* a detail study on binary packing is needed as the concept of equivalent granular void ratio, e^* originally came from the assumption of a binary mix.

4.3 BINARY PACKING AND *b*-VALUE

The factors that affect the density of a binary packing has a subtle correspondence to those affecting the *b*-value. The binary packing studies were mainly reported in the ceramic, concrete and powder technology areas and with the original objective of minimizing storage space or maximizing densities. A binary packing that can achieve high density means that the smaller particles can be fitted within the void space of the larger ones. Thus, unless the fines content is high, the smaller particle only has a secondary role in the force structure when the binary packing is loaded and thus the corresponding *b* value should be low. A binary packing that cannot achieve high

density means smaller particles must get between the larger ones and participate in the force structure. Thus, *b*-value at same fines content should be higher.

4.3.1 *Binary Packing*

The study of McGeary (1961) on the binary packing of spherical balls is particularly relevant to geotechnical engineering. The densities achieved by different binary packings of spheres, i.e. spheres of two different sizes and relative composition, placed using a special vibratory procedure were measured. The test results in Figure 4. 1 showed that if D/d > 7, where D is the diameter of the larger sphere and d is that of smaller sphere, the experimental density achieved would be close to the theoretical curve, because the smaller sphere migrating into the voids between the larger spheres. It is worth noting that geometric calculation of a small sphere inside of three large spheres required a diameter ratio of D/d ≈ 7 as shown in Figure 4. 2. However, test results for D/d < 4.7 deviated significantly from the theoretical curves thus showing the smaller spheres must move between the larger spheres.

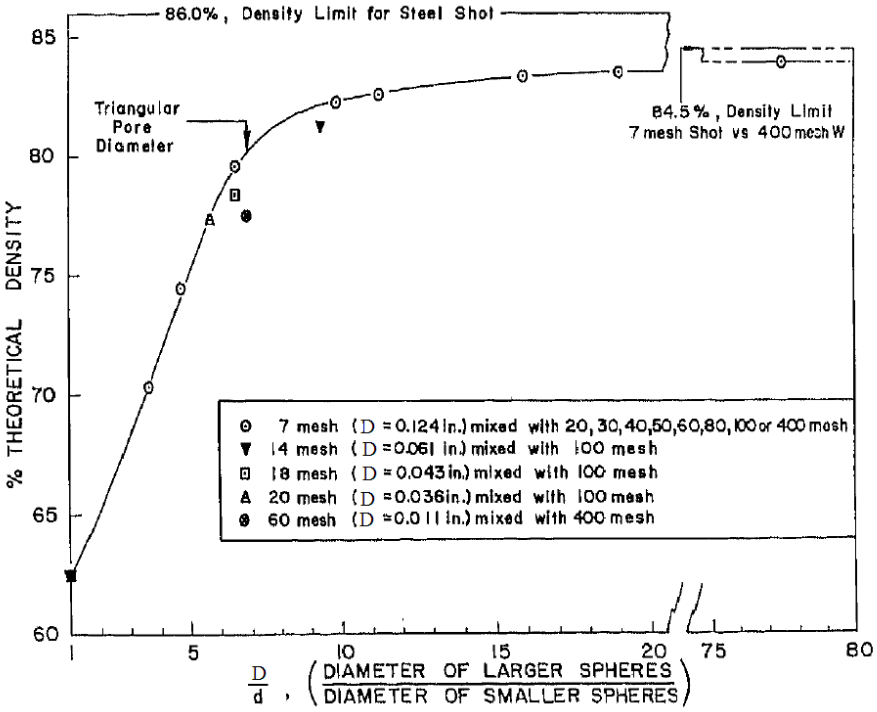

Figure 4. 1: **Effect of diameter ratio of binary packing density after McGeary (1961), slightly modified**

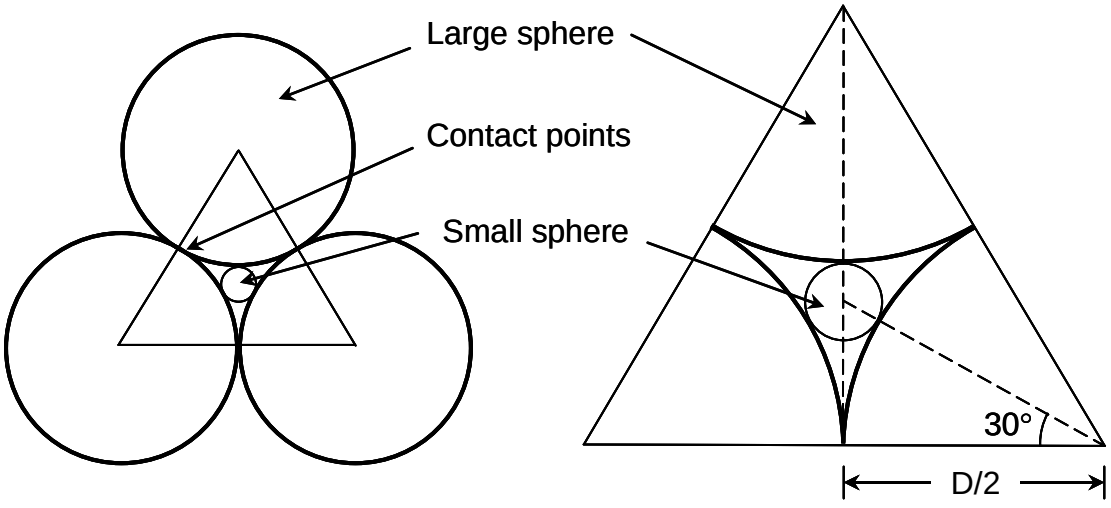

$$d = 2\left(\frac{D}{2}\times\frac{1}{\mathrm{Cos}30^{\circ}} - \frac{D}{2}\right) \approx \frac{1}{7}D$$

Figure 4. 2: **Geometric calculation of a small sphere fitting inside of three large spheres, modified from Lade et al. (1998)**

The study of McGeary (1961) was re-analyzed by Lade et al. (1998). The findings were presented in a slightly modified form as Figure 4. 3 of this chapter. The percentage of small spheres in the binary mixture is shown as fines content in the figure. The void ratio decreases with fines content until a threshold value is reached, but further increase in fines content leads to an increase in void ratio. This leads to a V-shaped curve with the first segment representing a "fines in coarse" packing, whereas the second segment is for a "coarse in fines" packing. Therefore, the trough of the V-curve is analogous to the concept of threshold fines content, TFC. For D/d > 6.5, where "D" is the diameter of the larger sphere and "d" is that of smaller sphere, the void ratios achieved are closed to the idealized line inferred by assuming the smaller spheres (fines) are all located in the void space between the large spheres. If D/d < 4.7, the void ratios achieved are significantly higher, thus implying that significant amount of smaller spheres are located between the larger spheres, and contribute more to the force structure (if loading is imposed on the binary packing). The V-shape curve becomes "flatter" relative to the ideal curve, thus implying that an increase in fines content increase participation of the fines in the force chain.

Figure 4. 4 was reproduced, with minor formatting modifications, from Lade et al. (1998). The minimum "void ratios" is defined by the trough points of the V-shaped curves of Figure 4. 3. At high size ratio, say D/d > 9, the minimum "void ratio" only reduces slightly with increase in D/d. Thus, size ratio only has a small influence on the contribution of fines to the force structure. For D/d < 6, the minimum "void ratio" varied rapidly with D/d because the smaller spheres have to get in between the larger ones. Therefore, the size ratio has a significant influence on the contribution of fines to the force structure. One can also infer a "sharp bend" delineating these two regimes

at D/d ≈ 7. Again, this value is consistent with the geometric calculation of fitting a smaller sphere between larger ones as shown in Figure 4. 2 and it is also observed in real soil behaviour (Cubrinovski and Ishihara 2002; Lade et al. 1998; Wickland et al. 2006). These finding on binary packing highlight the factors that influence the "extent of contacts" between large and small particles of a binary mix, and thus relevant to the prediction of *b*.

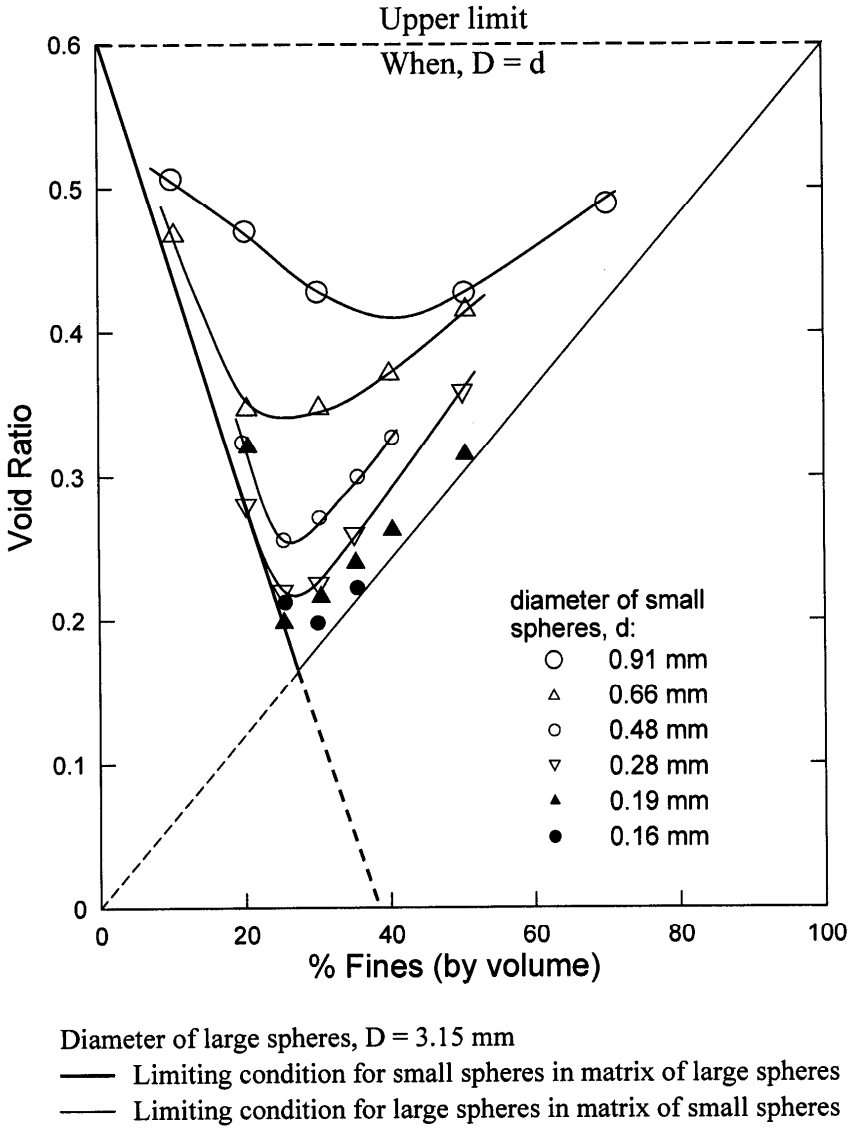

Figure 4. 3: **Effect of fines content on minimum void ratio of binary mix after Lade et al. (1998) (slightly modified).**

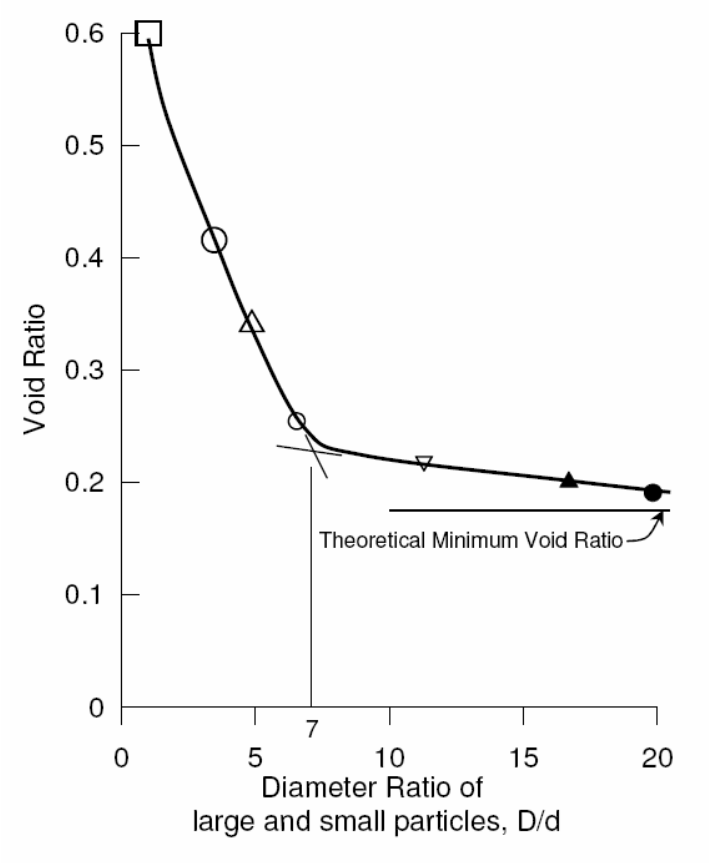

Figure 4. 4: Effect of diameter ratio on minimum void ratio of binary mix after Lade et al. (1998)

4.3.2 *Factors Affecting b*

The *b* value is a measure of the participation of the fines in the force structure. Fines that are between coarse particles are in the force chain whereas fines that are located in the gaps between the coarse grains have little contribution to the force structure. Therefore the factors that affect the void ratio of a binary packing, including the deviation of the V-shape curve from the theoretical curve of Figure 4. 3, can be used to infer the factors that affect the *b* value. Figure 4. 3 and Figure 4. 4 simply suggest that the void ratio of a binary packing is dependent on both the relative composition and the size ratio. Therefore, *b* is a function of both f_c and χ. This functional

relationship has to possess the following characteristics as inferred from the previous section on binary packing:

- The concept of a threshold fines content, TFC (for delineating the regime of "fines in sand" from "sand in fines") is valid and essential.
- For f_c < TFC, the *b* value increases with fines content. With increasing fines content, the first segment of the experimental V-shape curves gradually deviates more from the idealized one (Figure 4. 3). Such a deviation implies that more fines are located between the coarse grains and thus a higher *b* value.
- By assuming a correspondence between the transition void ratio and *b*-value, one can infer from the concept of a critical size ratio denoted as $(D/d)_{crit}$ that delineates two distinct zones (Figure 4. 4).
    - In the regime of D/d >> $(D/d)_{crit}$, "*b*" increases slowly with increase in fines content (because the fines can migrate into the void space between the coarse particles).
    - In the regime of D/d < $(D/d)_{crit}$, "*b*" increased rapidly with increase in fines content.
- Along the same argument as point 3 above, Figure 4. 4 shows that there is a transition region around $(D/d)_{crit}$ where "*b*" increases gradually with fines content because the fines can migrate into the void space or trapped between the large particles.

4.4 PREDICTION OF *b*

In this section, a functional relationship $b = F(\chi, f_c)$ is developed using a semi-empirical approach. As host sand and fines are not single size, the size of the host sand are characterized by the lower 10% fractile, D_{10} as mean void size of soil depends on the finest particle size (Aberg 1992), whereas that of fines are characterized by d_{50}, the median size. This is in line with the argument of Ni et al. (2004; 2005). Therefore, the size ratio, χ is defined as D_{10}/d_{50}. The "fines in sand" model implies that the grading curves of the host sand and fines are spaced apart. All the data sets studied in this thesis satisfy this requirement. To imply prediction formula with in "fines in sand" model, the threshold fines content, TFC has to be known before developing the functional relationship of *b*. Yang et al. (2006a) reported that TFC can be better determined from the location SS data points for sand with fines in *e*-log(*p*′) space. Alone the same line, an objective way to determine TFC from *e*-log(*p*′) space is discussed in next section and finally, a prediction formula is proposed from binary packing study and it can be used whenever enough data are not available to workout TFC.

4.4.1 *Prediction of TFC*

The value of TFC reported in published literature is in the range of 25% to 50% (Polito 1999; Yang et al. 2006a). However, the range reduces to 30% to 41% if only data points that satisfy the definition of TFC adopted in this chapter are included. Following the argument of Yang et al. (2006a), a standard way is proposed to determine TFC from SS data points of sand with fines in coming section.

Thevanayagam et al. (2002b) published a comprehensive set of data that showed the influence of fines content on the location of SS data points as illustrated in Figure 4. 5. The SS data points initially shifted downwards with increase in fines content but the trend was reversed at higher fines content. The fines content defining the lowest position of the SSL is the reversal point, thus the TFC. To determine this value objectively, e_{100} was plotted against fines content as presented in Figure 4. 6, where e_{100} is the void ratio on the SSL at p' = 100 kPa. The reversal point of the data defines the TFC. Thus, the TFC for Ottawa sand with non-plastic fines is about 36%.

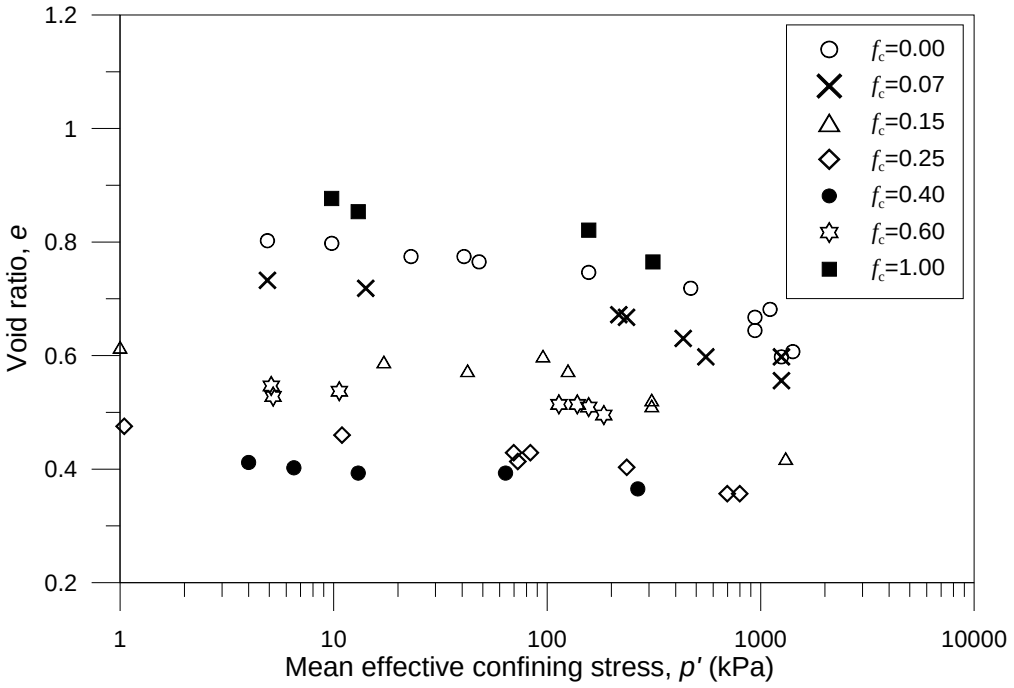

Figure 4. 5: Effects of fines content on SS data points for sand with fines after Thevanayagam et al. (2002b).

To examine the sensitivity of TFC on steady state mean confining pressure p', the above exercise was repeated using e_{50} and e_{300} at steady state mean confining pressure, p' of 50 kPa and 300 kPa respectively. The resultant plots are shown in the same Figure 4. 7. It shows that the fines content at the reversal points are evidently

only slightly different with steady state mean effective stress, p'. However, to reduce variability, TFC standardized at p' of 100 kPa.

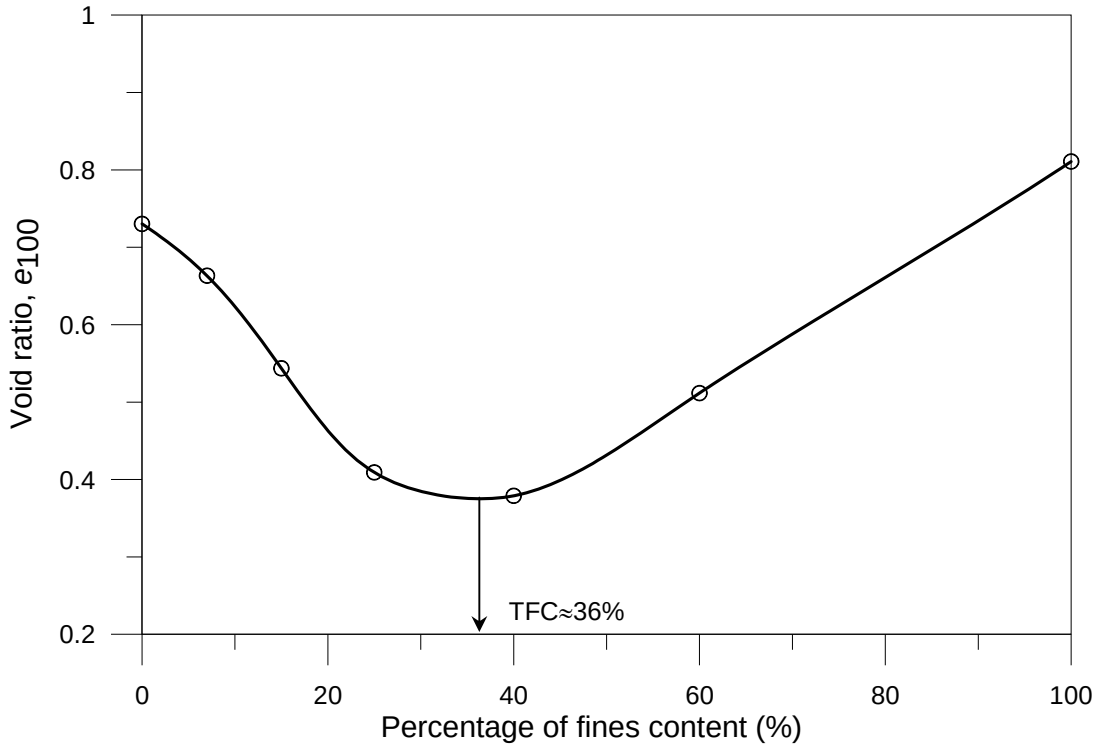

Figure 4. 6: Variation of steady state void ratio at mean effective stress, p' = 100kPa with fines content after Thevanayagam et al. (2002b).

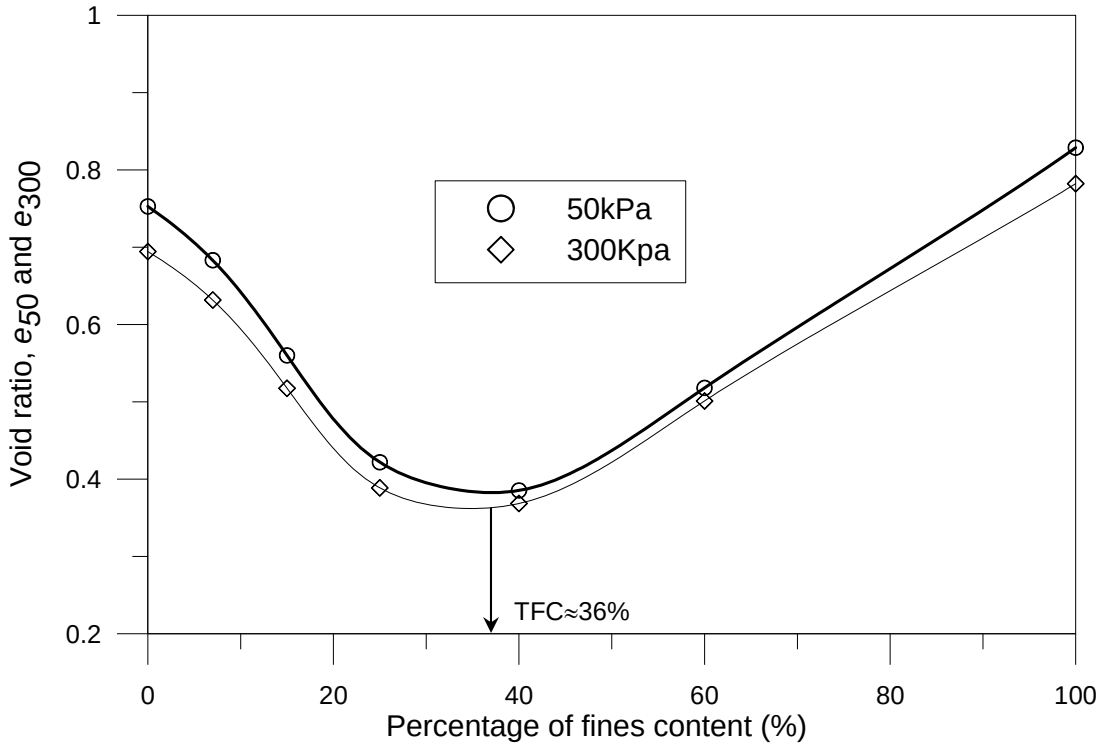

Figure 4. 7: Sensitivity of steady state void ratio for sand-fines mix with steady state confining pressure after Thevanayagam et al. (2002b).

The above procedure was repeated for six data sets and each data set gives one data point (TFC-χ space) as shown in Figure 4. 8. To maximize the number of data, data sets on the influence of f_c on CR is also included. For such a data set, TFC is also defined by the fines content where the influence of fines content on cyclic resistance reverses in direction. This gives a total of nine data point. These nine data points enable to study TFC-χ relationships. Figure 4. 8 shows that those data points reveal a distinct pattern with three important attributes:

- Firstly, TFC is at minimum value when particle diameter ratio (χ) is approximately at $(D/d)_{crit}$. This is consistent with the binary packing consideration that at $(D/d)_{crit}$, a minimum number of one small particle can

be fit in between the gap of large particles. Thus, it is expected to achieve minimum TFC around $(D/d)_{crit}$.

- Secondly, increase of χ beyond the turning point (when TFC is at a minimum) leads to a gradual increase of TFC to an asymptotic value. For a binary packing point of view, as the small particles get smaller in size, more particles can fit in the same void space between the large particles (thus giving a higher TFC) but there is an asymptotic limit to this increase.
- Thirdly, when diameter ratio is less than $(D/d)_{crit}$, TFC increases rapidly. This is because the small particles open up the gaps between large particles and give more space for the small particles to get it.

These features can be simulated by the following equation with three constants:

$$TFC = A_{TFC}\left(\frac{1}{1+e^{\alpha-\beta\chi}}+\frac{1}{\chi}\right) \qquad \textbf{4. 1}$$

The coefficient of A_{TFC} is the asymptotic value of 0.40. The other two parameters α and β are determined to yield a minimum TFC around $(D/d)_{crit}$ and the maximum TFC data point corresponding to the smallest χ of ~2.0, where, α = 0.50 and β = 0.13. Equation 4.1, also give a general shape that fits the data points well.

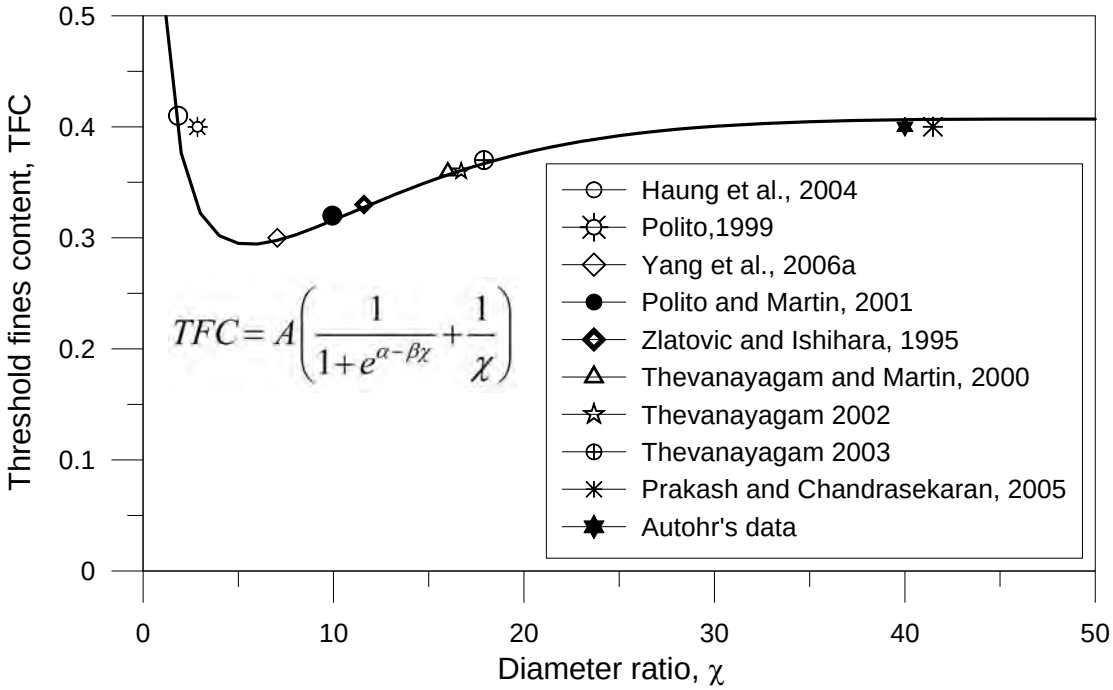

Figure 4. 8: Relation between TFC and particle diameter ratio

4.4.2 *General Equation of "b"*

A generalize function, $b = F(\chi, f_c)$ is proposed in this section that is able to simulate the various attributes as discussed in the previous sub-sections, and yet has a simple form. The equation can be expressed as

$$b = \left[1 - \exp\left(-m\frac{(f_c/TFC)^{n_b}}{k}\right)\right] \times \left(r\frac{f_c}{TFC}\right)^r \qquad \textbf{4. 2}$$

Where, f_c = fines content, $r = \chi^{-1}$ = d/D, $k = (1 - r^{0.25})$, and m, n_b are two empirical constants. The first factor gives the general shape of the b-χ curve. The second factor of the equation ensures that $b \rightarrow 0$ as $f_c/TFC. \rightarrow 0$.

To further simplifies the equation, one can assign $n_b = 1$. The parameter m can be determined by calibrating against the individual data set for sand with fines as explained below.

4.4.3 *Determination of "m"*

The data set of Thevanayagam et al. (2002b) is used to determine the parameter *m*. For Equation 4.2 to be valid, the equivalent granular void ratio calculated by this equation, should give a single correlation of SS data points in the e^*-log(p') space. In order to have an objective way to assess whether a single relation is achieved or not, a statistical measure, root-mean-square-deviation, RMSD is used. It is pertinent to note that data point described by Yang et al. (2006c) as "one trend line could represent the data points of the mixtures" have a RMSD value of 0.043. This value is thus used as the benchmark. The following steps are used to get the parameter *m*.

- Determine TFC as mentioned in section 4.4.1 as enough data are available to get TFC.
- Calculate the *b* values using Equation 4.2 with a first assumption of $m = 0.50$.
- Convert the void ratios of the data set to equivalent granular void ratios using Equation 2.14 and calculate RMSD of the trend line.
- By trial and error the parameter *m* has to find out where least RMSD of the trend is observed.

It is found that an essentially single relationship between e^* and log(p') was obtained by setting $m = 0.30$. The RMSD value of the data set is 0.0274 which is less than that of Yang et al. (2006c). Thus, the Equation 4.2 for Thevanayagam et al. (2002b) data set can be rewrite as following:

$$b = \left[1 - \exp\left(-0.3\frac{(f_c / TFC)}{k}\right)\right] \times \left(r\frac{f_c}{TFC}\right)^r \qquad \textbf{4. 2a}$$

Where, $m = 0.30$ and $n_b = 1$.

4.4.4 *Attributes of Prediction Equation*

The variation of b with χ, normalized with $b(20)$, is presented in Figure 4. 9a. Normalized plots are presented so that the b-χ plots corresponding to different fines content can be compared. It is evident that the general trend is independent of f_c. For $\chi \leq 4.5$, this factor changes rapidly with size ratio, but at a higher size ratio, say exceeding 9, b reduces very slowly with size ratio. The "turning point" may be inferred to be in the range of 6 to 8. These characteristics are in line with those listed in the previous section. This general trend implies that the predicted b-value is not sensitive to χ provided $\chi > 8$. However, at smaller size ratio, the input parameter χ has a significant effect on the predicted b-value. The general shape of the plots presented in Figure 4. 9a is attributed to the first factor, i.e. $\left[1-\exp\left(-0.3\frac{f_c/TFC}{k}\right)\right]$, of the prediction equation. This is illustrated by the normalized plots of Figure 4. 9b. The influence of χ on the value of the first factor is largely achieved through k. In general, a higher size ratio will give to a higher k value, which then leads to a lower value for the first factor.

The second factor $\left(r\frac{f_c}{TFC}\right)^r$ of the equation ensures that $b \rightarrow 0$ as $f_c \rightarrow 0$. Therefore, Equation 2.14 for defining e^* degenerates to Equation 2.12 for defining e_g. This is consistent with published work showing e_g (calculated with $b = 0$) is an adequate approximation for low fines content.

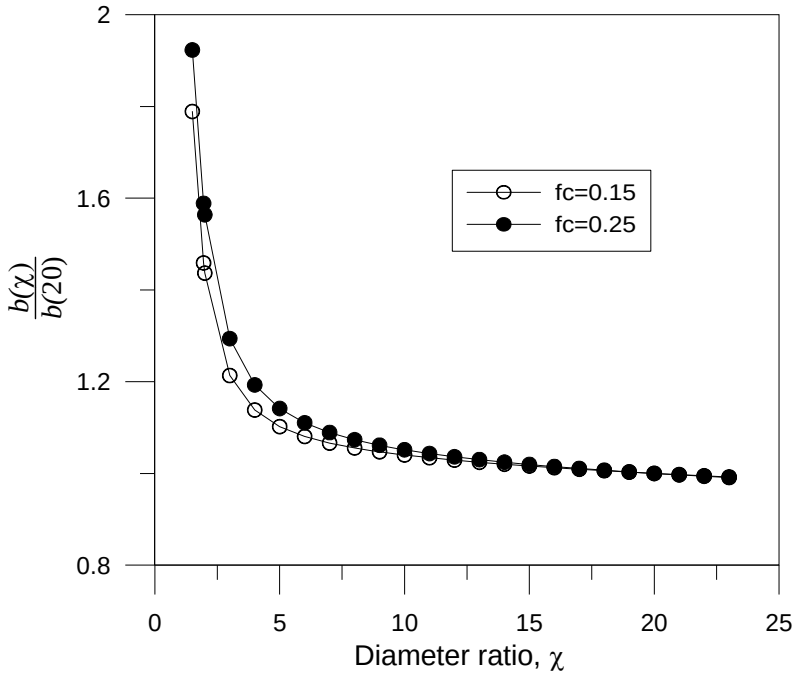

(a)

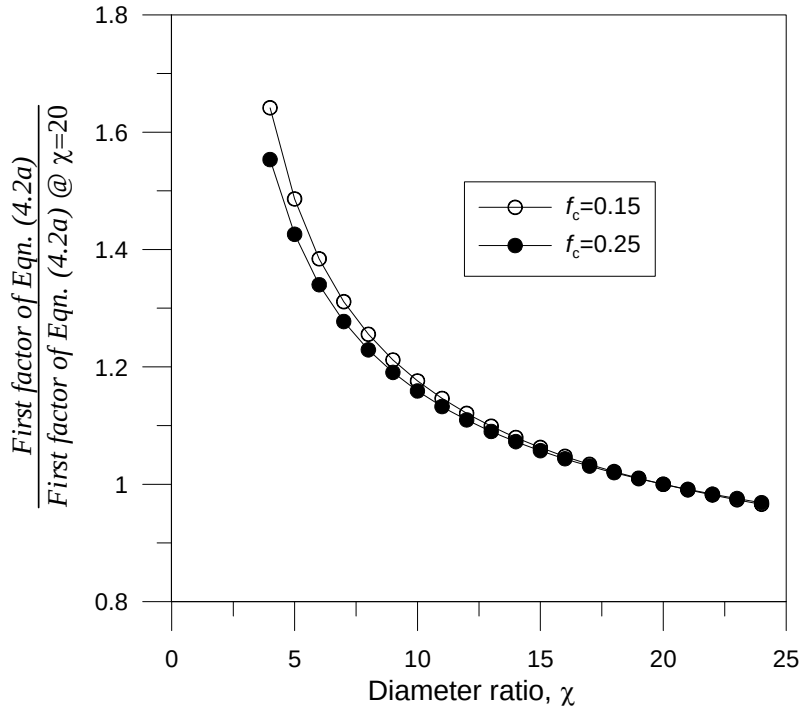

b)

Figure 4. 9: **Factors affecting *b*; (a) Influence of χ on *b* (TFC=35%), (b) Influence of χ on the first factor of Equation 4.2a (c) Influence of fines content on *b* (TFC=35%)**

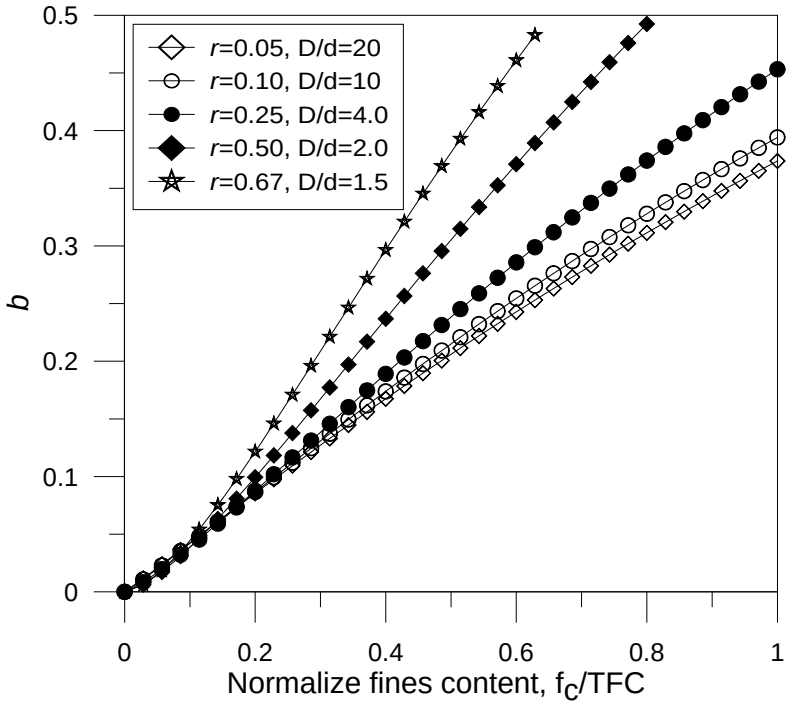

(c)

Figure 4. 9: Factors affecting *b*; (a) Influence of χ on *b* (TFC=35%), (b) Influence of χ on the first factor of Equation 4.2a (c) Influence of fines content on *b* (TFC=35%)

The resultant variation of *b* with fines content, normalized relative to threshold fines content, is shown in Figure 4. 9c. The plots showed at low fines content, both the value of *b* and $\partial b / \partial f_c$ are small. This is again consistent with published finding that e_g is an acceptable approximation for low fines content. It also meant that, at low fines content, the predicted *b*-value is not sensitive to the input parameters f_c and TFC. However, at higher fines content, $\partial b / \partial f_c$ begins to take a significant value. This implies the predicted *b*-value is dependent on getting reliable values of f_c and TFC.

4.5 VERIFICATION

To ensure the proposed Equation 4.2a, with m = 0.30, has general applicability, a validation exercise was conducted on nine different data sets extracted from published

literatures. These data sets cover a wide range of sand and fines from six countries. Two types of behaviour were examined: the SS data points from monotonic undrained shearing and the cyclic resistance behaviour from cyclic triaxial testing. A brief summary of the data sets is presented in Table 4. 1 and Table 4. 2. The validation procedure is as follows:

- Determine TFC, directly according to definition in section 4.4.1, if enough data points are available. Otherwise use prediction Equation 4.1, if enough data points are not available.
- Calculate the *b* values using Equation 4.2a.
- Convert the void ratios of the published data to equivalent granular void ratios using Equation 2.14.
- Examined whether a single behaviour trend independent of fines content can be obtained utilizing the equivalent granular void ratio as the alternative state parameter.

It is recognized that visual appearance of scatter may be subjectively influenced by the scale used in plotting, the number of data points and overall pattern of the data points. In order to have an objective assessment, two statistical quantities were calculated for each data set:

i) The half-spread of the source data in terms of e and

ii) The Root Mean Square Deviation, RMSD of the (e^*, p') data points from the best-fit trend line/curve.

The definitions of these two quantities are detailed in Appendix A. The magnitude of RMSD relative to the half-spread of the source data e-p' or e-CR space will provide an objective basis to assess whether the influence of fines content was significantly reduced by synthesizing data points in the e^*-p' or e^*-CR space.

Table 4. 1 Summary of steady state behaviour from previous study and the respective *b* values

Source	Sand			Fines			Input Parameter			Predicted *b*-value$^{\otimes}$
	Name	D_{10}	U_c	Name	d_{50}	U_f	$r = 1/\chi$	Fines Content (%)	Threshold Fines TFC (%)	
Yang et al. (2006a)	Hokksund sand	0.225	2.25	Chengbei	0.032	2.32	0.142	0 - 30	30*	0 to 0.410
Huang et al. (2004)	Mai Liao sand	0.080	1.75	Mai Liao sand	0.044	2.79	0.550	0 - 30	41*	0 to 0.480
Ni at al. (2004)	Old Alluvium	0.209	5.63	Old Alluvium	0.038	5.43	0.182	0 - 09	30†	0 to 0.137
Zlatovic and Ishihara (1995)	Toyoura Sand	0.116	1.61	Milled Toyoura sand	0.01	6.08	0.086	0 - 30	33†	0 to 0.360
Thevanayagam et al. (2002b)	OS00 #55	0.160	1.69	Sil-co-sil #40	0.010	7.50	0.063	0 - 25	36*	0 to 0.280

* Obtained from source data following the procedure describe in section 4.4.1

† Calculated value from Equation 4.1

$^{\otimes}$ *b*-value depends on fines content

Table 4. 2 Summary of cyclic mobility behaviour from previous study and the respective *b* value

Source	Sand			Fines			Input parameter			Predicted *b*-value$^{\otimes}$
	Name	D_{10}	U_c	Name	d_{50}	U_f	$r = 1/\chi$	Fines Content (%)	Threshold Fines *TFC*	
Vaid (1994)	Brenda 20/200	0.070	3.92	Non-plastic	0.007	2.97	0.100	0 - 21	32†	0 to 0.280
Polito and Martin (2001)	Monterey 0/30	0.311	1.55	Yatesville silt	0.031	4.38	0.100	0 - 25	32*	0 to 0.321
Polito, P.C. (1999)	Yalesville	0.089	2.39	Yatesville silt	0.031	4.38	0.348	0 - 37	37*	0 to 0.502
Thevanayagam and Martin (2002)	OS00 #55	0.160	1.69	Sil-co-sil #40	0.010	7.50	0.063	0 - 25	36*	0 to 0.280

* Obtained from source data following the procedure describe in section 4.4.1

† Calculated value from Equation 4.1

$^{\otimes}$ *b*-value depends on fines content

4.5.1 *Steady State Behaviour from Monotonic Undrained Shearing*

The evaluation exercise was conducted on five data sets extracted from published literatures. A brief summary of these data sets is presented in Table 4. 2. The RMSD value of SS data points for the trend line is compared with the RMSD value of Yang et al. (2006c) to assess whether the trend can be consider as single trend line.

Yang et al. (2006a) studied the influence of including Chengbei non-plastic silt in Hokksund sand, with fines content (FC) in the range of 0 to 30%. The SS data points as shown in Figure 4. 10a manifested significant spread as indicated by a half-spread value of 0.146. Furthermore, the SS data points moved downward with increase in FC. These data points were re-plotted in Figure 4. 10b using e^* in lieu of e (and with b calculated using the proposed Equation 4.2a). All the 18 data points can be described by a single trend curve as substantiated by a RMSD of 0.0172. Therefore, a single SSL independent of fines content by using equivalent granular void ratio as the state variable was obtained. The data was also analyzed with respect to intergranular void ratio, e_g, as defined in Equation 2.12. The corresponding SS data points as shown in Figure 4. 10c had a RMSD (measured now in e_g) is 0.073, which evidently is too high for a single correlation to be valid. The data points for FC = 30% fines appear to be a main contribution to the high scatter manifested in Figure 4. 10c. If only data points for FC in the range of 0 to 20% are used in the calculation, the RMSD based on e_g is reduced to about 0.041, which is still significantly higher than that in terms of e^*. This is consistent with the notion that e_g (defined by Equation 2.12) is an approximation of e^* (defined by Equation 4.2a) for low fines content.

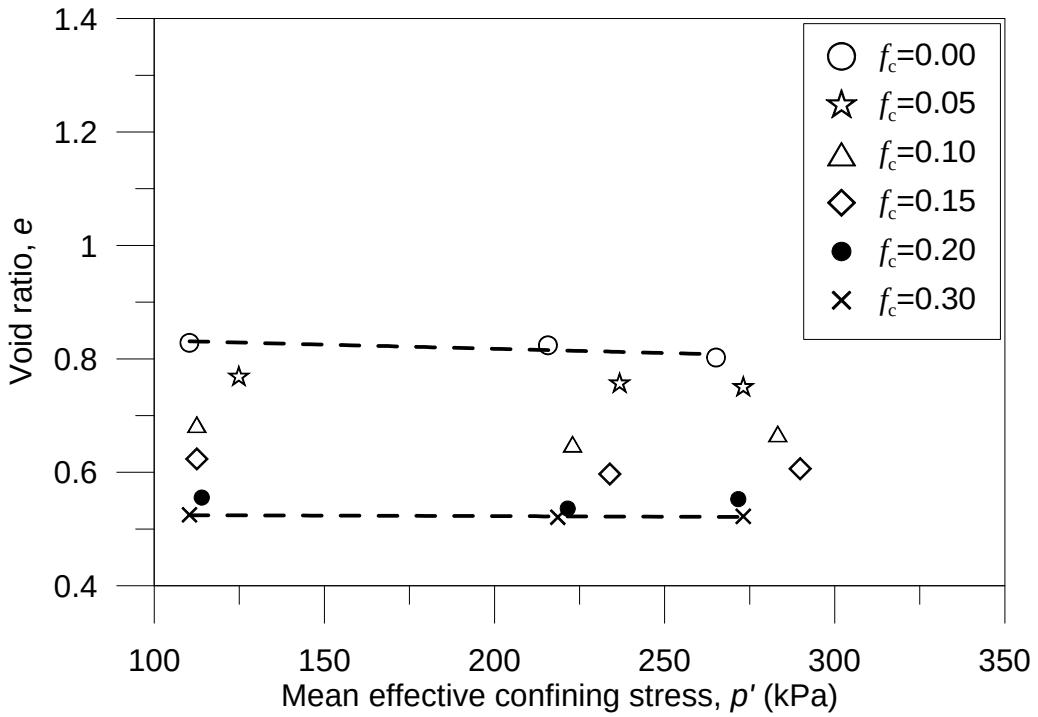

(a)

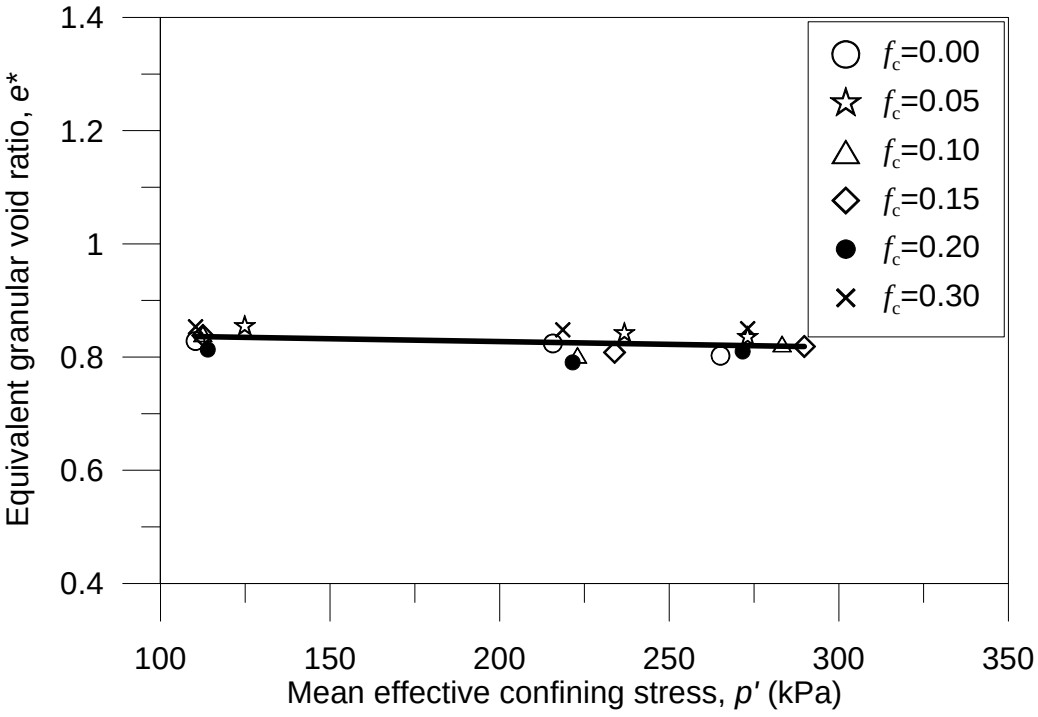

(b)

Figure 4. 10: **Steady state lines for Hokksund sand with Chengbei non-plastic fines; (a) source data after Yang et al. (2006a), (b) interpreted based on *e** using Equation. 4.2a and 2.14, (c) interpreted based on e_g using Equation 2.12.**

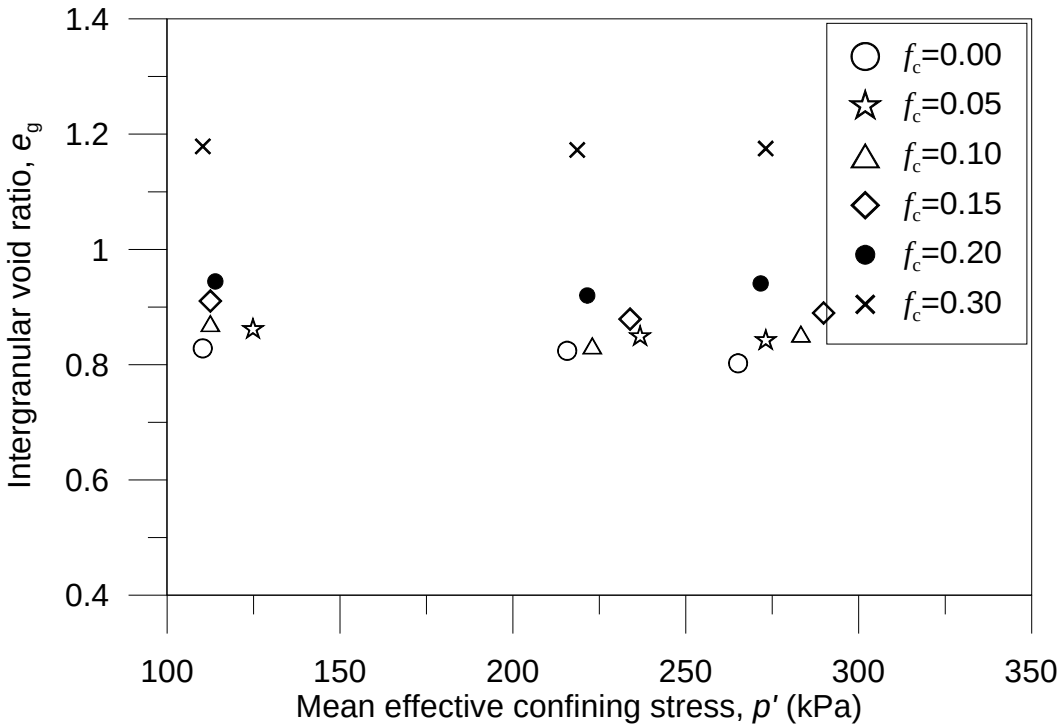

(c)

Figure 4. 10: Steady state lines for Hokksund sand with Chengbei non-plastic fines; (a) source data after Yang et al. (2006a), (b) interpreted based on *e using Equation. 4.2a and 2.14, (c) interpreted based on e_g using Equation 2.12.**

Huang et al. (2004) performed a series of laboratory tests on reconstituted sample of Mai Liao Sand (MLS) with silty fines from Central Western Taiwan. The SS source data points, with FC in the range of 0 to 30%, are shown in Figure 4. 11a. A significant and considerable spread is evident and the corresponding half-spread value of 0.131. These 26 data points plotted in the e^*-p' space (Figure 4. 11b) has a RMSD value of 0.0283, which is significantly less than the half-spread. Therefore, a single correlation between e^* (calculated using Equations 2.14 and 4.2a) and p' can be achieved.

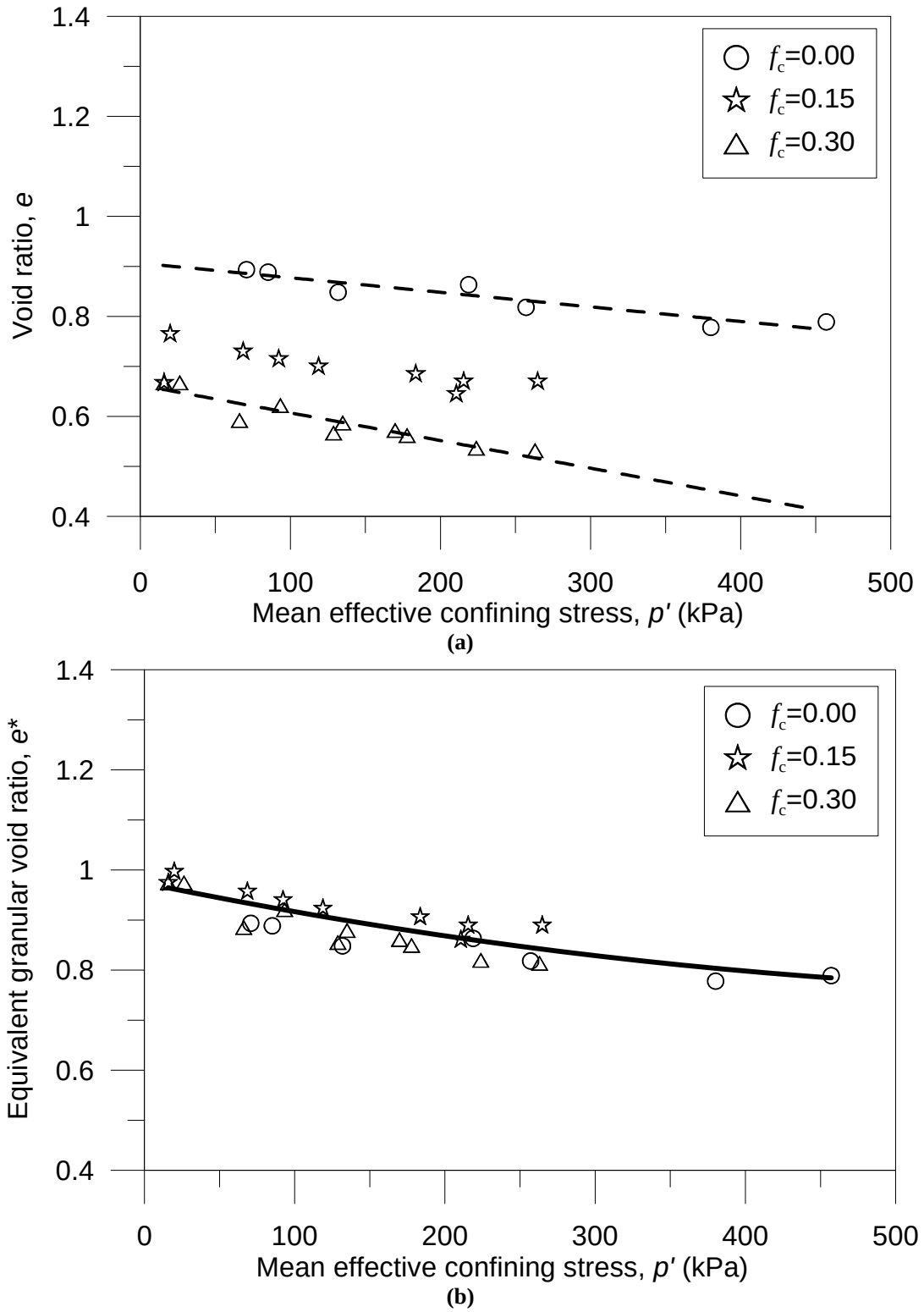

Figure 4. 11: **Steady state lines for Mai Liao sand with fines; (a) source data after Huang et al. (2004), (b) interpreted based on *e** using Equation 4.2a and 2.14.**

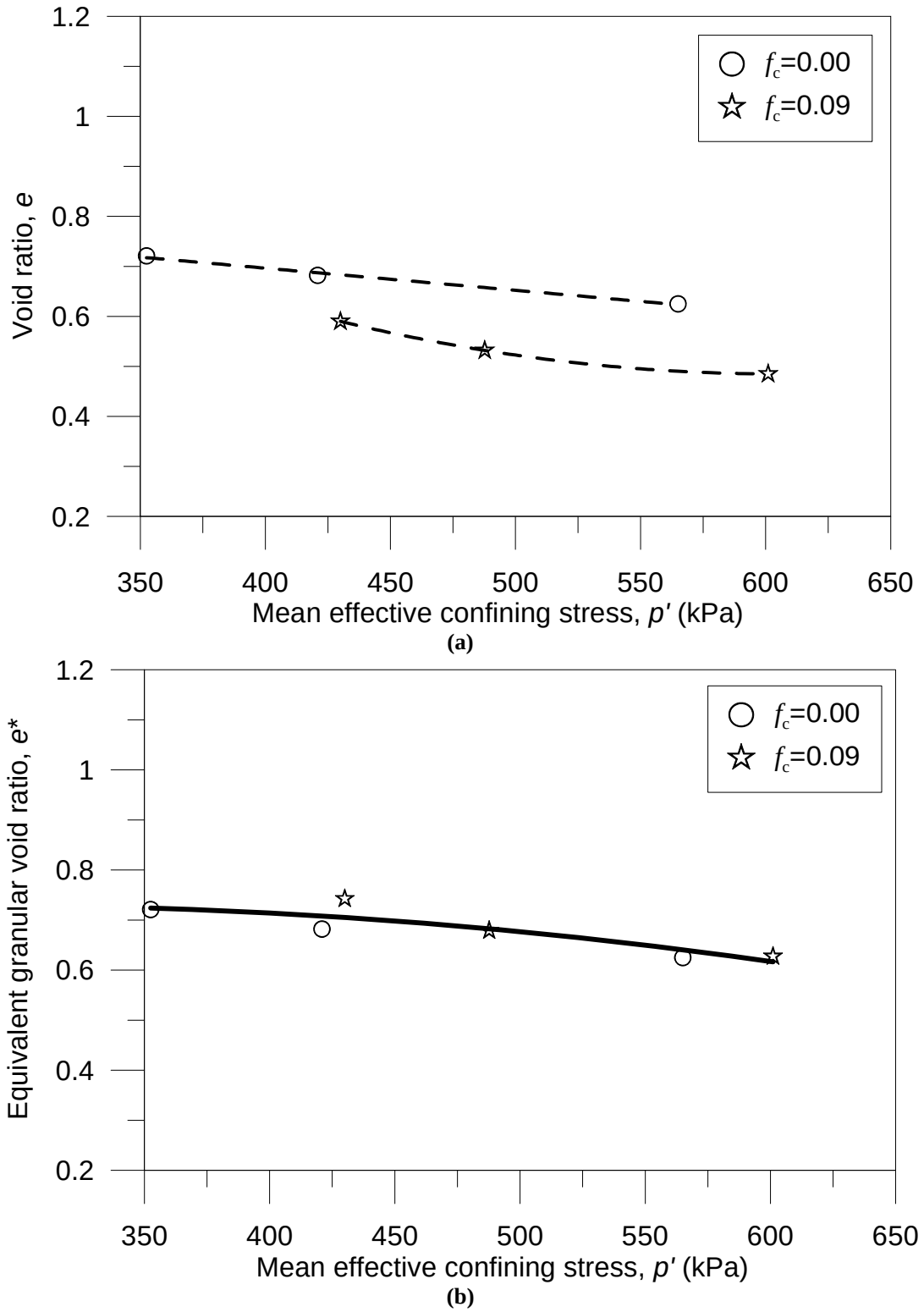

Figure 4. 12: **Steady state lines for Old Alluvium sand with fines; (a) source data after Ni et al. (2004), (b) interpreted based on e* using Equation 4.2a and 2.14.**

Ni et al. (2004) reported the influence of a non-plastic fines on Old Alluvium sand from Singapore. Their SS source data as shown in Figure 4. 12a had a half-spread of 0.062. However, if these data points were plotted in e^*-p' space as presented in Figure 4. 12b, these 6 data points followed essentially a single trend, with a small RMSD value of 0.017. It is interesting to note that Ni et al. (2004) selected $b = 0.7$ for calculating equivalent granular void ratio and also got a single trend line for all the SS data points. The prediction Equation 4.2a gives $b = 0.132$ for FC = 9%. This implies that multiple b-values can be obtained by targeting a unique correlation specific to data set. Indeed, the "fines-in-sand" model is not consistent with a high b-value of 0.70 at low fines content and high size ratio.

Zlatovic and Ishihara (1995) reported the influence of fines on Toyoura sand. The fines are milled Toyoura sand and FC is in the range of 0 to 30%. The SS source data points, as shown in Figure 4. 13a, manifested significant and considerable spread, as evidenced by a half-spread value of 0.201. If these 37 data points were plotted in the e^*-log(p') space as shown in Figure 4. 13b, the influence of fines content was significantly reduced as evidenced a RMSD value of 0.050 which might be consider as high for a single correlation. However, the RMSD value reduced to 0.0414 when $m = 0.20$ used in the Equation 4.2. This value is comparable with Yang et al. (2006c).

Thevanayagam et al. (2002b) presented SS data points for Foundary sand mixed with fines derived from crushed silica, and with FC in the range of 0 to 25%. The source SS data points in the e-log(p') space manifested significant spread (Figure 4. 14a) as evidenced by a half-spread value of 0.195. These 35 data points when plotted in the e^*-log(p') space (Figure 4. 14b), could be represented by a single SSL as evidenced by an RMSD value of 0.0274.

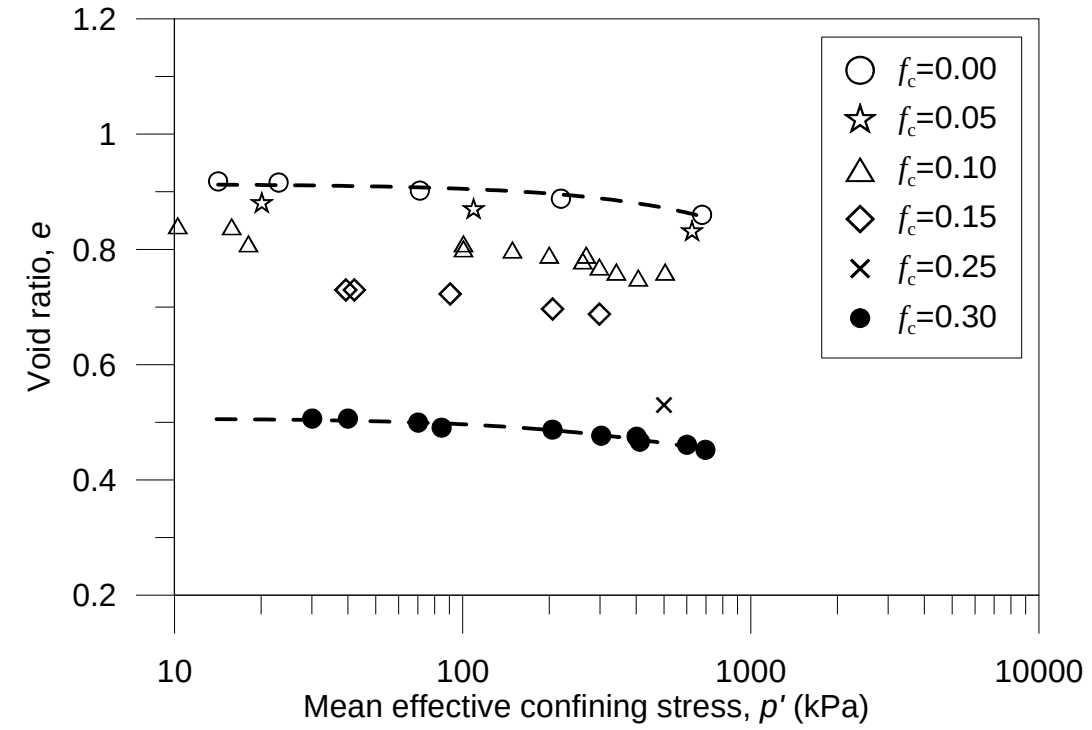

(a)

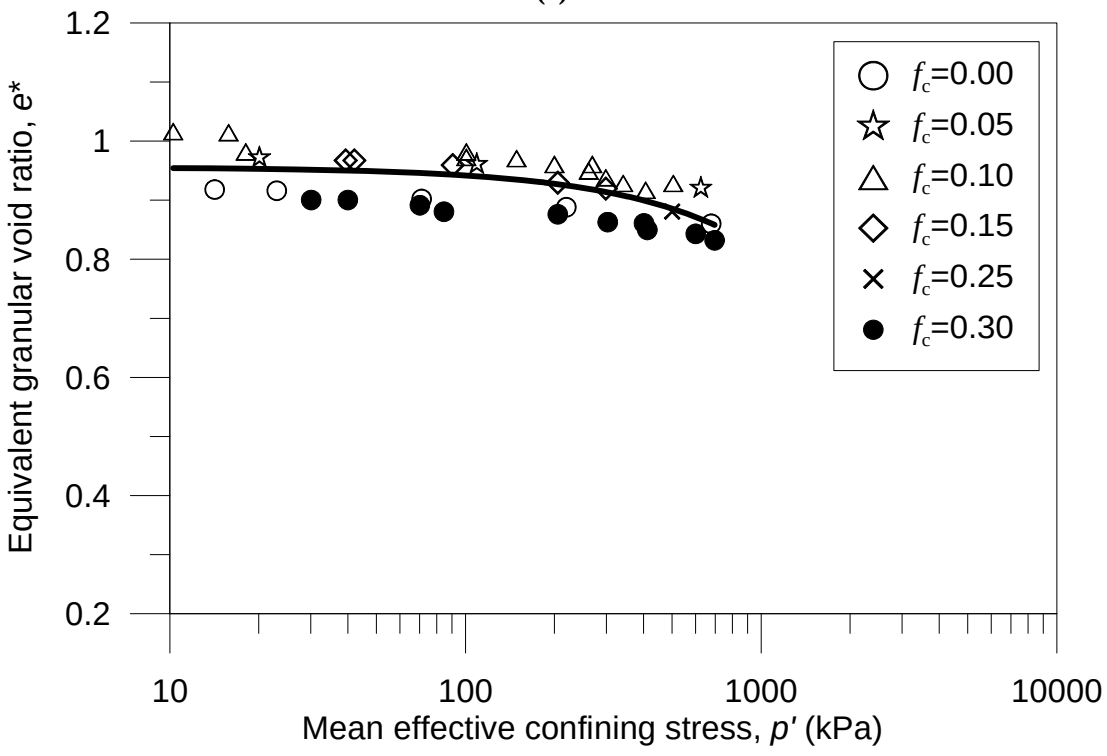

(b)

Figure 4. 13: Steady state lines for Toyoura sand with fines; (a) source data after Zlatovic and Ishihara (1995), (b) interpreted based on *e using Equation 4.2a and 2.14.**

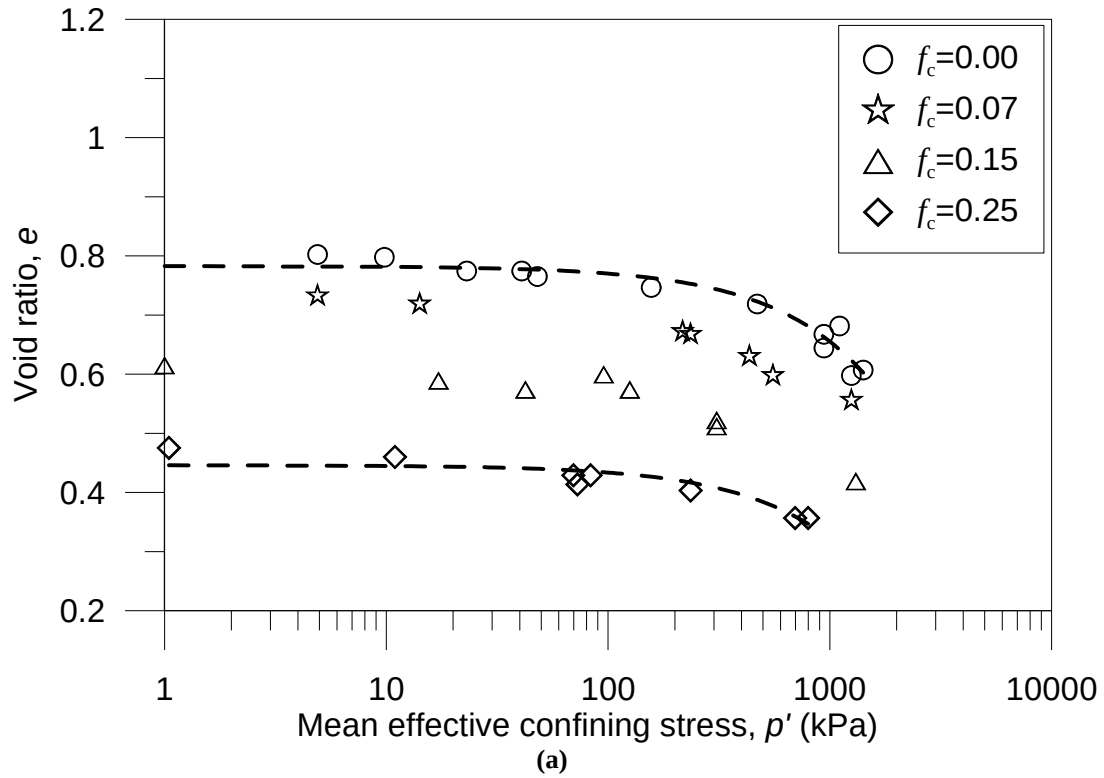

(a)

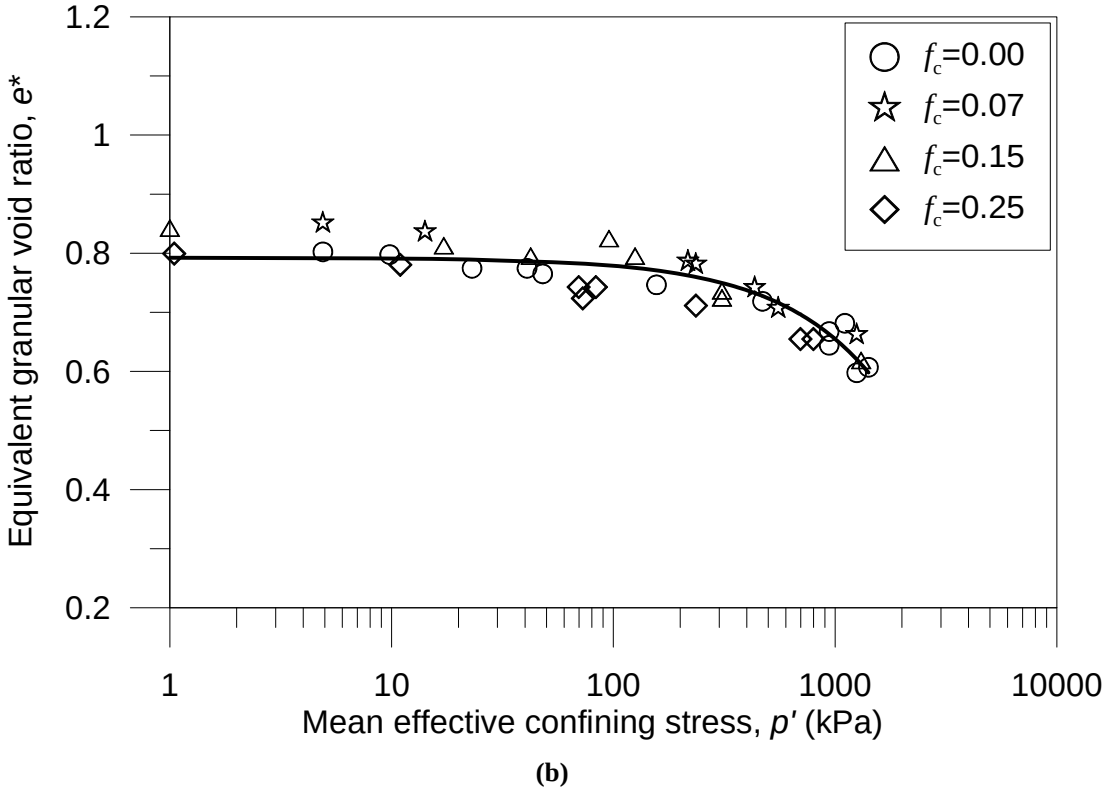

(b)

Figure 4. 14: **Steady state lines for Foundry sand with non-plastic fines; (a) source data after Thevanayagam et al. (2002b), (b) interpreted based on *e** using Equation 4.2a and 2.14.**

4.5.2 *Cyclic Mobility Behaviour*

This section investigate whether Cyclic Resistance (CR) as defined in Ishihara (1993) can be correlated to e^* in a manner that is approximately independent of fines content. This evaluation exercise was conducted on four data sets as summarized in Table 4. 2. It is pertinent to note that the last data set, as explained in a later paragraph, can only be used indirectly. Following the same argument presented for SS data points, the half-spread of the source data based on void ratio, e and the RMSD of the reduced data points based on equivalent granular void ratio, e^* were calculated to provide an objective basis for this investigation.

Vaid (1994) performed cyclic triaxial tests on Brenda 20/200 sand with non-plastic fines, and with FC ranges from 0 to 21%. Brenda sand is an angular tailing sand. As shown in Figure 4. 15a, the Cyclic Resistance versus void ratio relationship is dependent on FC, and the trend lines moves downward with increase in FC. These 13 source data points have a half-spread of 0.170. However, if these data points were re-plotted based on e^* (Figure 4. 15b), an essentially single correlation between e^* and CR , with a low RMSD of 0.0255, was obtained.

Polito and Martin (2001) preformed a series of cyclic triaxial tests on Monterey No. 0/30 sand with Yatesville fines. As shown in Figure 4. 16a, the Cyclic Resistance versus void ratio relationship is dependent on FC, and the trend lines moves downward with increase in FC. The half-spread of these source data is 0.156. However, if these 24 data points were re-plotted in terms of e^* as presented in Figure 4. 16b, a single correlation between e^* and CR was obtained as evidenced by a low RMSD value of 0.029.

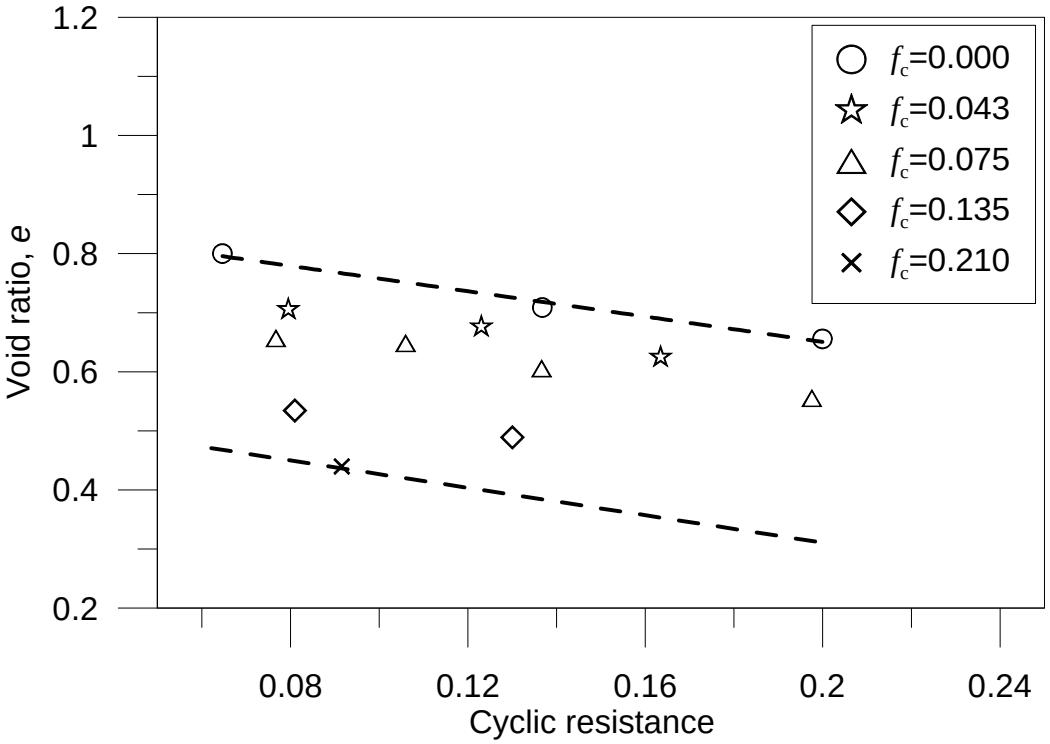

(a)

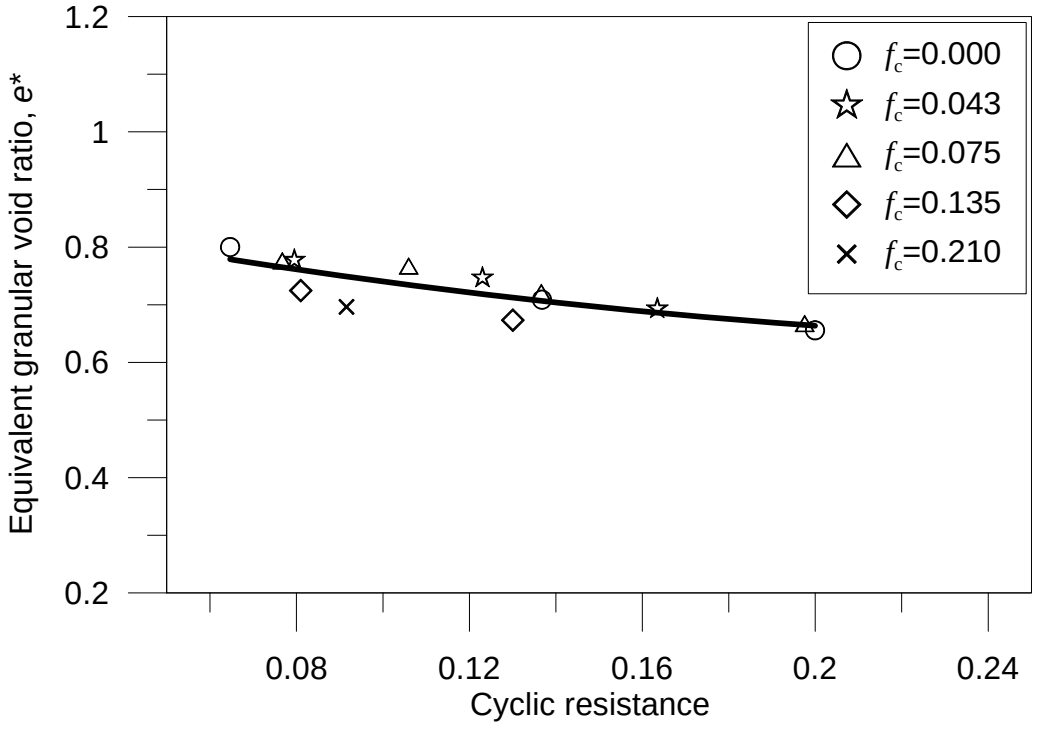

(b)

Figure 4. 15: Cyclic Resistance for 20/200 Brenda sand with silty fines; (a) source data after Vaid (1994), (b) interpreted based on *e using Equation 4.2a and 2.14.**

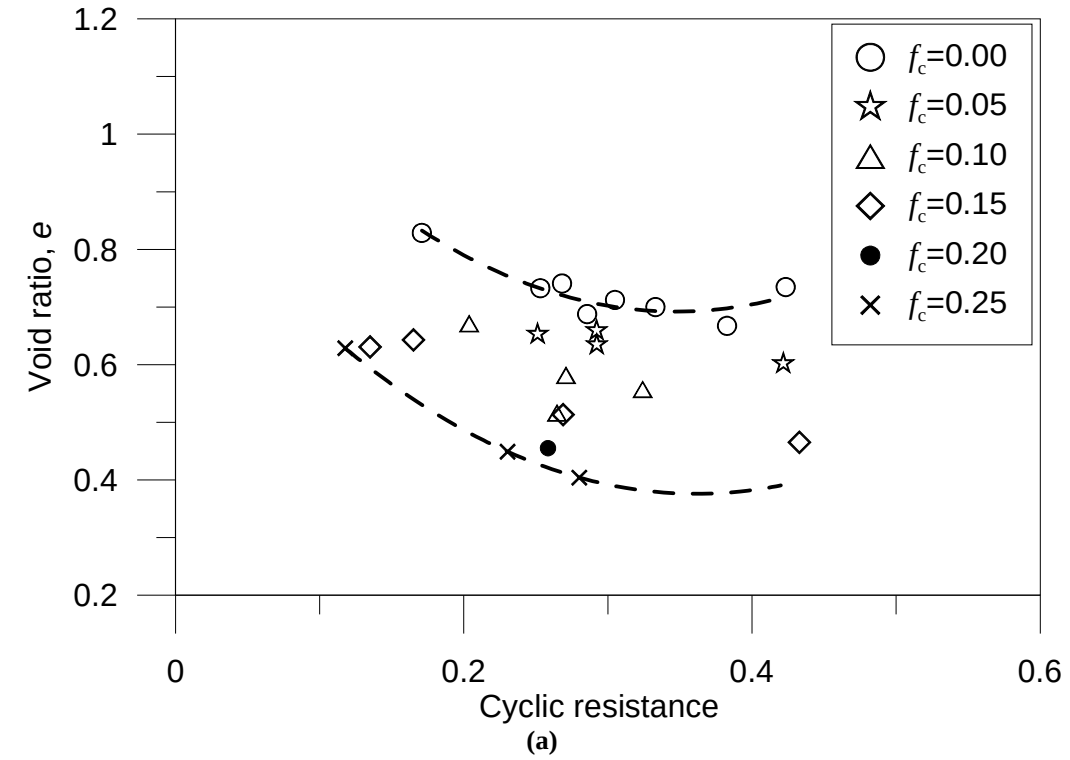

(a)

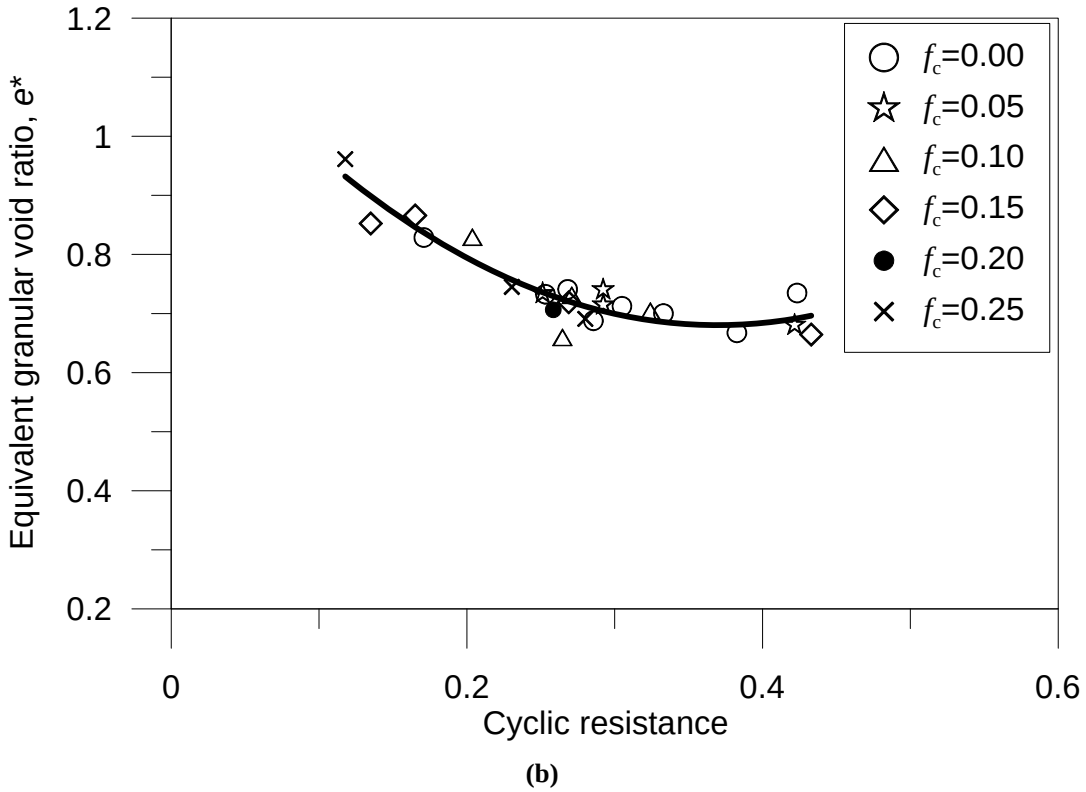

(b)

Figure 4. 16: **Cyclic resistance for Monterey sand and Yatesville fines; (a) source data after Polito and Martin (2001), (b) interpreted based on *e** using Equation 4.2a and 2.14.**

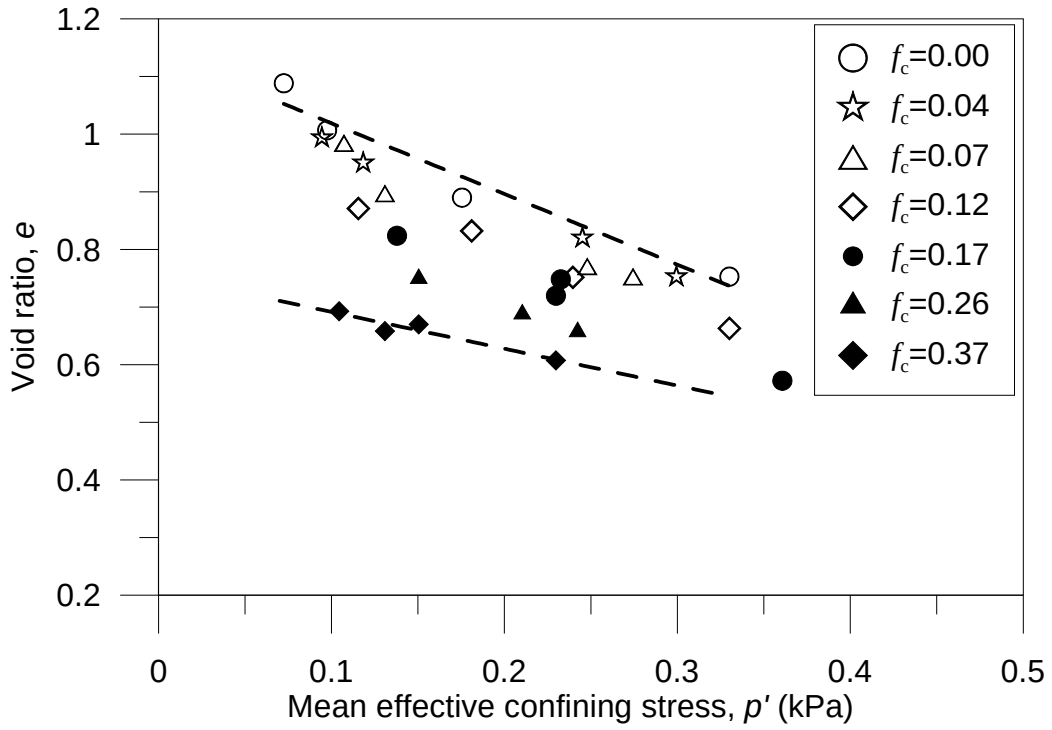

(a)

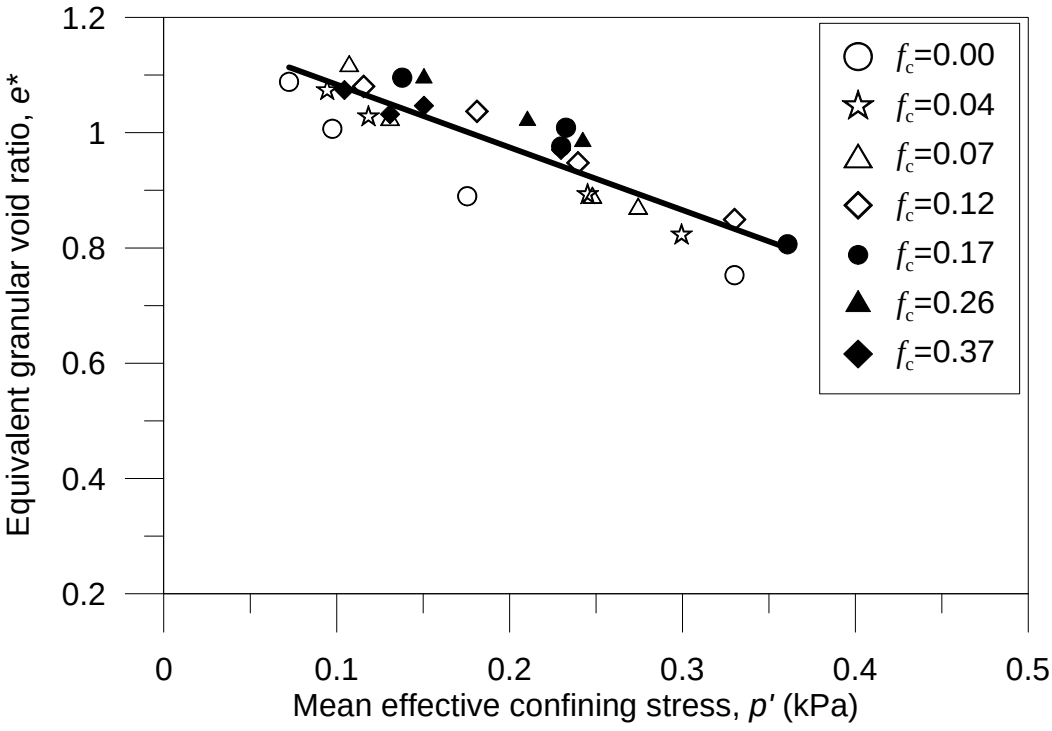

(b)

Figure 4. 17: Cyclic resistance for Yatesville sand with fines; (a) source data after Polito (1999), (b) interpreted based on *e using Equation 4.2a and 2.14.**

Polito (1999) preformed cyclic triaxial tests on Yatesville sand with Yatesville fines. Yatesville sand is a poorly graded, medium to fine sand obtained from a dam site in Louisa County, Kentucky. The fines was derived from the fine-grained portion of Yatesville silty sand. As shown in Figure 4. 17a, the Cyclic Resistance versus void ratio relationship was dependent on fines content, as evidenced by a high half-spread value of 0.148. Furthermore, the trend lines for the source data points moved downward with increase in FC. If these 28 data points were re-plotted using equivalent granular void ratio as the alternative state variable (Figure 4. 17b), the data points has a RMSD value of 0.0448 (about the "best-fit" correlation). Although this RMSD value may be considered as high, this value can be reduced to 0.0407 when m = 0.35 is used in Equation 4.2. Therefore, the influence of fines content on the correlation with cyclic resistance is significantly reduced if e^* is used as the alternative state variable.

Thevanayagam and Martin (2002) studied the effect of fines on liquefaction using Ottawa sand with non-plastic silt. N_L, the number of cycles required to achieve cyclic liquefaction at an imposed cyclic stress ratio of 0.20, were used as a parameter for studying the influence of fines. As such, N_L is only an indirect measure of Cyclic Resistance and this data set can only be used to investigate whether the influence of fines content can be significantly reduced by using e^* in lieu of e. As shown in Figure 4. 18a, these 30 source data points plotted in the e-N_L space manifested considerable spread and scatter. The half-spread of the source data is 0.138. However, if the data was re-plotted in the e^*-N_L space, the resultant RMSD was 0.045 which showed the influence of FC was significantly reduced via the use of e^* (Figure 4. 18).

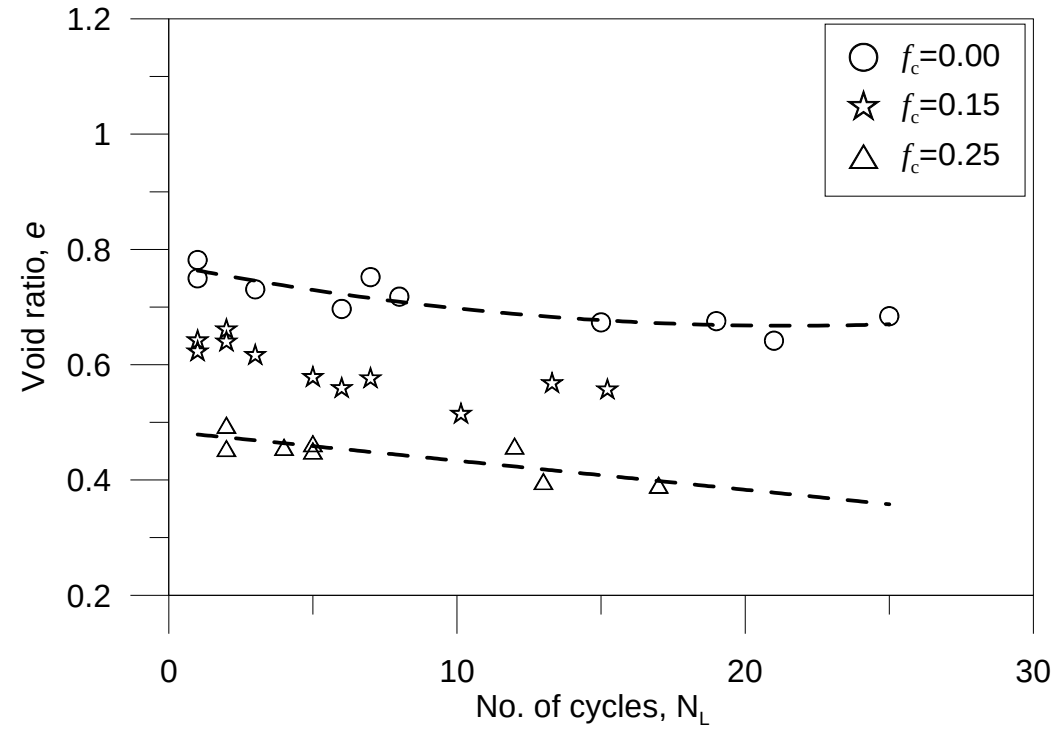

(a)

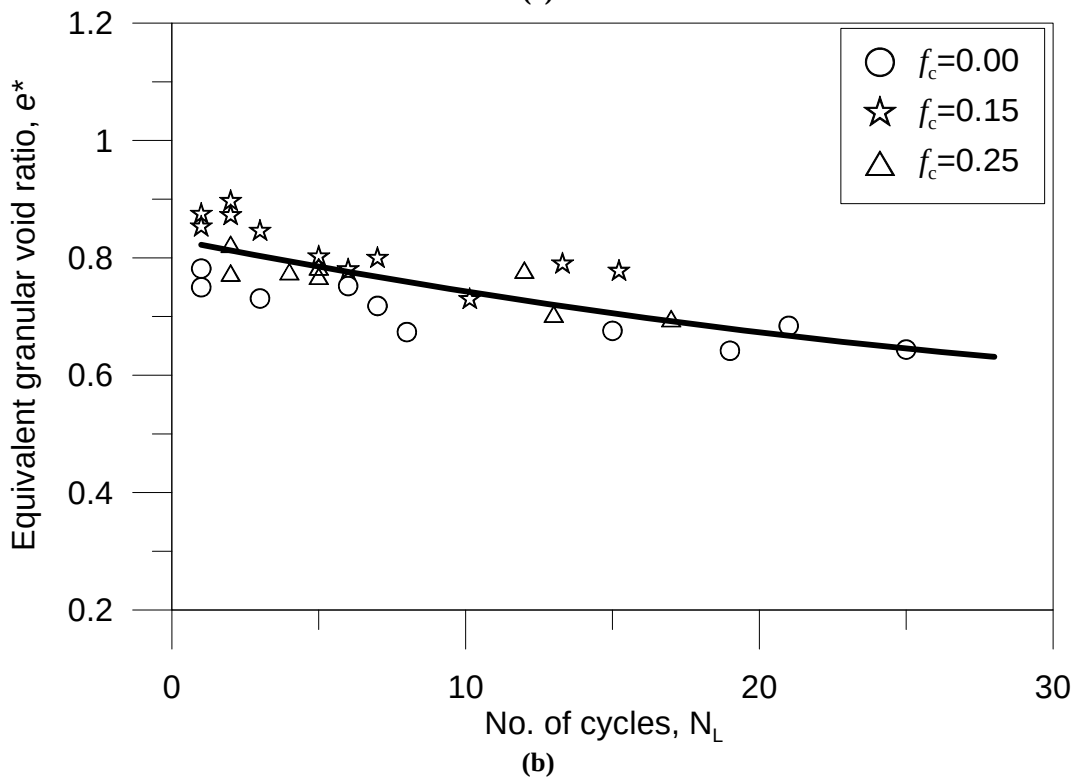

(b)

Figure 4. 18: **No. of cycles (NL) required to trigger cyclic liquefaction for Ottawa sand with non-plastic fines at cyclic stress ratio of 0.20; (a) source data after Thevanayagam and Martin (2002), (b) interpreted based on *e** using Equation 4.2a and 2.14.**

4.5.3 *Discussion*

A total of nine data sets were examined. Six of which could be described by a single correlation in terms of e^*, and this was evidenced by RMSD values less than 0.028. The scatter manifested by the remaining data sets deserves further discussion. The SS data set of Zlatovic and Ishihara (1995), when analyzed in term of e^*, gave a RMSD value in the range of 0.050 to 0.041, depending on the value of m in Equation 4.2 This range is comparable to the RMSD value of data points described by Yang et al (2006c) as could be represented by a single trend line. The remaining 2 data sets (Figure 4. 17b and Figure 4. 18b), when analyzed in terms of e^*, had RMSD values of 0.045; and a single correlation in terms of e^* can only be assumed as a first approximation. However, this RMSD value is still significantly less than the half-spread of the source data, and thus the influence of fines contents is significantly reduced if e^* is used as the alternative state variable.

Differentiation of Equation 2.14 with respect to b also showed that e^* calculated with Equation 4.2a is sensitive to the predicted b-value. Therefore, the exercise undertaken in this section provides a stringent evaluation of the proposed concept.

It needs to be re-iterated that Equation 2.14 implies that e^* may be approximated by e_g (calculated with b=0) at low fines content and therefore, the significance of predicting a b-value (by Equation 4.2a) is only of significance for higher fines content. However, having the same framework for the whole spectrum of fines content that satisfy the “fines-in-sand” model is an essential objective of this chapter, in particular in relation to the application of Critical State Soil Mechanics framework as presented in the next chapter.

4.5.4 *Variation of m between Different Data Sets*

A different value of *m* can be observed for a different data set by following the same procedure discussed in section 4.4.3. Thus, a study has been done on the variation of *m* for different data sets in this section. Exactly same procedure was followed, but only in some cases the TFC had to be determined by Equation 4.1 where enough data was not available to follow the procedure in section 4.4.1. The Table 4. 3 shows that most of the data shows a single relation.

Table 4. 3 Variation of the calibrated *m* for different data sets

Data Source	Calibrated *m*	
	m	RMSD
Yang et al. (2006a)	0.31	0.0168
Huang et al. (2004)	0.30	0.0283
Ni et al. (2004)	0.25	0.0171
Zlatovic and Ishihara (1995)	0.20	0.0414
Thevanayagam et al. (2002b)	0.30	0.0274
Vaid (1994)	0.20	0.0200
Polito and Martin (2001)	0.28	0.0288
Polito (1999)	0.35	0.0407
Thevanayagam and Martin (2002)	0.35	0.0440

The table shows that the calibrated *m* varies from 0.20 to 0.35. However, the value obtain from Thevanayagam et al. (2002b) data set, $m = 0.30$ which is very close to average value (≈ 0.28) was used in Equation 4.2a. The statistical measure, root-mean-square-deviation, RMSD was used for sensitivity analysis between calibrated *m* and $m = 0.30$. It was done in two steps; First, a constant $m = 0.30$ was used in the Equation

4.2 and the RMSD was calculated with best fit trend for all data sets. Second, the obtain data is then compared with calibrated *m* that found for least RMSD for each data set. A comparison of RMSD is presented in Table 4. 4.

Table 4. 4 Sensitivity of *m* over all data sets

Data Source	Constant $m = 0.30$	Calibrated *m*	
	RMSD	*m*	RMSD
Yang et al. (2006a)	0.0172	0.31	0.0168
Huang et al. (2004)	0.0283	0.30	0.0283
Ni et al. (2004)	0.0173	0.25	0.0171
Zlatovic and Ishihara (1995)	0.0505	0.20	0.0414
Thevanayagam et al. (2002b)	0.0274	0.30	0.0274
Vaid (1994)	0.0255	0.20	0.0200
Polito and Martin (2001)	0.0293	0.28	0.0288
Polito (1999)	0.0448	0.35	0.0407
Thevanayagam and Martin (2002)	0.0450	0.35	0.0440

4.6 SUMMARY

The main focus of this chapter was to develop a prediction formula for *b* which is required in the calculation of equivalent granular void ratio. The concept of equivalent granular void ratio, e^* as defined by Equation 2.14 is only valid for "fines in sand" model, and this is only applicable when the fines contents are less than an upper limit referred to as threshold fines content, TFC. This parameter is also an input parameter in Equation 4.2a for predicting *b*. Considering the importance of TFC, a standard way to determine TFC is presented and, a prediction formula is developed.

A generalize functional relationship, $b = f(\chi, f_c)$ is developed. This function requires one calibration parameter, *m*. A detail calibration study shows that the calibration parameter *m* can be approximately assigned by a constant value of 0.30 for all data sets. However, the correlation of individual data sets can be improved by having *m* specific to individual data set.

A detail evaluation study has been done with nine data sets from six countries around the world. Three out of nine data sets showed a little scatter around the trend line. However, these data sets shows a good correlation (compared with Yang et al. (2006c)) when calibration is done by individual data sets.

It worth noting that the data sets used in the evaluation exercise are extracted data from previous studies. The original objectives of most these of studies are different from our objective and thus the accuracy of these data are not optimize for our purpose. This might introduce additional scatter in the correlation.

CHAPTER 5

Equivalent Granular Steady State Line

5.1 INTRODUCTION

In general, the SSL for a sand with a particular fines content can be used to predict the undrained behaviours within CSSM framework. However, the steady state, SS data points for sand with fines are dependent on fines content. Therefore, extensive amount of testing and time will be needed to establish a family of SS data points for a range of fines content.

It has been discussed in previous chapter, how Steady State, SS data points for sand with different fines contents can be described by a single trend in e^*-log(p') space irrespective of fines contents provided f_c < TFC. This single trend is referred to as Equivalent Granular Steady State Line, EG-SSL, in the previous chapter. Now, the issue is whether the EG-SSL can be used to predict undrained behaviours of sand with fines irrespective to fines contents within CSSM framework.

5.2 CONCEPTUAL FRAMEWORK OF EG-SSL

It is discussed in the previous chapter that the concept of equivalent granular void ratio, e^* was supported on the observation that sand and sand with fines ($f_c \leq$ TFC) may have a single steady state line in e^*-log(p') space. In the determination of equivalent granular void ratio e^*, many researchers back analyzed the parameter, *b*

based on the criteria of achieving a single steady state line (Ni et al. 2004; Ni et al. 2005; Thevanayagam 1999; Thevanayagam 2000; Yang et al. 2006a; Yang et al. 2006b; Yang et al. 2006c). It was also shown in Chapter 4 that *b* can be predicted by a formula that depends on only three input parameters: particles diameter ratio, χ, percentage of fines, f_c and threshold fines content, TFC. The validity of the prediction formula was also justified by a single steady state line i.e. EG-SSL both for sand and sand with fines. As such, the *b*-value may be considered as being based on the assumption of a single EG-SSL. Thus, this is a desirable condition for developing a prediction formula for *b* and the concept of EG-SSL. However, achieving a single EG-SSL does not guarantee that it can be used to predict the behaviour of sand with fines within CSSM framework. If the EG-SSL can function as an "alternate SSL" within the CSSM framework, then it should fulfill the followings:

- First, all SS data points for sand with fines must come to a single trend i.e. the EG-SSL irrespective to their fines contents.

- The EG-SSL can be used in conjunction with initial state in e^*-log(p') space to predict the overall undrained behaviour i.e. flow or limited flow or non-flow.

- One can define an equivalent granular state parameter (as discussed in section 5.4.3) relative to the EG-SSL to predict/evaluate undrained responses of sand with fines in terms of effective stress path, ESP and deviator stress-strain behaviour.

5.3 EXPERIMENTAL INVESTIGATION

It is noted during literature review that there is lack of detailed published data that can be used for the evaluation of EG-SSL within CSSM framework. The only publication available to the author at the time of drafting this thesis is the work of Thevanayagam and Mohan (2000) which does not provide all necessary information and, assumptions need to be made for the evaluation as discussed in section 5.5.

To provide reliable data for a comprehensive evaluation of whether the EG-SSL can use for predicting behaviour pattern within the framework of CSSM, an experimental program was designed. This experimental program also overcomes the following limitations of published studies:

- The fines are mostly non-plastic and only few publications have been found with plastic fines (Ni et al. 2004; Thevanayagam and Mohan 2000). However, those data had not been evaluated within CSSM framework.

- The fines had a relatively low uniformity coefficient: an average value of 4.82 and a maximum value of 7.50 (Thevanayagam et al. 2002b). The effect of higher uniformity coefficient of fines has not been investigated.

A fines referred to as MII fines is designed in such a way so that it has low-plasticity (PI = 27) and a higher uniformity coefficient of 12.56. The details of material properties and the improved experimental technique for accurate measurement of void ratio are given in Chapter 3. The data obtained from the experimental program is then used to evaluate the predictive ability of EG-SSL within the CSSM frame works.

The testing program is given in Table 5. 1. A name convention has been adopted to identify a particular test and the testing condition. An example of such name is S-MII-XX-YY. The first letter in the name convention indicates the type of sand; in this case it is "S" for Sydney sand. "MII" indicates MII fines; "XX" indicates the percentage of fines and "YY" is the tests number.

The testing program covers; i) a wide range of fines content: from 0 to 50%, ii) a wide range of confining pressure: from 100kPa to 1300kPa and iii) a wide range of void ratio at the end of consolidation: from 0.455 to 0.886. At the end of the test most of the samples reached the Steady State, SS. This is because of extreme care and advanced techniques applied during sample preparation as explained in details in Chapter 3. Only a few samples didn't reach to the Steady State, SS and they are denoted by superscript (^{N}) in Table 5. 1. In such a case, the steady state was obtained by following the extrapolation method proposed by Murthy et al. (2007).

Table 5. 1 Summary of triaxial tests, continue

Test Name	Fines Content, (%)	*b*-value	p'_0 (kPa)	$e_{(0)}$	$e^*_{(0)}$	$\psi^*_{(0)}$	p'_{SS} (kPa)	Observed behaviour
S-MII-00-04	00	0.000	350	0.864	0.864	0.020	139.0	LF
S-MII-00-05	00		350	0.851	0.851	0.007	311.5	LF
S-MII-00-06	00		350	0.743	0.743	-0.100	1216.0	NF
S-MII-00-07	00		600	0.850	0.850	0.035	350.0	LF
S-MII-00-08*	00		600	0.852	0.852	0.037	213.7	F
S-MII-00-09^N	00		600	0.735	0.735	-0.080	760.0	NF
S-MII-00-10	00		850	0.886	0.886	0.097	150.0	F
S-MII-00-11	00		850	0.848	0.848	0.059	220.9	F
S-MII-15-01^N	15	0.150	100	0.617	0.853	-0.029	110.0	NF
S-MII-15-02	15		350	0.658	0.900	0.056	9.9	F
S-MII-15-03	15		600	0.655	0.896	0.081	36.5	F
S-MII-15-04	15		600	0.623	0.860	0.045	87.3	F
S-MII-15-05	15		600	0.628	0.866	0.051	120.4	F
S-MII-15-06^N	15		600	0.535	0.759	-0.056	1140	NF
S-MII-15-07^N	15		600	0.588	0.819	0.004	431.2	LF
S-MII-15-08	15		850	0.647	0.887	0.098	71.5	F
S-MII-15-09	15		1100	0.645	0.885	0.119	119.5	F
S-MII-15-10	15		1300	0.569	0.797	0.050	901.5	LF

*** The test consider as "F" though they shows a transition behavior between "F" and "LF"**

Table 5. 1 Summary of triaxial tests, continue

Test Name	Fines Content, (%)	*b*-value	p'_0 (kPa)	$e_{(0)}$	$e^*_{(0)}$	$\psi^*_{(0)}$	p'_{SS} (kPa)	Observed behaviour
S-MII-20-01	20	0.200	350	0.588	0.892	0.048	26.9	F
S-MII-20-02	20		600	0.573	0.874	0.059	69.7	F
S-MII-20-03	20		850	0.576	0.877	0.088	124.9	F
S-MII-20-04	20		1100	0.560	0.858	0.092	132.5	F
S-MII-30-01	30	0.280	350	0.611	0.926	0.082	68.3	F
S-MII-30-02	30		600	0.485	0.893	0.078	138.8	F
S-MII-30-03	30		850	0.460	0.861	0.072	197.3	F
S-MII-30-04	30		1100	0.455	0.855	0.089	318.6	F
S-MII-50-01	50	┆	600	0.508	---	---	313.0	F

where, p'_0 = Initial mean effective stress, at the end of consolidation,

$e_{(0)}$ = Void ratio at the end of consolidation,

$e^*_{(0)}$= Equivalent granular void ratio at the end of consolidation,

$\psi^*_{(0)}$= Equivalent granular state parameter at the end of consolidation,

p'_{SS} = Mean effective stress at steady state

F = Flow,

LF = Limited Flow,

NF = Non-Flow.

5.4 EVALUATION OF EG-SSL CONCEPT

The evaluation of the EG-SSL for Sydney sand with fines in e^*-log(p') space as an "alternate SSL" within CSSM framework are done in 3 steps. The steps are followings:

- The EG-SSL for Sydney sand with fines are verified whether a single trend can be achieved with equation 4.2a and 2.14 in e^*- log(p') space.
- The correlation between EG-SSL and the overall undrained behaviour patterns (i.e. F, NF, LF) within CSSM framework are evaluated in second step.
- Then, an equivalent granular state parameter based on EG-SSL is introduced as discussed in section 5.4.3. This equivalent granular state parameter is then used to predict the patterns of undrained effective stress, ESP, and deviatoric stress-strain responses.

5.4.1 *EG-SSL for Sydney Sand with Fines*

Following the procedure in Chapter 4, the variation of e_{SS} at 300 kPa with f_c is plotted in Figure 5. 1 and a TFC of 39% was obtained. e_{300} was used instead of e_{100} because only one SS data point for 50% fines content obtained at round 300kPa. However, it is shown in Chapter 4 that TFC does not very much from e_{100} to e_{300}.

The TFC is also calculated with the prediction Equation 4.1 which gives a TFC of 40.17%. These two different methods give nearly same TFC (≈ 40%). Therefore, TFC = 40% is use to predict b values with Equation 2.14, which in turn enables the conversion of e to gave e^* for the range of fines contents.

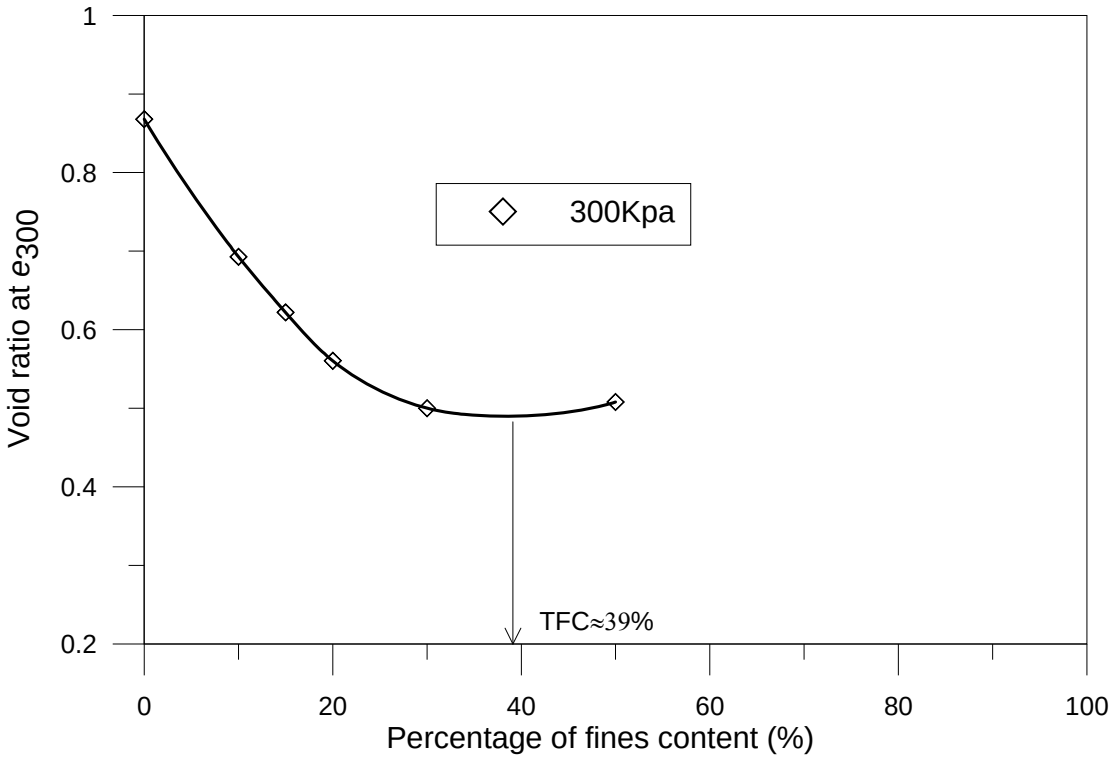

Figure 5. 1: Threshold fines content, TFC for Sydney sand with fines

This enabled, plotting of the SS data points in the e^*-log(p') space as shown in Figure 5. 2b. Evidently, all SS data points in e^*-log(p') space followed a single trend i.e. a single EG-SSL was obtained.

However, this EG-SSL is not a straight line rather a curve which is consistent with many publications (Bobei and Lo 2005; Rahman and Lo 2007; Wang et al. 2002). Thus, the curvature should be born in mind though it is usually referred to as line (as discussed in Chapter 2). These data points can be presented by a quadratic function presented as Equation 5. 1 below:

$$e = 1\times10^{-7}\times(p')^2 - 0.0003\times p' + 0.9601 \qquad \textbf{5. 1}$$

where, p' is mean effective stress at SS. It gives a very good fit with a RMSD of 0.024. Alternatively one can also use a power function (Wang et al. (2002)):

$$e^* = 0.908 - 0.0266 \times \left(\frac{p'}{p_a} \right)^{0.7} \qquad \textbf{5. 2}$$

It also gives a good fit with a RMSD of 0.019. The power function is preferred as the shape of the curve does not change with extrapolation to higher mean effective stress. It is noted, the spread of the family of SSLs for Sydney sand with 0-30% fines in *e*-log(p') space was about 0.20 which is large relative to RMSD of EG-SSL. Thus, the concept of a single equivalent granular steady state line, EG-SSL, is valid for Sydney sand with fines.

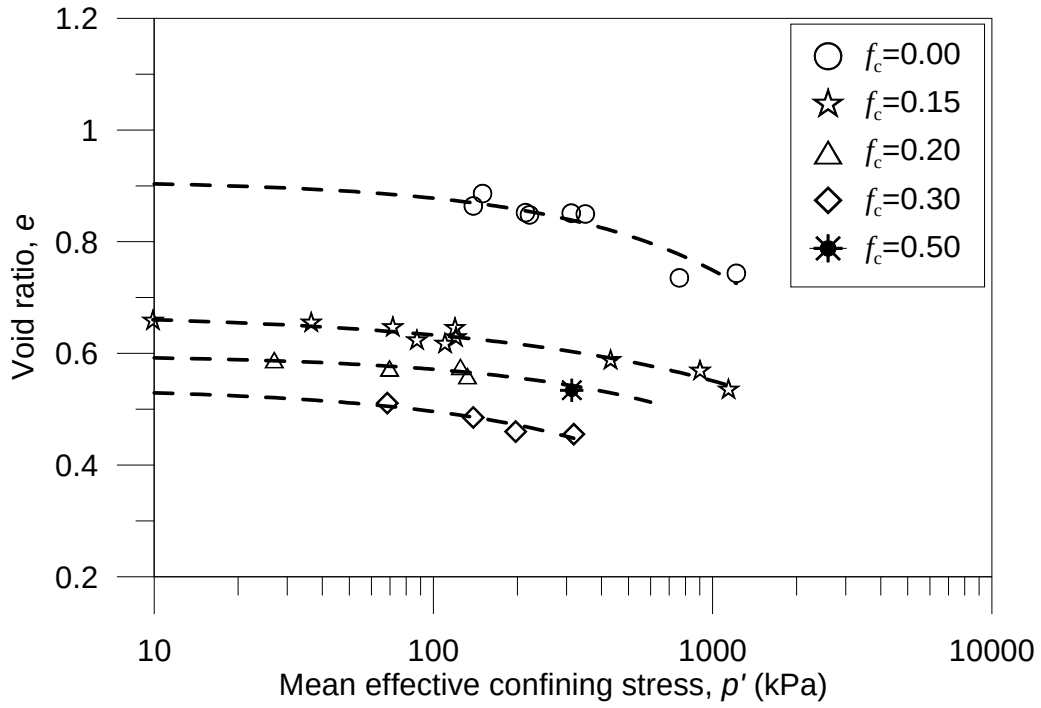

(a)

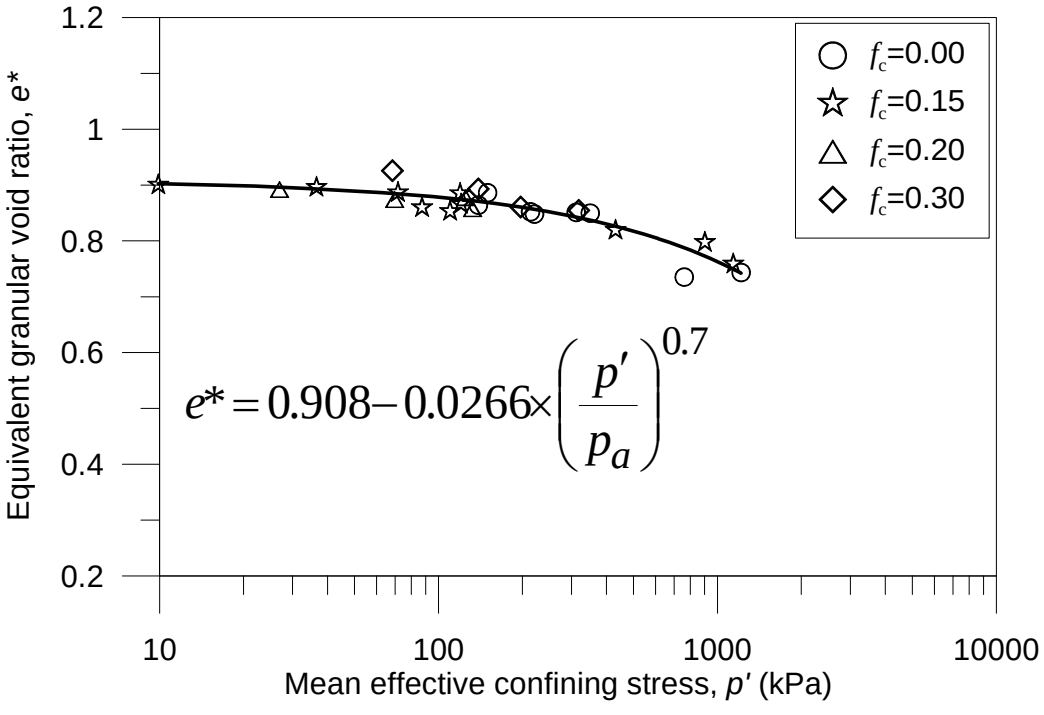

(b)

Figure 5. 2: **Effect of fines on SS data points for sand with fines, (a) Effect of fines on SS data points in *e*-log(*p′*) space, (b) A single EG-SSL for sand with fines in *e**-log(*p′*) space**

5.4.2 *Overall Evaluation of EG-SSL within CSSM framework*

5.4.2.1 Preliminary Investigation

Prior to a detailed evaluation of whether the proposed EG-SSL line can be used as an "alternate SSL" in context of CSSM framework, a preliminary evaluation exercise was done on Sydney sand with 15% fines. For this purpose, two tests were designed in such a way that, according to the CSSM framework, one exhibit non-flow and the other limited-flow behaviours. Replication of soil fabric of these two samples was ensured by the following procedure:

- These two samples were prepared by same sample preparation method and same amount of material. Thus, nearly same void ratios were achieved at the beginning of consolidation.

- Essentially same consolidation curves were achieved during consolidation as shown in Figure 5. 3. This also ensured same fabric at the end of consolidation.

The two tests were S-MII-15-01 and S-MII-15-07. The state of test S-MII-15-01 at the end of consolidation at 100kPa was below the SSL and the state of test S-MII-15-07 was on the SSL at the end of consolidation at 600 kPa as shown in Figure 5. 3. Note that there were enough SS data points to define SSL for Sydney sand with 15% fines. According to the CSSM, the test S-MII-15-01 should show non-flow behaviour and the test S-MII-15-07 should show limited flow behaviour. In Figure 5. 5, it is found that S-MII-15-01 exhibits non-flow behaviour and S-MII-15-07 exhibits limited flow behaviour. Thus, their behaviours are consistent with conventional SSL within CSSM framework.

However, if EG-SSL is applicable within the CSSM framework, then the initial states of these two tests before shear relative to the EG-SSL in e^*-log(p') space, should be the same as those for conventional SSL. Note that this verification condition is very stringent as the initial states just located above and below the conventional SSL Figure 5. 4 shows that their initial states relative to the EG-SSL are consistent with CSSM framework i.e. at the end of consolidation test S-MII-15-01 was below the EG-SSL and the test S-MII-15-07 should be slightly above the EG-SSL. It gives an indication that EG-SSL can be used as an "alternate SSL" for sand with fines.

5.4.2.2 Prediction of F, NF and LF behaviour for all tests

The above illustration only provides a preliminary evaluation for 15% fines content. In order to evaluate for sand with a wide range of $f_c \leq$ TFC, the initial state (i.e. just prior to shearing) of each tests and the EG-SSL in e^*-log(p') space are plotted in Figure 5. 6. It shows all tests with flow behaviour are well above the EG-SSL and tests with non-flow behaviour are well below the EG-SSL. Several tests with initial state around the EG-SSL show limited-flow behaviour. It should be noted that the test results showing 'flow', 'limited flow' or 'non-flow' are presented in later this chapter, thus they are not included in this section. This gives over all verification that the EG-SSL, in conjunction with the initial states in e^*-log(p') space, can be used within the CSSM framework in predicting the overall undrained behaviour patterns. The next step is to extend the concept of state parameter to equivalent granular state parameter as discussed in next section.

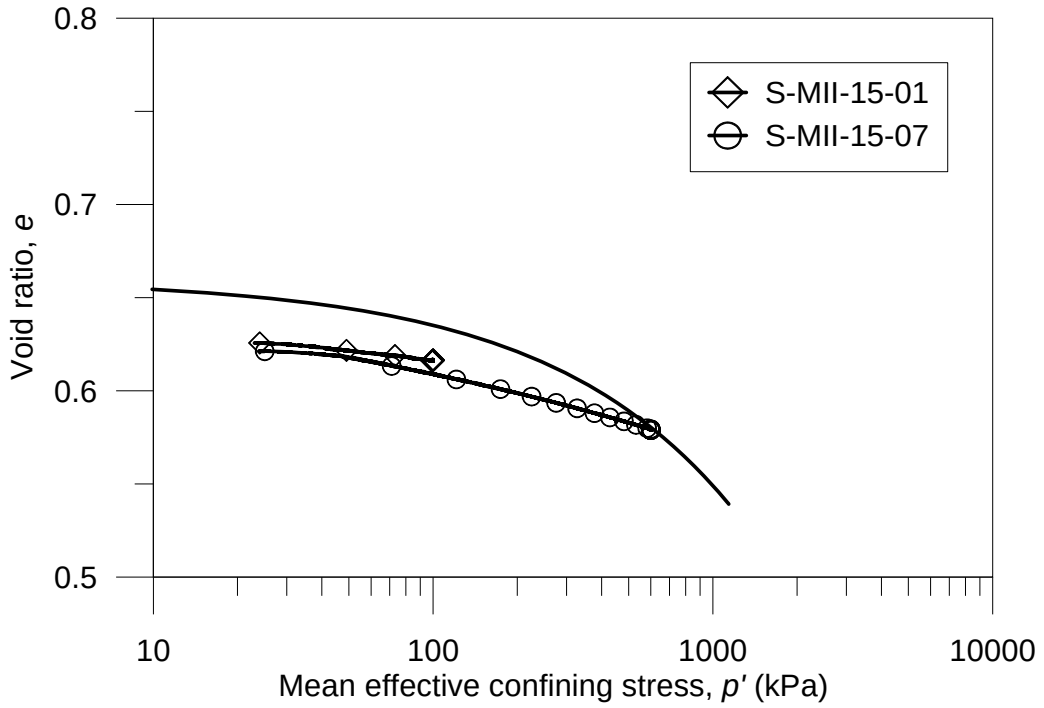

Figure 5. 3: **SSL for Sydney sand with 15% MII fines and consolidation curve of two special tests in *e*-log(*p′*) space**

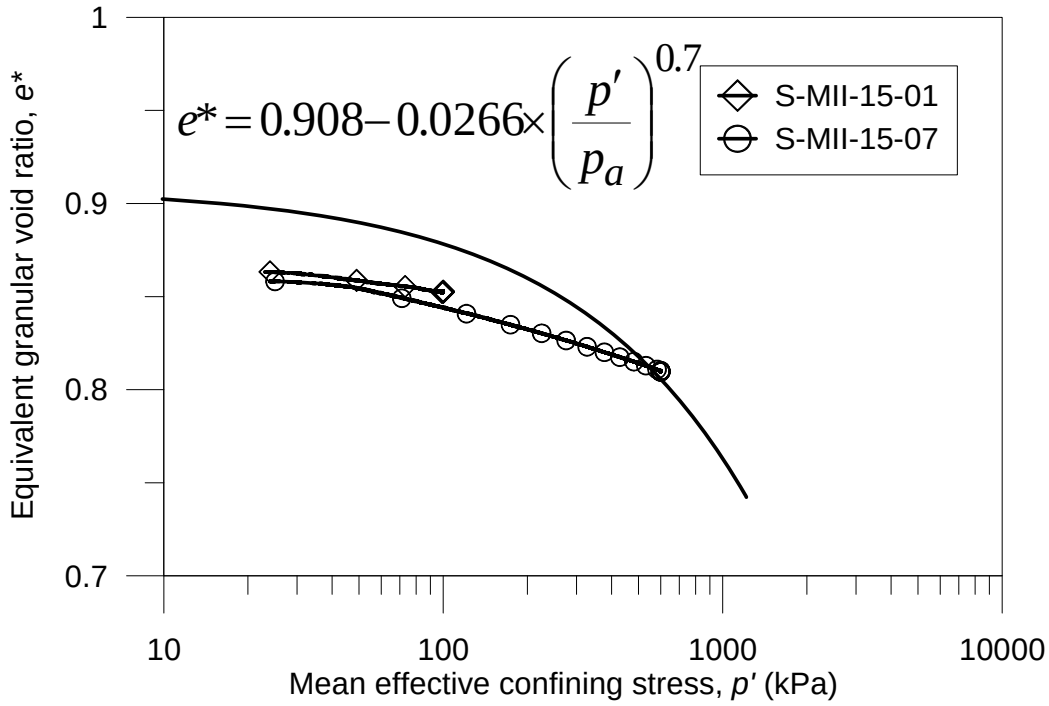

Figure 5. 4: **EG-SSL for Sydney sand with 15% MII fines and consolidation curve for two special tests in *e**-log(*p′*) space.**

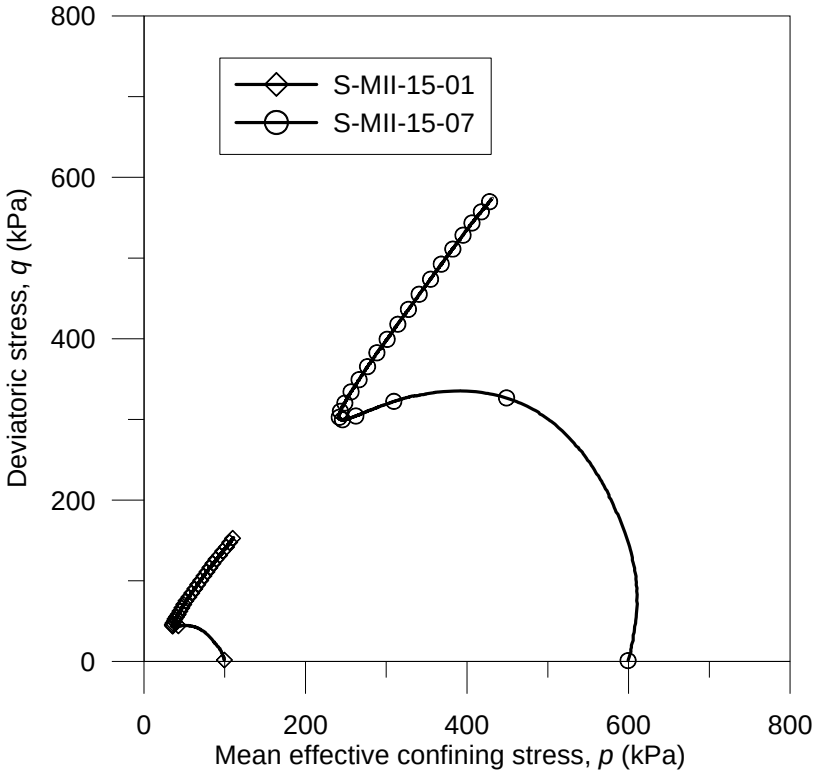

(a)

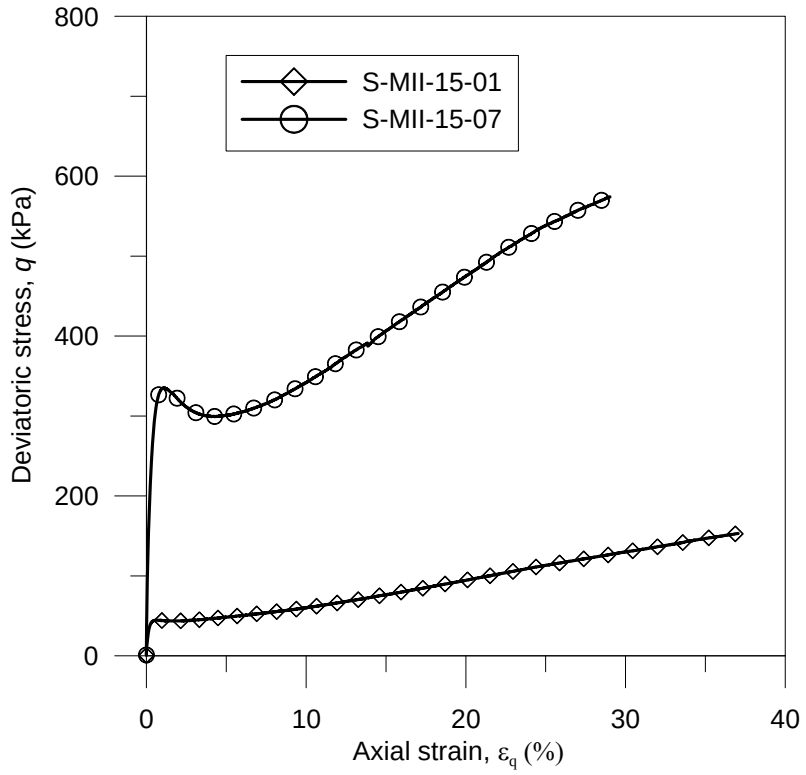

(b)

Figure 5. 5: Non-flow and limited flow behaviour for special tests; (a) stress path behaviour, (b) stress-strain behaviours

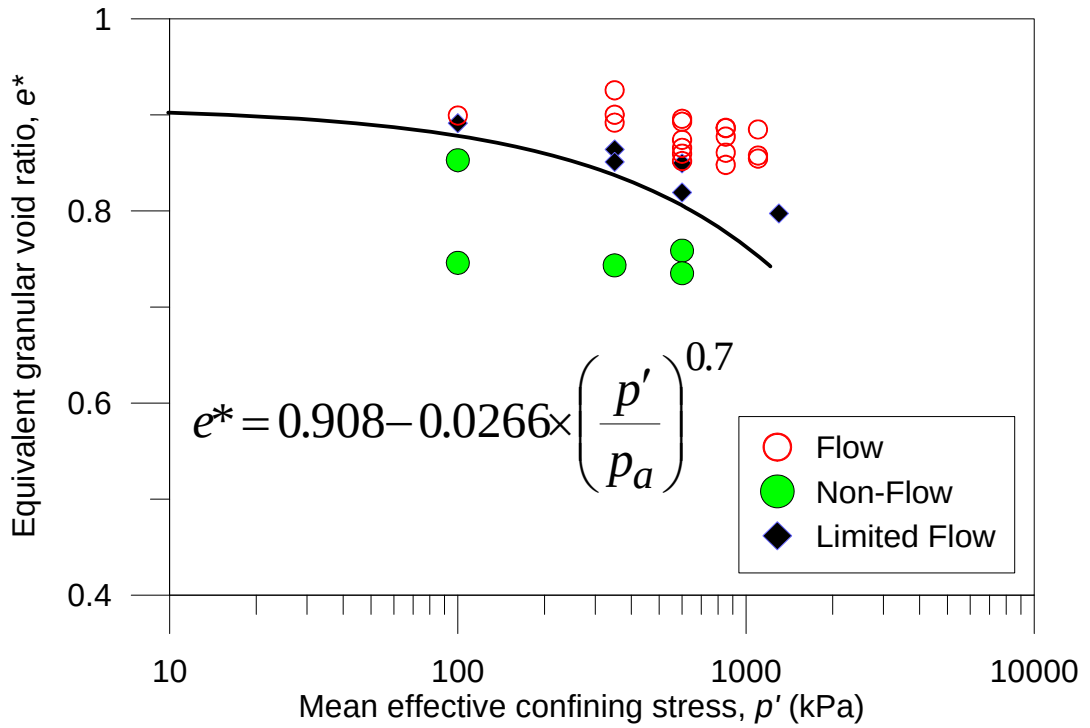

Figure 5. 6: **Initial state of all tests for sand and sand with fines (up to 30%) relative to EG-SSL.**

5.4.3 *Concept of Equivalent Granular State Parameter*

Been and Jefferies's (1985) defined state parameter as following

$$\psi = e - e_{SS} \qquad \textbf{5. 3}$$

Detail discussion of the state parameter is given in Chapter 2. It can be used to predict the behaviour patterns of sand or sand with fines content. Since ψ is defined relative to SSL, then a separate SSL is needed for each fines content, and it is also difficult to compare the implications of different ψ values obtained from sand with different fines content. On the hypothesis that EG-SSL may be used as the single "alternative SSL" in the e^*-log(p') space in the context of CSSM framework, ψ^* can be defined in lieu of state parameter, ψ as following

$$\psi^* = e^* - e^*_{SS} \qquad \textbf{5. 3a}$$

where, ψ^*= equivalent state parameter, e^* = current equivalent granular void ratio of the sample, e^*_{SS} = equivalent granular void ratio at EG-SSL for same mean effective stress. Figure 5. 7 shows the definition of equivalent granular state parameter, ψ^*. Denoting the ψ^* value at start of undrained shearing as $\psi^*_{(0)}$, one may hypothesis (based on the application of CSSM framework to e^* and EG-SSL), that $\psi^*_{(0)} > 0$ implies flow behaviour during undrained shearing irrespective of fines contents, and similarly $\psi^*(0) < 0$ implies NF. One may also expect that the ESP and q-ε_q responses can also be correlated to $\psi^*_{(0)}$.

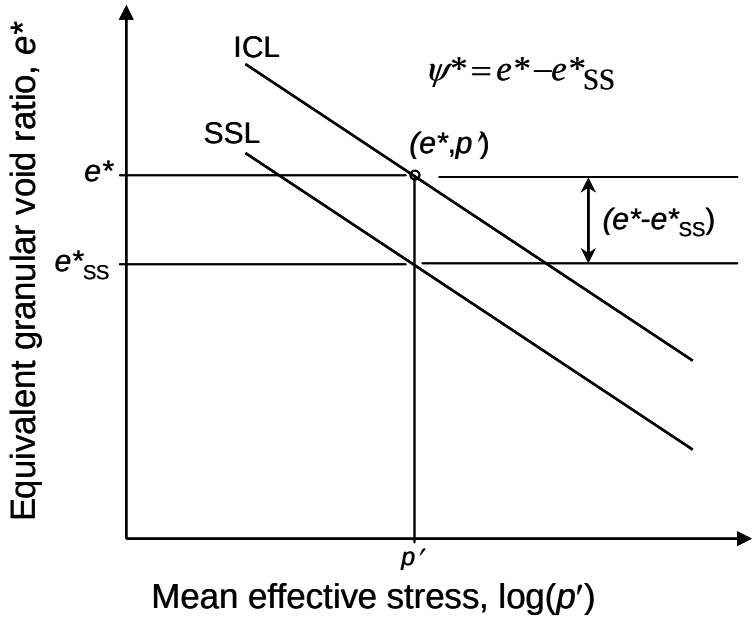

Figure 5. 7: Definition of equivalent state parameter, ψ^*

The value of $\psi^*_{(0)}$ and overall undrained behavior (F, NF, LF) are also listed in Table 5. 1, tests with positive equivalent state parameter manifested flow behaviour and tests with negative equivalent granular state parameter showed non-flow behaviour. Tests with $\psi^*_{(0)}$ around zero showed limited flow behaviour.

5.4.4 *Relationship between Undrained Behaviour and $\psi^*_{(0)}$*

This section presents a more comparative study on the relationship between $\psi^*_{(0)}$ and the ESP and deviatoric stress-strain responses during undrained shearing. In studying the role of $\psi^*_{(0)}$, the comparison is extended to the tests with different initial mean effective stress, $p'_{(0)}$. However, ESPs at different initial mean effective stress, $p'_{(0),}$ are not directly comparable. To eliminate the effect of initial mean effective stress, p'_0, the ESPs are plotted in a $q/\ p'_{(0)}$- $p'/p'_{(0)}$stress space i.e. the stresses are normalized with respect to the initial mean effective stress, $p'_{(0)}$.

5.4.4.1 Influence of $\psi^*_{(0)}$ on ESP Responses of Clean Sand: a Consistency Check

It is understood form the formulation of the equivalent granular void ratio that the EG-SSL for sand with fines is in fact SSL for clean sand (Rahman and Lo 2008). Thus, it is expected that EG-SSL will be capable of predicting undrained behaviour of clean sand. However as a consistency check, three tests with $\psi^*_{(0)}$ being -0.08 to 0.097 are presented in Figure 5. 8. The tests are: S-MII-00-10, S-MII-00-09 and S-MII-00-07 and their initial mean effective stress, $p'_{(0)}$ varies from 600kPa to 850kPa. The ESP responses can be correlated to $\psi^*_{(0)}$. Test S-MII-00-10 has the highest $\psi^*_{(0)}$ = 0.097. The location of its ESP is the lowest among three tests. Its ESP traced leftward during the entire test. After attaining a peak deviator stress, the ESP plummeted toward origin. The test S-MII-00-07 has a mid-value of equivalent granular state parameter, $\psi^*_{(0)}$ of 0.035. Although ESP also bent left, it is not as significant as the 1st test S-MII-00-10. Furthermore, the ESP manifested a PT point at which the ESP reversed its direction and turn back towards $dp' > 0$. The value of

$q/p'_{(0)}$showed some reduction after attaining a peak value. Eventually the ESP traced right and climbed upwards. It achieved both high deviator stress and high p' at end of the test. The 3rd test S-MII-00-09 has the lowest equivalent state parameter of $\psi^*_{(0)}$ of -0.097. Its ESP traced only slightly to the left and then turned right (i.e. towards $dp' > 0$). Its ESP climbed upward throughout the test. High deviator stress and high mean effective stress were achieved at the end of test

The q-ε_q behaviour the above three tests in $q/p'_{(0)}$-ε_q space are shown in Figure 5. 8b. The test S-MII-00-10 (largest $\psi^*_{(0)}$) shows that it reached to an initial peak and then showed rapid strain softening to the SS. The test S-MII-00-07 (mid-value for $\psi^*_{(0)}$) showed a gradual strain softening after attaining a peak $q/p'_{(0)}$value. The behaviour at higher strain reverted back to a gradual strain hardening. The q-ε_q response of test S-MII-00-09 (lowest $\psi^*_{(0)}$) showed a continuous strain hardening towards the SS. Thus, ESP and q-ε_q responses of the above three tests for clean sand can be correlated $\psi^*_{(0)}$. This demonstrates overall consistency of the framework.

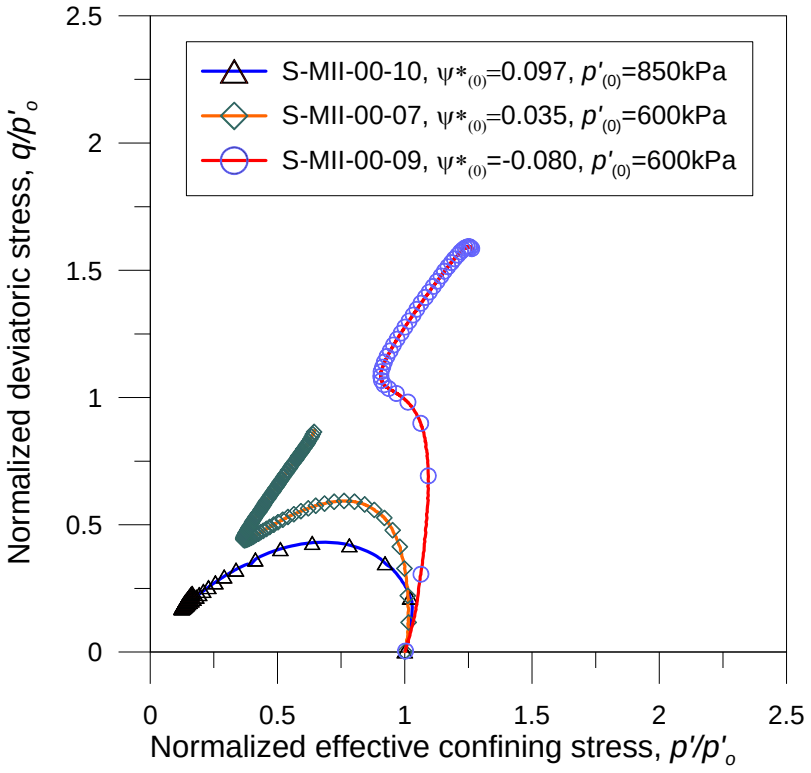

(a)

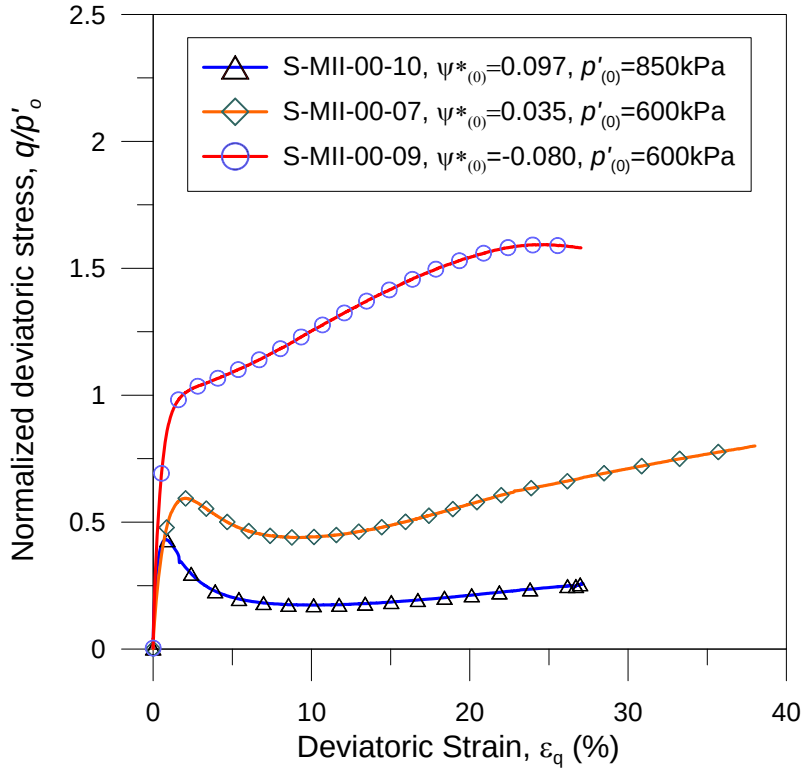

(b)

Figure 5. 8 **Different equivalent granular state parameter for different undrained behaviour for clean sand; (a) $q/p'_{(0)}$- $p'/p'_{(0)}$space, (b) $q/p'_{(0)}$- ε_q space.**

5.4.4.2 Influence of $\psi^*_{(0)}$ with ESP and Deviator Stress-Strain Responses of Specimen with 15% Fines Content

The ESP and q-ε_q curve of three tests with 15% fines contents are compared in Figure 5. 9. Their $p'_{(0)}$ varies from 350kPa to 600 kPa. The locations of ESPs are shifting downward with increase in $\psi^*_{(0)}$. The test S-MII-15-02 has the highest $\psi^*_{(0)}$ of 0.056. Its ESP traced leftward during the entire test. After attaining a peak deviator stress, the ESP plummeted toward the origin. The test S-MII-15-07 has a mid-value $\psi^*_{(0)}$ of 0.004 although the ESP also bend left, it is not as significant as the 1st test. Furthermore, the ESP eventually reversed its direction, i.e. turn back towards $dp' > 0$. The value of $q/p'_{(0)}$ showed some reduction after attaining a peak value. Eventually the ESP traced right and climbed upwards. It achieved both high deviator stress and high p' at end of test. The test S-MII-15-06 has the lowest $\psi^*_{(0)}$ of -0.056 and its ESP was located at the top. Its ESP traced only slightly to the left and then turned right i.e. towards $dp' > 0$ and $q/p'_{(0)}$ increased continuously. Its ESP climbed upward throughout the test. Highest deviator stress and high mean effective stress achieved at the end of test. Thus, the equivalent granular state parameter, $\psi^*_{(0)}$ for these tests can predict the patterns of ESP for sand with 15% fines.

The q-ε_q behaviour the above three tests are shown in Figure 5. 9b. The deviator stress of test S-MII-15-02 (highest $\psi^*_{(0)}$ value) reached an initial peak and then showed rapid strain softening to the SS. The q-ε_q response of test S-MII-15-07 (mid-value for $\psi^*_{(0)}$) showed a gradual strain softening after attaining a peak deviator stress. The behaviour at higher strain reverted back to a gradual strain hardening. The q-ε_q response of test S-MII-15-06 (lowest $\psi^*_{(0)}$ value) showed a continuous strain hardening towards the SS. Thus,

the undrained behaviour pattern of the above four tests for sand with different fines content can be predicted with $\psi^*_{(0)}$ within CSSM framework.

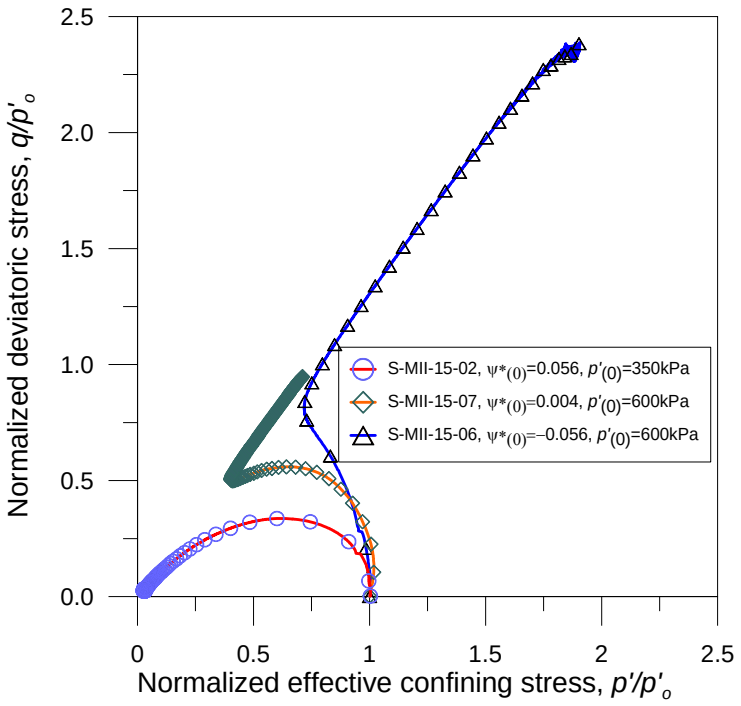

(a)

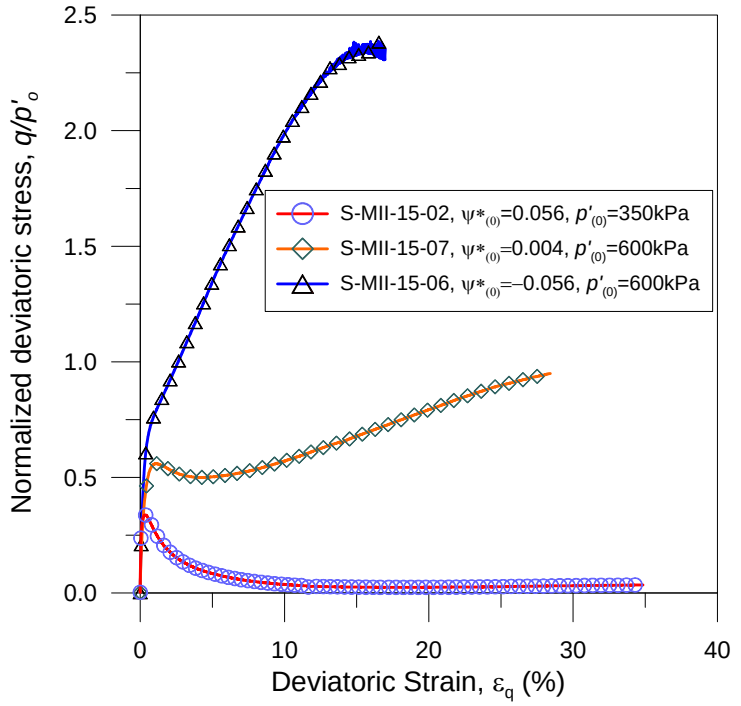

(b)

Figure 5. 9 Different equivalent granular state parameter for different undrained behaviour for same fines content, (a) $q/p'_{(0)}$- $p'/p'_{(0)}$space, (b) $q/p'_{(0)}$-ε_q space.

5.4.4.3 Influence of $\psi^*_{(0)}$ on the ESP and Deviator Stress-Strain Responses for Specimens with Different Fines Content

Four tests for specimens with different fines content were examined. These four tests have different $\psi^*_{(0)}$ values and their corresponding ESP and q-ε_q responses are examined in Figure 5. 10. A correlation between the overall location of ESPs and their corresponding $\psi^*_{(0)}$ was manifested by the downward shift of ESP with increase in $\psi^*_{(0)}$. Test S-MII-30-01 and S-MII-20-02 have $\psi^*_{(0)}$ values of 0.082 and 0.059 respectively, which are positive and higher than other two tests. Their ESPs located lowest, always traced leftward (i.e. $dp' < 0$) during shearing, and plummeted toward the origin after attaining the peak deviator stress. Test S-MII-15-07 has a $\psi^*_{(0)}$ of 0.004. Its ESP also traced leftward, but to a lesser extent compare with the 1st two tests. Furthermore, the ESP eventually reversed its direction, i.e. turn back towards $dp' > 0$. The value of q/p'_0 showed some reduction after attaining a peak value. Eventually the ESP traced right and climbed upwards, achieving both high deviator stress and high p' at end of test. Test S-MII-00-09 has the lowest $\psi^*_{(0)}$ value of -0.080. Its ESP traced only slightly to the left and then turned right i.e. towards $dp' > 0$ and $q/p'_{(0)}$increased continuously. Its ESP climbed upward throughout the test. Highest deviator stress and high mean effective stress reached at the end of test. The q-ε_q responses the above four tests are shown in Figure 5. 10b. Test S-MII-30-01 and S-MII-20-02 showed rapid strain softening to the SS after attaining their respective deviator stresses. The q-ε_q response of test S-MII-15-07 (mid-value for $\psi^*_{(0)}$) showed a gradual strain softening after attaining a peak deviator stress. The behaviour at higher strain reverted back to a gradual strain hardening. The q-ε_q response of test S-

MII-00-09 (lowest and negative $\psi^*_{(0)}$ value) showed a continuous strain hardening towards the SS. Thus, the undrained behaviour pattern of the above four tests for sand with different fines content can be predicted with $\psi^*_{(0)}$ within CSSM framework.

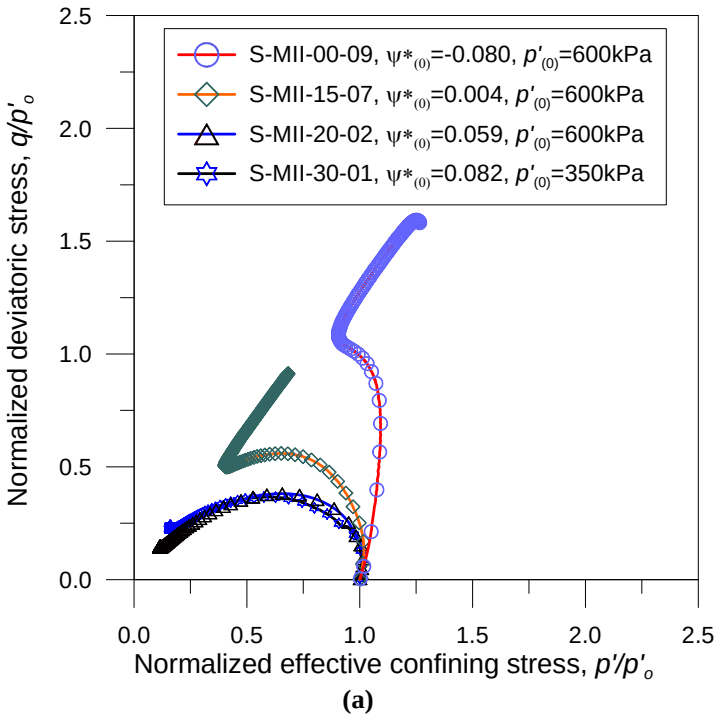

(a)

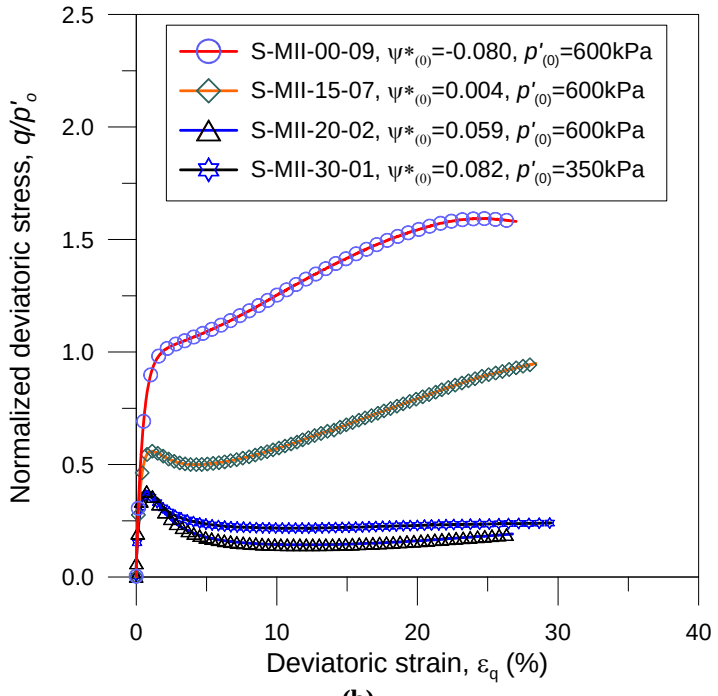

(b)

Figure 5. 10 Different undrained behaviours for different $\psi^*_{(0)}$ for different fines content; (a) $q/p'_{(0)}$- $p'/p'_{(0)}$space, (b) $q/p'_{(0)}$-ε_q space.

5.4.4.4 ESP and Deviator Stress-Strain Responses of Specimen with Different Fines Content but Same $\psi^*_{(0)}$

To further substantiate the hypothesis that undrained behaviour is largely governed by $\psi^*_{(0)}$, tests on specimens of different fines content and also different e_0 are compared in this section. It was extremely difficult to achieved near-identical $\psi^*_{(0)}$ for specimens with different fines contents. However, two sets of comparison were achieved as discussed below.

Figure 5. 11a compares three tests with different fines contents but the value of $\psi^*_{(0)}$ is in a small range of 0.092 to 0.097. As such it may be considered as essentially having the same $\psi^*_{(0)}$. The fines contents of these 3 tests vary from 0% to 20%. The $p'_{(0)}$ and e_0 values of these 3 tests are also different. The ESPs manifested by these three tests were close: tracing leftward and then plummeting to the origin after attaining their respective peak deviator stresses. Their q-ε_q responses as plotted in Figure 5. 11b in the $q/p'_{(0)}$-ε_q space are also similar. A second set of comparison is for 3 tests with fines content varying from 15%, to 30%. The $\psi^*_{(0)}$ values of these 3 tests were in a narrow range of 0.081 to 0.088. The ESP and q-ε_q responses are shown in Figure 5. 12. The ESPs manifested by these 3 tests were close irrespective to fines content. Figure 5. 12b compares the deviator stress strain responses in the $q/p'_{(0)}$-ε_q space. Although test S-MII-15-03 for 15% fines appeared to strain soften to a lower SS strength, the three curves in $q/p'_{(0)}$-ε_q space are essentially similar. Once again, their undrained behaviour responses (ESP, q-ε_q) can be correlated with $\psi^*_{(0)}$.

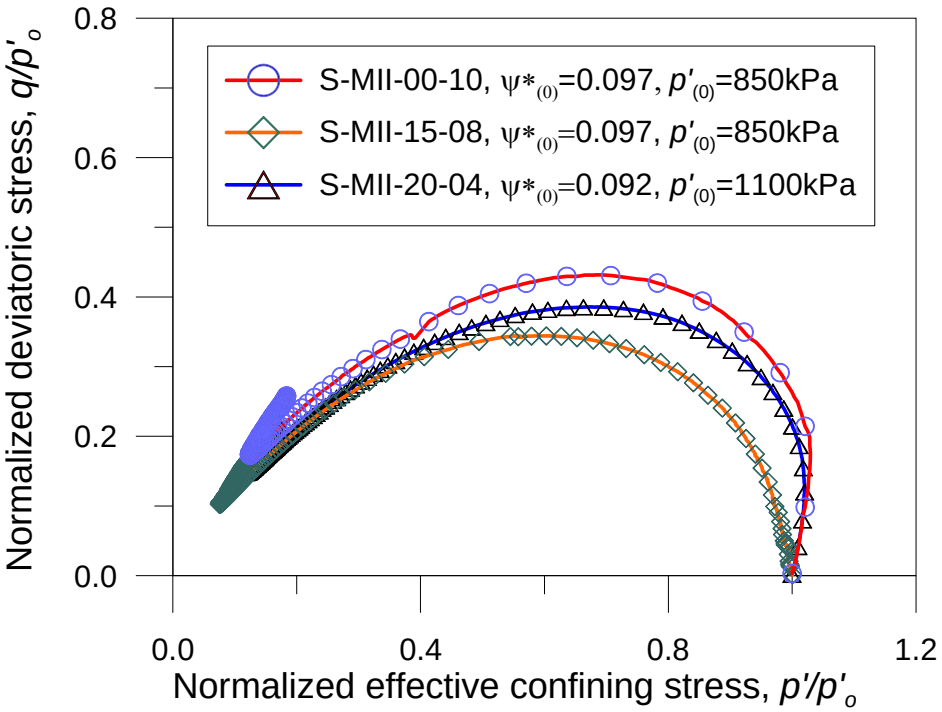

(a)

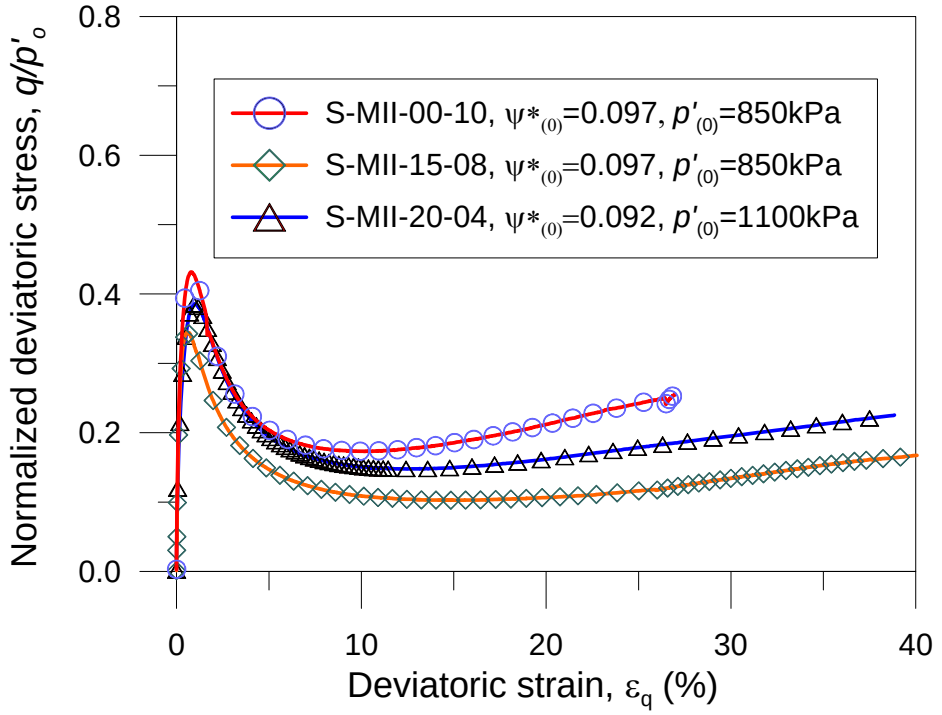

(b)

Figure 5. 11 **Comparison at same equivalent granular state parameter, $\psi^*_{(0)}$ = 0.97 for different fines contents; (a) in $q/p'_{(0)}$- $p'/p'_{(0)}$space, (b) in $q/p'_{(0)}$-ε_q space.**

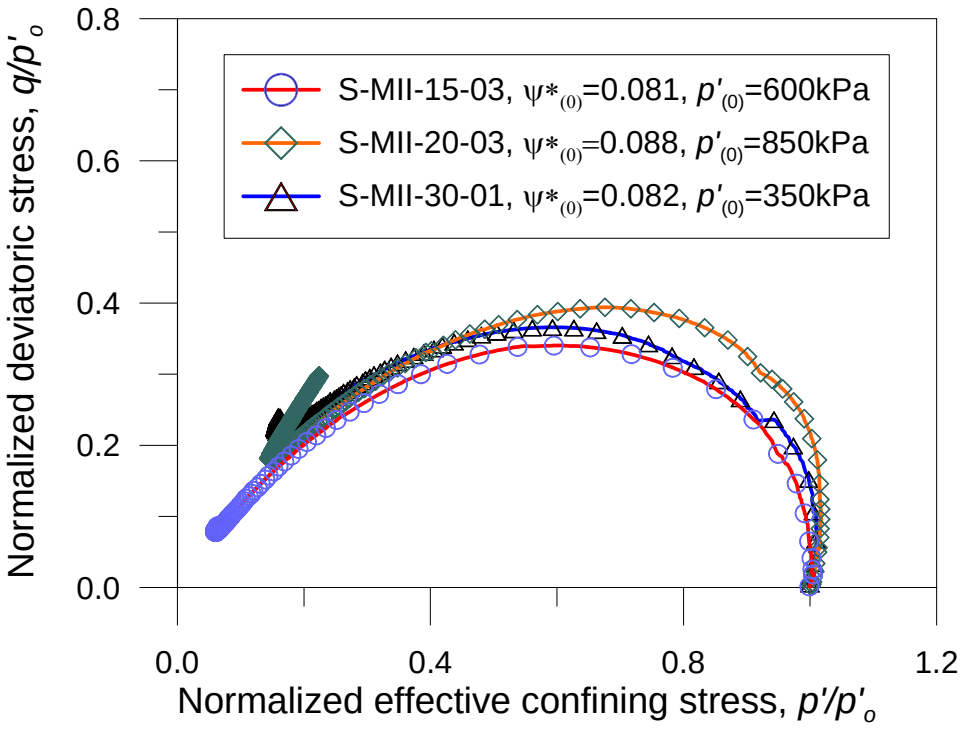

(a)

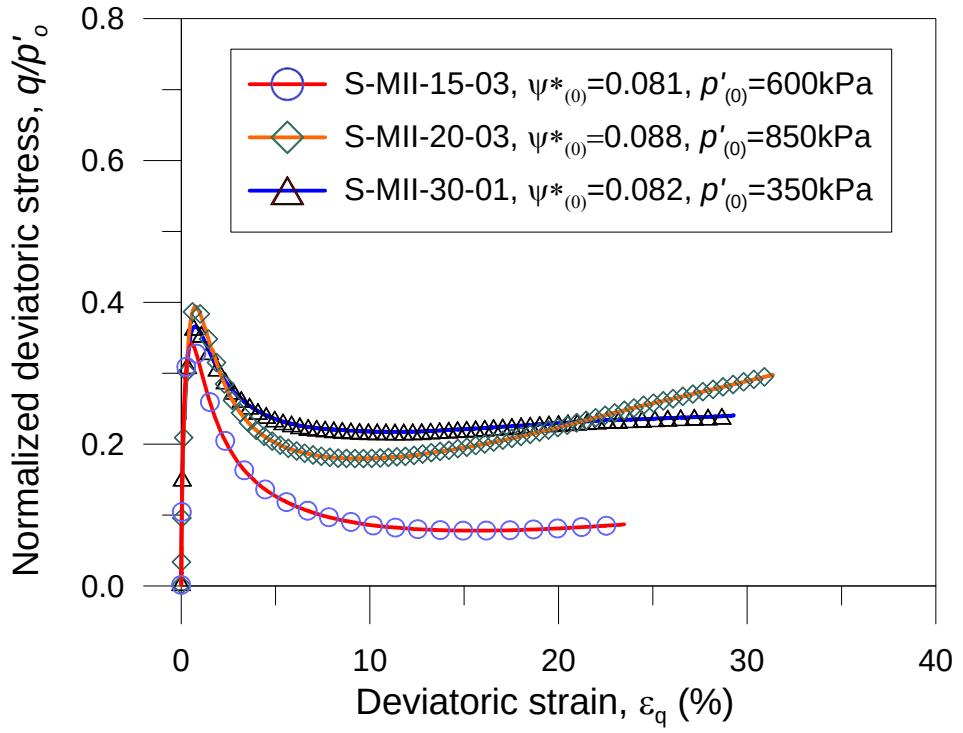

(b)

Figure 5. 12 **Comparison at same equivalent granular state parameter, $\psi^*_{(0)}$=0.81 for different fines contents; (a) in $q/p'_{(0)}$- $p'/p'_{(0)}$space, (b) in $q/p'_{(0)}$-ε_q space.**

5.5 VERIFICATION WITH PUBLISHED DATA SETS

The validity of predicting undrained behaviour pattern using $\psi^*_{(0)}$ was further evaluated using the published data of Thevanayagam and Mohan (2000). The specimens used in this study were prepared using a single host sand mixed with two different types of fines and at different fines content. The fines are: Ground silica fines (GS) and kaolin (KS). The grain size distribution curves for sand with fines are given in Figure 5. 13. It is noted, the sand in a naturally occurring state contained 2% fines. Thus the natural sand deposit, analytically, is the host sand plus 2% fines and this is denoted as A2. The host sand is obtained by washing off the fines and the corresponding tests are denoted by A0. The name convention and the percentage in the tests are given in Table 5. 2. Note that for test series S2 to S4 (with added fines), the combined fines contents are used to synthesize the test data. The parameters required to calculate TFC and equivalent granular void ratio are extracted from the grain size distribution curve as shown in Figure 5. 13 and they are also presented on Table 5. 2.

Table 5. 2 The details of material tested

Test series	Fines Reference	Natural Fines	Artificial fines		Total fines content	D_{10}	d_{50}	TFC
			Type	(%)				
S1.	A0	0	--	--	0	0.16	--	--
S1.	A2	2	--	--	0	0.16	--	--
S2.	KS-10	2	KS	10	12	--	0.0091	36
S3.	KS-25	2	KS	25	27	--	0.0090	36
S4.	GS-10	2	GS	10	12	--	0.0090	36

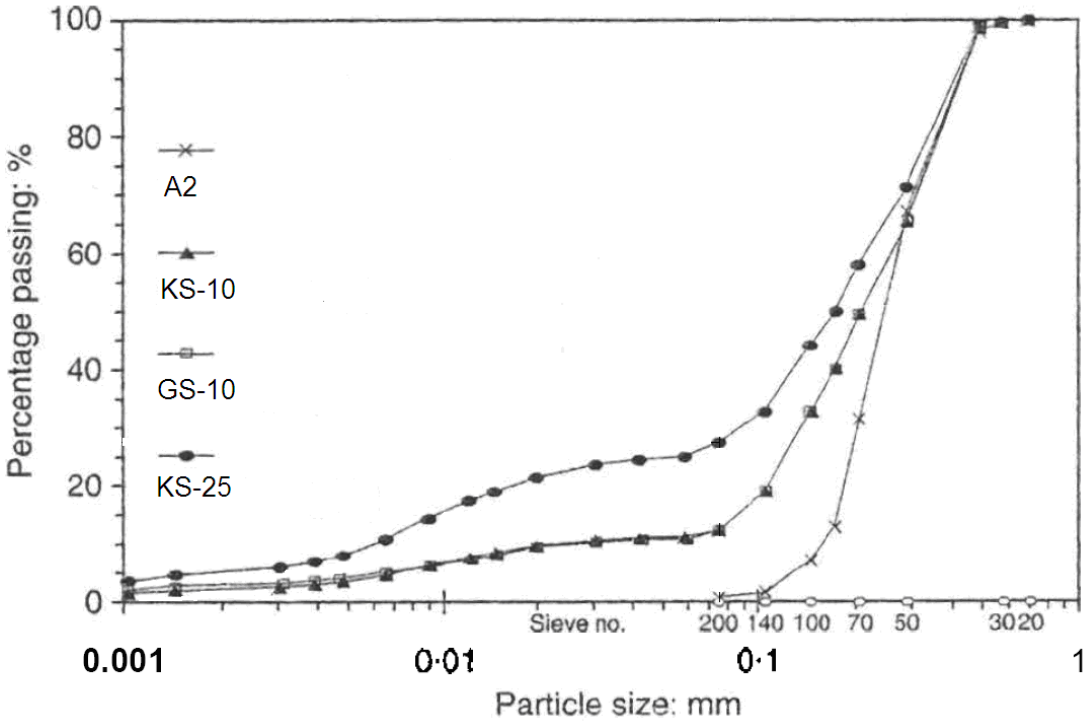

Figure 5. 13 Grain size distribution curve of Host sand with fines.

5.5.1 *Evaluation of the EG-SSL concept*

5.5.2 *EG-SSL for Host sand with two different types of fines*

Figure 5. 14a shows that the SSL for sand with fines shifted downward with increase in fines content. The spread of these SS data points are about 0.550 in terms of void ratio, e. However, all SS data points plotted in e^*-log(p') space can be approximated by a single trend line as shown in Figure 5. 14b. Note that the threshold fines content, TFC is calculated using Equation 4.1 and the equivalent granular void ratio, e^* is calculated by Equation 4.2a & 2.12. This single trend line, which is the EG-SSL, can be approximated by a power function as following:

$$e^* = 1.0 - .047\left(\frac{p'}{p'_a}\right)^{0.71} \qquad \textbf{5. 4}$$

where, e^* is void ratio at SS, p' is effective confining pressure at SS and p'_a is atmospheric pressure equal to 100 kPa. The RMSD of the data points around the EG-SSL is about 0.060 which is on the high side relative to those of other data sets discussed in this thesis. A close examination of Figure 5. 14 showed that the steady state data points of KS-25 at $p'_{SS} > 100$ kPa appears to be a significant contributor to the scatter. A examination of the SS data points for KS-25 in either the e-log(p') space or e^*-log(p') space revealed that the data points for with $p'_{SS} > 100$ kPa appear to be follow a trend different from those at $p'_{SS} \leq 100$ kPa. This was recognized in the original publication. Furthermore, the trend manifested by the 3 data points at $p'_{SS} > 100$ kPa appears to suggest negligible change in e_{SS} with significant increase in p'_{SS}. This is inconsistent with expectation. Therefore, the calculation was repeated without using these 3 data points, and a RMSD of 0.043 can be achieved without these data points. Therefore, Equation 5. 4 can be consider as a single trend and it can be used for further evaluation.

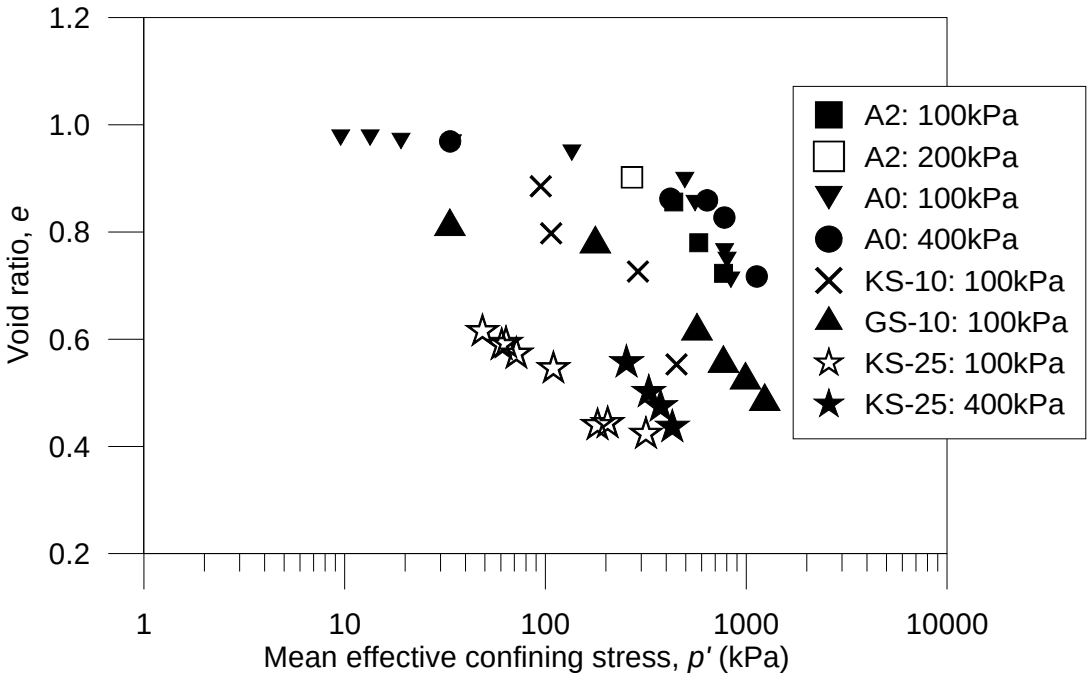

(a)

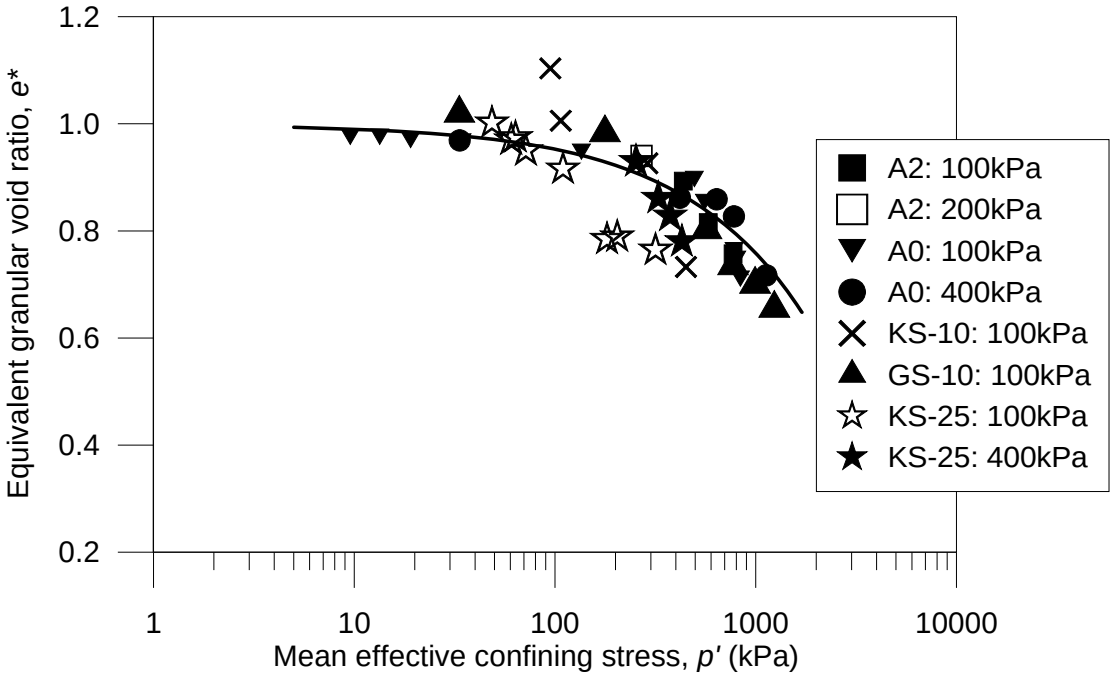

(b)

Figure 5. 14 Effect of fines on SS data points for Host sand with fines; (a) Effect of fines in *e*-log(*p′*) space, (b) A single EG-SSL *e-log(*p′*) space.**

5.5.3 *Overall evaluation of EG-SSL with in CSSM framework*

Thevanayagam and Mohan (2000) classified undrained behaviours as contractive, dilative and contractive-dilative which are based on pore water pressure generation. In this thesis, the overall undrained behaviours are classified as flow, non-flow and limited-flow which are based on strain softening (static liquefaction). One may not be able to obtain the strain softening classification from pore water pressure response classification. It can be better understood by the partial derivative of deviator stress, $q=\eta p'$, with respect to ε_q

$$\frac{\partial q}{\partial \varepsilon_q} = \frac{\partial \eta}{\partial \varepsilon_q} \cdot p' + \frac{\partial p}{\partial \varepsilon_q} \cdot \eta \qquad \textbf{5. 5}$$

Noting, $du = - dp'$, the Equation 5. 5 can be rewrite as

$$\frac{\partial q}{\partial \varepsilon_q} = \frac{\partial \eta}{\partial \varepsilon_q} \cdot p' - \frac{\partial u}{\partial \varepsilon_q} \cdot \eta \qquad \textbf{5. 5a}$$

In strain softening (flow/limited flow) behaviour, $\partial q/\partial \varepsilon_q$, by definition, is less than zero. In contractive/ behaviour the second term of Equation 5. 5a is negative due to pore water pressure generation but the resultant $\partial q/\partial \varepsilon_q$ may not be less than zero because $\partial \eta/\partial \varepsilon_q > 0$. Thus, strain softening behaviour may not be seen in contractive behaviours. Therefore the ESP or deviator stress strain responses as published in Thevanayagam and Mohan (2000) were used to classify flow/non-flow behaviour pattern the Table 5. 3 and some of the tests could not be classified due to inadequate information.

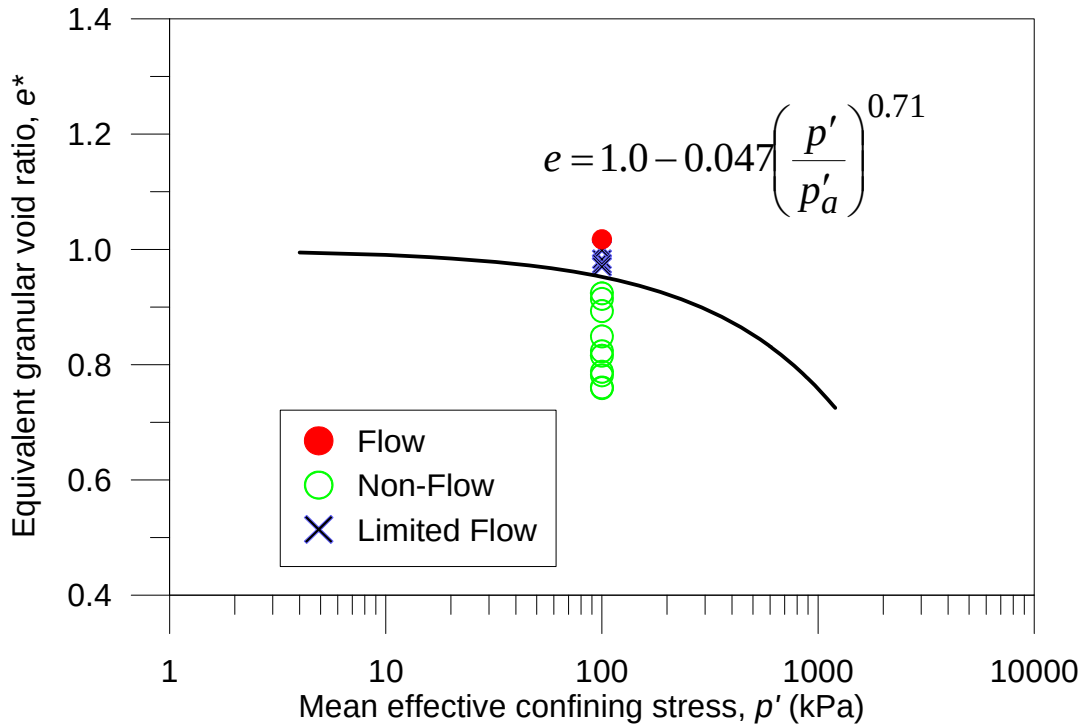

Figure 5. 15 EG-SSL and initial state of tests with flow/non-flow behaviours for 0%-27% fines.

To examine the ability of the EG-SSL in predicting overall behaviour pattern, the initial state (i.e. at start of undrained shearing) of all tests are plotted in the e^*-log(p') space as shown in Figure 5. 15. Different symbols are used depending on whether the overall behaviour is F, NF or LF. This Figure 5. 15 shows that initial states located below the EG-SSL manifested Flow behaviour, but initial states plotted well above the EG-SSL manifested flow behaviour. Tests that manifested limited flow behaviour had their initial states plotted around the EG-SSL. This gives an overall verification that e^* and EG-SSL can be used within CSSM framework to predict overall behaviour pattern.

Table 5. 3 Summary of tests data after Thevanayagam and Mohan (2000), continue

Test Name	Fines content, (%)	Types of Fines	*b*-value	p'_0 (kPa)	$e_{(0)}$	$e^*_{(0)}$	$\psi^*_{(0)}$	Observed behaviour
S1.1	0	--	0.02	100	0.893	0.893	-0.060	NF
S1.3	0	--		100	0.849	0.849	-0.108	NF
S1.2	2	--		100	0.854	0.891	-0.062	--
S1.4	2	--		100	0.780	0.816	-0.137	NF
S1.5	2	--		100	0.725	0.759	-0.193	NF
S2.1[N]	12	KS	0.135	100	0.880	1.098	0.145	--
S2.2	12	KS		100	0.795	1.003	0.050	LF
S2.3	12	KS		100	0.724	0.924	-0.029	NF
S2.4	12	KS		100	0.634	0.823	-0.129	NF
S2.5[X]	12	KS		100	0.521	0.697	-0.256	--
S2.6[X]	12	KS		100	0.551	0.731	-0.222	NF
S3.1	25	KS	0.284	100	0.612	0.998	0.046	LF
S3.2	25	KS		100	0.593	0.975	0.022	LF
S3.3	25	KS		100	0.589	0.970	0.172	LF
S3.4	25	KS		100	0.544	0.914	-0.038	NF
S3.5	25	KS		100	0.442	0.788	-0.165	NF
S3.6	25	KS		100	0.437	0.781	-0.171	NF
S3.7	25	KS		100	0.420	0.760	-0.192	NF
S3.12[X]	25	KS		100	0.574	0.951	-0.002	--

[X] ESP and q-ε_1 was not presented in original paper

[N] Unable to digitize due to lack of resolution in original paper

Table 5. 3 Summary of tests data after Thevanayagam and Mohan (2000), continue

Test Name	Fines content, (%)	Types of fines	*b*-value	p'_0 (kPa)	$e_{(0)}$	$e^*_{(0)}$	$\psi^*_{(0)}$	Observed behaviour
S4.1	12	GS	0.139	100	0.808	1.017	0.065	F
S4.2	12	GS		100	0.777	0.983	0.030	LF
S4.3	12	GS		100	0.615	0.802	-0.151	NF
S4.4	12	GS		100	0.555	0.735	-0.218	NF
S4.5	12	GS		100	0.523	0.699	-0.253	NF
S4.6[X]	12	GS		100	0.484	0.655	-0.297	NF

[X] ESP and q-ε_1 was not presented in original paper

[N] Unable to digitize due to lack of resolution in original paper

5.5.4 *Undrained Behaviours with respect to EG-SSL*

In this section, it is further evaluated whether equivalent granular state parameter, $\psi^*_{(0)}$ can be used as predictor of effective stress path, ESP and deviatoric stress-strain responses.

5.5.4.1 Influence of $\psi^*_{(0)}$ on the ESP Spectrum at Same GS Fines Content

Five tests from S4 series are plotted in Figure 5. 16 which contain sand with GS-10 fines (non-plastic). Overall pattern shows that the ESPs are going downward with increase in equivalent granular state parameter, $\psi^*_{(0)}$. Tests S4.1 and S4.2 have equivalent granular state parameters of 0.065 and 0.030 which are the higher than other three tests and their ESP shows lower deviatoric stress among five tests. Their ESPs also show maximum leftward movement. S4.3 and S4.4 have equivalent

granular state parameter form -0.151 and -0.218 and they show less leftward movement and their ESPs turn right to higher mean effective stress. It should be noted that S4.5 showed unusual leftward movement. It's $\psi^*_{(0)} < 0$ and void ratio, e is smaller than other tests, thus it should manifest strong non-contractive tendency from the beginning. But, it manifested initial contractive (leftward movement) behaviour which is also observed in q-ε_1 space in Figure 5. 16b. However, at the end of the test, S4.5 reached to a highest deviatoric stress, q of around 1150 kPa whereas tests S4.4 and S4.3 reached to around 850 kPa and 700 kPa respectively which are also consistent with equivalent granular state parameter. Again, the q-ε_1 paths in Figure 5. 16b also show that highest deviatoric stress is achieved at lowest equivalent granular state parameter of -0.253. Theses observations confirmed that equivalent granular state parameter can be used to predict undrained behaviour of host sand with GS-10 non-plastic fines.

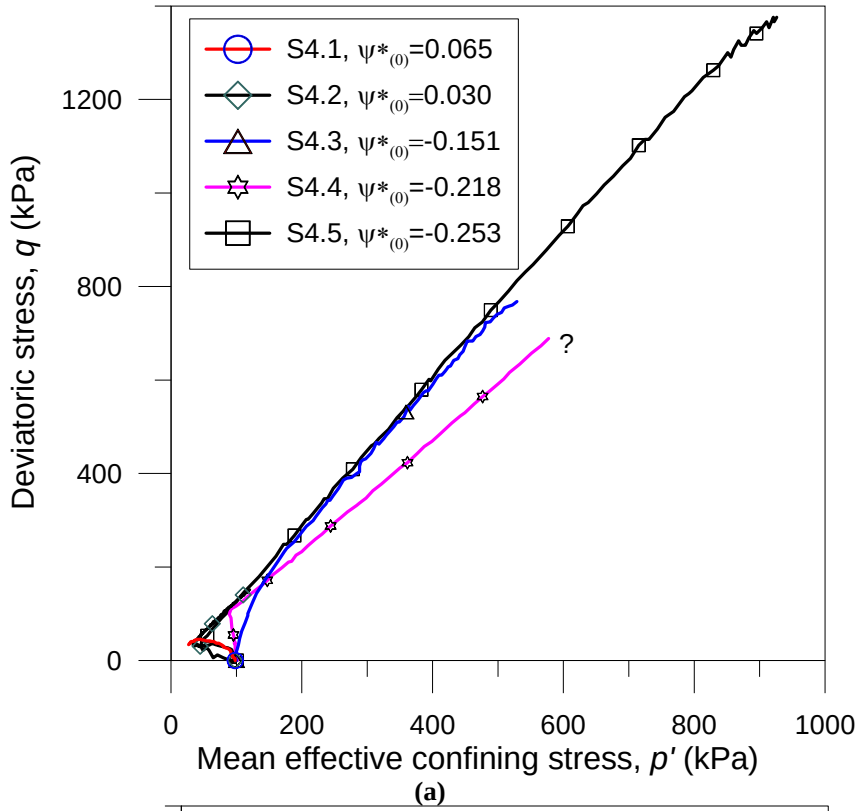

(a)

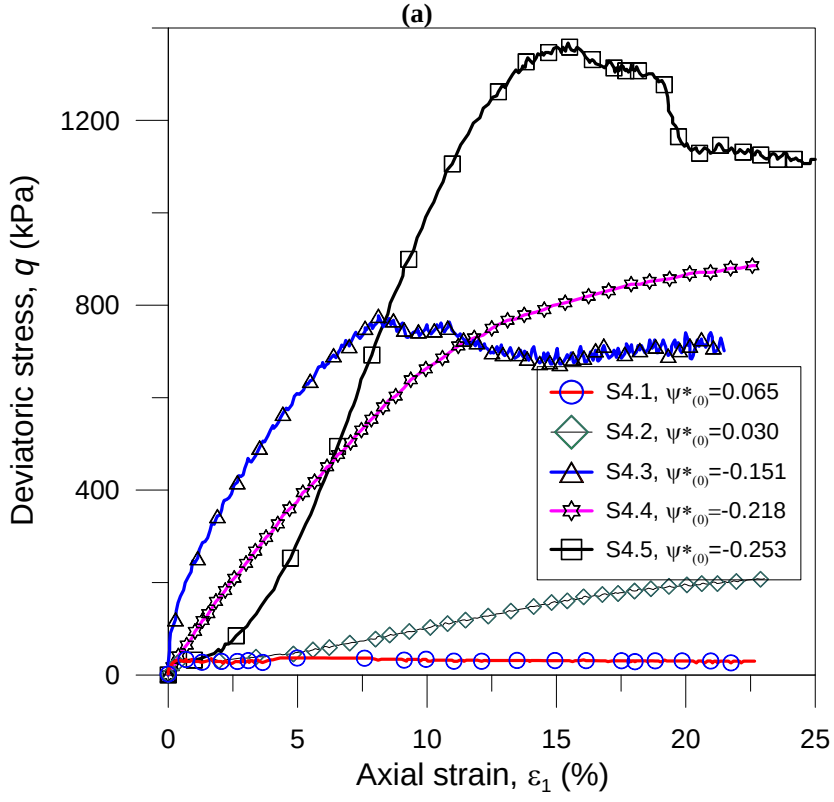

(b)

Figure 5. 16 **Equivalent granular state parameter and different ESP behaviour for host sand with GS-10 fines; (a) *q*-*p′* space, (b) *q*-ε_1 space, reproduced from Thevanayagam and Mohan (2000) .**

5.5.4.2 Sand with KS-10 materials

Three tests from S2 series are shown in Figure 5. 17. This test series is for sand with KS-10 fines. Although all 3 ESPs initially bent left and eventually turns right, test S2.2 with a positive $\psi^*_{(0)}$ value of 0.050 traced most to the left compared with the other two test which had negative $\psi^*_{(0)}$ values. Furthermore, the ESP of test 2.2 manifested a shape characteristic of Limited flow (dipped downward after attaining a peak deviator stress, and then bend sharply upward at the PT point). The other two tests with positive $\psi^*_{(0)}$, although still manifested PT points, were always tracing upwards (i.e. strain hardening). The correlation between $\psi^*_{(0)}$ and q-ε_1 curves is more evident. Test S2.2 with a positive $\psi^*_{(0)}$ of 0.05 manifested a low peak deviator stress, limited flow and the lowest q_{SS} of 112. The test S2.3 with an intermediate $\psi^*_{(0)}$ of -0.029 showed continuous strain hardening and attained a high q_{SS} of 410kPa. Test S2.4 with the most negative $\psi^*_{(0)}$ of -0.129 had a q-ε_1 curve located on the top and attained the highest q_{SS} of 470kPa. The above comparison supports the use $\psi^*_{(0)}$ as the predictor of ESP and q-ε_1 responses for sand with KS-10 fines.

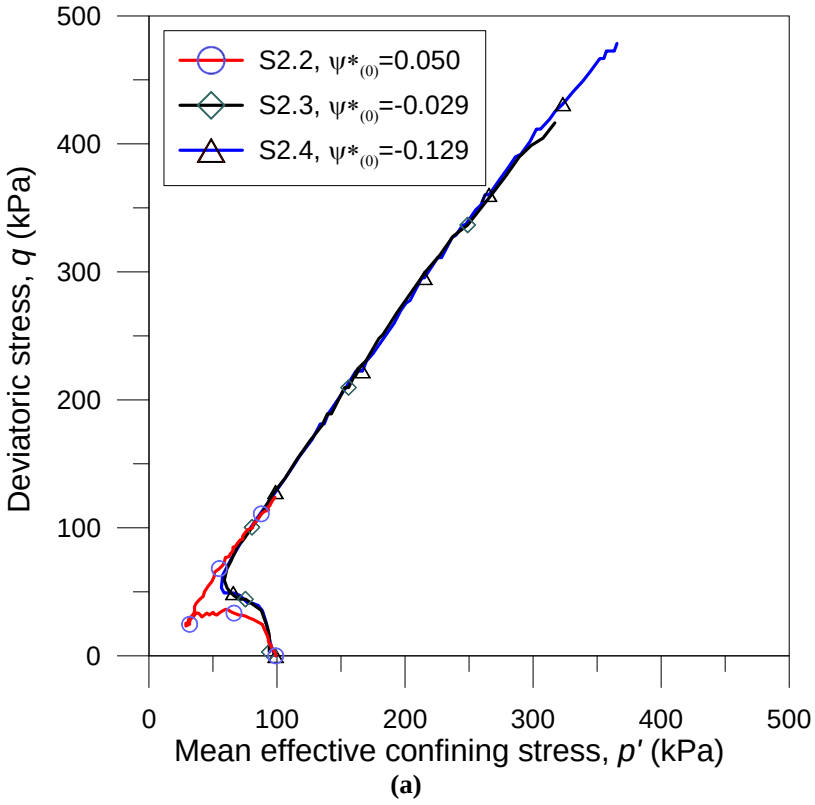

(a)

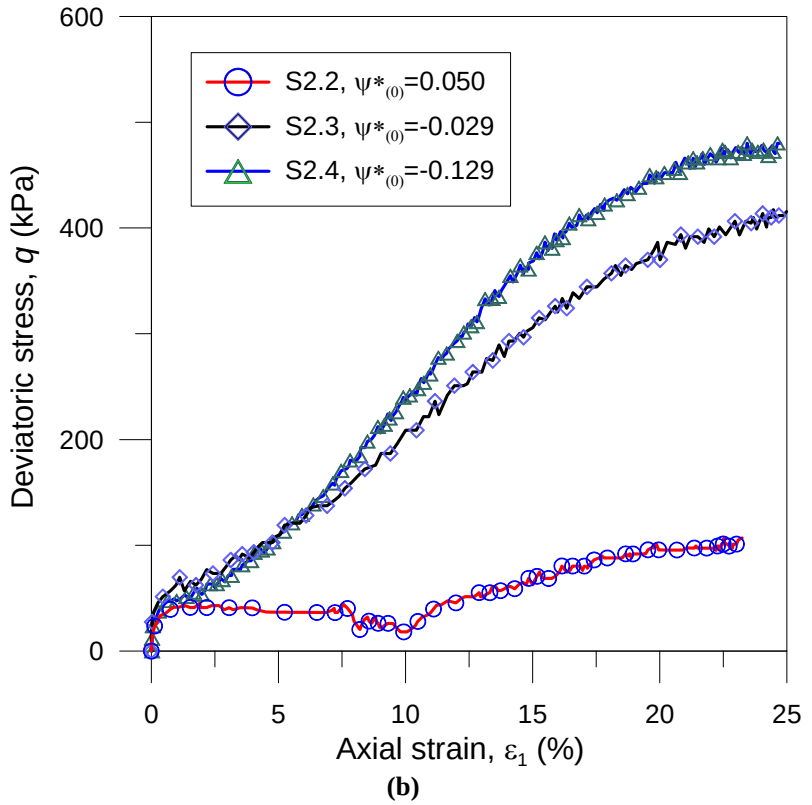

(b)

Figure 5. 17 **Influence of $\psi^*_{(0)}$ on the ESP Spectrum of same KS-10 fines; (a) in q-p' space, (b) in q-ε_1 space, reproduced from Thevanayagam and Mohan (2000).**

5.5.4.3 Sand with Different Fines Content and Types

Four test results are shown in Figure 5. 18 These four test covers all three fines type (A2, KS & GS) and with fines content ranging from 02% to 27%. The $\psi^*_{(0)}$ of these four tests ranges from 0.065 to -0.193. S4.1 has a positive $\psi^*_{(0)}$ value of 0.065 and its ESP manifested leftward movement and dipped after attaining the maximum deviator stress, no PT observed. S3.3 has a lower and slightly positive $\psi^*_{(0)}$ value 0.017. Its ESP manifested a PT point. The portion of ESP prior to the PT point was similar to S4.1, but bend right sharply and climb upwards after the PT point. S2.3 has a negative $\psi^*_{(0)}$ value of -0.029 and its ESP moved leftward to a lesser extent compared with S4.1 or S3.3 (both with a higher $\psi^*_{(0)}$ value). After the PT point, The ESP turned right and climbed to higher effective stress compared with S3.3 (with slightly positive $\psi^*_{(0)}$. S1.5 had a negative $\psi^*_{(0)}$ value of -0.193 and its ESP did not manifested any evident leftward movement but showed continuous increase in deviatoric stress.

The correlation between $\psi^*_{(0)}$ and q-ε_1 curves as shown in Figure 5. 17b are even more evident: a reduction in $\psi^*_{(0)}$ value is always associated with an upward shift in the q-ε_1 curve. S4.1 and S3.3 (with positive $\psi^*_{(0)}$ values) had the lowest deviatoric stress at SS. Test S2.3 (with a slightly negative $\psi^*_{(0)}$ value) manifested a continuous strain hardening to SS. Test S1.5 (with the most negative $\psi^*_{(0)}$) manifested the stiffest response and attained the highest peak deviator stress.

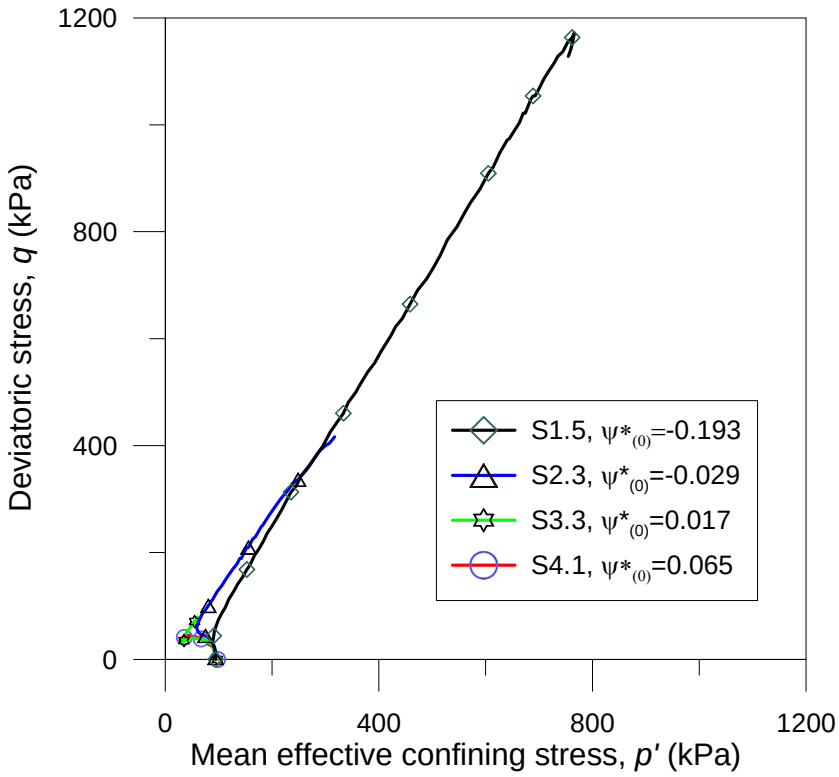

(a)

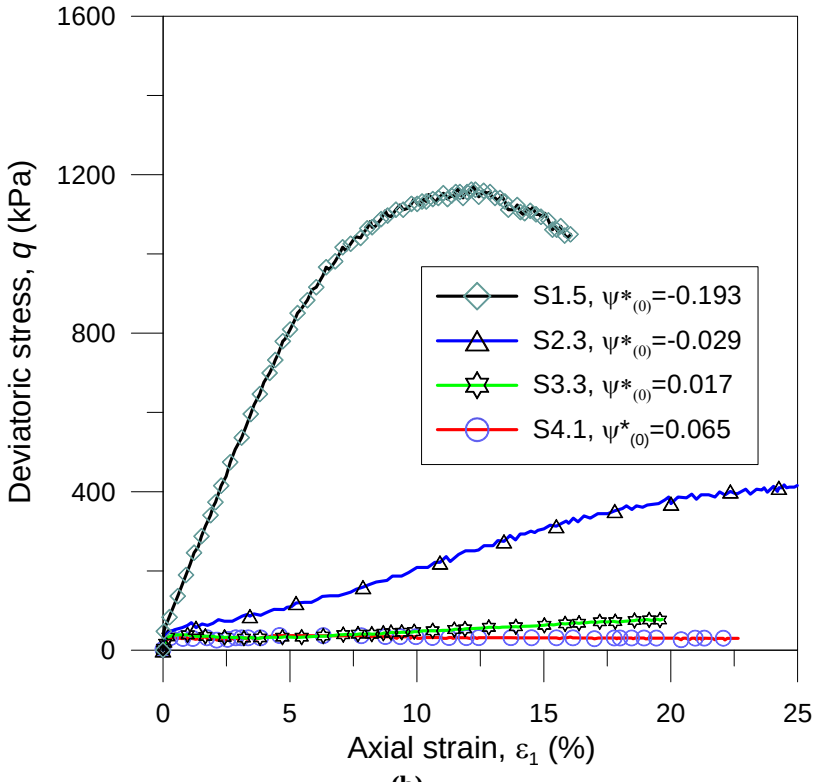

(b)

Figure 5. 18 **Influence of $\psi^*_{(0)}$ on the ESP Spectrum of different fines content; (a) in q-p' space, (b) in q-ε_1 space, reproduced from Thevanayagam and Mohan (2000) .**

5.5.4.4 Sand at Similar $\psi^*_{(0)}$ but Different Fines Content and Types

Two tests are presented in Figure 5. 19 with nearly same equivalent granular state parameter of $\psi^*_{(0)}$ (maximum difference is 0.014). S1.4 and S4.3 are the tests with 2% and 12% GS fines respectively. S4.3 and S1.4 have equivalent granular state parameter of -0.151 and -0.137 respectively. Their ESPs shows almost negligible leftward movement. Moreover, S4.3 shows stronger behaviour than S1.4 which is consistent with their equivalent granular state parameter. Their strain paths are also shown in Figure 5. 19b. They show a continuous strain hardening. Thus the equivalent granular state parameter can be used to predict over all spectrums of ESP and the concept of EG-SSL is consistent with the with CSSM framework.

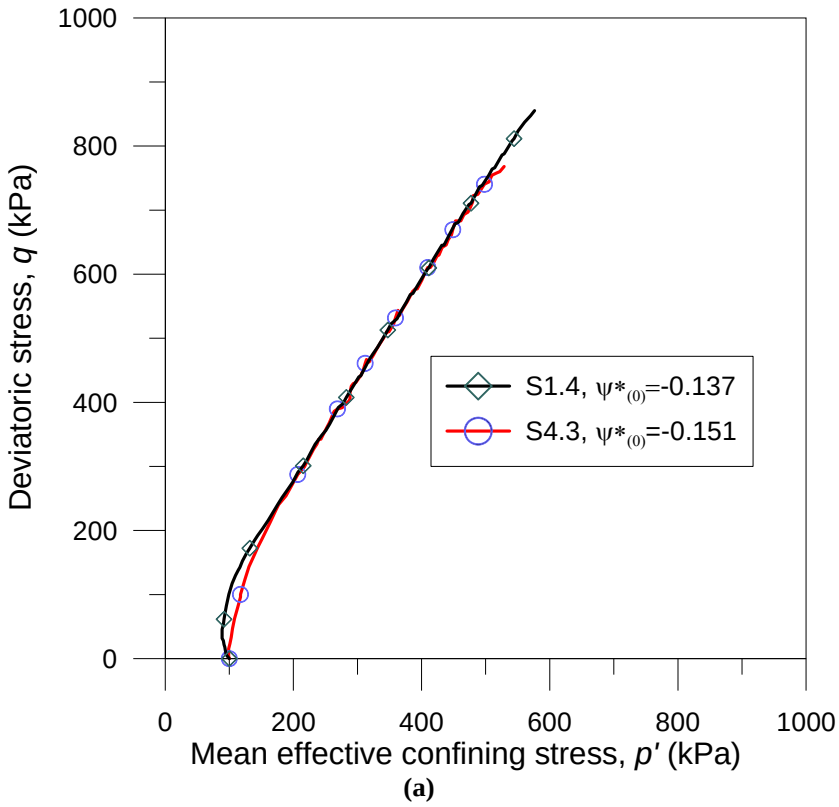

(a)

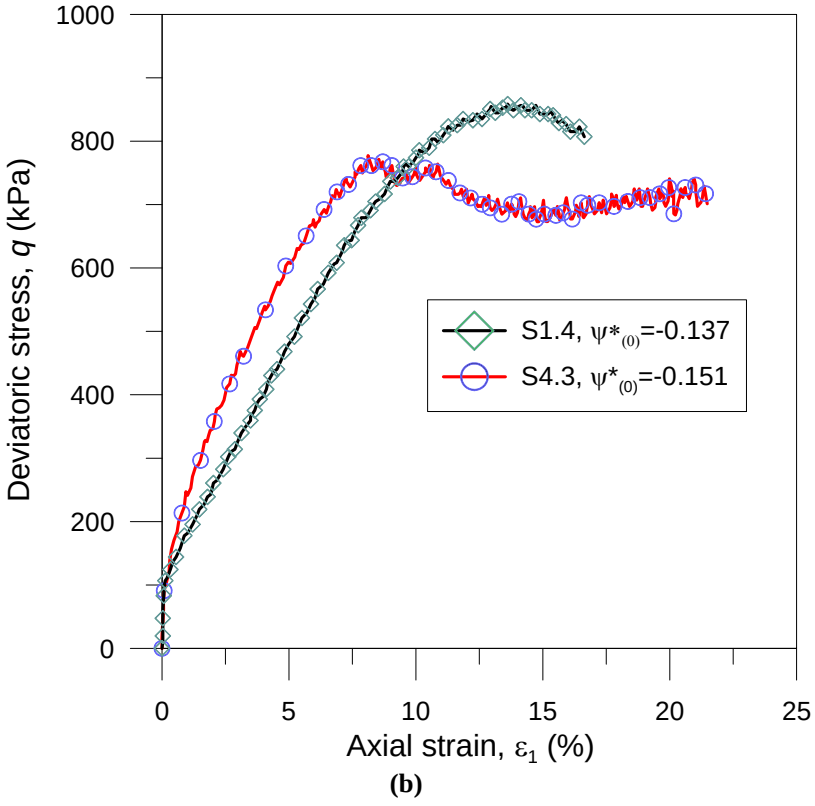

(b)

Figure 5. 19 ESP spectrum at different fines content but same $\psi^*_{(0)}$; (a) in q-p' space, (b) in q-ε_1 space, reproduced from Thevanayagam and Mohan (2000) .

5.6 SUMMARY

The main focus of this chapter was to evaluate the concept of EG-SSL and equivalent granular state parameter, $\psi^*_{(0)}$ within critical state soil mechanics, CSSM framework using two different data sets: author's experimentation and Thevanayagam and Mohan (2000). The following two issues were investigated:

- The initial state of soils relative to EG-SSL to predict flow, non-flow and limited flow behaviour and
- The correlation between equivalent state parameter, $\psi_I{}^*_{(0)}$ and undrained responses (ESP and q-ε_q).

It is found that EG-SSL can be used predict F, NF, LF and equivalent granular state parameter, $\psi^*_{(0)}$ can be correlate with the undrained responses for both data sets with CSSM framework.

CHAPTER 6

Modelling of Sand with Fines

6.1 INTRODUCTION

The concept of equivalent granular void ratio, e^* and equivalent granular state parameter, ψ^* are discussed in previous Chapters. It is shown that the equivalent granular state parameter, ψ^* can effectively predict undrained behaviour of sand with fines irrespective of fines contents. Thus, the next step is to implement these concepts in an existing constitutive model and to predict undrained behaviour of sand with fines independent of fines contents. This Chapter discusses about the selection of an appropriate model, determination of model parameters and success in predicting undrained behaviour irrespective of fines contents. The model was also used to predict undrained behaviour for sand with 10% fines from literature (Bobei 2004) and a good agreement is also observed. The details are discussed in subsequent section.

6.2 MODEL SELECTION

There are many elasto-plastic constitutive models are available for soils. However, since a clean sand is a special (limiting) case of sand with fines, a clean sand model is selected for modification/extension to include the effects of fines. The resultant model then can be degenerated back to the special case of f_c = 0% i.e. clean sand. There are two possible options in modifying an existing clean sand model so as to incorporate the influence of fines.

Option 1: modifying an existing model by introducing extra terms or factors that are function of fines contents.

Option 2: starting from a state dependent constitutive model for sand and replace $e \rightarrow e^*$, $\psi \rightarrow \psi^*$. The equivalent granular state parameters are then absorbed the effects of fines. The input parameters of this model may or may not be independent of fines content.

A major modification of the constitutive model has to be made in option 1. On the other hand, the concept of equivalent granular void ratio, e^* and ψ^* for reflecting the influence of fines is already verified in previous Chapters. Thus, option 2 is chosen for the modification.

The state dependent constitutive model should also satisfy the following conditions:

- e and ψ are parameters in the model.
- The constitutive model should be well verified and documented for sand.
- It is not too complicated.
- The input parameter can be determined from triaxial tests.

The state dependent constitutive model by Li and co-workers satisfies all above requirements (Li et al. 1999; Li 1997; Li 2002; Li and Dafalias 2000; Li and Ming 2000). This model is well documented and verified for Toyoura sand. In addition to the parameters needed for defining the CS/SS, it needs eleven input parameters and they can be all determined from triaxial tests.

The equation of this constitutive model governs both the plastic and elastic component and they are presented below.

6.2.1 *Elastic Components*

Two elastic modulus are used to be defined its elastic part. They are: shear modulus, *G* and bulk modulus, *K*.

Shear modulus, *G*

The elastic shear modulus, *G* of this model is expressed by the following empirical equation (Richart et al. 1970):

$$G = G_0 \frac{(2.97 - e)^2}{1 + e} \sqrt{p' p_a} \qquad \textbf{6. 1}$$

where, *G* is elastic shear modulus, G_0 is a material constant, *e* is current void ratio, p' is mean effective confining stress and p_a is atmospheric pressure. Note that the initial void ratio was used in the original work of Richart et al. (1970).

Bulk Modulus, *K*

Considering the isotropic condition, the elastic bulk modulus is -

$$K = G \frac{2(1 + \nu)}{3(1 - 2\nu)} \qquad \textbf{6. 2}$$

where, *K* is elastic bulk modulus and ν is the Poisson's ratio which is consider as a material constant independent of pressure and density for this model.

6.2.2 *Plastic Components*

The plastic part of the model consists of flow rule, yield function and hardening function. The equations govern these components are given below.

Flow Rule

Li and Dafalias (2000) proposed the following generalized equation for state dependent dilatancy.

$$\frac{\mathrm{d}\varepsilon_v^p}{\mathrm{d}\varepsilon_q^p} = \Delta = \Delta_0\left(e^{m_d\psi} - \frac{\eta}{M}\right) = \frac{\Delta_0}{M}\left(Me^{m_d\psi} - \eta\right) \qquad \textbf{6. 3}$$

where, Δ_0 and m_d are two positive modeling parameters, η is effective stress ratio, M is the effective stress ratio at steady State, ψ is state parameter and superscript "p" indicate plastic part. It is noted that Cam-clay dilatancy, $\Delta = M - \eta$ is a special case of state dependent dilatancy when $m_d = 0$ and $\Delta_0 = M$. Again it satisfy the condition, dilatancy equal zero at critical state, when $\psi = 0$ and $\eta = M$.

Yield Function

A linear yield function was used as a matter of simplicity.

$$f(q, p) = q - \eta\, p' = 0 \qquad \textbf{6. 4}$$

Plastic Hardening Modulus, *K*p

For plastic hardening modulus K_p, the following constitutive relation was proposed.

$$\frac{\mathrm{d}\eta}{\mathrm{d}\varepsilon_q^p} = \frac{K_p}{p'} \qquad \textbf{6. 5}$$

where,

$$K_p = hG\left(\frac{M}{\eta} - e^{n\psi}\right) \qquad \textbf{6. 6}$$

where, *K*p is plastic hardening modulus, h and n are two positive plastic model parameters.

6.3 THE MODIFIED COSTITUTIVE MODEL

The above model can be modified for sand with fines as following:

- The void ratio, e should be expressed in terms of equivalent granular void ratio, e^*.
- The equivalent granular state parameter, ψ^* should be used instead of state parameter, ψ.

The detail modification of the selected model in terms equivalent granular void ratio, e^*, equivalent granular state parameter, ψ^* and the EG-SSL is presented in coming sub-sections.

6.3.1 *Elastic Components*

The two elastic modulus can be modified in term of equivalent granular void ratio, e^* as following.

Shear modulus, *G*

The elastic shear modulus, G can be expressed by the following equation.

$$G = G_0 \frac{(2.97 - e^*)^2}{1 + e^*} \sqrt{p' p_a} \qquad \textbf{6. 7}$$

where, e^* is current equivalent granular void ratio.

Bulk Modulus, *K*

The equation of elastic bulk modulus can be written as:

$$K = G \frac{2(1+\nu)}{3(1-2\nu)} \qquad \textbf{6. 8}$$

where, G is a function of equivalent granular void ratio, e^*.

6.3.2 *Plastic Components*

The plastic part of the model can be modifies as following.

Flow Rule

The dilatancy equation can be written in terms of equivalent granular state parameter, ψ^* as following:

$$\Delta = \Delta_0\left(e^{m_d\psi^*} - \frac{\eta}{M}\right) = \frac{\Delta_0}{M}\left(Me^{m_d\psi^*} - \eta\right) \qquad \textbf{6. 9}$$

where, ψ^* is equivalent granular state parameter.

Yield Function

The yield function remained unchanged as:

$$f(q, p) = q - \eta\ p' = 0 \qquad \textbf{6. 4}$$

Plastic Hardening Modulus, *K*p

The hardening modulus can be written as:

$$\frac{\mathrm{d}\eta}{\mathrm{d}\varepsilon_q^p} = \frac{K_p}{p'} \qquad \textbf{6. 5}$$

where,

$$K_p = hG\left(\frac{M}{\eta} - e^{n\psi^*}\right) \qquad \textbf{6. 10}$$

where, *K*p is plastic hardening parameter, *h* and *n* are two positive plastic model parameters.

Based on elasto-plastic formulation of $\mathrm{d}\varepsilon_{ij} = \mathrm{d}\varepsilon_{ij}^e + \mathrm{d}\varepsilon_{ij}^p$, we have

Total deviatoric strain increment,

$$\mathrm{d}\varepsilon_q = \left(\frac{1}{3G} + \frac{1}{K_p}\right)\mathrm{d}q - \frac{\eta}{K_p}\mathrm{d}p' \qquad \textbf{6. 11}$$

Total volumetric strain increment,

$$\mathrm{d}\varepsilon_v = \frac{\mathrm{d}p'}{K} + \Delta \times \frac{\mathrm{d}q - \eta \mathrm{d}p'}{K_p} = \frac{\Delta}{K_p}\mathrm{d}q + \left(\frac{1}{K} - \frac{\Delta \times \eta}{K_p}\right)\mathrm{d}p' \qquad \textbf{6. 12}$$

where G, K, Kp, Δ are function of e* and ψ*.

6.4 CRITICAL STATE PARAMETERS

The critical state parameter can be obtained from critical state line. In this case it is EG-SSL. Mathematically, the EG-SSL is defined by

- The slope of the EG-SSL, M, in the q-p' space.

- The function defining the equation of EG-SSL in e*-p' space

Figure 6. 1 shows that the EG-SSL in q-p' space for sand with fines. It is essentially a single line for f_c in the range of 0% to 30%. The slope of the line, M is 1.305 i.e. M remain constant with increase in fines content up to 30%.

The following equation of EG-SSL in e*-log(p') space was given in Chapter 5.

$$e^* = 0.908 - 0.0266 \times \left(\frac{p'}{p_a}\right)^{0.7} \qquad \textbf{5.2}$$

where, e_Γ = 0.908, λ = 0.0266 and ξ = 0.70. Thus, all critical state parameters are extracted from Figure 6. 1 and Equation 5.2. They are summarized in Table 6. 1.

Table 6. 1: Critical/ Steady state parameters of constitutive model

Critical State Parameters	
M	1.305
e^*_Γ	0.908
λ	0.0266
ξ	0.70

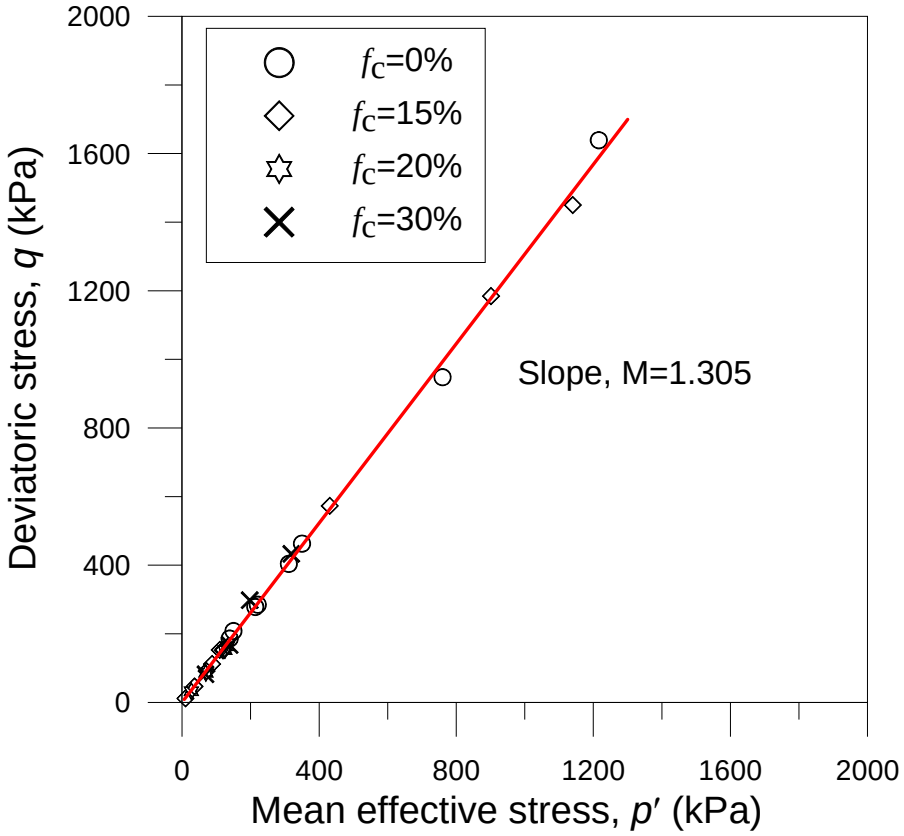

Figure 6. 1: The slope of Critical or Steady State Line, *M* in *q*-*p′* space.

6.5 DETERMINATION OTHER MODEL PARAMETERS

This section discussed about the determination of other seven model parameters. These parameters can be classified in three groups: elastic, dilatancy and hardening parameters as shown in Table 6. 2. Both drained and undrained tests can be used to determine these parameters. However, only drained tests are used to obtain these parameters because, the intension is to-

i) Predict undrained behaviour with the proposed model and compared with the undrained test results.

ii) Therefore, to have a prediction rather than a simulation of undrained behaviour, the input parameters have to be obtained from different test conditions (in this case drained).

The details of the testing program for model parameter determination exercise is given in Table 6. 3. Six drained tests for sand with 10% fines content were used for this purpose. Four out of six test were obtained form Bobei (2004). The tests cover initial confining stress from 100kPa to 600kPa and equivalent granular void ratio from 0.719 to 0.955.

Table 6. 2: The other parameters required for the proposed model

Elastic parameter	Dilatancy parameter	Hardening parameter
G_0	Δ_0	h_1
ν	m_d	h_2
		n

Table 6. 3: Details of drained tests used in determination of model parameters

Test Name	Source	Fines content, (%)	p'_0 (kPa)	Beginning of shearing	End of shearing
				Eq. granular void ratio, e^*	
S-MII-10-01	Author	10	300	0.772	0.829
S-MII-10-02	Author	10	350	0.719	0.821
A1	(Bobei 2004)	10	100	0.955	0.875
A2	(Bobei 2004)	10	300	0.921	0.843
A3	(Bobei 2004)	10	400	0.903	0.882
A4	(Bobei 2004)	10	600	0.892	0.807

6.5.1 *Elastic Parameters*

The Equation 6. 7 can be rewritten as following:

$$G = p_a G_o \frac{(2.97 - e^*)^2}{1 + e^*} \sqrt{\left(\frac{p'}{p_a}\right)} \qquad \textbf{6. 13}$$

Replacing Equation 6. 13 into Equation 6. 8

$$K = \left(\frac{\mathrm{d}p'}{\mathrm{d}\varepsilon_v^e}\right) = G_o \frac{(2.97 - e^*)^2}{1 + e^*} \frac{2(1+\nu)}{3(1-2\nu)} \sqrt{\left(\frac{p'}{p_a}\right)} \times p_a \qquad \textbf{6. 14}$$

This can be rewritten as

$$\left(\frac{d\varepsilon_v^e}{dp'}\right) = A\left(\frac{p'}{p_a}\right)^{-0.5} {p_a}^{-1} \qquad \textbf{6. 15}$$

where,

$$\frac{1}{A} = G_0 \frac{(2.97 - e^*)^2}{(1 + e^*)} \times \frac{2(1+\nu)}{3(1-2\nu)} \qquad \textbf{6. 15a}$$

The value of ν for Sydney sand was reported 0.30 in literature (Lo and Lee 1990). Therefore, G_0 is known once A is known. Experimental data of a purely elastic response can be used to obtain A, following the Equation 6.15. There are several ways to achieve elastic response in tri-axial testing system (Atkinson and Richardson 1985). However, most reliable and easy way to achieve elastic response is the isotropic unloading. To achieve an unloading response, the test S-MII-10-02 was isotropically loaded to 350kPa and then gradually unloaded to 32kPa. The unloading response of the test was used to determine G_0 by following procedure:

- Triaxial isotropic p' - $\Delta\varepsilon_v$ response of test S-MII-10-02 is shown in Figure 6. 2. The maximum isotropic load (350kPa) and its corresponding volumetric strain (0.006%) were set as bench mark.

- Simulated unloading p' - $\Delta\varepsilon_v$ response were also simulated from Equation 6. 15 for different value of A by an incremental calculation from the maximum isotropic stress of S-MII-10-02. The simulated paths were compared with unloading path of S-MII-10-02. They are also presented in Figure 6. 2.

- Appropriate A = 0.0019 was obtained for a close match of unloading response of S-MII-10-02 and the theoretical response.

- The equivalent granular void ratio, e^* during test was varied from 0.725 to 0.719. Hence an average e^* of 0.721 was taken for calculation.

- Then, G_0 = 82 was determined from Equation 6. 15a. The obtained data is presented in Table 6. 4.

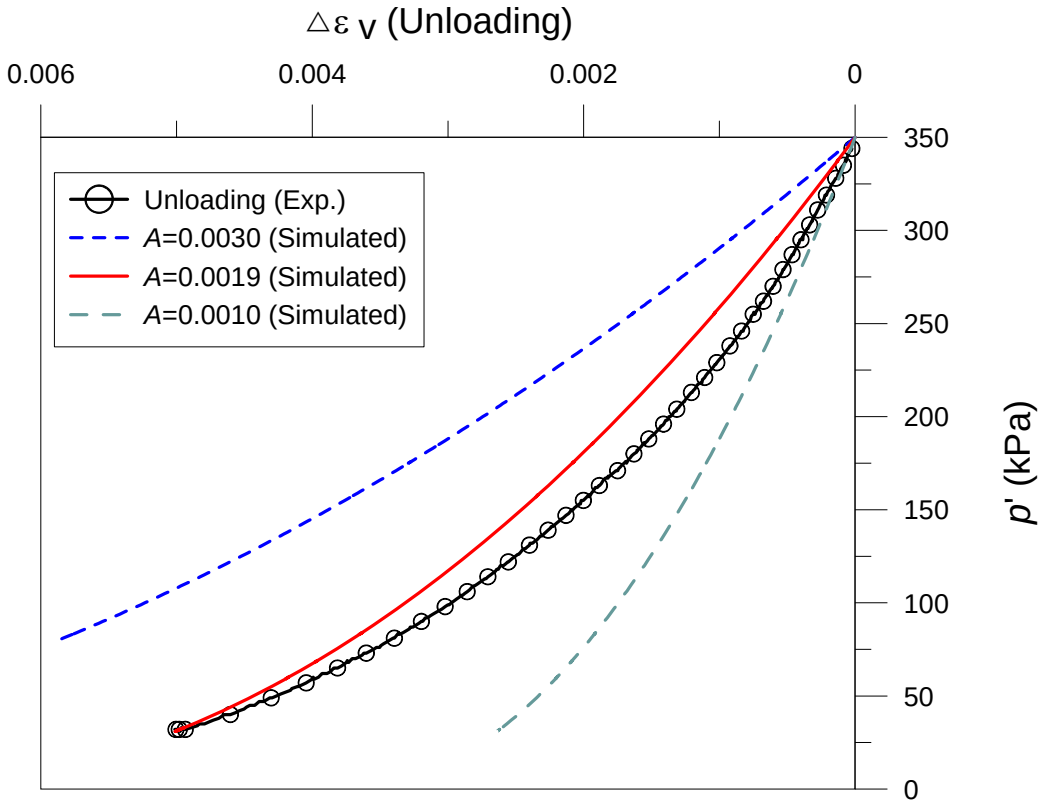

Figure 6. 2: Determination of *A* to obtain G_0

Table 6. 4: Dilatancy parameters for sand and sand with fines

Test name	A (10^{-3})	ν	e^*	G_0
S-MII-10-02	1.90	0.30	0.721	82

6.5.2 *Dilatancy parameters*

The dilatancy parameters: m_d and Δ_0 were obtained from calibration with a conventional drained tri-axial test data. Test A2 was used for this purpose. The calibration is done in such a way that, for a suitable set of m_d and Δ_0, the simulated flow rule in η-(1-Δ) space obtain a close match with the experimental flow rule. The

Figure 6. 3 shows that the simulated and the experimental flow rule are in close match for Δ_0 = 1.06 and m_d = 0.50. However emphasis was given to achieve a better match in higher stress ratio, η because the data at higher stress ratio, η are most reliable. The calibrated dilatancy parameters are given in Table 6. 5.

Table 6. 5: Dilatancy parameters for Sydney sand with 10% M-II fines

Test Name	Source	Fines (%)	p'_0 (kPa)	Dilatancy parameters	
				m_d	Δ_0
A2	(Bobei 2004)	10	300	0.50	1.06

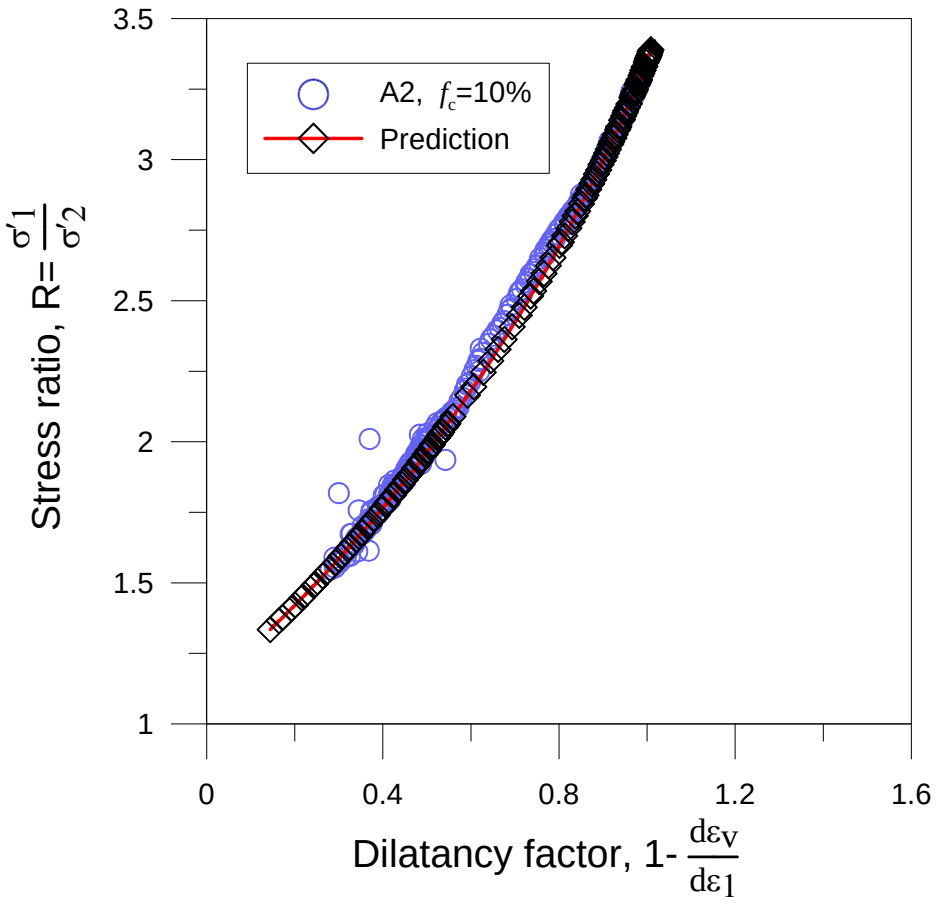

Figure 6. 3: Determination of dilatancy parameters from Test A2.

6.5.3 *Hardening parameter*

The hardening parameters were determined from the conventional drained triaxial test data. They are explained below:

6.5.3.1 Determination of "*n*"

At drained failure, *K*p = 0; thus the following can be obtained from Equation 6. 10.

$$n = \frac{1}{\psi_f^*} \ln \frac{M}{\eta_f} \qquad \textbf{6. 16}$$

For a medium dense sand with $\eta_f > M$ and $\psi_f^* \neq 0$, therefore *n* can be obtained from such a failure condition. A value of *n* = 0.95 obtained from Test S-MII-10-01.

6.5.3.2 Determination of "*h*"

The second parameter, *h* can be deduced by the following procedure. For a conventional drained tri-axial test, the hardening Equation 6. 10 can be written as:

$$\frac{dq}{d\varepsilon_q} \approx \frac{dq}{d\varepsilon_q^p} = \frac{K_p}{1 - a\eta} = hG_0 \left\{ \frac{(2.97 - e^*)^2 \left[(M/\eta) - e^{n\psi^*} \right] \sqrt{p' p_a}}{(1 + e^*)\left(1 - \frac{1}{3}\eta\right)} \right\} \qquad \textbf{6. 17}$$

The plot $\frac{dq}{d\varepsilon_q^p}$ Vs $\left\{ \frac{(2.97 - e^*)^2 \left[(M/\eta) - e^{n\psi^*} \right] \sqrt{p' p_a}}{(1 + e^*)\left(1 - \frac{1}{3}\eta\right)} \right\}$ should be linear and G_0h is the slope. Such a plot was presented in Figure 6. 4, for test S-MII-15-02 where G_0h is 67.5 and *h* is 0.82. Note that *e** is variable.

Since, *h* for each test corresponds to a range of *e**. So in the plot of *h* verses *e**, each test gave a bar instead of giving one point as shown in Figure 6. 5.

The process was repeated for 5 other tests with different initial e^* and hence 5 more bars were achieved as shown in Figure 6. 5. The bars are quite narrow and therefore, a linear fit can be assumed. This is consistent with Li and Dafalias (2000). The linear fit can be presented by the following equation.

$$G_0 h = G_0 (h_1 - h_2 e^*) = 365 - 345 e^* \qquad \textbf{6. 18}$$

where, G_0 is equal to 82, thus the Equation 6. 18 can be rewrite as

$$h = 4.45 - 4.20 e^* \qquad \textbf{6. 19}$$

Thus one can obtain, h_1 = 4.45 and h_2 = 4.20.

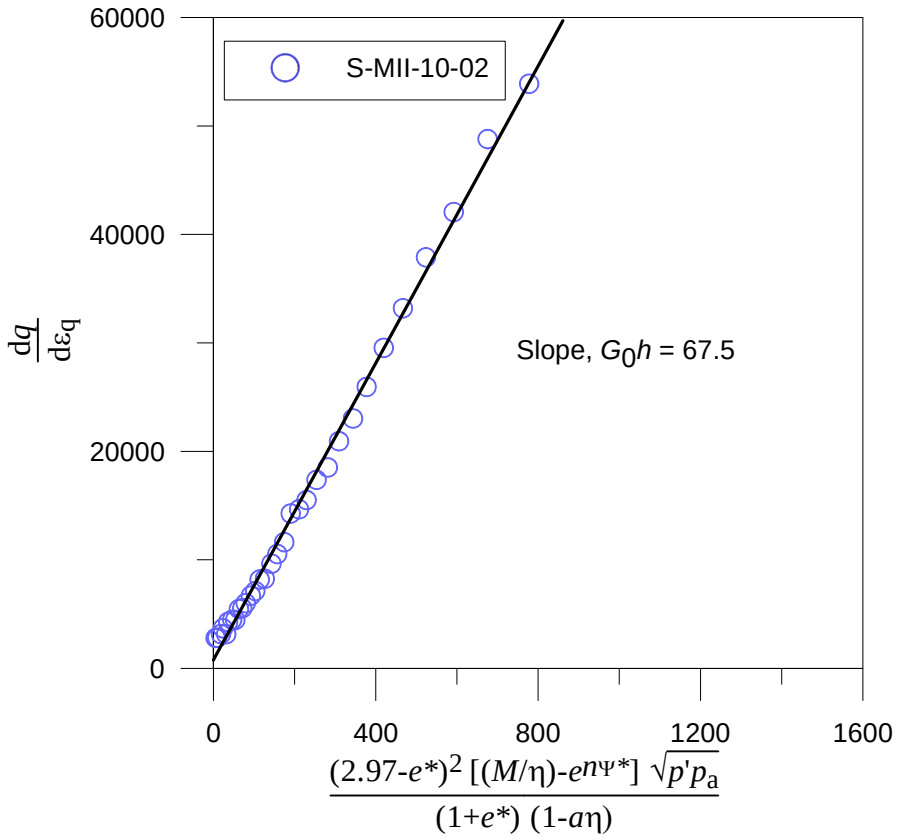

Figure 6. 4: Determination of hardening parameters from test S-MII-10-01

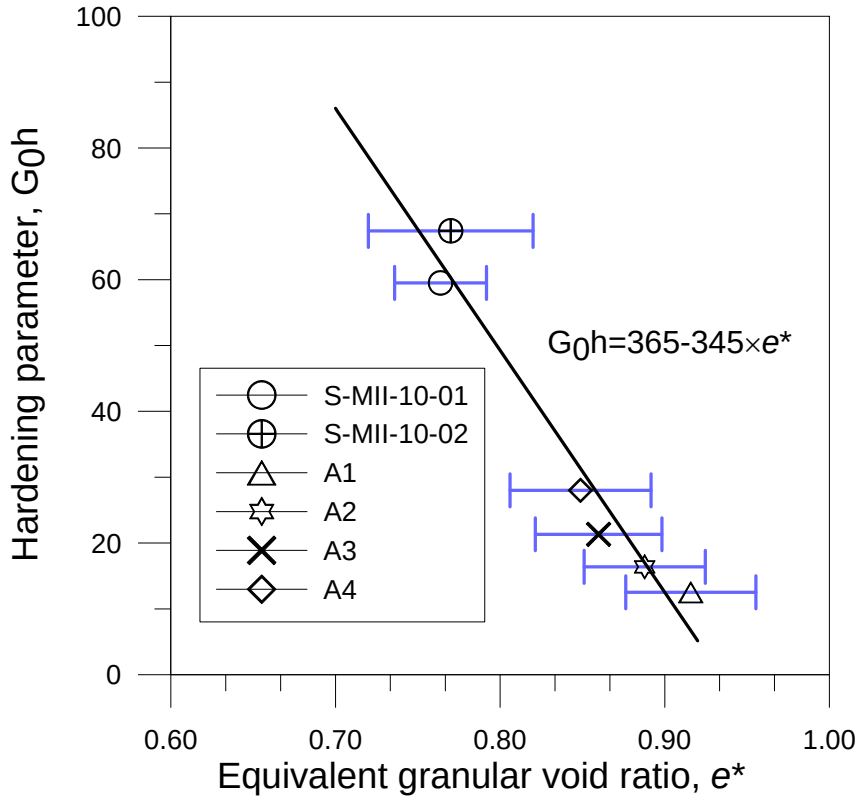

Figure 6. 5: Relation between hardening parameter and equivalent granular void ratio, *e

This concluded the determination of model parameters. Note that all the model parameters were obtained from sand 10% fines with the intension that it can be used to predict drained/undrained behaviour for sand with a range of fines contents. All the eleven parameters, including CS/SS parameters are summarized in Table 6. 6.

Table 6. 6: All parameters for the model from drained test.

Elastic parameter		Critical state parameter		Dilatancy parameter		Hardening parameter	
G_0	82	M	1.305	Δ_0	1.06	h_1	4.45
ν	0.30	e^*_Γ	0.908	m_d	0.50	h_2	4.20
		λ	0.0266			n	0.95
		ξ	0.70				

6.6 PREDICTION OF FLOW RULE OF DRAINED TESTS

Partial evaluation of the model was done by predicting flow rule (stress dilatancy response) of drained tests other than the tests used in model parameter determination. Thus, it is also an independent model prediction exercise. Drained test for clean sand, sand with 10%, 15% and 25% fines are used in the evaluation exercise. The details of the testing program is given in Table 6. 7. Thus, it gives a primary evaluation whether the model can used to predict independent of fines content.

Table 6. 7: Summary of the tests used for flow rule prediction

Test Name	Source	Fines content, (%)	p'_0 (kPa)	Beginning of shearing	End of shearing
				Eq. granular void ratio, e^*	
H2	(Bobei 2004)	0	50	0.907	0.858
A1	(Bobei 2004)	10	100	0.955	0.875
S-MII-15-11	Author	15	350	0.941	0.862
S-MII-25-02	Author	25	600	0.857	0.788

Note that test H2 was used for the model evaluation for 0% fines content. The conventional stress-strain and volume change diagram for these tests are shown in Figure 6. 6. The predicted flow rule is evaluated over wide range of fines content, including clean sand using input parameter determined form 10% fines content. The comparisons are shown in Figure 6. 7 and Figure 6. 8. Evidently good perditions were achieved for different fines content.

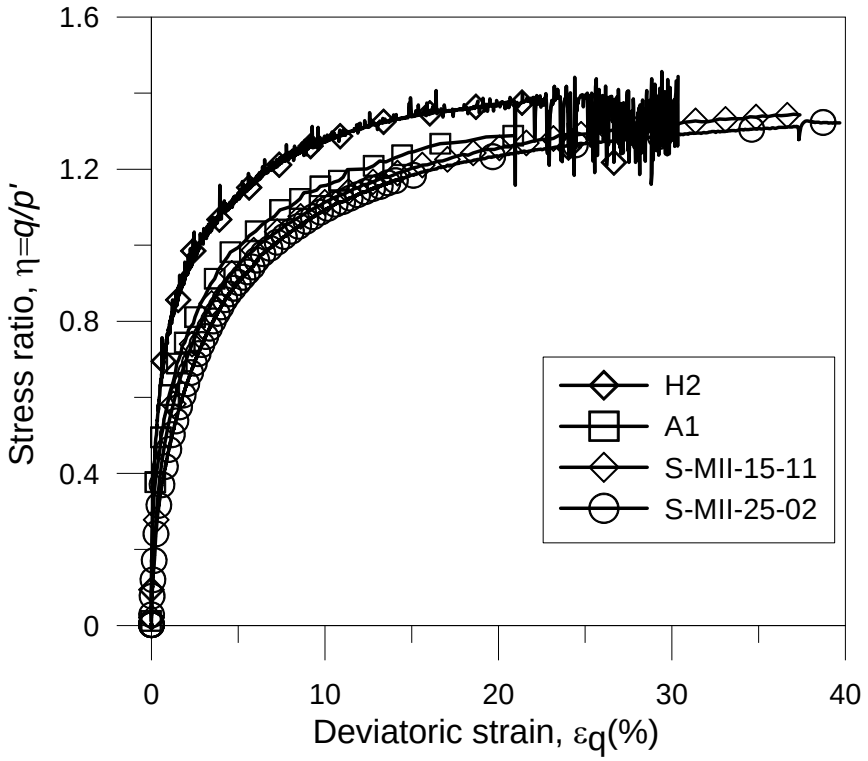

(a)

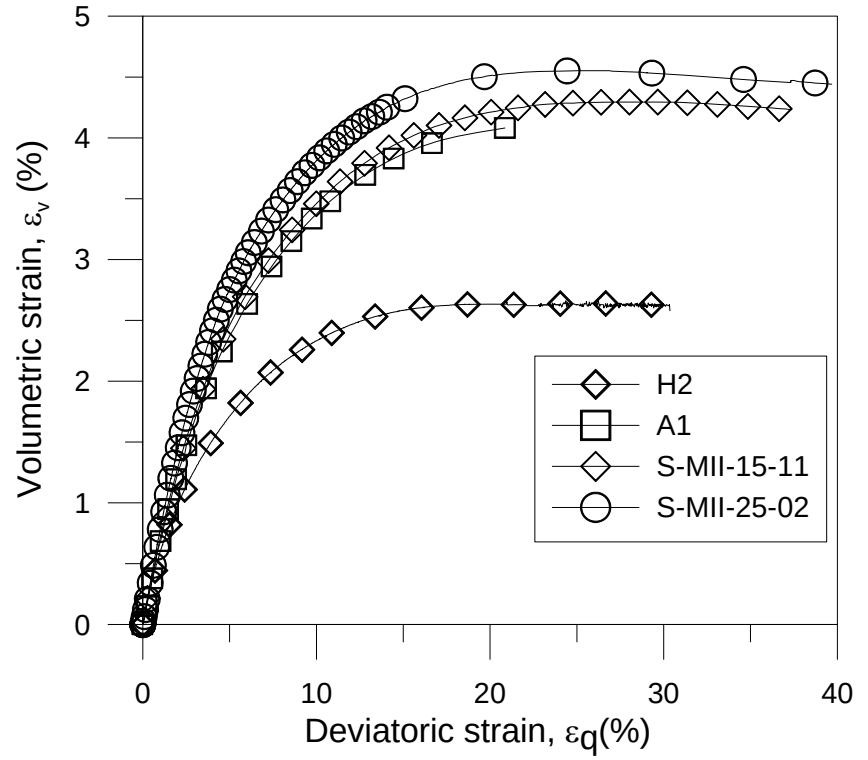

(b)

Figure 6. 6: The conventional stress-strain and volume change diagram for the tests used in flow rule prediction.

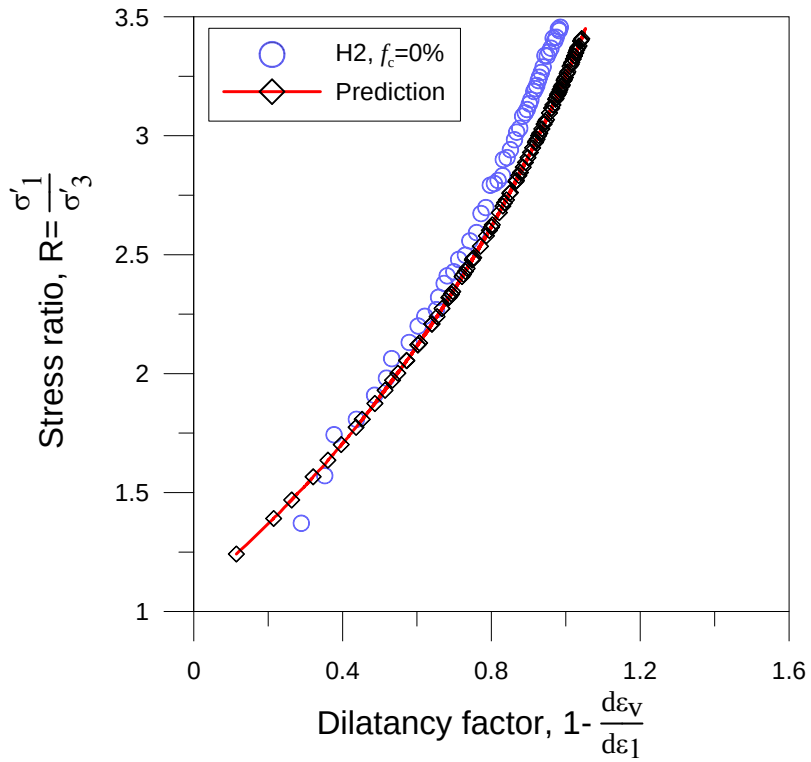

(a)

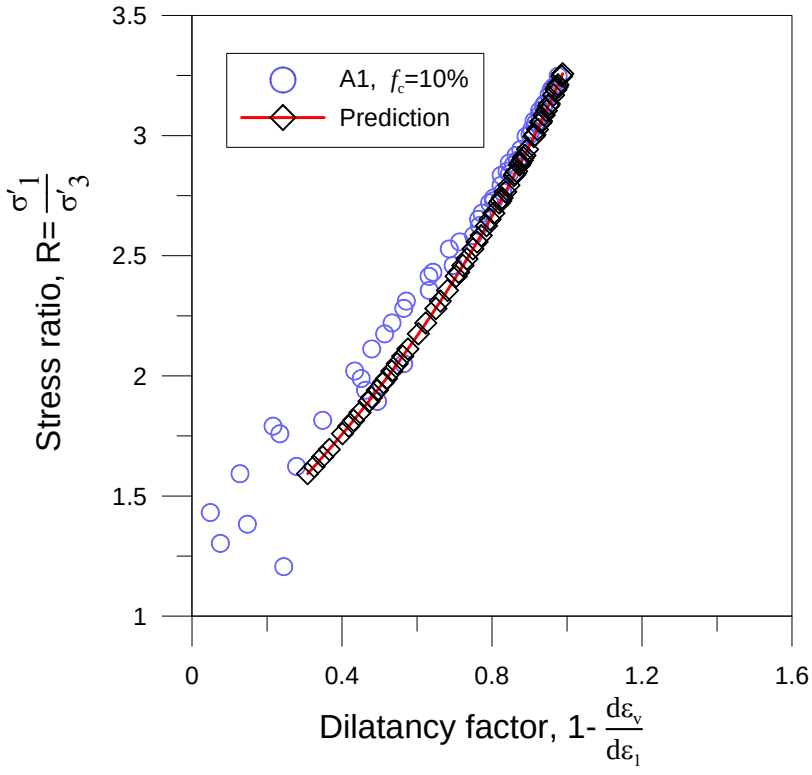

(b)

Figure 6. 7: Prediction of flow rule; (a) Sydney sand, (b) Sydney sand with 10% M-II fines.

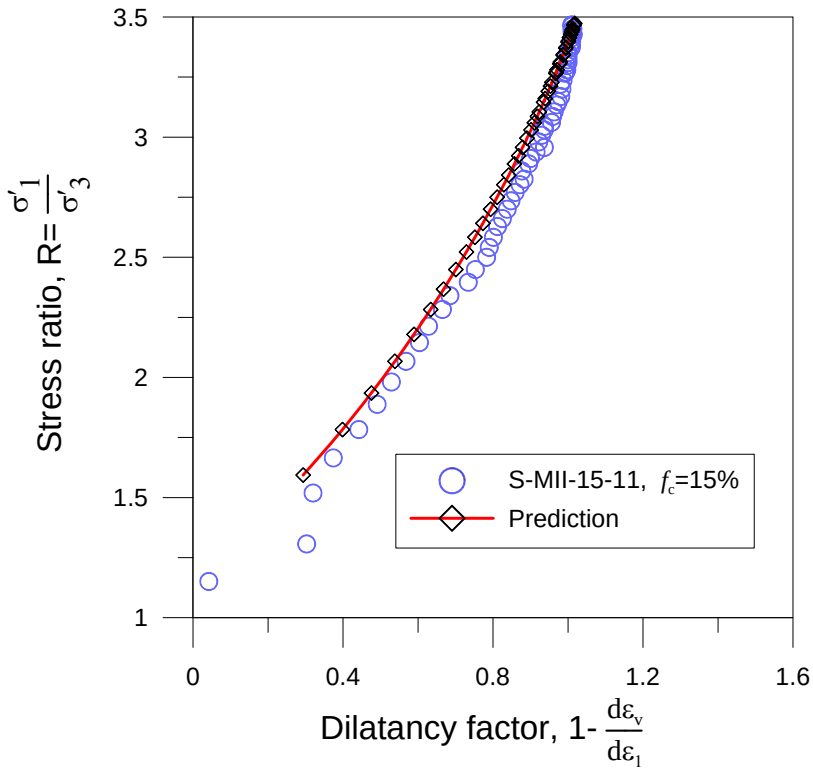

(a)

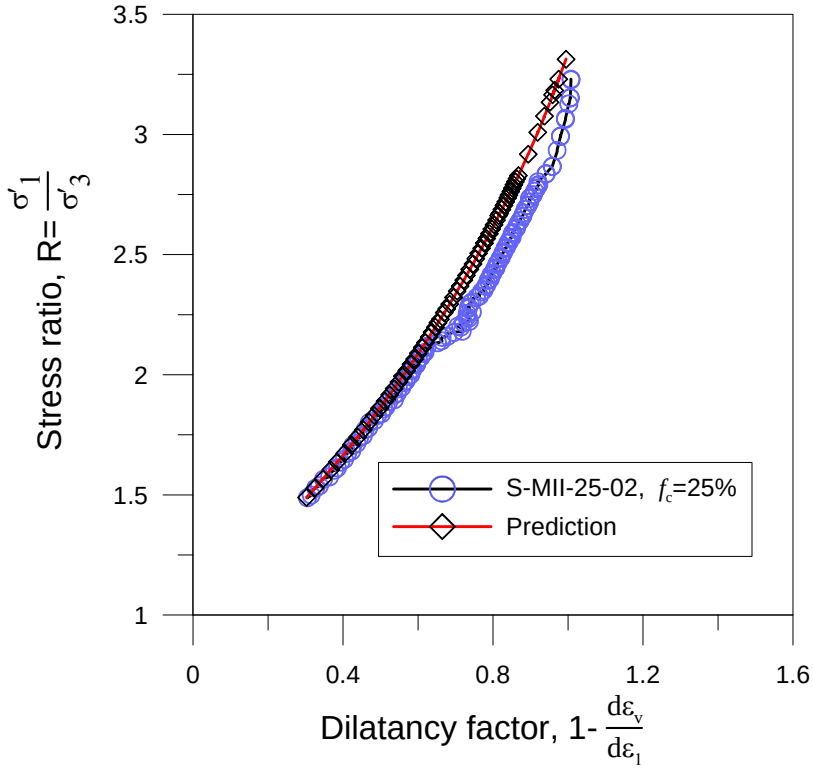

(b)

Figure 6. 8: Prediction of flow rule; (a) Sydney sand with 15% M-II fines, (b) Sydney sand with 25% M-II fines.

6.7 PREDICTION OF UNDRAINED TESTS

In undrained test, the volume of the sample remains unchanged. Thus, replacing $d\varepsilon_v = 0$ in the Equation 6. 12, one can obtain-

$$d\varepsilon_v = 0 = \frac{dp'}{K} + \Delta\frac{dq - \eta dp'}{K_p} = \frac{\Delta}{K_p}dq + \left(\frac{1}{K} - \frac{\Delta\eta}{K_p}\right)dp' \qquad \textbf{6. 20}$$

Re-writing the above equation

$$dp' = -p'K\frac{\Delta}{K_p}d\eta \qquad \textbf{6. 21}$$

This is the key equation to predict the effective stress path, ESP response. The ESP of undrained test can be obtained by the following procedure/algorithm which is based on finite difference with forward stepping:

1. Initial condition of the test i.e. $p'_{(0)}$, $q_{(0)}$, $e^*_{(0)}$ and model parameters are assigned.

2. Read current state of sample and calculate $\psi^*, \eta = \frac{q}{p'}$, G, K, Δ and Kp.

3. Stepping $\delta\eta$ (approximating $d\eta$ by $\delta\eta$).

4. Calculate $\delta p'$ from Equation 6. 21 and p' as $(p')_{i+1} = (p')_i + \delta p'$.

5. Calculate δq as $dq = p'\delta\eta + \eta\delta p'$ and q as $(q)_{i+1} = (q)_i + \delta q$.

6. Calculate $\delta\varepsilon_q$ from Equation 6. 11 and $(\varepsilon_q)_{i+1} = (\varepsilon_q)_i + \delta\varepsilon_q$.

7. Repeat the step 2 to 6 until it reached to the steady state.

where the subscript "*i*" denote the *i*-th step.

Note that for isotropic consolidation, a numerical calculation can not start at $q = 0$, thus a small value $q \approx 0.01$ was assigned. The stepping $\delta\eta$ need to be carefully chose around M to avoid over shooting; $\delta\eta$ have to be small to achieve smooth 'limited flow' responses. Thus, the $\delta\eta$ for $(i + 1)$ step was $\delta\eta_{(i+1)} = \delta\eta_i\left[1 - \frac{\eta}{M}\right]$.

Now, the above steps can produced complete ESP and deviatoric stress-strain response i.e. undrained prediction by the model. Thus, a comparison between undrained response of triaxial tests and the model prediction can be present in this section. Three types of undrained behaviours: flow, limited flow and non flow are compared with model prediction in separate subsections. The flow behaviour is discussed first. Then limited flow and non-flow behaviour are also discussed in subsequent section. The organization of evaluation exercise can be presented below:

- Prediction of flow behaviours
    - with different fines content at different p'_0.
    - with different fines content at same p'_0.
    - with different fines content at same $\psi^*_{(0)} \approx 0.090$.
    - with different fines content at same $\psi^*_{(0)} \approx 0.080$.
- Prediction limited flow behaviour.
- Prediction of non-flow behaviour.

6.7.1 *Prediction of Flow Behaviour*

Four sets of model prediction for flow behaviour are presented in this section. First set covers a variation of fines contents from 0% to 30% and mean effective stress from 350kPa to 1100 kPa. The comparisons between effective stress path ESP and the model prediction for 0% and 30% are compared in Figure 6. 9a. The ESP prediction for S-MII-00-10 and S-MII-30-01 are very good. The prediction q-ε_q responses are shown in Figure 6. 9b. The prediction for S-MII-30-01 is very good where as prediction for S-MII-00-10 deviates from experimental results in large strain. However, the over all model prediction are in good agreement with experimental results. The prediction of ESP for 15% and 20% are shown in Figure 6. 10a. The model prediction are excellent. The prediction for q-ε_q responses are shown in Figure 6. 10b. the prediction are in very good agreement with experimental results. Thus, the overall model predictions are independent of fines content with in a range of confining stress from 350kPa to 1100kPa.

The second set of data compares model prediction for three tests with three different fines content (15%, 20%, 30%) at same initial effective stress of 850kPa as shown in Figure 6. 11a&b to Figure 6. 13a&b. The prediction of ESP and q-ε_q responses are excellent for all three tests. Once again, the prediction is independent of fines contents.

The third sets present a comparison between experimental results and the model prediction for same equivalent granular state parameter, $\psi^*_{(0)}$ of 0.097 but different fines content. Figure 6. 14a&b presents a comparison between ESP and deviatoric stress-strain responses. The prediction of ESP are excellent and the prediction of

deviatoric stress-strain responses are also in very good agreement. Again, the overall prediction closely match with experimental results despite of their difference in fines content and initial mean effective stress.

The forth set also presents comparison between experimental results and the model prediction for same equivalent granular state parameter, $\psi^* \approx 0.080$ but different fines contents and initial confining stress, p' as shown in Figure 6. 15a&b and Figure 6. 16a&b. Figure 6. 15a&b shows a comparison between the experimental results and the model prediction for the test S-MII-15-03. The model predictions for ESP and q-ε_q responses are excellent. Figure 6. 16a&b shows a comparison between the experimental results and the model prediction for the tests S-MII-20-03 and S-MII-30-01. The model predictions for ESP and q-ε_q responses for corresponding tests are also in very good agreement. Thus, the state dependent constitutive model in conjunction with equivalent granular void ratio, e^* and state parameter, ψ^* can be used to predict undrained flow behaviour of sand with fines independent of fines contents.

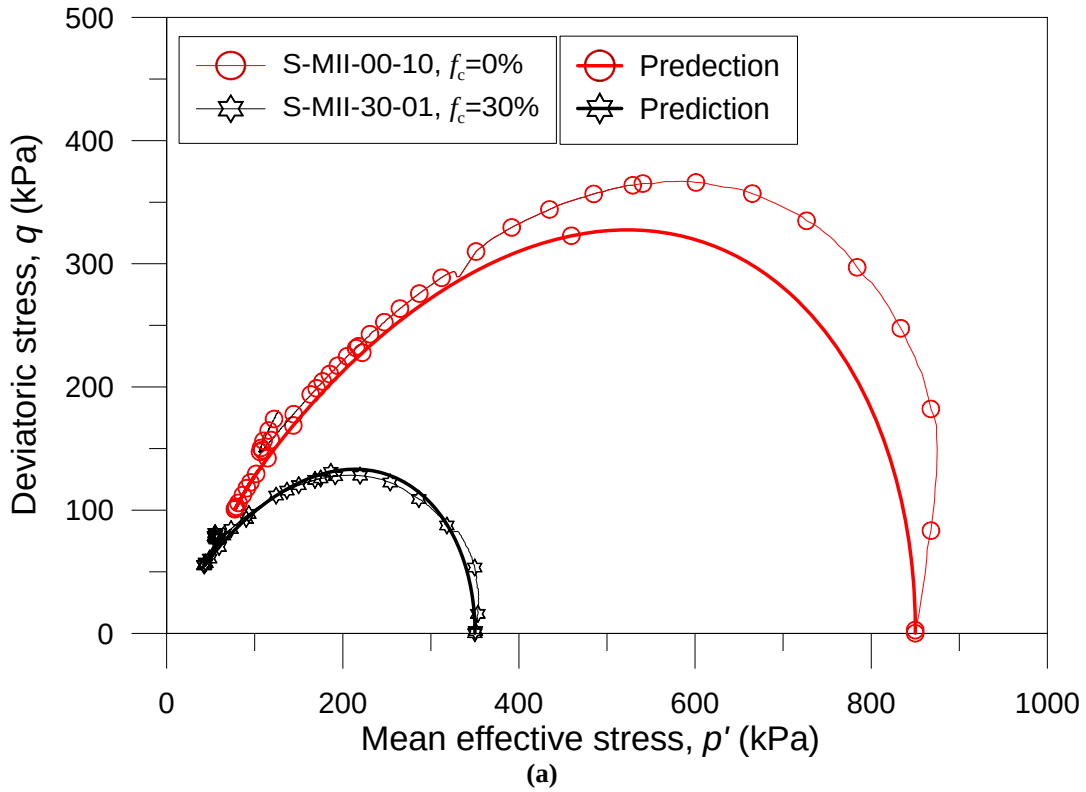

(a)

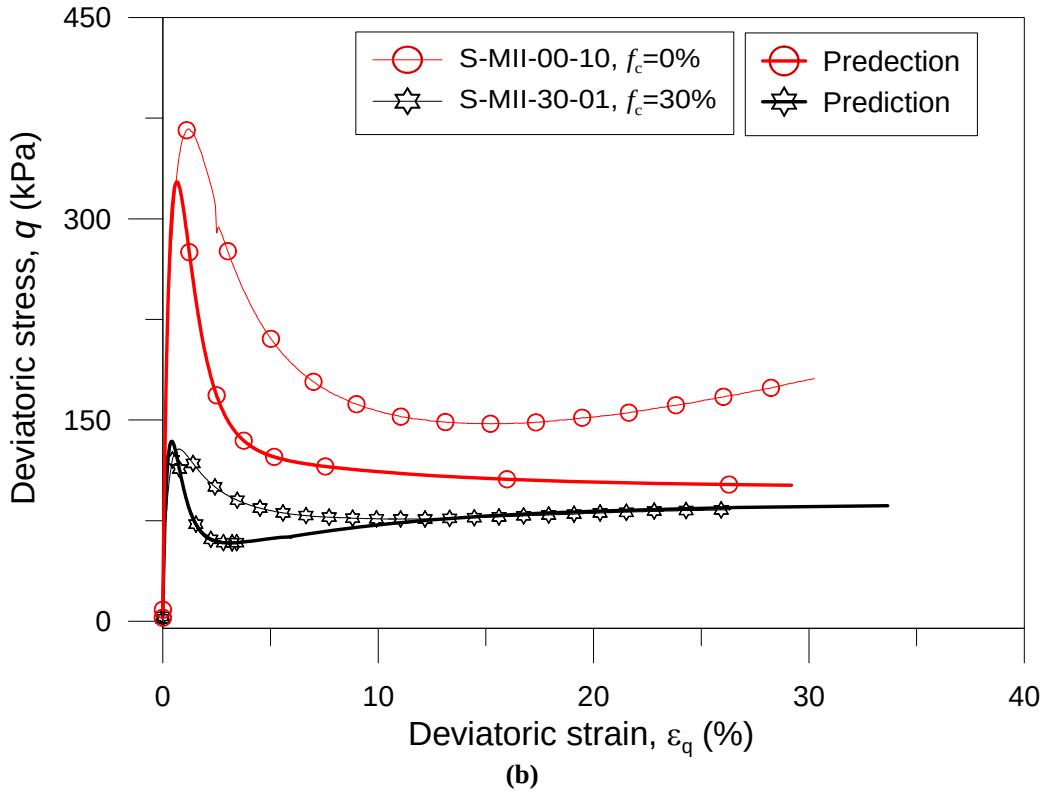

(b)

Figure 6. 9 **Comparison between undrained triaxial compression tests results and model prediction for different fines content, f_c and different initial mean effective stress, p'_0.**

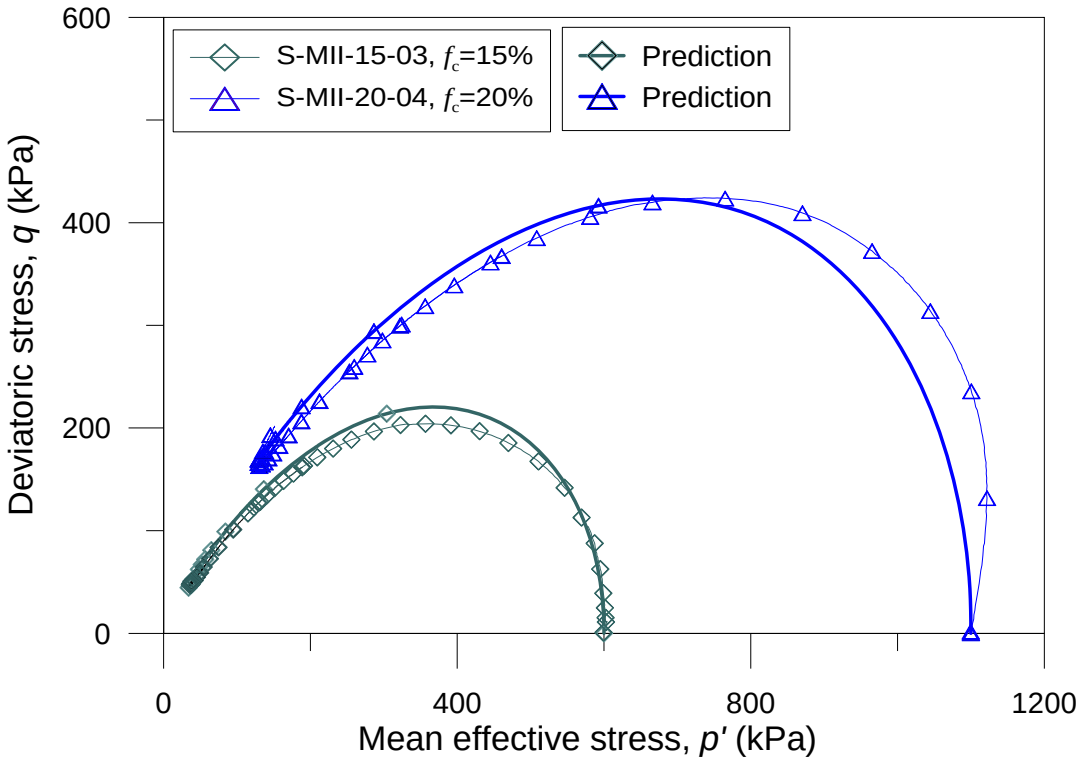

(a)

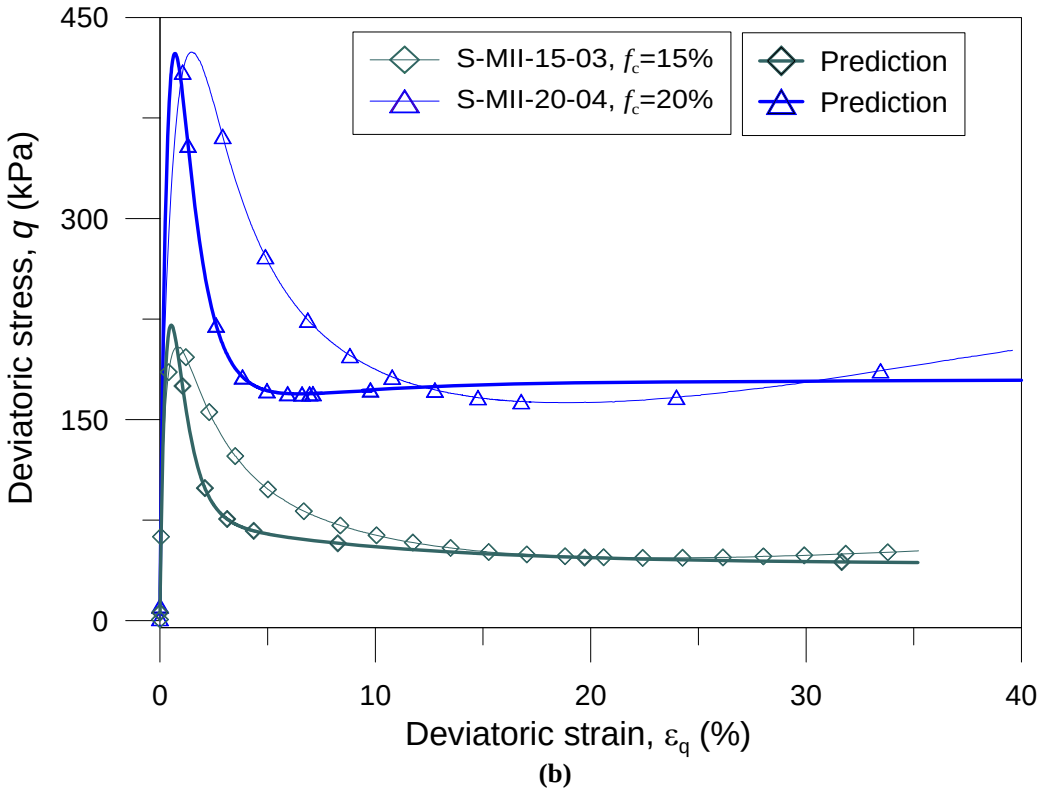

(b)

Figure 6. 10 **Comparison between undrained triaxial compression tests results and model prediction for different fines content, f_c and different initial mean effective stress, p'_0.**

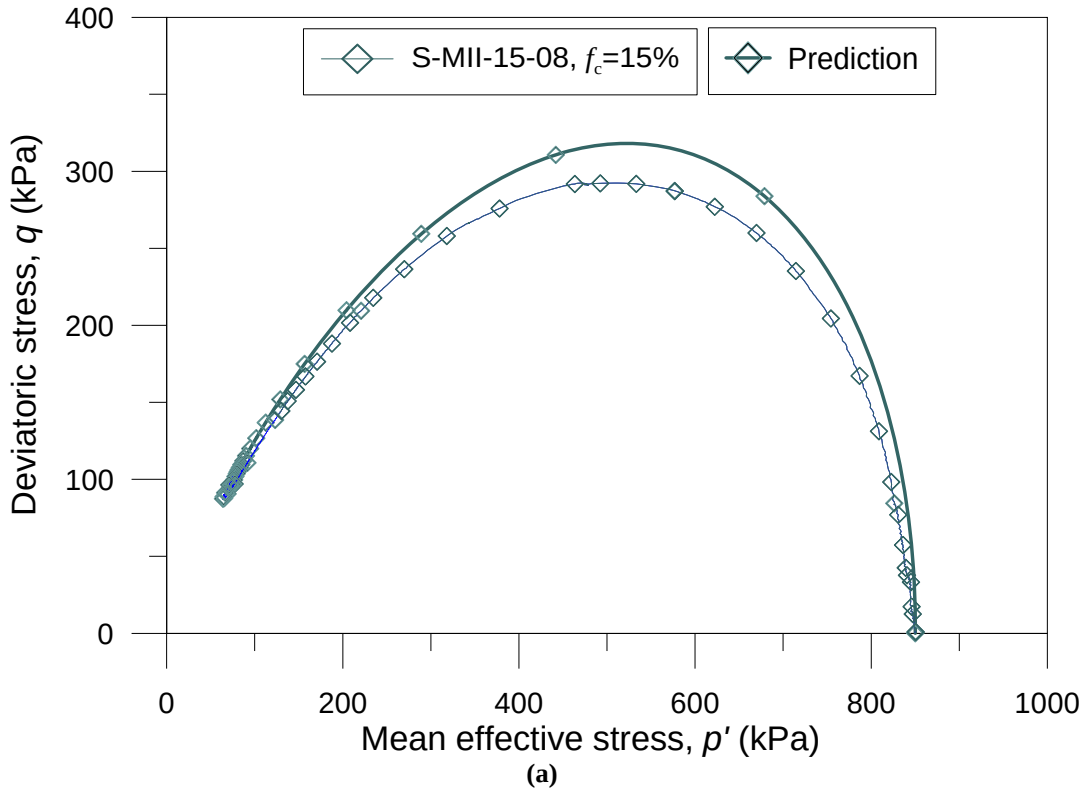

(a)

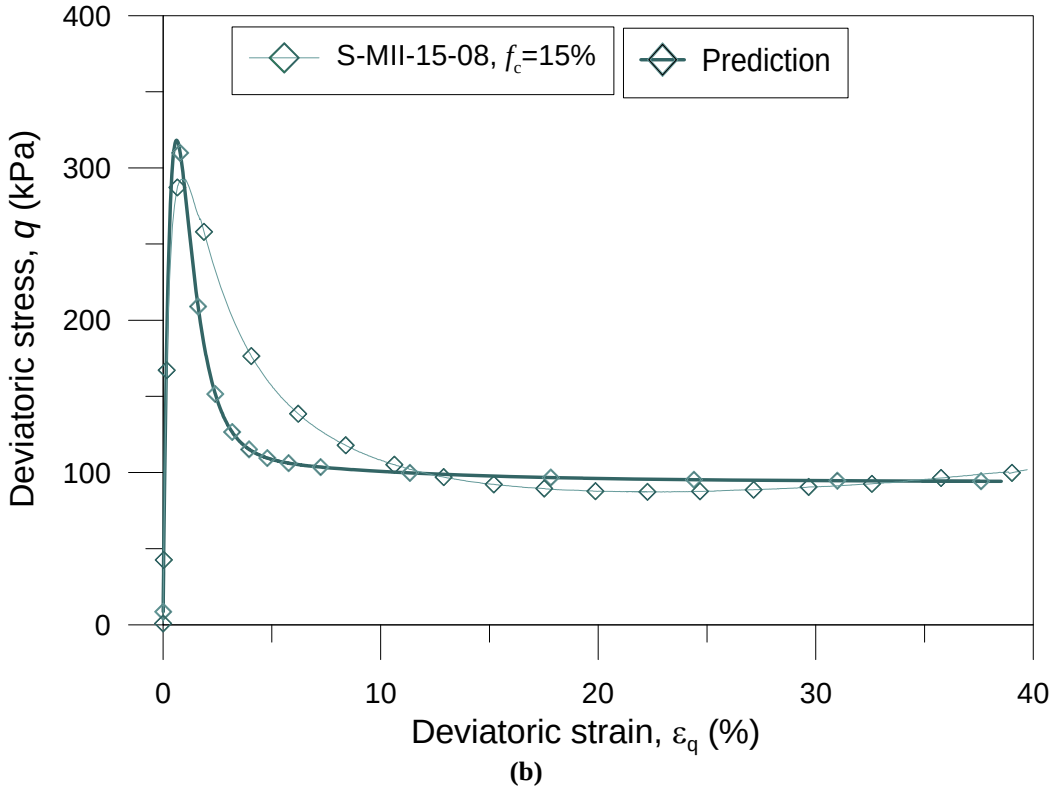

(b)

Figure 6. 11 **Comparison between undrained triaxial compression tests results and model prediction for different fines content, f_c at same initial mean effective stress, p'_0 = 850kPa.**

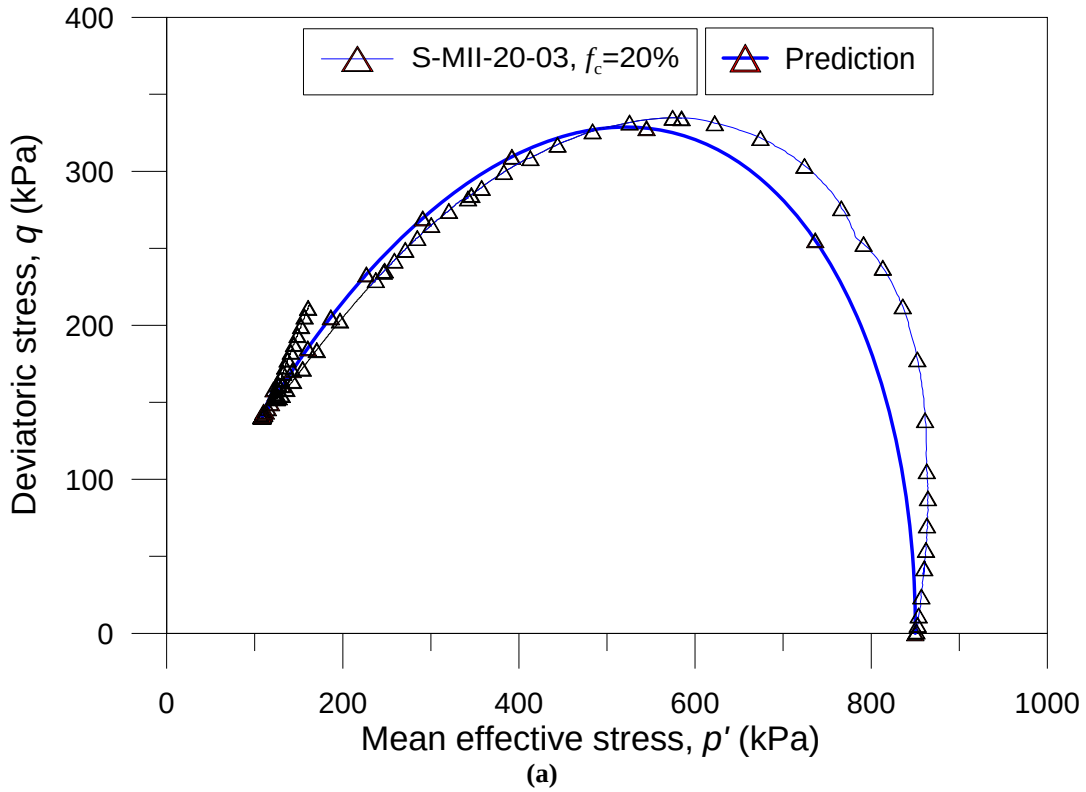

(a)

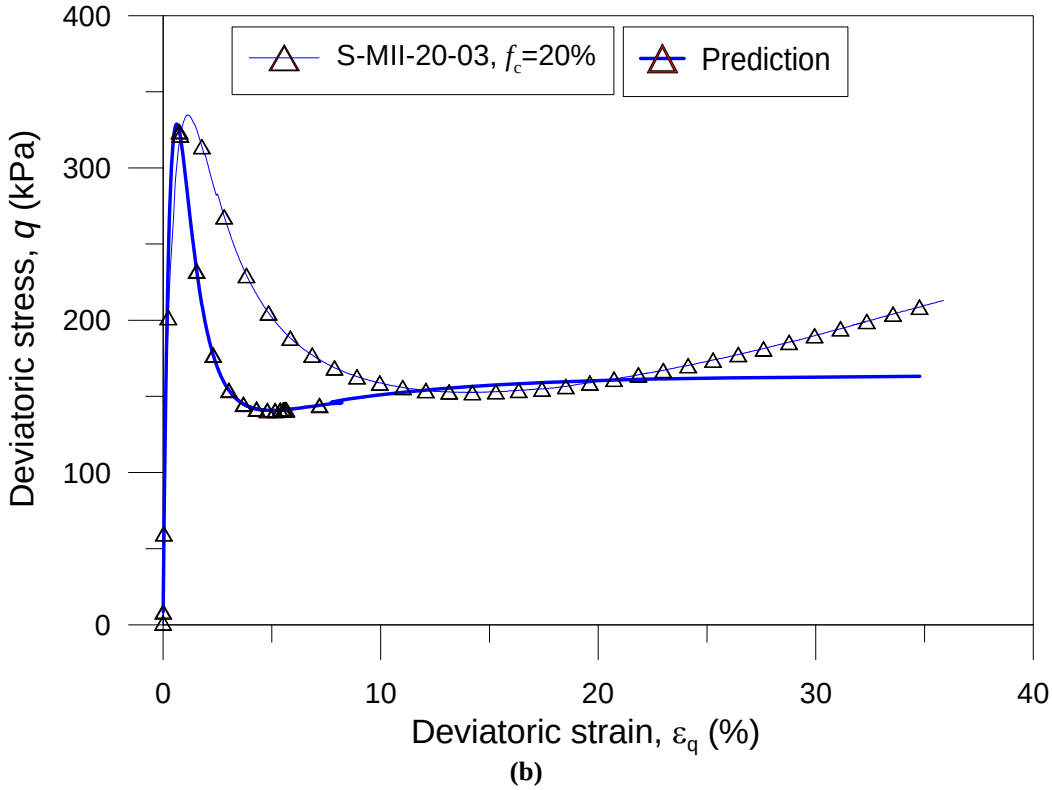

(b)

Figure 6. 12 **Comparison between undrained triaxial compression tests results and model prediction for different fines content, f_c at same initial mean effective stress, p'_0 =850kPa.**

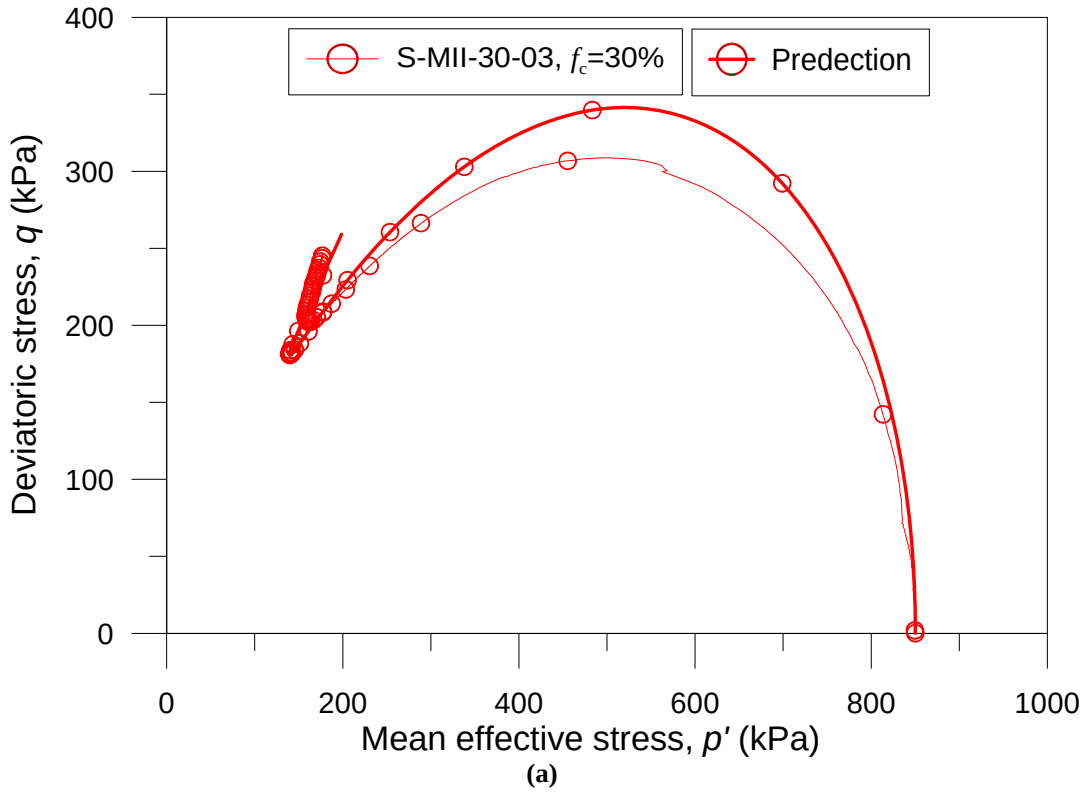

(a)

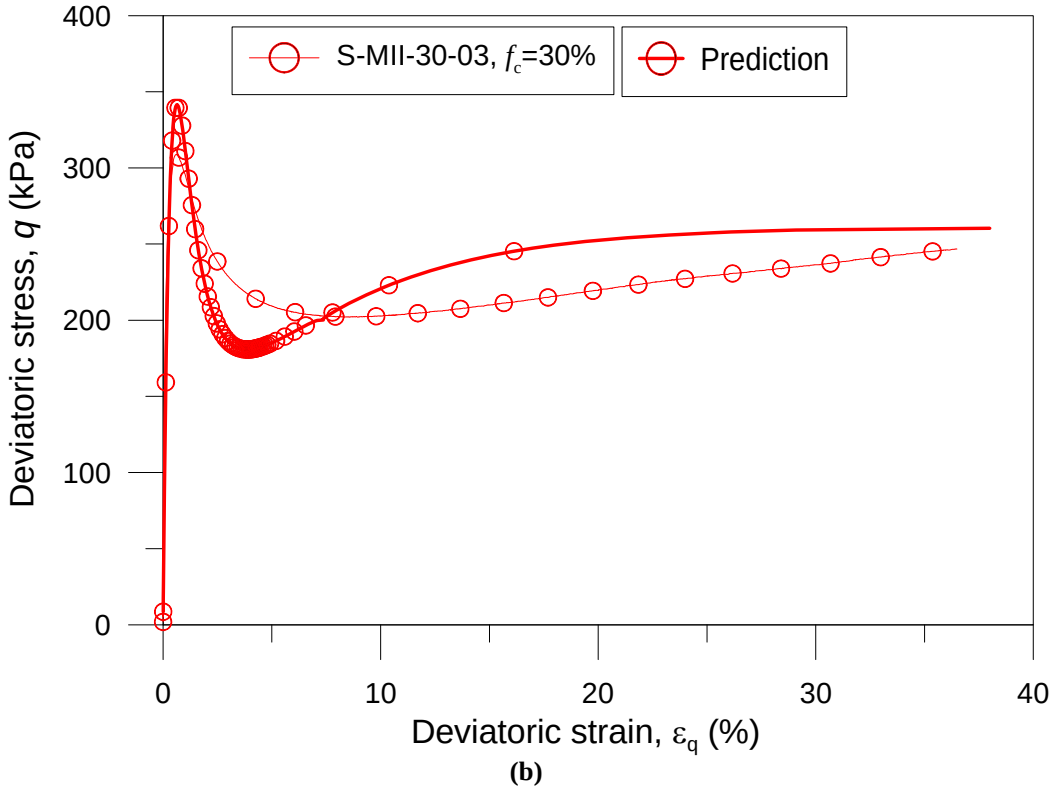

(b)

Figure 6. 13 **Comparison between undrained triaxial compression tests results and model prediction for different fines content, f_c at same initial mean effective stress, p'_0 =850kPa.**

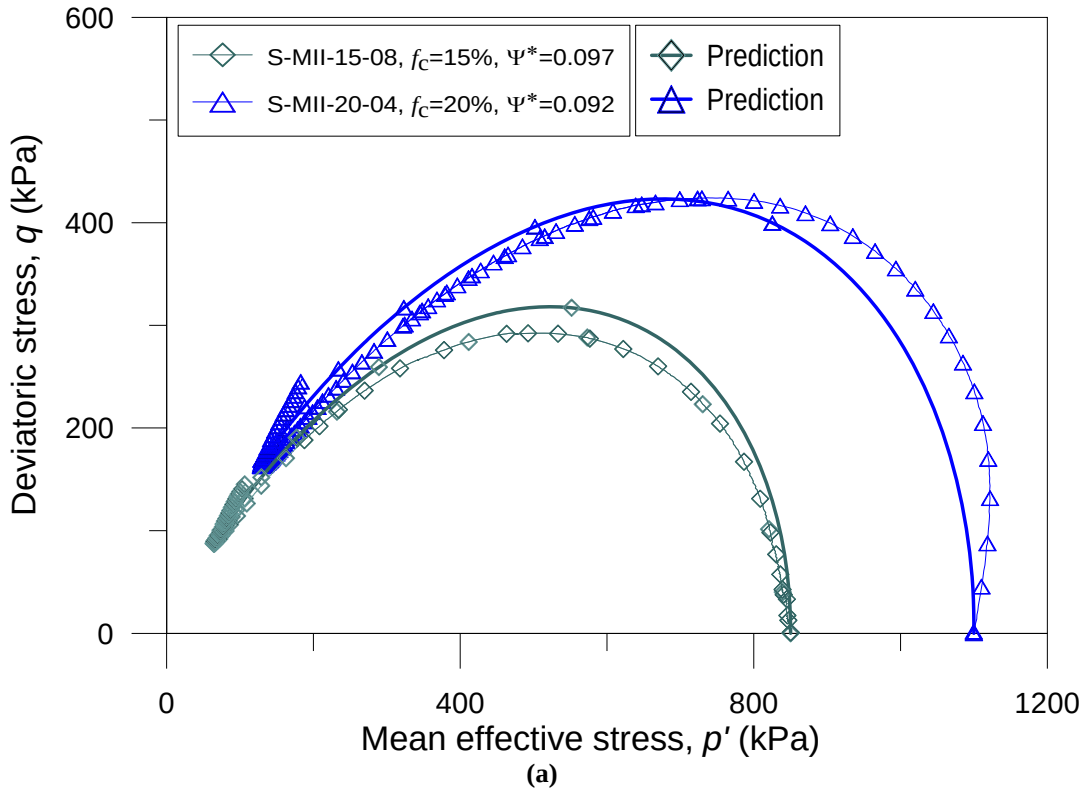

(a)

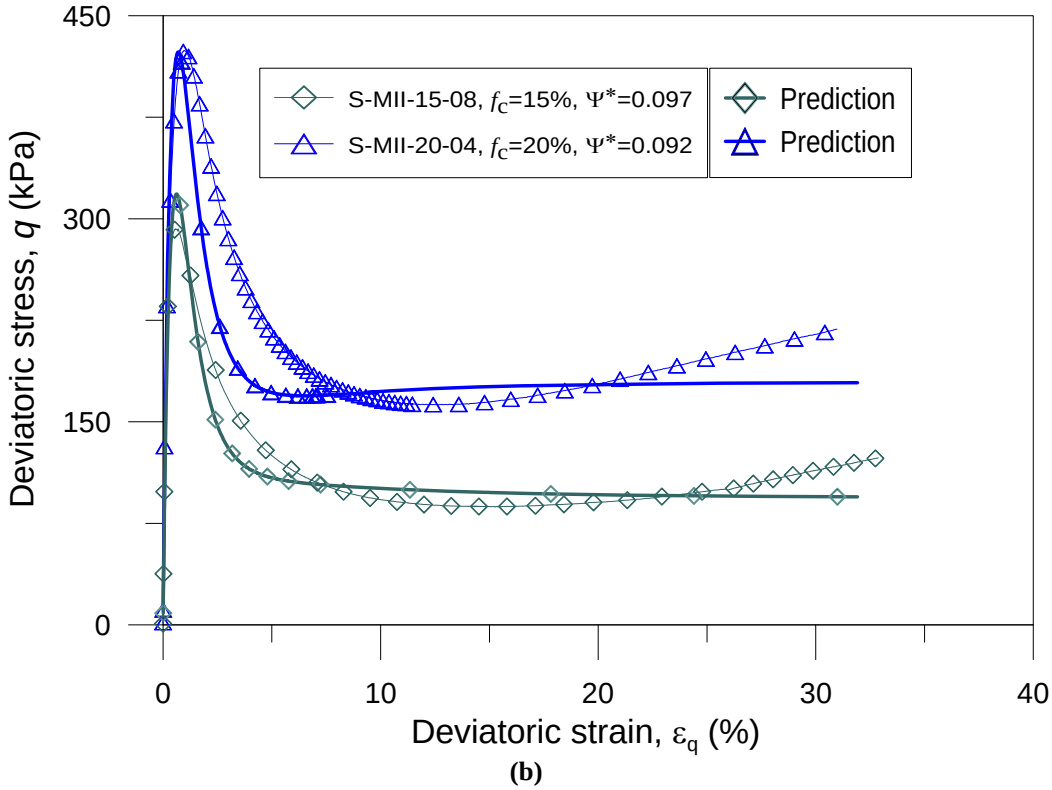

(b)

Figure 6. 14 **Comparison between undrained triaxial compression tests results and model prediction for different fines content, f_c but same equivalent granular sate parameter, $\psi^*_{(0)} \approx 0.09$.**

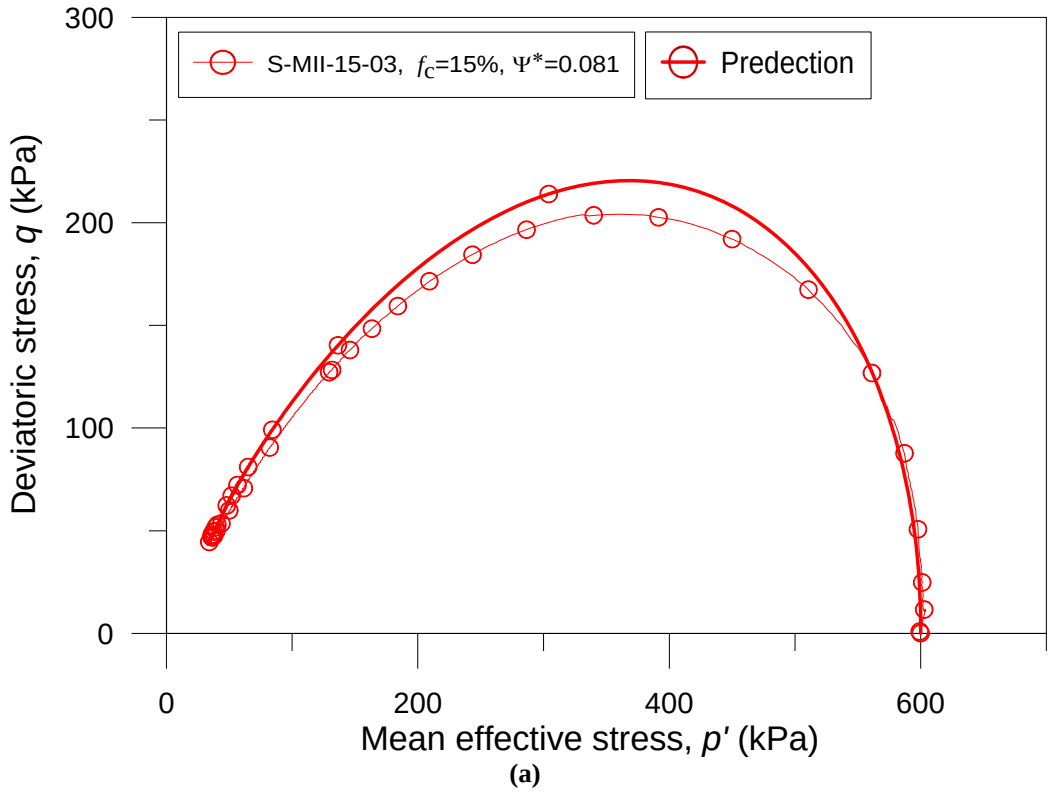

(a)

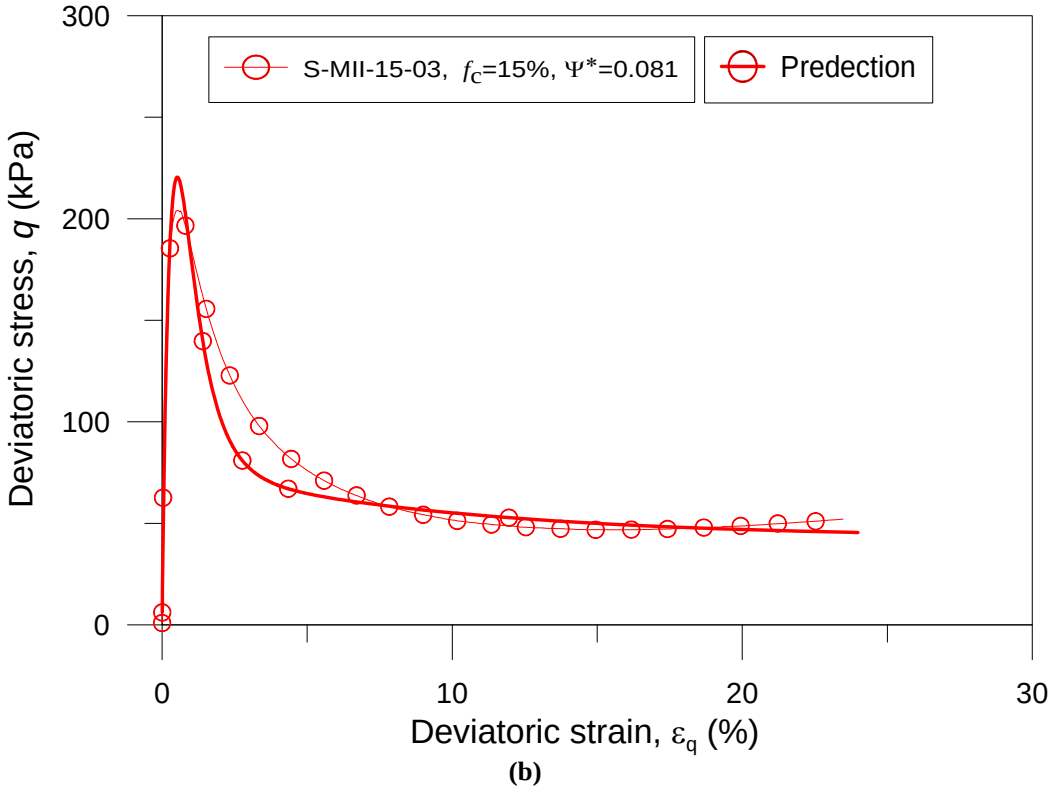

(b)

Figure 6. 15 **Comparison between undrained triaxial compression tests results and model prediction for different fines content, f_c but same equivalent granular sate parameter, $\psi^*_{(0)} \approx 0.08$.**

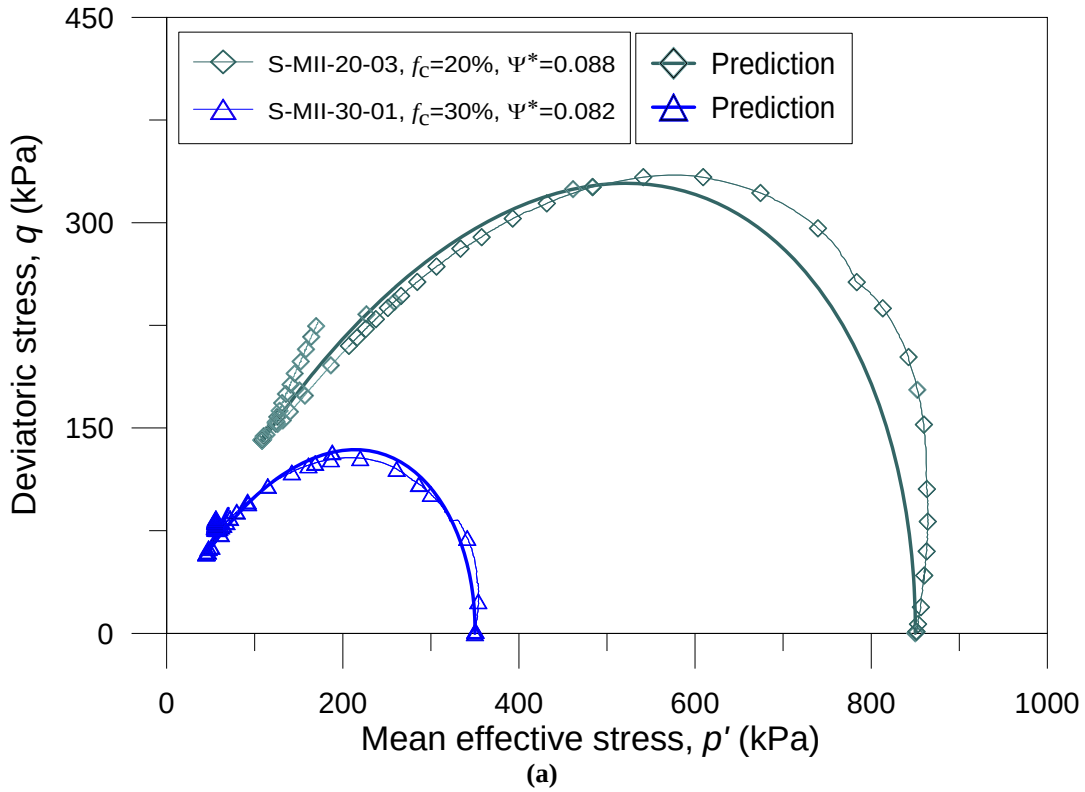

(a)

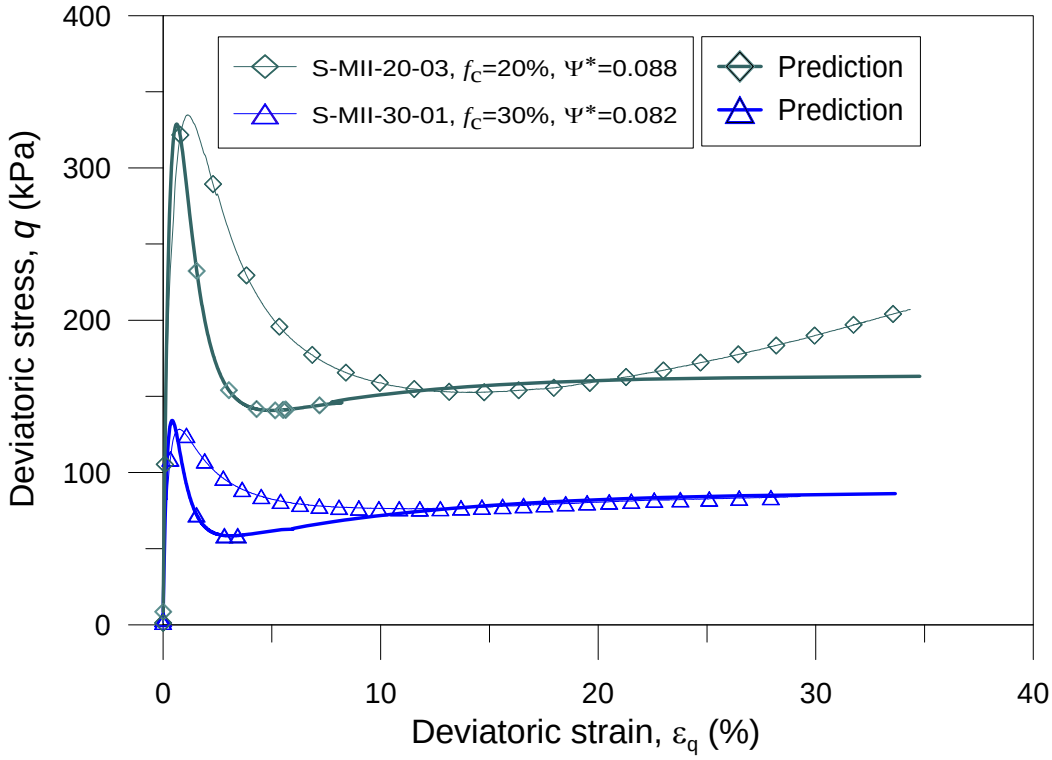

(b)

Figure 6. 16 **Comparison between undrained triaxial compression tests results and model prediction for different fines content, f_c and same equivalent granular sate parameter, $\psi^*_{(0)} \approx 0.08$.**

6.7.2 *Prediction of Limited Flow Behaviour*

A comparison of model prediction and limited flow behaviour for sand with 0% and 15% fines contents are presented in Figure 6. 17a&b. The experimental results show a significant strain hardening after phase transformation (PT) followed by initial strain hardening. The prediction behaviour also shows significant strain hardening after PT followed by initial strain hardening. Though the prediction PT in q-ε_q space are limited, the overall spectrum of the prediction is in good agreement with the experimental results.

6.7.3 *Prediction of Non Flow Behaviour*

A comparison of model prediction and the ESP of non-flow behaviour with 0 to 15% fines content are presented in Figure 6. 18a. the ESP and the prediction are in good agreement. However, discrepancy observed at the point of PT; the predicted ESP shows greater leftward movement at PT than the experimental results. Figure 6. 18b shows that the undrained behaviour and the prediction in q-ε_q space are in good agreement.

Thus, it can be seen that the model prediction broadly match with the experimental results for flow, limited flow and non flow behaviour independent of fines contents. It indicates the effectiveness of the proposed constitutive model in conjunction with equivalent granular state parameter, ψ^* irrespective of fines contents.

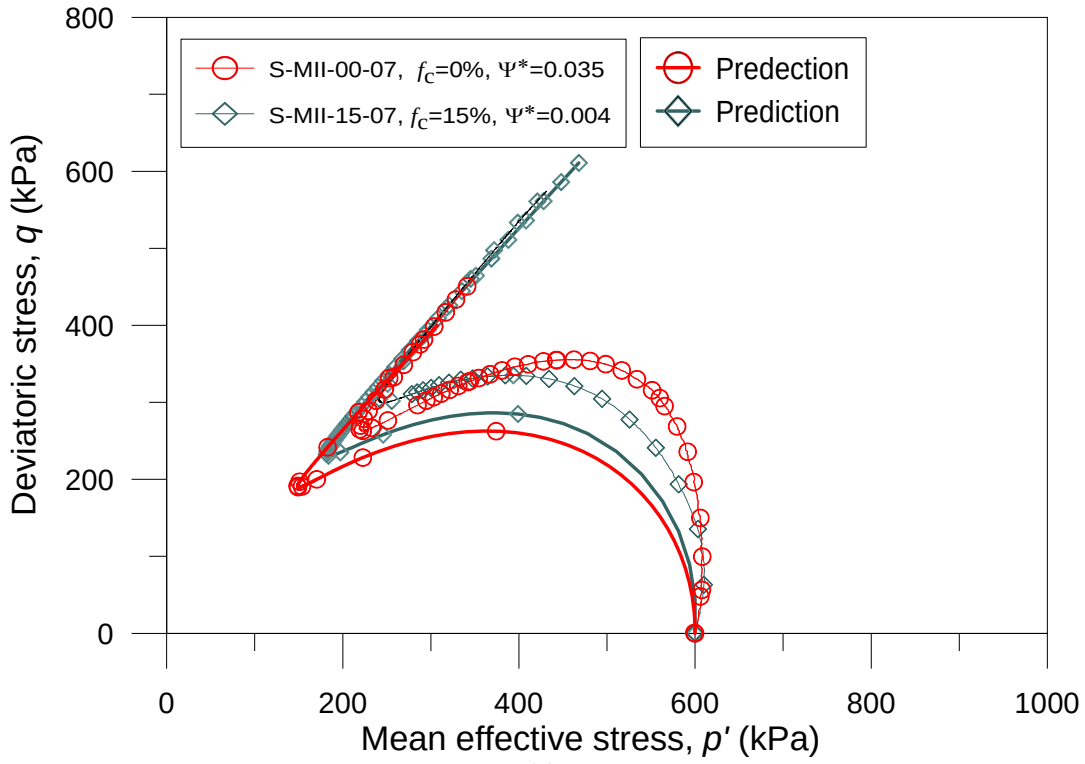

(a)

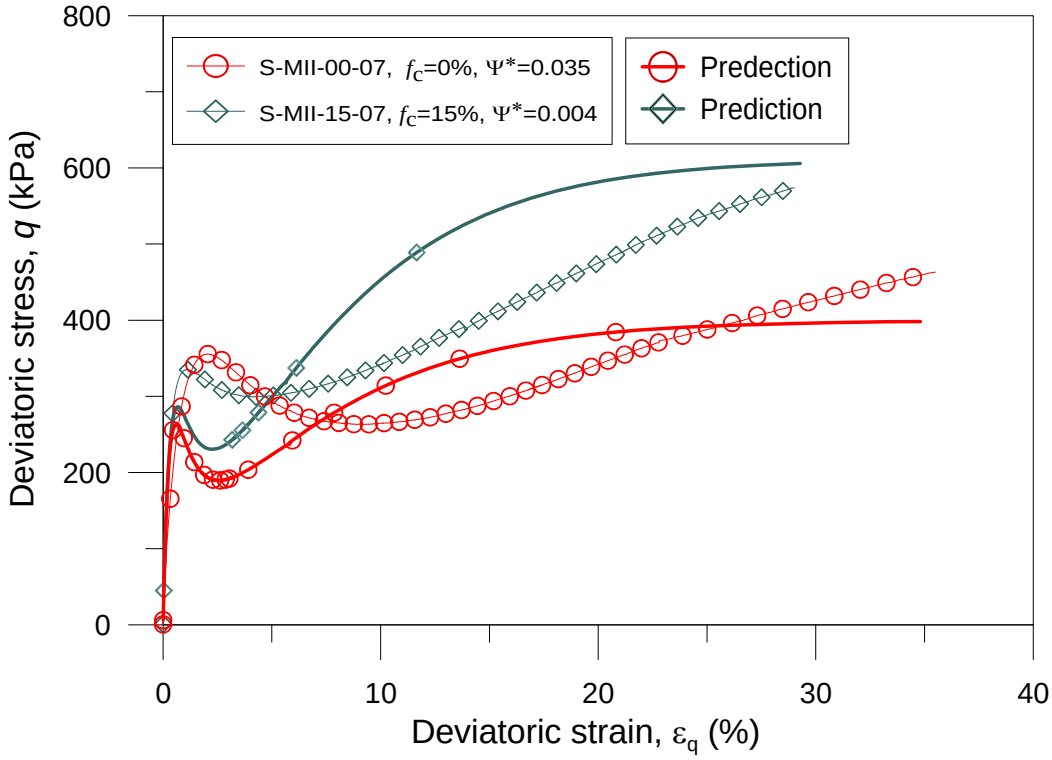

(b)

Figure 6. 17 Comparison of limited flow between undrained triaxial compression tests results and model prediction for different fines content, f_c.

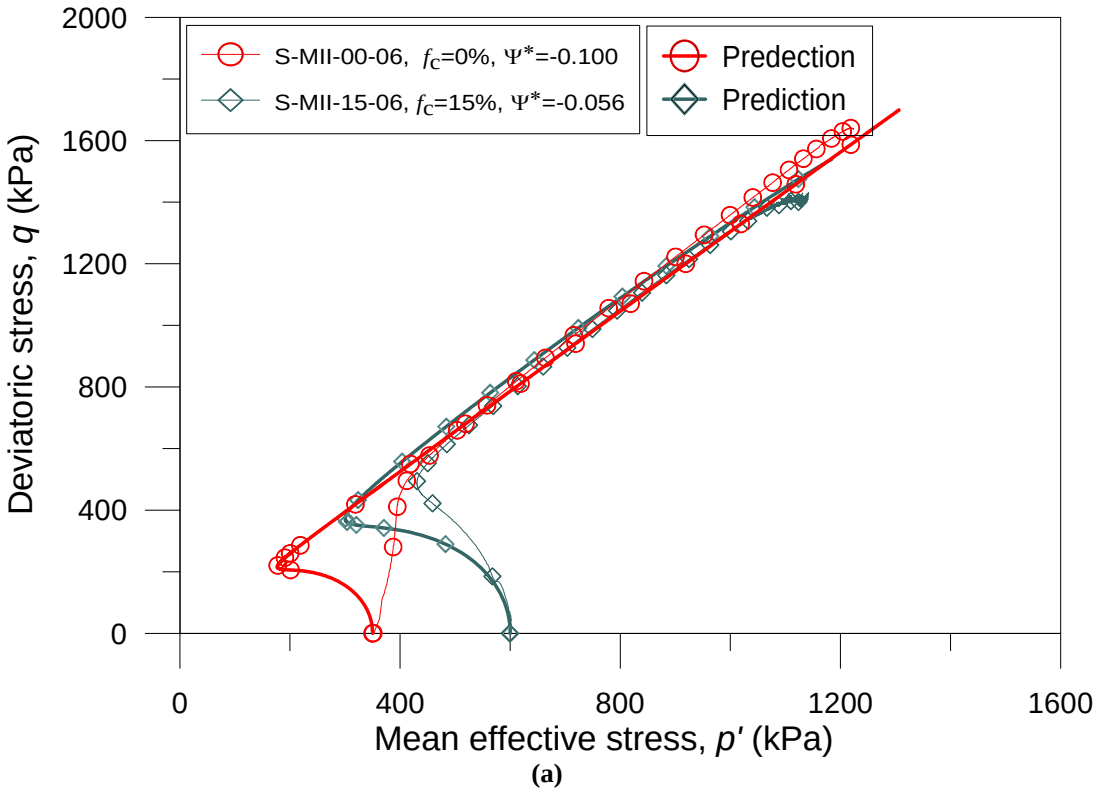

(a)

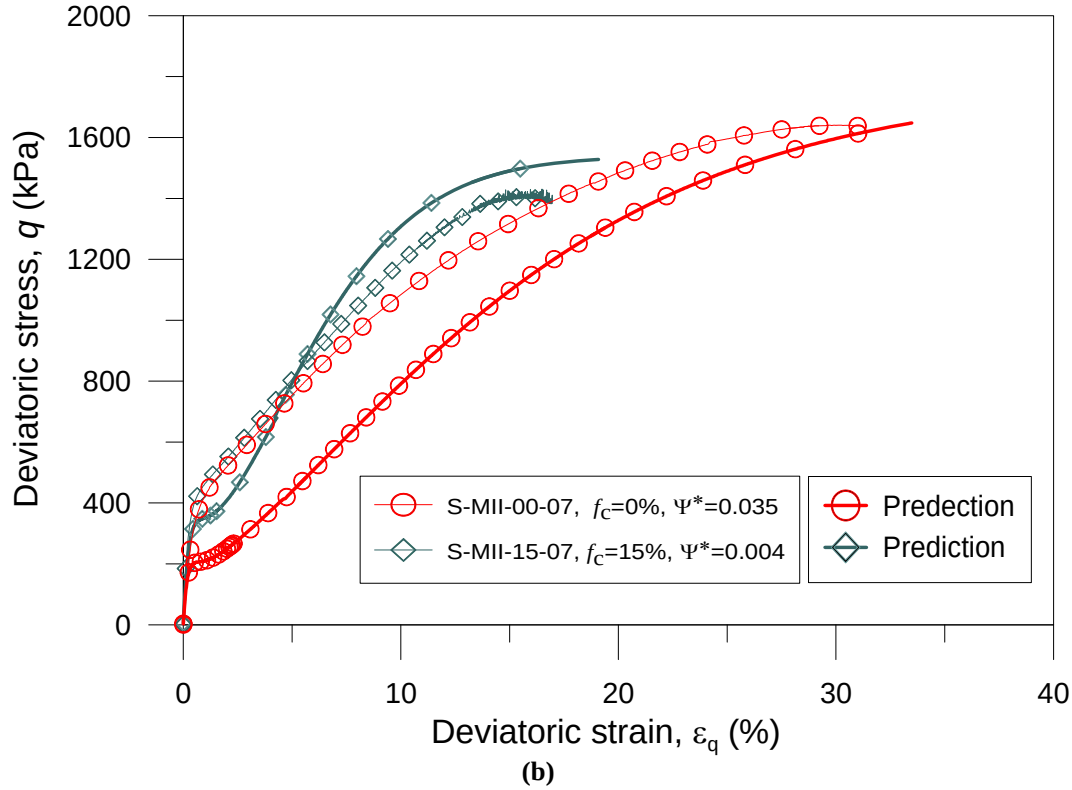

(b)

Figure 6. 18 **Comparison of non flow behaviour between undrained triaxial compression tests results and model prediction for different fines content, f_c.**

6.8 PREDICTION FOR OTHER INDEPENDENT RESEARCH

The model prediction capability is further evaluated for sand with 10% fines. The data was extracted from an independent research (Bobei 2004). The details of the testing condition are given on the Table 6. 8. It shows that all of the tests manifested flow behaviour. A comparison of model prediction and experimental results are presented in Figure 6. 19a&b to Figure 6. 21a&b. Figure 6. 19a&b shows model prediction for a low initial mean effective stress. The prediction of undrained response are in good agreement. Figure 6. 20 shows model prediction for initial mean effective stress of 300kPa and 400kPa. The prediction of undrained response is in good agreement. Finally, Figure 6. 21 shows model prediction for initial mean effective stress of 600kPa and 1115kPa. The prediction of undrained response is also in good agreement.

Table 6. 8: The details testing condition for Sydney sand with 10% M-II fines (Bobei 2004).

Test Name	Fines Content, (%)	*b*-value	p'_0 (kPa)	$e_{(0)}$	$e^*_{(0)}$	$\psi^*_{(0)}$	p'_{SS} (kPa)	Observed behaviour
C1	10	0.103	100	0.772	0.947	0.066	--	F
C2	10		300	0.757	0.930	0.079	--	F
C3	10		400	0.736	0.907	0.069	14.8	F
C4	10		600	0.728	0.898	0.083	93.6	F
C5	10		1115	0.700	0.867	0.103	128.5	F

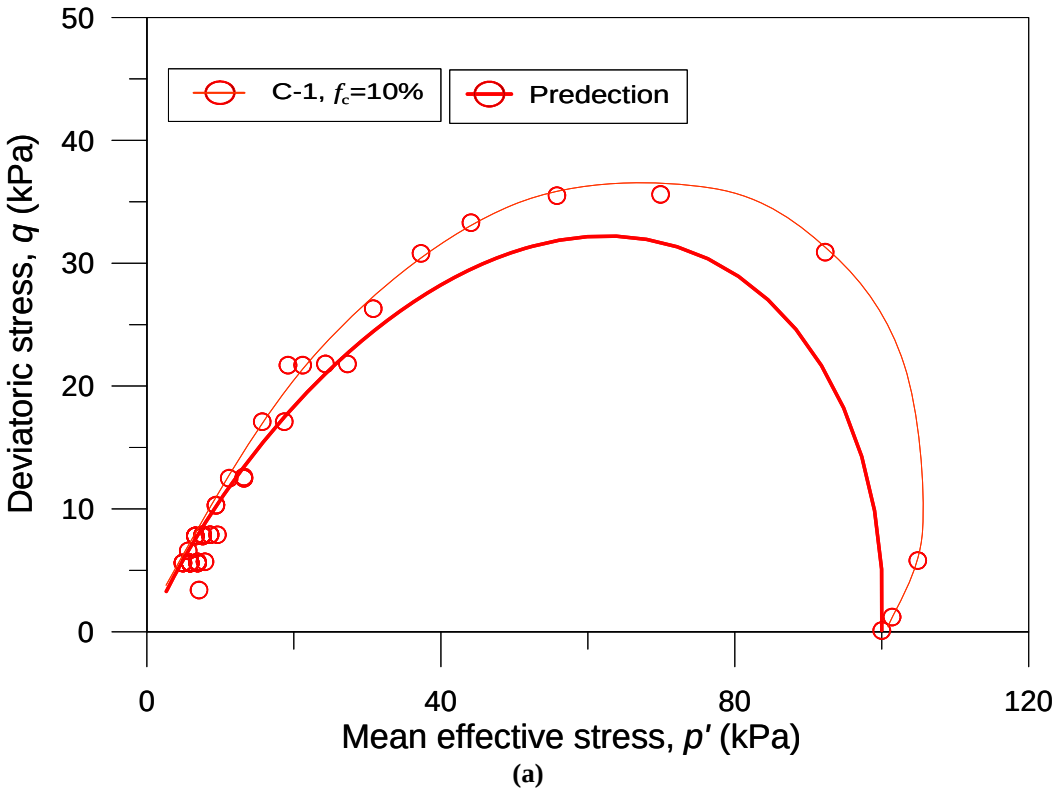

(a)

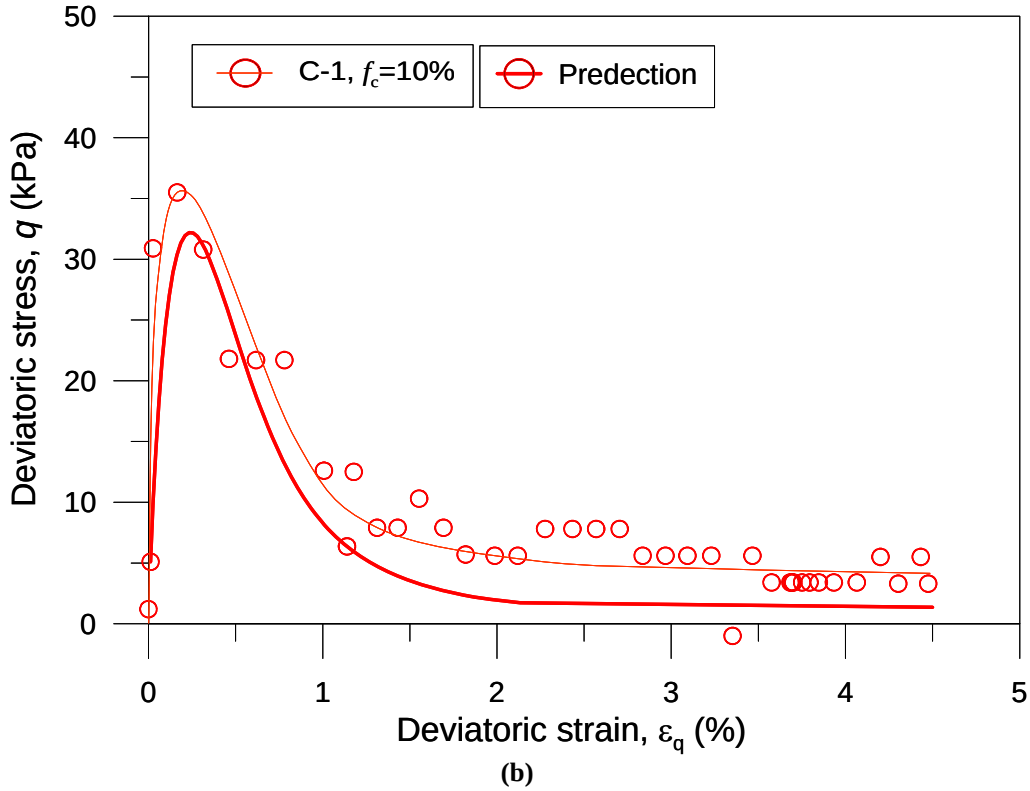

(b)

Figure 6. 19 **Comparison between undrained triaxial compression tests results and model prediction for 10% fines content, f_c at a initial mean effective stress, p'_0 = 100kPa, after Bobei (2004).**

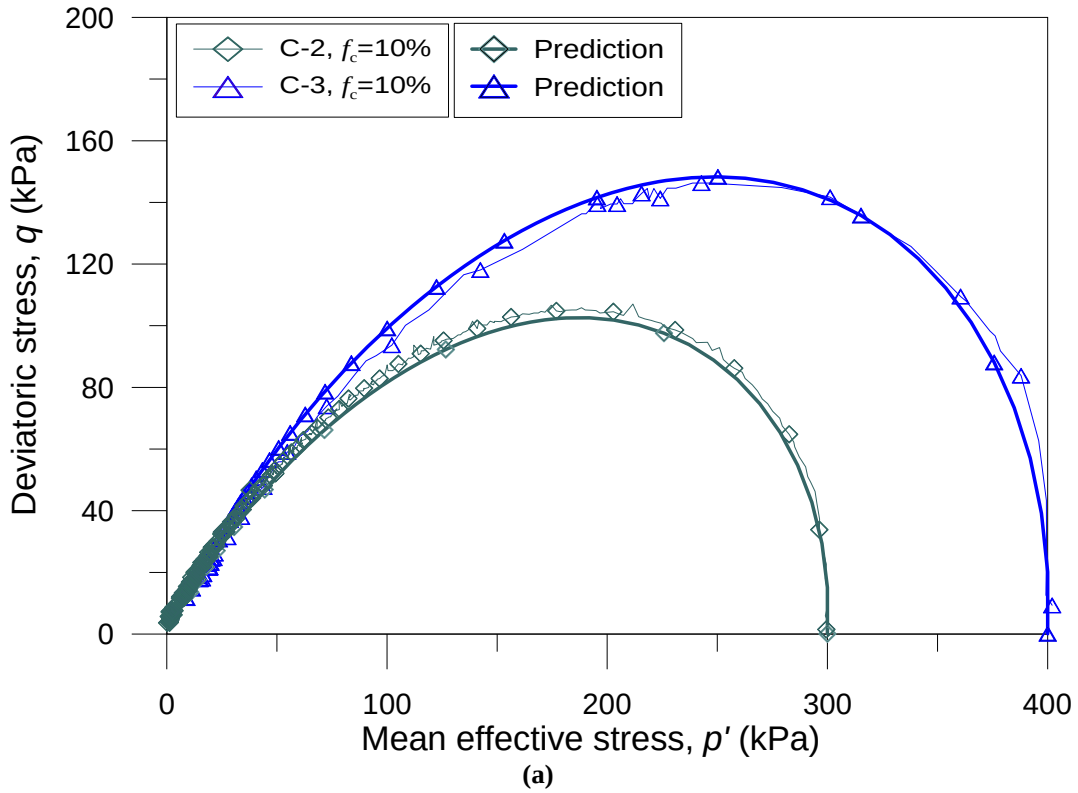

(a)

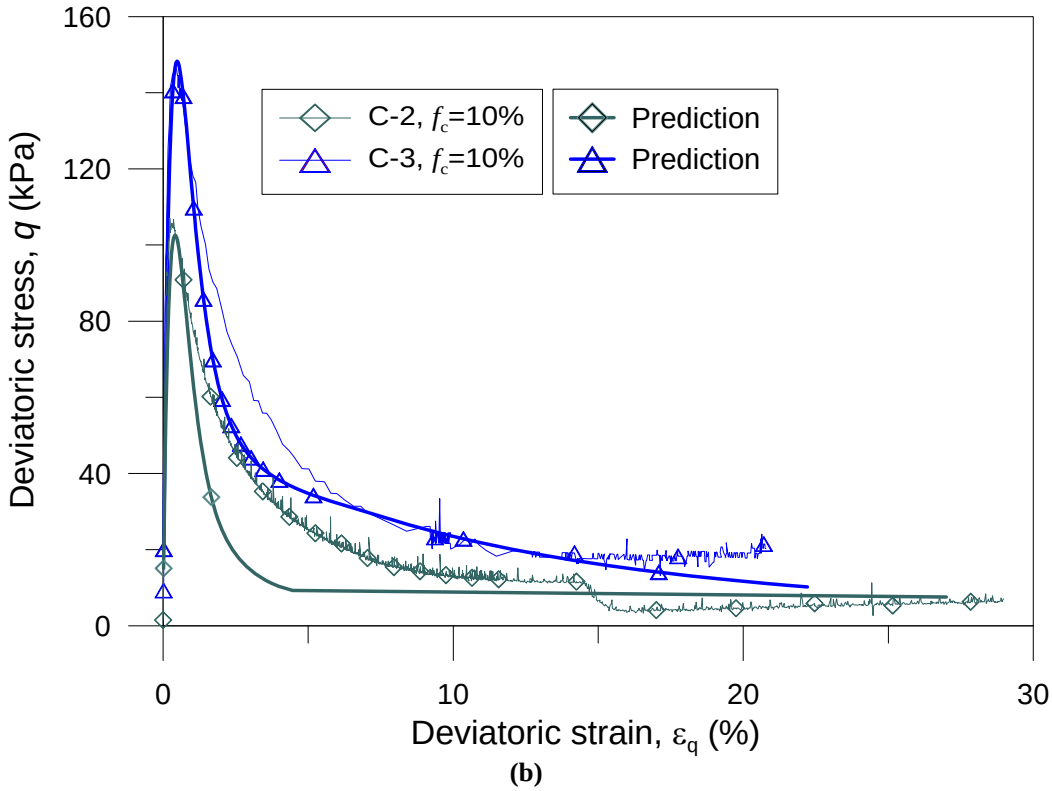

(b)

Figure 6. 20 **Comparison between undrained triaxial compression tests results and model prediction for 10% fines content, f_c at initial mean effective stress, p'_0 of 300kPa and 400kPa, after Bobei (2004).**

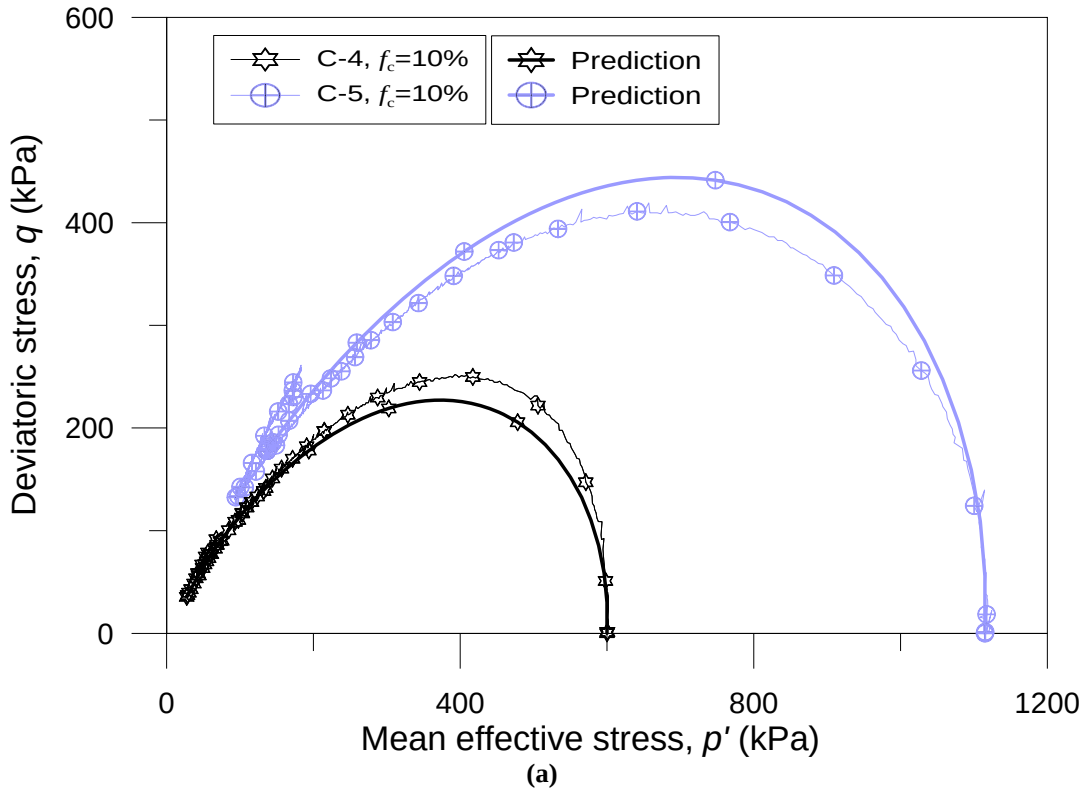

(a)

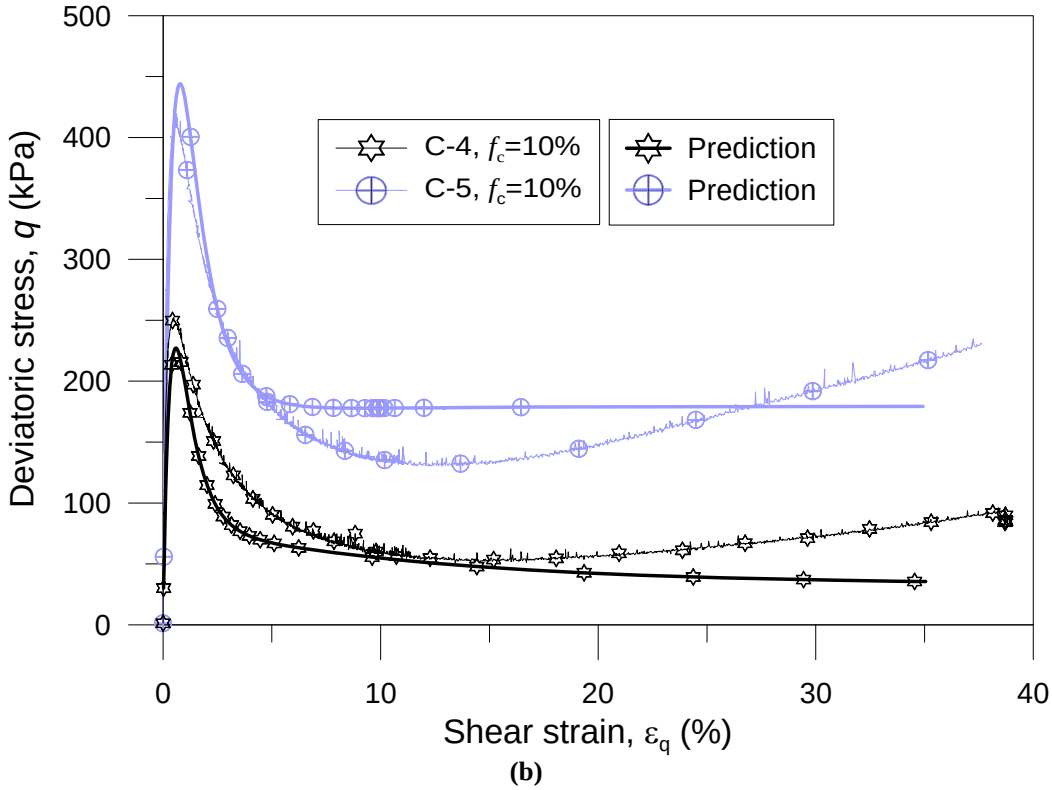

(b)

Figure 6. 21 **Comparison between undrained triaxial compression tests results and model prediction for 10% fines content, f_c at initial mean effective stress, p'_0 of 600kPa and 1115kPa, after Bobei (2004).**

6.9 SUMMARY

A state dependent constitutive model is modified in conjunction with equivalent granular void ratio, e^* and state parameter, ψ^* to predict undrained behaviour of sand with fines irrespective of fines contents.

Eleven parameters are needed for the proposed model. Four of them are critical state parameters and readily available from Chapter 5. All other parameters of the model were determined from drained tests for sand with 10% fines.

The evaluation of model prediction was done in three steps with drained and undrained tests.

First, the flow rule was predicted for drained test. The data obtained form two sources; author and Bobei (2004) and it covered sand with 0%, 10%, 15%, 25% fines contents. The predicted flow rule showed good agreement with experimental results for sand with fines irrespective of fines contents and data sources.

Secondly, the prediction was evaluated with undrained behaviour covering F, NF, LF behaviour for sand with 0-30% fines contents. All test results used for this evaluation are obtained from authors experimentations. The overall undrained behaviour and the model prediction were in good agreement despite of the different testing conditions such as different fines content, different initial mean effective stress, different/same equivalent granular state parameter, ψ^*.

Finally, the model predictions were compared with an independent data source (Bobei 2004). The test results covered confining pressure from 100kPa to 1115kPa for sand with 10% fines content. The predictions were in good agreement with

experimental results. It emphasizes the model effectiveness independent of data sources.

CHAPTER 7

Effect of Fines Type on Liquefaction

7.1 INTRODUCTION

It is discussed in Chapter 4 & 5, how equivalent granular void ratio, e^* can be used to obtain a single framework for sand with fines (for $f_c \leq$ TFC) under Critical State Soil Mechanics, CSSM. Finally, it is shown in Chapter 6, how an equivalent granular state parameter, ψ^* dependent constitutive model can be used to predict drained and undrained behaviour of sand with fines. This completes the development of the single conceptual framework for sand with fines under CSSM. However, the whole conceptual frame work was justified for sand with a single type of fines. The effects of fines types (i.e. fines angularity, plasticity etc.) were not addressed. This chapter discusses about the effect of fines types in sand-fines mix.

7.2 THE EFFECT OF FINES TYPE AND METHODOLOGY

Fines types can be characterized by their size, shape factor (spheresity/angularity), mineralogy (plasticity) etc. This section discussed about the limitation of prediction equation of b parameter for different types of fines and the methodology to examine their effect.

Three input parameters are used in the prediction equation of the b parameter: particle size ratio, χ threshold fines content, TFC and fines content, f_c. It was inherently assumed that b is independent of other parameters such as angularity and plasticity.

For a particular sand-fines mix the particle size ratio, angularity and plasticity remain the same. Thus, the effect of fines plasticity and angularity could not observe in previous chapters.

To examine the effect of fines types, four different types of fines are mixed with Sydney sand. They are MI, MII, SI and SII. The suffix indicates numbers of materials were used to synthesize them. 'I' indicates fines was synthesize from one type of material and 'II' indicates fines was synthesize from two types of materials. The alphabet indicates the major part of the fines: 'M' for Majura fines and 'S' for crushed Sydney sand. The second component of fines as indicated by 'II" is kaolin. Its plasticity index is 31 which is higher than 'M' and 'S' fines. Thus, an increasing effect of plasticity was expected in SII and MII than SI and MI. The plasticity index of MII is 27 where as for MI is 18. Similarly, the plasticity index of SII is 16 whereas SI is non-plastic. The details of the material properties and size distribution of these fines can be found in Chapter 3.

The three materials used in the synthesis of fines are collected from three distinct sources and their microscopic structures are different. For example, MI was obtained from naturally occurring river deposited. The SEM photograph shows that it has some rounded particles and they are surrounded by clay particles as shown in Figure 7. 1. On the other hand, SI (artificial angular fines) is prepared by crushing Sydney sand. The SEM photograph of SI is shown in Figure 7. 2. It shows that SI particles are highly angular. Thus, the SI and MI fines can be used to examine the effect of changing fines angularity.

The SEM photograph of kaolin shows that they are “spongy” like balls and clusters and their relative size is much smaller than other two materials (Figure 7. 3). The SEM photograph of MII shows that it consists of rounded particles with “spongy” balls and clusters on the surface as shown in Figure 7. 5. The number/intensity of “spongy” balls and clusters on the surface of MII fines were higher than MI. The SEM photograph of SII also shows some spread of “spongy” balls and clusters on the surface of angular particles.

Based on these four types of fines, the following study on the effect fines types can be made-

- Effect of fines types on prediction formula of *b*
- Effect of angularity
  - Effect of fines angularity on ‘I’ fines
  - Effect of fines angularity on ‘II’ fines.
- Effect of plasticity
  - Effect of fines plasticity on ‘M’ fines
  - Effect of fines plasticity on ‘S’ fines,

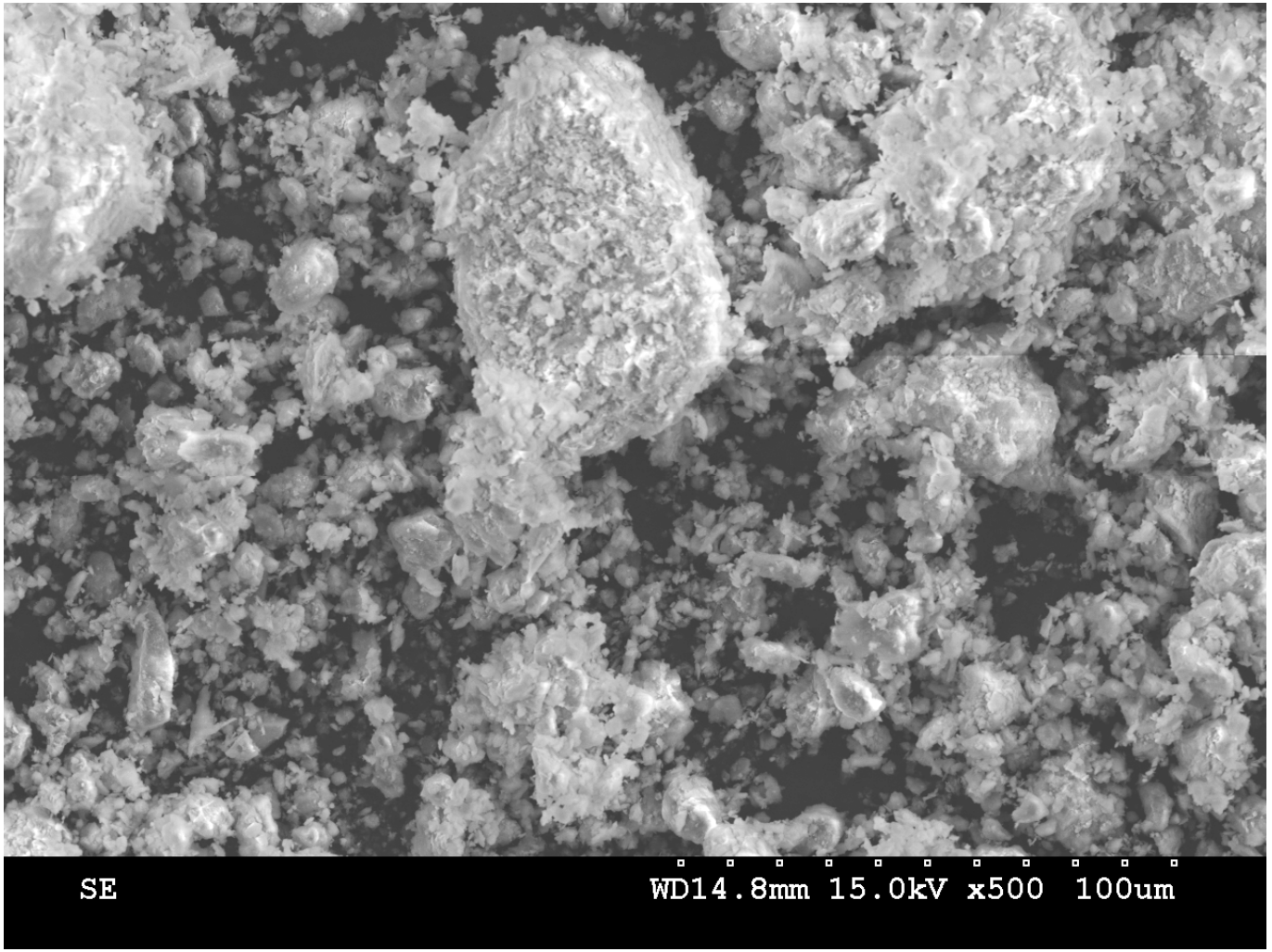

Figure 7. 1: SEM photograph of MI fines (500x magnification)

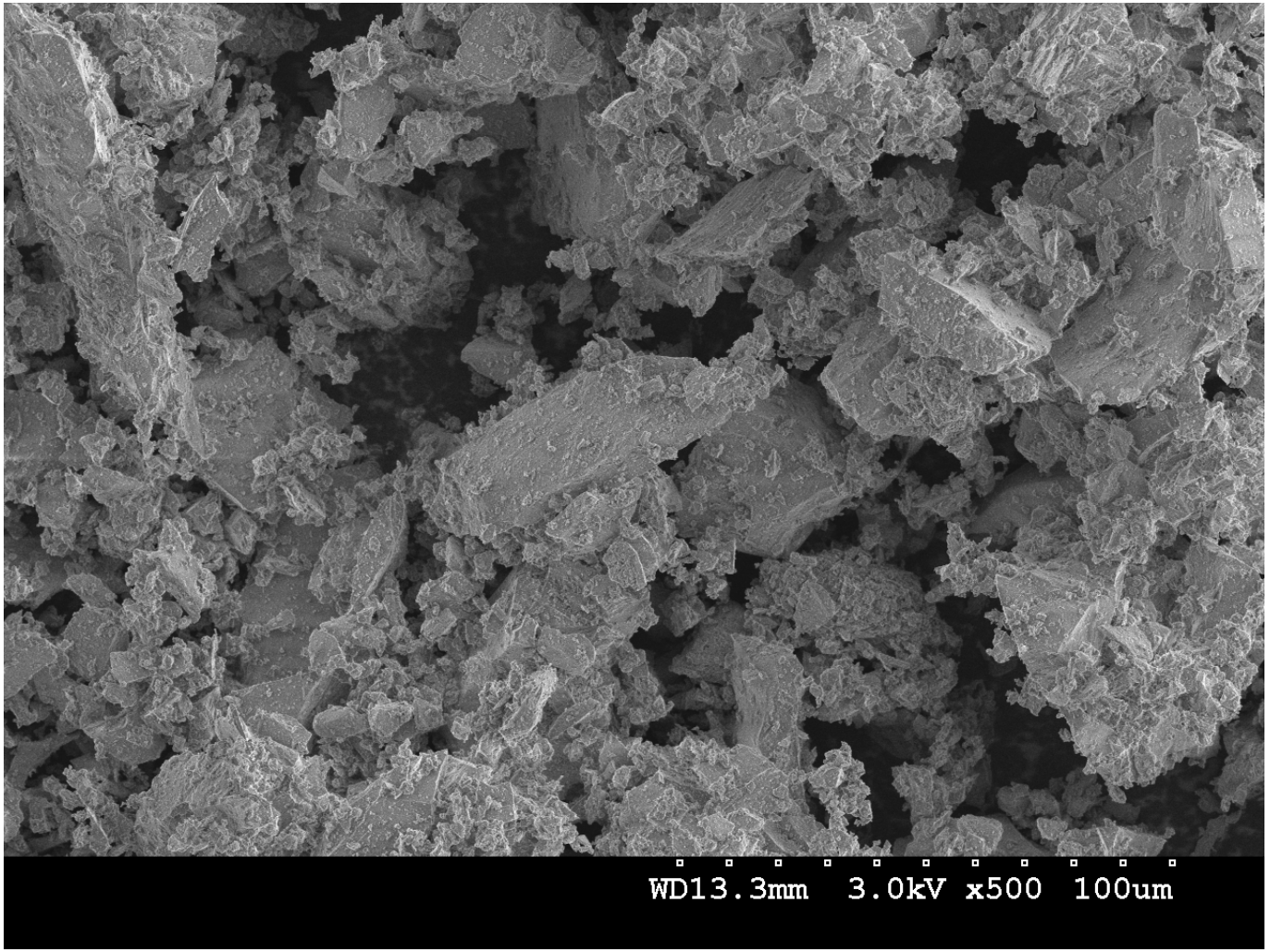

Figure 7. 2: SEM photograph of SI fines (500x magnification)

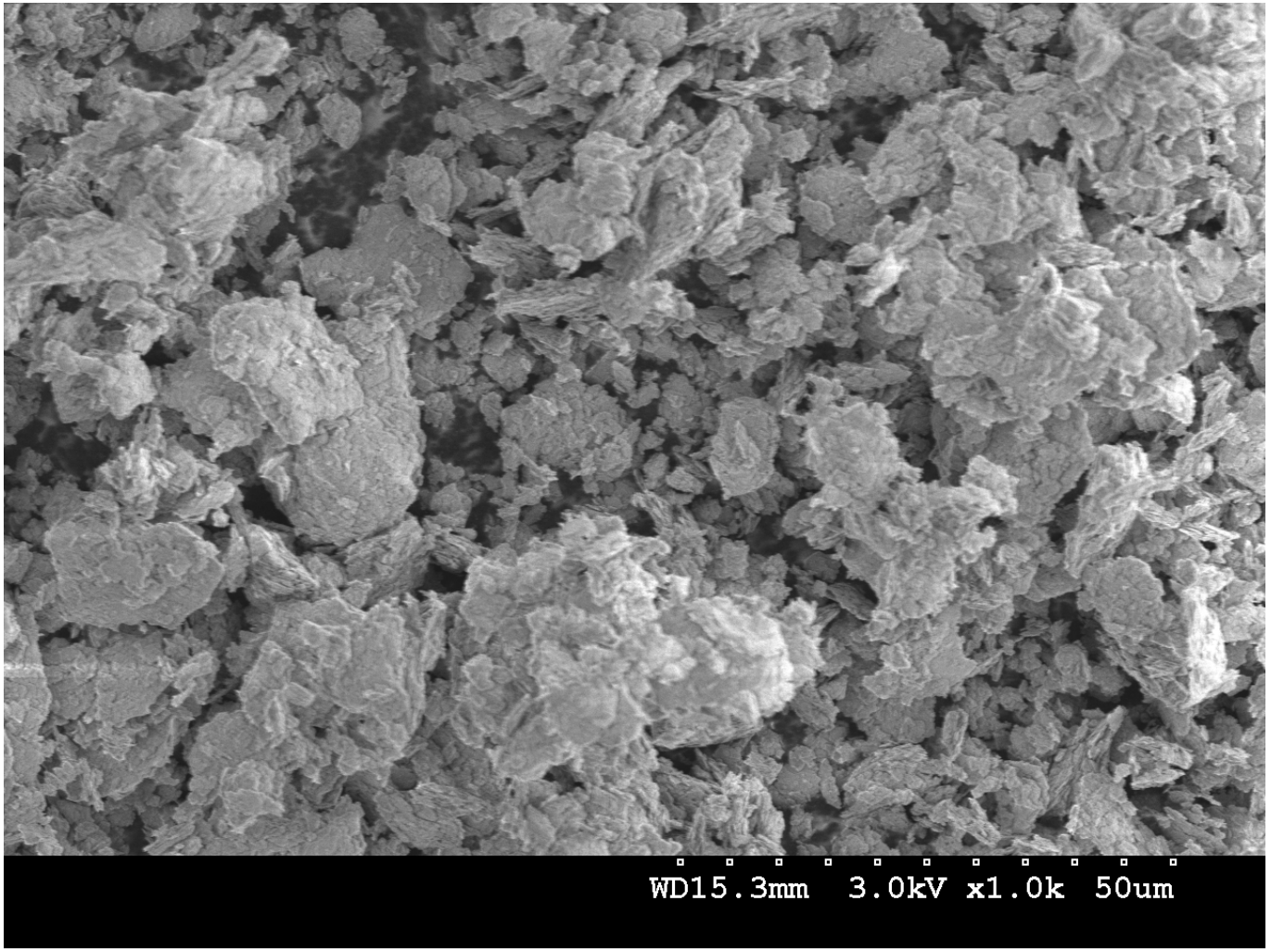

Figure 7. 3: SEM photograph of kaolin (1000x magnification)

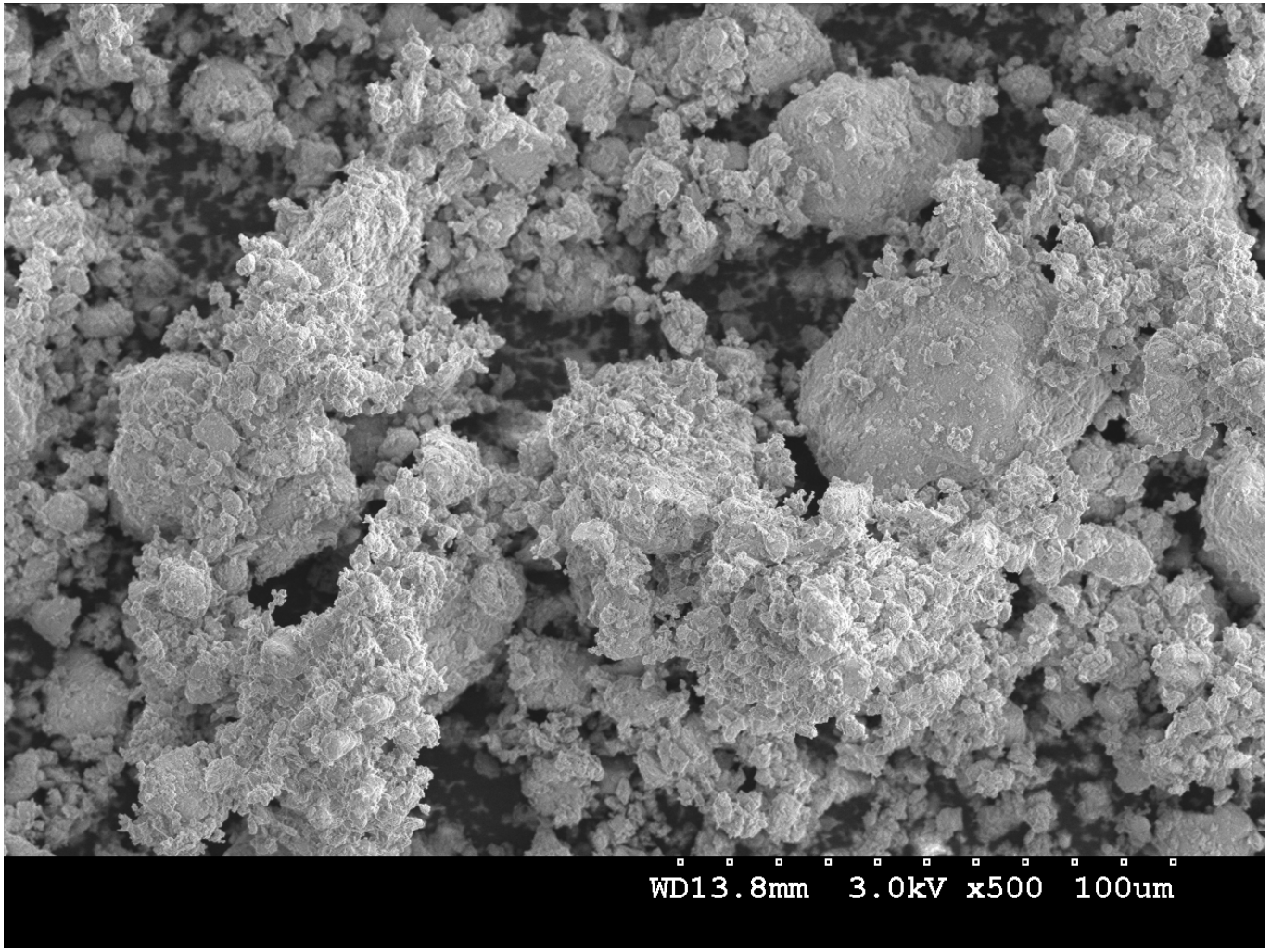

Figure 7. 4: SEM photograph of MII fines (500x magnification)

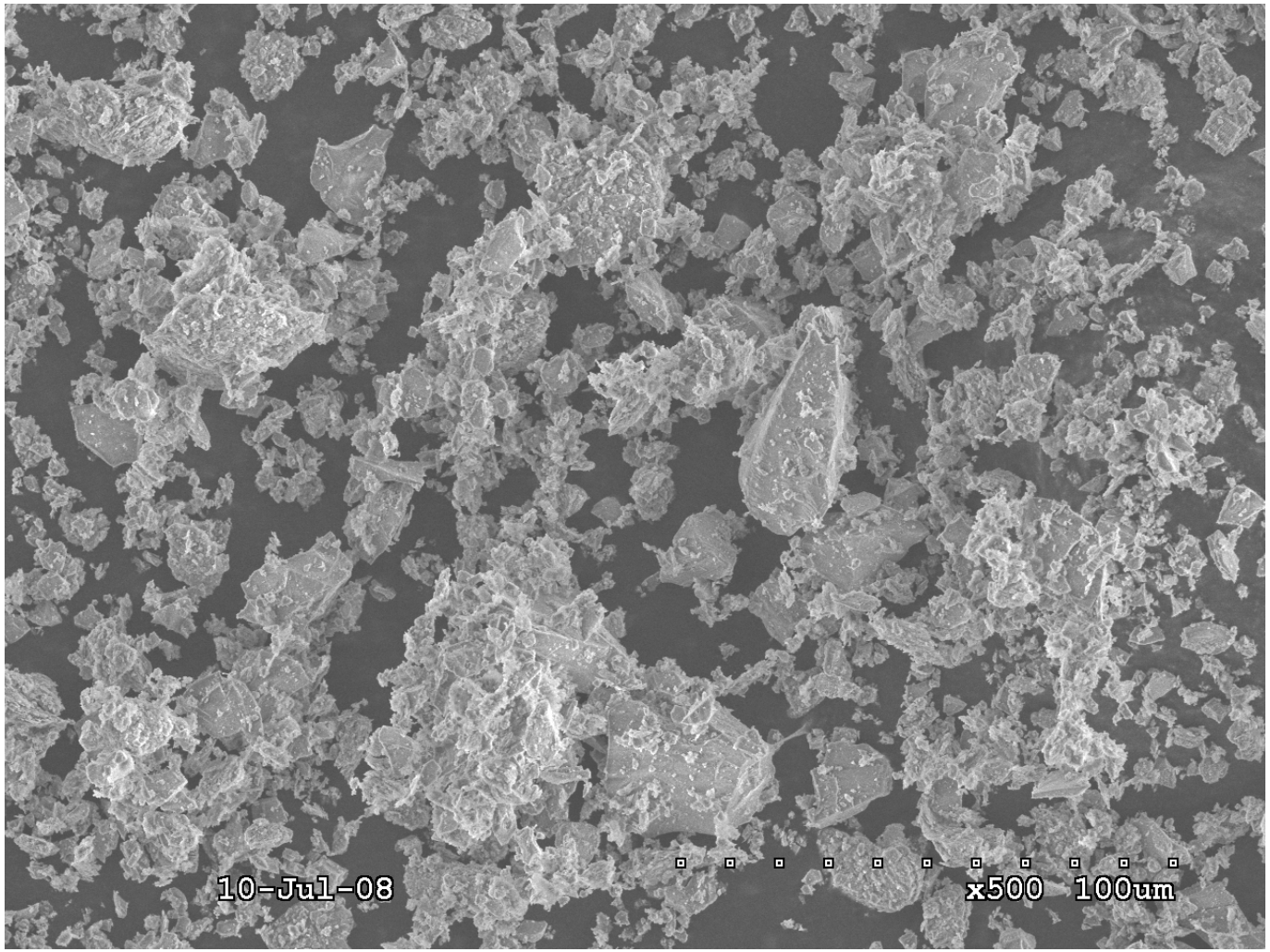

Figure 7. 5: SEM photograph of SII fines (500x magnification)

7.3 TESTING PROGRAM

The testing program is given in Table 7. 1a&b. The same name convention as Chapter 5 is used for this testing program except fines identities are changed according to fines types. For example a test is identified as S-MII-XX-YY in Chapter 5. where, "MII" indicates MII fines. In this Chapter, fines identities are changed according to fines types such as MI, MII, SI and SII. The other alphabet indicates their usual meaning i.e. "XX" indicates the percentage of fines and "YY" is the tests number.

The testing program covers-

i) four different types of fines,

ii) the fines types cover non-plastic to plastic (PI=27) fines,

iii) the fines type cover wide range of particles angularity,

iv) a wide range of confining pressure, from 350kPa to 850kPa.

Most of the samples reached the Steady State, SS at the end of shearing. This is because of extreme care and advanced techniques applied during sample preparation as explained in details in Chapter 3. If a sample did not reached to the steady state, the steady state was obtained by following the extrapolation method proposed by Murthy et al. (2007). These test are denoted by "^{N}" in Table 7. 1a&b.

Table 7. 1: Summary of the testing program: (a) for MI & MII fines

Test Name	Fines Content, (%)	*b*-value	p'_0 (kPa)	$e_{(0)}$	$e^*_{(0)}$	$\psi^*_{(0)}$	p'_{SS} (kPa)	Observed behaviour
S-MI-15-01	15	0.211	350	0.685	0.912	0.066	65	F
S-MI-15-02	15		350	0.692	0.919	0.074	34	F
S-MI-15-03	15		600	0.664	0.888	0.071	94	F
S-MI-15-04	15		850	0.662	0.885	0.093	350	F
S-MI-15-05	15		850	0.667	0.891	0.099	200	F
S-MII-15-01^N	15	0.150	100	0.617	0.853	-0.029	110.0	NF
S-MII-15-02	15		350	0.658	0.900	0.056	9.9	F
S-MII-15-03	15		600	0.655	0.896	0.081	36.5	F
S-MII-15-04	15		600	0.623	0.860	0.045	87.3	F
S-MII-15-05	15		600	0.628	0.866	0.051	120.4	F
S-MII-15-06^N	15		600	0.535	0.759	-0.056	1140	NF
S-MII-15-07^N	15		600	0.588	0.819	0.004	431.2	LF
S-MII-15-08	15		850	0.647	0.887	0.098	71.5	F

where, p'_0 = Initial mean effective stress, at the end of consolidation,

$e_{(0)}$ = Void ratio at the end of consolidation,

$e^*_{(0)}$= Equivalent granular void ratio at the end of consolidation,

$\psi^*_{(0)}$ = Equivalent granular state parameter at the end of consolidation,

p'_{SS} = Mean effective stress at steady state

F = Flow, LF = Limited Flow, NF = Non-Flow

Table 7.1: Summary of the testing program: (b) for SI & SII fines

Test Name	Fines Content, (%)	*b*-value	p'_0 (kPa)	$e_{(0)}$	$e^*_{(0)}$	$\psi^*_{(0)}$	p'_{SS} (kPa)	Observed behaviour
S-SI-15-01	15	0.191	350	0.700	0.935	0.089	5	F
S-SI-15-02	15		600	0.690	0.923	0.106	35	F
S-SI-15-03	15		850	0.729	0.911	0.094	135	F
S-SI-15-04	15		1100	0.762	0.890	0.098	123	F
S-SII-15-01	15	0.143	350	0.675	0.922	0.077	1	F
S-SII-15-02	15		350	0.665	0.911	0.065	23	F
S-SII-15-03	15		600	0.664	0.909	0.093	45	F
S-SII-15-04	15		600	0.652	0.896	0.079	103	F
S-SII-15-05	15		600	0.659	0.904	0.087	218	F
S-SII-15-06	15		850	0.640	0.882	0.090	245	F

where, p'_0 = Initial mean effective stress, at the end of consolidation,

$e_{(0)}$ = Void ratio at the end of consolidation,

$e^*_{(0)}$= Equivalent granular void ratio at the end of consolidation,

$\psi^*_{(0)}$ = Equivalent granular state parameter at the end of consolidation,

p'_{SS} = Mean effective stress at steady state

F = Flow, LF = Limited Flow, NF = Non-Flow

7.4 RESULTS AND DISCUSSION

The test results and discussions are synthesized in two aspects. The first aspect to be studied is the effect of fines types on the validity of the proposed equation of *b* parameter and then the conversion of *e* to *e**. The second aspect is the effect of fines types on the correlation between equivalent granular state parameter, $\psi^*_{(0)}$ and undrained responses (in terms of effective stress path, ESP and deviatoric stress-strain responses).

7.4.1 *The Effect of Fines Types on Prediction Equation of 'b'*

In previous Chapters, the prediction equation for *b* was supported by a single EG-SSL. The effectiveness of this approach and *e** was evaluated by the scatter of SS data points around the EG-SSL. Note that the proposed equation does not have fines types as input parameter. Thus, along the same line, the effect of fines types on the prediction equation of *b* parameter and *e** can be examined by the flowing procedure-

i) Calculate the *b* parameter with the proposed Equation 4.2a and thus, *e** for sand with different types of fines.

ii) Then, plot SS data points in *e**-log(*p*′) space.

- If the SS data points can be described by a single trend of EG-SSL, then the effect of fines types are negligible in the prediction equation *b*.

- If the SS data points can not be described by a single trend of EG-SSL, then the effect of fines types are not negligible in the

prediction equation *b*. The fines types have to be considered as input parameter in the prediction equation of *b*.

The required parameters for calculating equivalent granular void ratio, *e** are given in Table 7. 2. The particle size ratios for sand with different types of fines are different and thus, the TFC for different types of fines are different (as they are calculated from the Equation 4.1). Hence, the *b* parameters for different types of fines are different even though PI and angularity were not the input parameters.

Table 7. 2 The required parameters for equivalent granular void ratio for different types of fines.

Fines	PI	D_{10}	d_{50}	TFC	f_c	*b*
S-I	---	0.225	0.0180	0.334	0.15	0.191
S-II	16	0.225	0.0025	0.404	0.15	0.143
M-I	18	0.225	0.0250	0.309	0.15	0.211
M-II	27	0.225	0.0055	0.400	0.15	0.152

The SS data points for different types of fines are presents in *e*-log(*p*′) space in Figure 7. 6a. A single trend for sand with different types of fines are observed, that means, plasticity and angularity of fines do not have significant effects on SS data points. On the other hand, the SS data points are presented in *e**-log(*p*′) space as shown in Figure 7. 6b. The SS data points can also be presented as a single trend i.e. EG-SSL. Hence the effect of fines types on *b* parameter for achieving a single EG-SSL is negligible. However, the scatter of SS data points in *e*-log(*p*′) and *e**-log(*p*′) space assessed by

root-mean-square-deviation, RMSD around the trend line. The RMSD of SS data points around average trend line in e-log(p') space is 0.028, on the other hand the RMSD for equivalent granular SS data points around EG-SSL is 0.020. It shows that the prediction equation of b reduced the original scatter of the SS data in e^*-log(p') space .

However, achieving a single EG-SSL does not grantee that it can be used as an "alternate SSL" under Critical Sate Soil Mechanics, CSSM. According to CSSM, the equivalent granular state parameter, $\psi^*_{(0)}$ is adequate to predict undrained responses (in terms of effective stress path, ESP and deviatoric stress-strain response) of sand with fines. Therefore, the effect of fines types need to further investigate by studying the undrained responses with respect to equivalent granular state parameter, $\psi^*_{(0)}$.

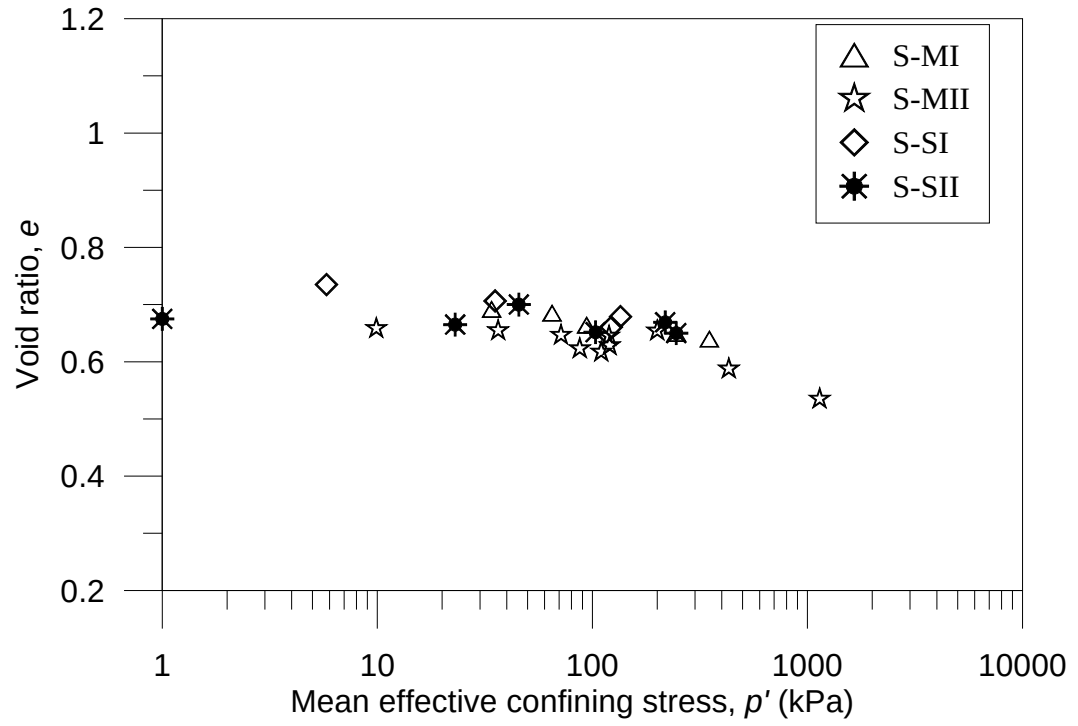

(a)

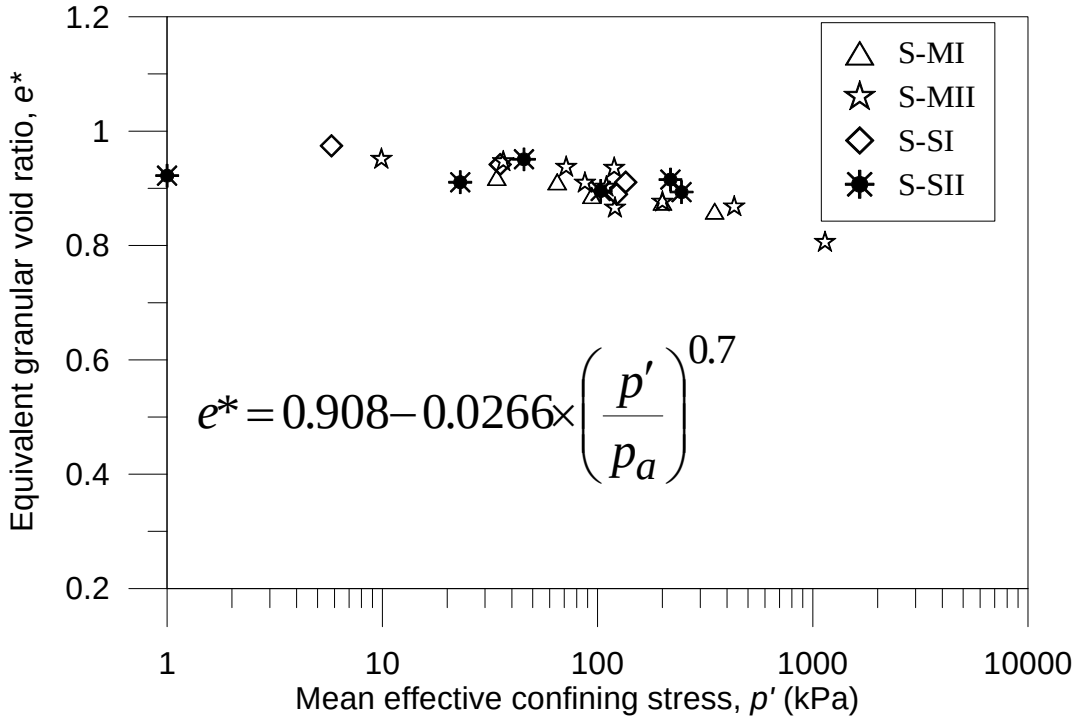

(b)

Figure 7. 6: Effect of different types of fines; (a) SSL in *e*-log(*p*′) space, (b) EG-SSL in *e-log(*p*′) space**

7.4.2 *The Effect of Angularity of Fines*

To examine the effect of angularity two sets of tests are presented in this section. First set compares tests on sand with SI and MI fines i.e. sand with "I" fines. Second set compares tests on sand with SII and MII fines i.e. sand with "II" fines. Each set consists of three pair of tests at initial confining pressure of 350kPa, 600kPa and 850kPa and they are referred as first, second and third pair in the following discussions.

SI fines are highly angular where as MI fines rounded. Thus, the comparison of the ESP and q-ε_q responses of the sand with SI and MI fines should manifest the effect of angularity of fines in a sand-fines mix.

7.4.2.1 Comparison between SI and MI

The over all behaviour of these three pair of tests in q-p' and q-ε_q space manifested flow behaviour as shown in Figure 7. 7a&b. The equivalent granular state parameters of these tests are in a range of 0.071 to 0.099 which is consistent (large enough) with the flow behaviour. However, the relative behaviour of sand with SI and MI fines with respect to their individual equivalent granular state parameter, $\psi^*_{(0)}$ deserve further discussion.

The equivalent granular state parameter, $\psi^*_{(0)}$ for sand with SI fines in first and second pairs are higher than the corresponding test with MI fines. In general, a test with higher equivalent granular state parameter should manifest lower q_{peak} than a test with smaller $\psi^*_{(0)}$. But the test for sand with SI fines manifested higher q_{peak} for both tests. Again, in the third pair, sand with SI fines manifested higher q_{peak} than the

corresponding test for sand with MI fines though they have almost same equivalent granular state parameter, $\psi^*_{(0)}$. The over all ESP for sand with SI fines located above of sand with MI fines. Thus, the ESP behaviour manifested by sand with SI and MI fines can not be correlated with equivalent granular state parameter, $\psi^*_{(0)}$ with in a same framework as the ESP depends on fines types.

The reason of such behaviour is the presence of highly angular particles in SI fines (crushed Sydney sand) than MI fines. Due to the angularity, SI fines exhibit more inter-locking effect in between sand grains. Thus, sand with SI fines manifested lower compressibility during consolidation and achieved higher equivalent granular void ratio, $e^*_{(0)}$ than sand with MI fines at the end of consolidation. This is the reason of getting higher $\psi^*_{(0)}$ for sand with SI fines. The initial higher q_{peak} behaviour during shearing for sand with SI fines was also due to the inter-locking effects. On the other hand, sand with MI fines exhibited lower initial q_{peak} and lower compressibility due to their rounded smooth shape. The angularity, apparently, is the reason of these two different responses though it does not have any effect on the EG-SSL.

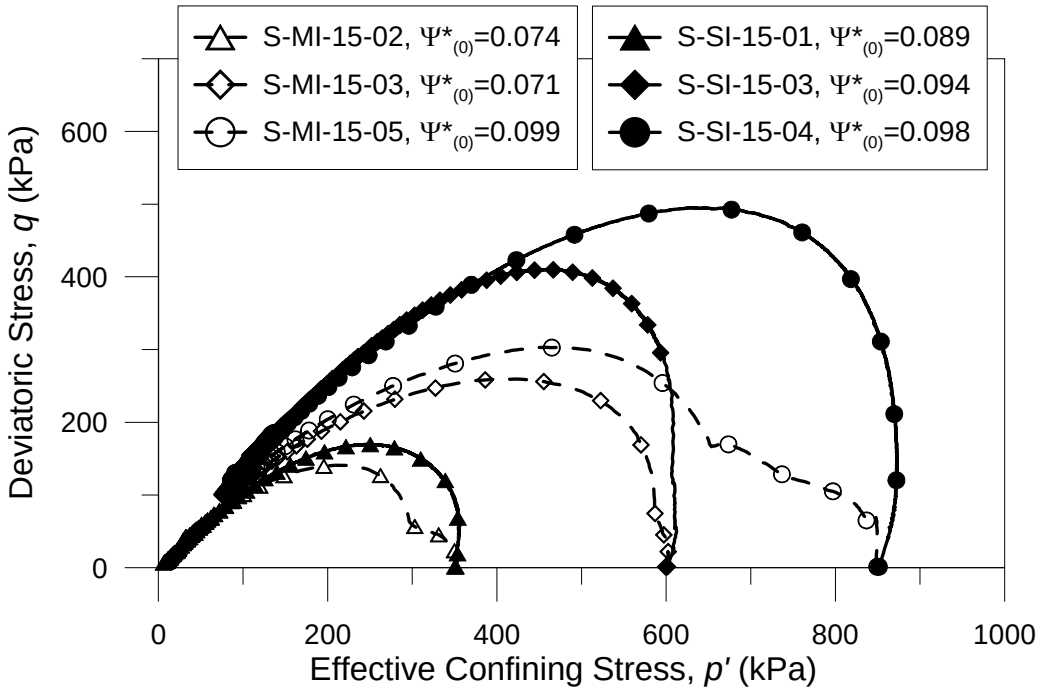

(a)

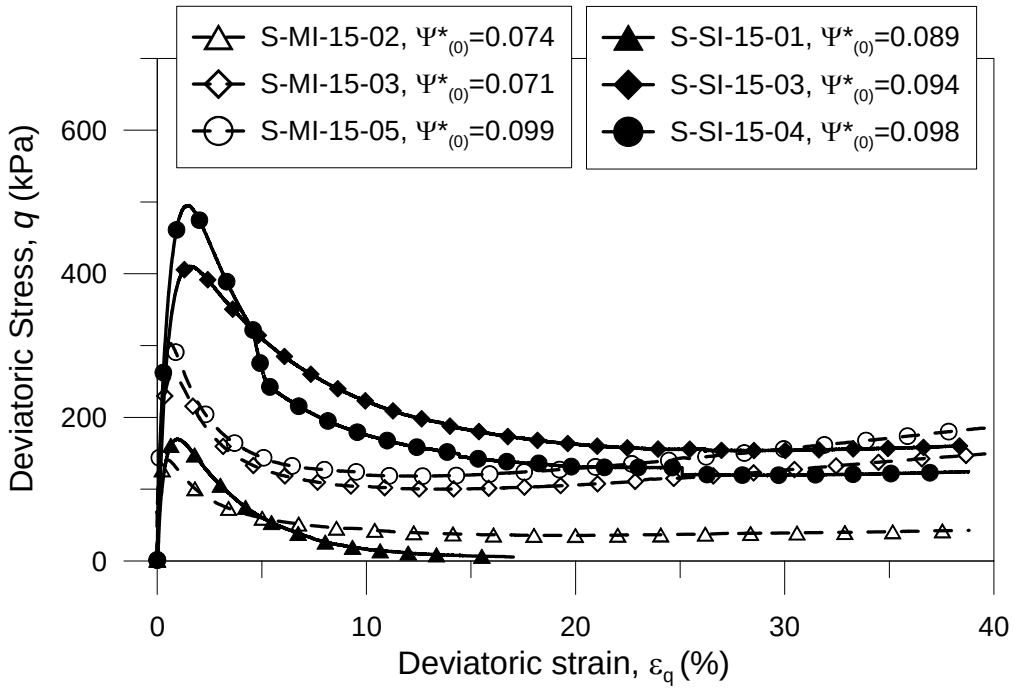

(b)

Figure 7. 7: The effect of increasing plasticity on "I" fines to; (a) in *q*-*p′* space, (b) in *q*-ε_q space.

7.4.2.2 Comparison between SII and MII

The effects of angularity of 'II' fines are discussed in this section. SII fines are highly angular where as MII fines rounded but both of them contain some plastic particles (kaolin). Thus, the comparison of the ESP and q-ε_q responses of the sand with SII and MII fines should manifest the effect of angularity of low-plastic fines.

The over all behaviour of these three pair of tests in q-p' and q-ε_q space manifested flow behaviour as shown in Figure 7. 8a&b. The equivalent granular state parameters of these tests are in a range of 0.056 to 0.098 which is consistent to the flow behaviour. However, the relative behaviour of sand with SII and MII fines with respect to their individual equivalent granular state parameter, $\psi^*_{(0)}$ deserve further discussion.

The equivalent granular state parameter, $\psi^*_{(0)}$ for sand with SII fines in first pair is higher than MII fines where as in second and third pairs are lower than MII fines. But, in general, the initial q_{peak} for sand with SII fines are higher than that of sand with MII fines irrespective of their equivalent granular state parameters, $\psi^*_{(0)}$. Again, at the end of the test, the deviatoric stresses at SS for sand with SII fines were higher than sand with MII fines. Thus, the ESP behaviour manifested by sand with SII and MII fines can not be correlated with equivalent granular state parameter, $\psi^*_{(0)}$ with in a same framework as the ESP depends on fines types.

The reason of such behaviour is the presence of highly angular particles with some spongy-cluster like particles in SII fines. The initial higher q_{peak} behaviour during shearing for sand with SII fines was also due to the inter-locking effects of angular

particles. Thus, the angularity with reinforcement by plastic particle is the reason of these responses.

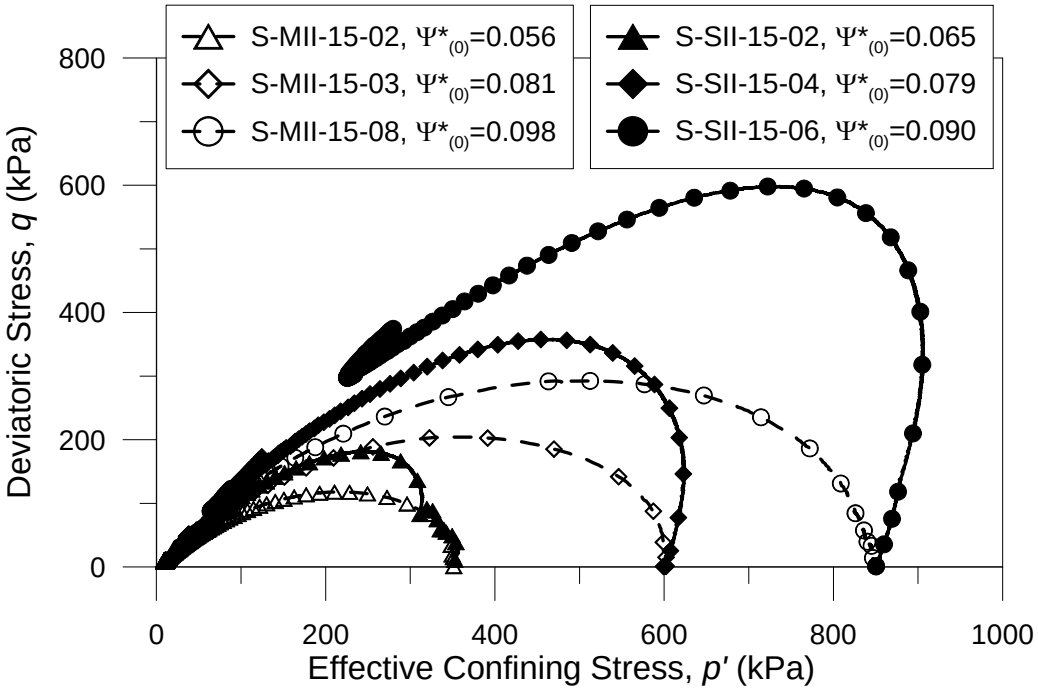

(a)

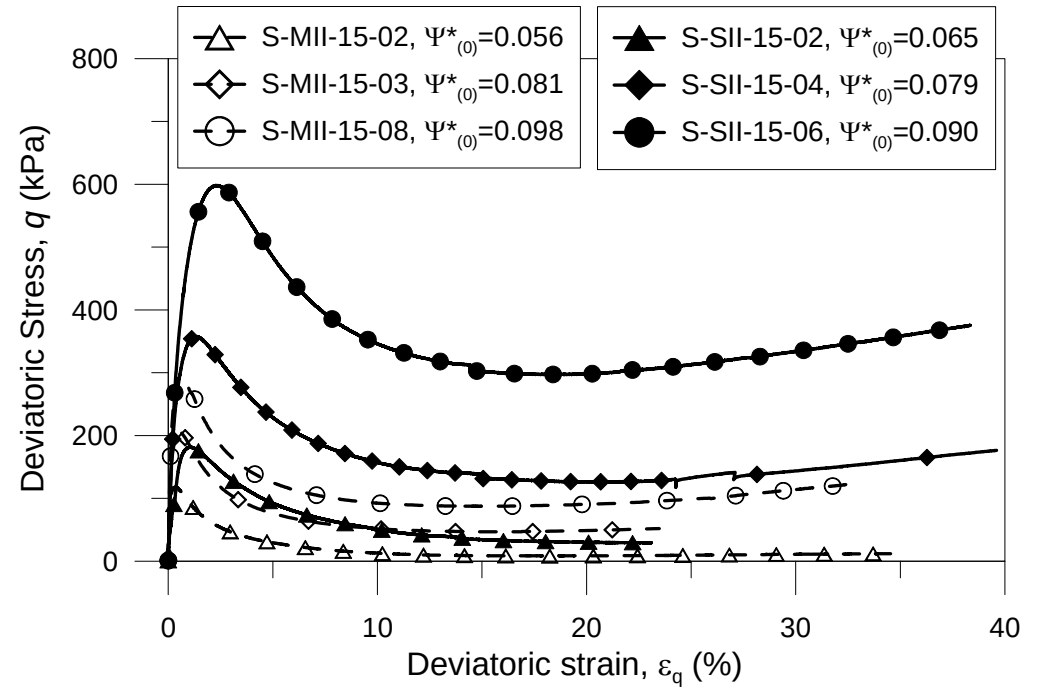

(b)

Figure 7. 8: The effect of increasing plasticity on "II" fines to; (a) in *q*-*p′* space, (b) in *q*-ε_q space.

7.4.3 *Effect of Plasticity of Fines*

To examine the effect of plasticity two sets of tests are also presented in this section. First set compares tests on sand with MI and MII fines i.e. sand with "M" fines. Second set compares tests on sand with SI and SII fines i.e. sand with "S" fines. Each set consists of three pair of test at confining pressure of 350kPa, 600kPa and 850kPa and they are referred as first, second and third pair in the following discussion.

7.4.3.1 Comparison between MI and MII

The effects of plasticity of 'M' fines are discussed in this section. The plasticity index for MI fines is 18 and for MII fines is 27. The comparison of the ESP and q-ε_q responses of the sand with MI and MII fines should manifest the effect of plasticity of fines.

The over all behaviour of these three pair of tests in q-p' and q-ε_q space manifested flow, with/without small post QSS strain hardening as shown in Figure 7. 9a&b. The equivalent granular state parameters, $\psi^*_{(0)}$ of these tests are in a range of 0.056 to 0.099 which is large enough to predict flow behaviour. However, the relative behaviour of sand with MI and MII fines with respect to individual equivalent granular state parameter, $\psi^*_{(0)}$ deserve further discussion.

The equivalent granular state parameter, $\psi^*_{(0)}$ for sand with MII fines in first and third pairs are smaller than MI fines but higher than sand with MI fines in second pair. However, in general the initial peak deviatoric stress q_{peak} and deviatoric stress at SS are higher for sand with MI fines than corresponding test of sand with MII fines irrespective of $\psi^*_{(0)}$. Thus, the ESP behaviour manifested by sand with MI and MII

fines can not be correlated with equivalent granular state parameter, $\psi^*_{(0)}$ with in a same framework as the ESP depends on fines types.

The reason of such behaviour is the presence of “spongy” like balls and cluster. There are more plastic particles in MII fines than MI fines. The “spongy” particle that falls in between the contacts of sand grains are compressed during shearing and exhibited lower deviatoric stress at peak and SS though they may have lower equivalent granular void ratio, e^*. Apparently, the plasticity is the reason of lowering deviatoric stress between these two types of fines though it does not have any effect on the EG-SSL.

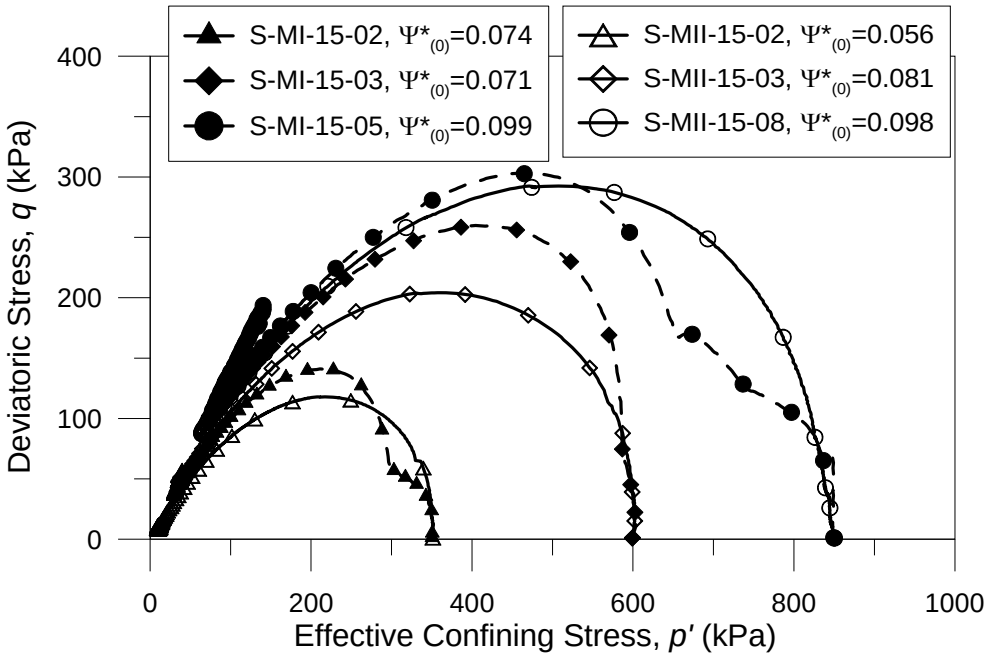

(a)

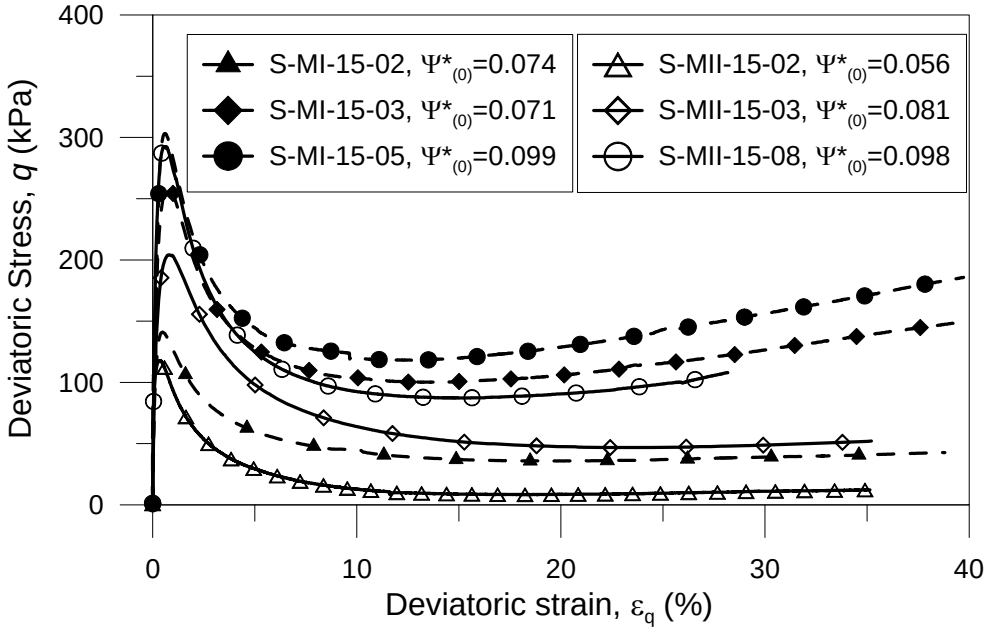

(b)

Figure 7. 9: The effect of increasing plasticity on "M" fines to; (a) in *q*-*p′* space, (b) in *q*-ε_q space.

7.4.3.2 Comparison between SI and SII

The effects of increasing plasticity of 'S' fines are discussed in this section. The SI fines are non-plastic where as the plasticity index of SII fines is 16. The comparison of the ESP and q-ε_q responses of the sand with MI and MII fines should manifest the effect of plasticity of in angular fines.

The over all behaviour of these three pair of tests in q-p' and q-ε_q space manifested flow, with/without small post QSS strain hardening as shown in Figure 7. 10a&b. The equivalent granular state parameters, $\psi^*_{(0)}$ of these tests are in a range of 0.065 to 0.104 which is large enough to predict flow behaviour. However, the relative behaviour of sand with SI and SII fines deserve further discussion.

The equivalent granular state parameter, $\psi^*_{(0)}$ for sand with SI fines are higher than that of sand with SII fines. But, a general trend for initial q_{peak} SI and SII fines can not be observed on their ESP as shown in Figure 7. 10a. However, sand with SII fines exhibits higher deviatoric SS strength than sand with SI fines as shown in Figure 7. 10b. Thus, the ESP behaviour manifested by sand with SI and SII fines can not be correlated with equivalent granular state parameter, $\psi^*_{(0)}$ with in a same framework as the ESP depends on fines types.

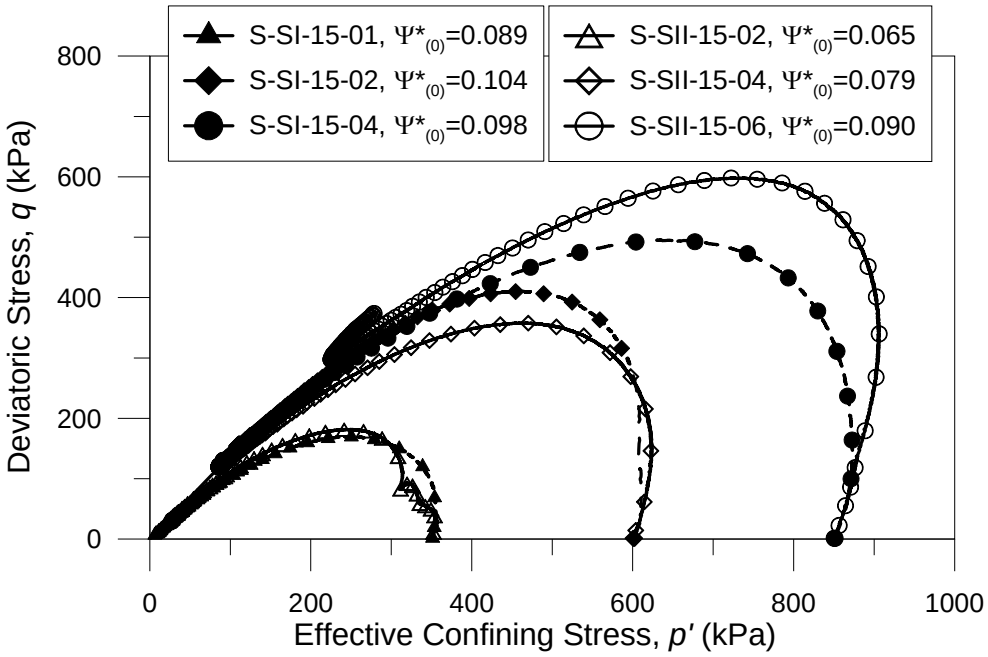

(a)

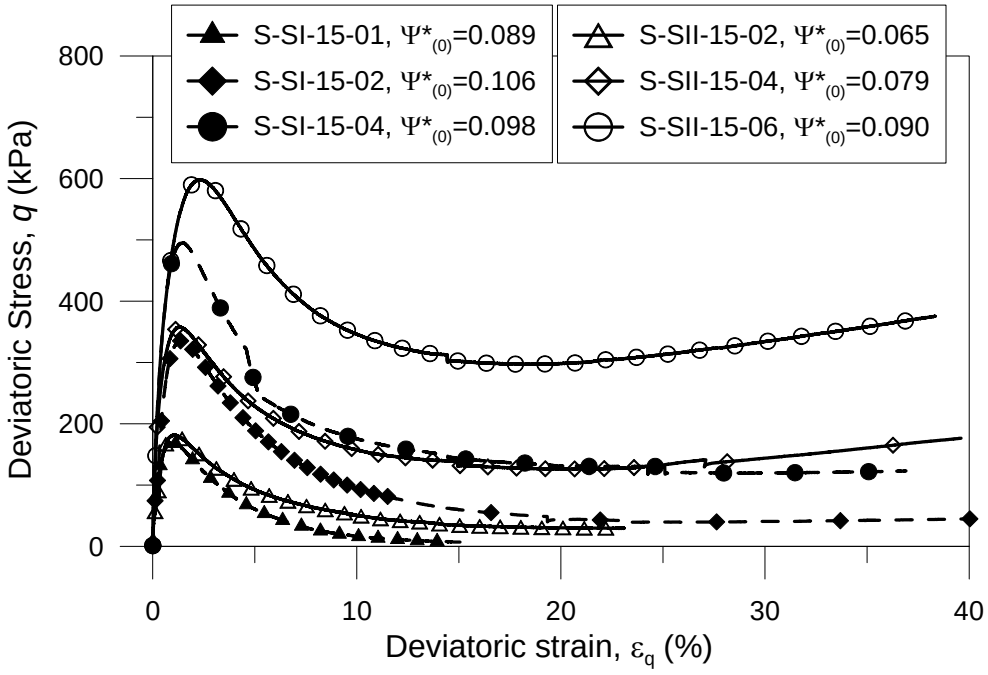

(b)

Figure 7. 10: The effect of increasing plasticity on "S" fines to; (a) in *q*-*p′* space, (b) in *q*-ε_q space.

7.5 SYNTHESIS OF RESULTS

The effect of fines angularity and plasticity on the prediction equation of *b* and the conversion from *e* to *e** are presented in section 7.4.1. It shows that the effect of angularity and plastic has negligible effect on the prediction equation of *b* and EG-SSL. However, Ni et al. (2006) proposed a force carrying hierarchy for silty and plastic fines in equivalent granular void ratio, *e** formula (as discussed in Chapter 2). This study indicates that the force carrying hierarchy for silty and plastic fines may not be necessary to consider in equivalent granular void ratio formula, *e** for sand with different type of fines (at least for the four types of fines discussed in this Chapter).

However, the angularity and plasticity of fines have significant effect on undrained behaviour (in terms of their ESP and deviatoric stress-strain response). In constitutive modelling point of view, the EG-SSL can be used to define the relative state of same soil by equivalent granular state parameter, $\psi^*_{(0)}$ and then the corresponding $\psi^*_{(0)}$ can also be used to predict undrained responses. But this study shows that the undrained responses manifested by sand with different types of fines can not be correlated with equivalent granular state parameter, $\psi^*_{(0)}$ within a same framework. Their undrained responses depends on fines types and thus can not be treated as same soil.

The undrained responses (in terms of ESP and deviatoric stress-strain) of sand with different types of fines are largely depended on their corresponding flow rule and plastic hardening parameters. These parameters for sand with different types of fines are expected to be different due to their difference in micro-structure. Thus, only

achieving the EG-SSL was not enough for explain the undrained behaviour of sand with different types of fines.

7.6 SUMMARY

An equivalent granular void ratio, e^* and equivalent granular state parameter, ψ^* based constitutive model for sand with fines was discussed in Chapter 6. The equivalent granular void ratio, e^* depends on a parameter b and a prediction formula for b was developed in Chapter 4. The only three input parameters used to obtain the b parameter are particle size ratio, χ threshold fines content, TFC and fines content, f_c. It was inherently assumed that b is independent of other parameters such as angularity and plasticity. For particular sand-fines mix the particle size ratio, angularity and plasticity are remain same and the effect of these parameters can not be observed on the b parameter. Thus, the effect of fines plasticity and angularity could not observe in previous chapters as it only used sand with MII fines. Thus, to examine the effect of fines types, the test results of sand with four different types of fines are discussed in this Chapter. These four different types of fines are characterized by their angularity and plasticity. Thus, their effects on prediction equation of b, EG-SSL and undrained response are examined. The following are the out come of this study-

- The fines types do not have significant effect the prediction equation of b and the conversion from void ratio, e to equivalent granular void ratio, e^*. Thus their effect on EG-SSL is negligible.

- Only EG-SSL can not be used to predict undrained responses (ESP and deviatoric stress strain responses) for sand with different types of fines in a

same CSSM framework as sand with different types of fines effectively represent different soil.

- Significant effect of fines angularity was observed on undrained responses though it did not have influence on EG-SSL. The sand with highly angular particles exhibited higher q_{peak} than sand with rounded particles even though low plastic property added to angular particles.

- The effect of fines plasticity was observed on their undrained responses though they did not have significant influence on EG-SSL. In general, the sand with high plasticity fines exhibited lower q_{peak}. However, the effect of plasticity can be suppressed by the presence of highly angular particles.

CHAPTER 8

Effect of Fines on Cyclic Loading

8.1 INTRODUCTION

The study of the mechanical behaviour of saturated sands under undrained monotonic loading condition has lead to important research development on soil liquefaction due to cyclic loading. A number of research works suggested that the over all key feature of cyclic loading behaviour of soil can be partly related to monotonic behavioural frame i.e. there is a link between monotonic and cyclic loading (Chu et al. 2003; Gennaro et al. 2004; Georgiannou et al. 1991; Konrad 1993; Mohamad and Dobry 1986; Yamamuro and Covert 2001). However, experimental evidence to support this finding is limited. Thus, the main focus of this Chapter is to present experimental evidence directly verifying the link between monotonic and cyclic loading, particularly strain hardening behaviour after quasi steady state, QSS. It also clarifies the effect of fines contents on the linkage between monotonic and cyclic loading condition.

8.2 THE CONCEPTUAL FRAMEWORK

Significant progress has been made, since the 80s, in linking instability behaviour between undrained monotonic and cyclic undrained loading condition.

CHAPTER 8

Effect of Fines on Cyclic Loading

8.1 INTRODUCTION

The study of the mechanical behaviour of saturated sands under undrained monotonic loading condition has lead to important research development on soil liquefaction due to cyclic loading. A number of research works suggested that the over all key feature of cyclic loading behaviour of soil can be partly related to monotonic behavioural frame i.e. there is a link between monotonic and cyclic loading (Chu et al. 2003; Gennaro et al. 2004; Georgiannou et al. 1991; Konrad 1993; Mohamad and Dobry 1986; Yamamuro and Covert 2001). However, experimental evidence to support this finding is limited. Thus, the main focus of this Chapter is to present experimental evidence directly verifying the link between monotonic and cyclic loading, particularly strain hardening behaviour after quasi steady state, QSS. It also clarifies the effect of fines contents on the linkage between monotonic and cyclic loading condition.

8.2 THE CONCEPTUAL FRAMEWORK

Significant progress has been made, since the 80s, in linking instability behaviour between undrained monotonic and cyclic undrained loading condition.

- Mohamad and Dobry (1986) reported that the monotonic behaviour of soil must be considered in analyzing the undrained cyclic behaviour of saturated sand. Georgiannou et al. (1991) reported the same finding for Ham river sand .

- Konrad (1993) reported that the undrained peak strength envelope in the normalized effective stress space could be used to define the triggering of strain softening in both monotonic and cyclic undrained loading.

- Yamamuro and Covert (2001) confirmed that cyclic instability in loose 50/200 Nevada sand with 40% silt was triggered when effective stress path, ESP "crossed" the instability line. Vaid and Sivathayalan (2000) reported that strain softening under undrained cyclic loading occurred at the instant when the mobilized friction angle attained the value that triggered strain softening under monotonic undrained loading. Gennaro et al. (2004) reported similar finding.

Based on the above studies, a conceptual framework for linking liquefaction behaviour under static and cyclic undrained loading is presented in Figure 8. 1. In this framework liquefaction is a manifestation of instability and this is different from cyclic mobility. One can define an instability stress ratio, η_{IS}, by the effective stress state at peak undrained strength under monotonic undrained loading. When the effective stress state crosses the line defined by η_{IS} as a result of pore water pressure generation due to either monotonic or cyclic undrained loading, instability will be triggered. It is evident from Figure 8. 1 that the deviatoric stress pulse required to trigger instability under cyclic loading can be less than that in monotonic loading.

Furthermore, the ESP of monotonic undrained loading defines the boundary of admissible stress state during cyclic loading.

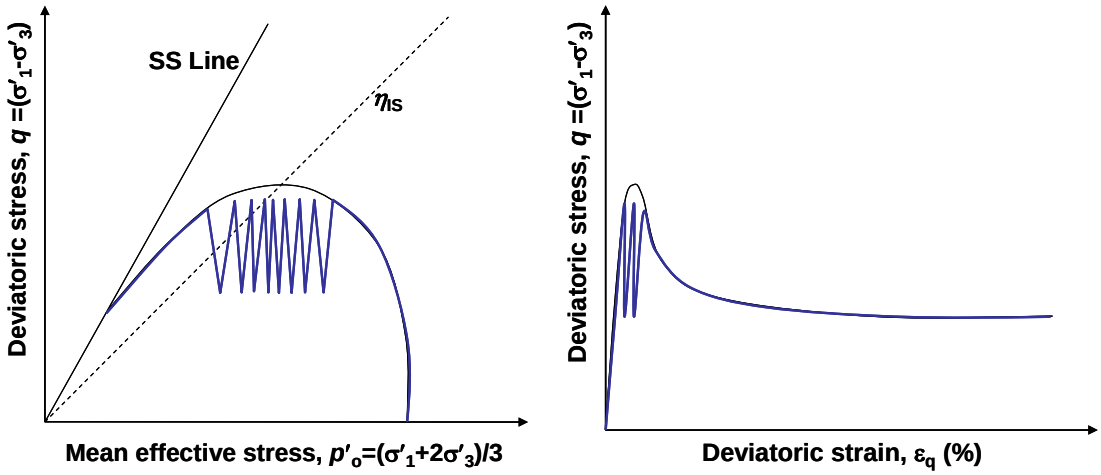

(a) **(b)**

Figure 8. 1: **Relation between cyclic and monotonic behaviour for strain softening type triaxial tests; (a) in q-p' space, (b) in q-ε_q space.**

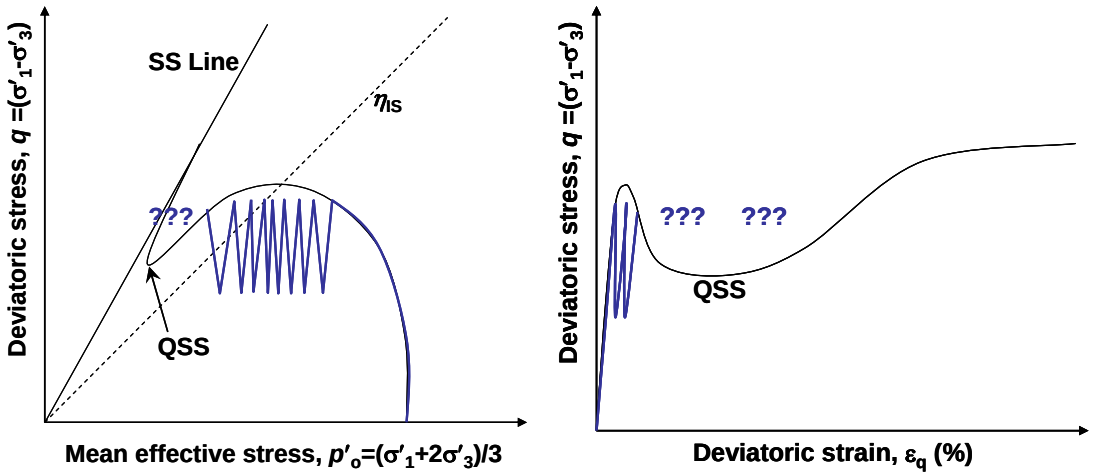

(a) **(b)**

Figure 8. 2: **Limited understanding for strain hardening type behaviour.**

However, experimental evidence directly verifying the above conceptual framework is relatively limited, in particular, in relations to the case of strain hardening for sand with fines. One particular issue is the dilemma presented in Figure 8. 2, whether

stability will be re-gained in cyclic loading when the soil is sheared, cyclically, to a condition beyond the quasi-steady state (QSS). There is also the question about the influence of fines content on cyclic behaviour.

To address the above issues, as series of monotonic and cyclic triaxial tests were conducted on a sand with varying amount of fines. A synthesis of the test results serves three purposes.

- The first one is to establish some linkages between monotonic and cyclic instability, mainly in the case of strain hardening.
- The second one is to investigate the influence of fines content, if any, on the linkages between monotonic and cyclic behaviour. The equivalent granular void ratio, e^* and equivalent state parameter, ψ^* are used to examine whether the relation between monotonic and cyclic loading can be established independent of fines contents.
- The third one is to investigate the effect of the stress pulse (in terms of effective stress ratio, η at first cycle) on triggering cyclic insatiability.

8.3 TESTING PROGRAM

The testing program was designed to give pairs of tests, one for monotonic loading and the other one for cyclic loading. Two tests of a given pair have similar equivalent granular void ratio, e^* and equivalent state parameter, $\psi^*_{(0)}$. But different pairs have different equivalent granular void ratio, e^* and equivalent state parameter, $\psi^*_{(0)}$. The testing program is presented in

Table 8. 1. It contains seven pairs of isotropically consolidated undrained tests for sand with up to 20% fines content. It covers the following spectrum of strain hardening behaviours:

- Type A: significant strain softening to QSS followed by slight strain hardening,
- Type B: significant strain softening to QSS followed by significant strain hardening,
- Type C: slight strain softening to QSS followed by significant strain hardening.

The material used for this study is Sydney sand and MII fines. To examine the effect of fines content, different percentage of fines were added to the sand. A simplified name convention is used in this Chapter. A test is identified by a name in the format of “alphabet-xx-yy”, where alphabet is either “M” for monotonic and “C” for cyclic, “xx” is the fines content in percentages, and “yy” is an additional reference number. It is noted that most of monotonic tests used in this Chapter to complete pairs are also discussed in previous Chapter. However, they are also indentified by the new name convention.

Table 8. 1: The summary of triaxial testing

Test Name		Fines Content, (%)	*b*-value	p'_0 (kPa)	$e_{(0)}$	$e^*_{(0)}$	$\psi^*_{(0)}$	Observed Behaviour
M-15-04	Mono	15	0.150	600	0.623	0.860	0.045	Type A
C-15-20	Cyclic	15		600	0.617	0.853	0.038	
M-15-05	Mono	15	0.150	600	0.628	0.866	0.051	
C-15-21	Cyclic	15		600	0.613	0.848	0.034	
M-20-02	Mono	20	0.200	600	00.573	0.874	0.059	
C-20-20	Cyclic	20		600	0.568	0.868	0.053	
M-00-08	Mono	00	00	600	0.852	0.852	0.037	Type B
C-00-20	Cyclic	00		600	0.845	0.845	0.030	
M-00-07	Mono	00	00	600	0.850	0.850	0.035	
C-00-21	Cyclic	00		600	0.840	0.840	0.025	
M-15-05	Mono	15	0.150	600	0.628	0.886	0.051	
C-15-22	Cyclic	15		600	0.625	0.862	0.047	
M-00-05	Mono	00	00	350	0.851	0.851	0.007	Type C
C-00-22	Cyclic	00		350	0.851	0851	0.007	
M-15-07	Mono	15	0.150	600	0.588	0.819	0.004	
C-15-23	Cyclic	15		600	0.591	0.822	0.008	

where, $e_{(0)}$ = Void ratio at the end of consolidation,

$e^*_{(0)}$ = Equivalent granular void ratio at the end of consolidation,

$\psi^*_{(0)}$ = Equivalent granular state parameter at the end of consolidation.

8.4 COMPARISON BETWEEN CYCLIC AND MONOTONIC LOADING BEHAVIOUR

Seven pair of tests covering 0% to 20% fines are presented in this section to clarify the issues on the link between monotonic and cyclic loading behaviour with a emphasis on strain hardening after QSS. The three types of strain hardening behaviours are discussed in coming sub-sections. The effect of fines contents are also discussed and analyzed in terms of equivalent granular state parameter, $\psi^*_{(0)}$ in subsequent sub-sections.

8.4.1 *Type A: significant strain softening to QSS followed by slight strain hardening*

Three test pairs that manifested "type A" behaviour are compared in coming three sub-section. In this type of behaviour a significant strain softening behaviour observed before QSS and only slight strain hardening behaviour observed after QSS.

8.4.2 *Type A: Test pair M-15-05 for monotonic loading and C-15-21 for cyclic loading*

This section presents a comparison in between test pair M-15-05 for monotonic loading and C-15-21 for cyclic loading. Both tests have 15% fines content. The equivalent granular void ratios at the end of consolidation, $e^*_{(0)}$ for C-15-21 and M-15-05 are 0.848 and 0.866 which lead to equivalent granular state parameter, $\psi^*_{(0)}$ of 0.034 and 0.051 respectively. The equivalent state parameters, $\psi^*_{(0)}$ are almost same and they can be compared meaningfully. The comparison in terms of ESP and q-ε_q responses is presented in Figure 8. 3a&b, whereas the cyclic load-time trace of the cyclic test was plotted in Figure 8. 3c.

The specimen for the cyclic test was first sheared to a static deviator stress from which stress pulses were commenced. Three packets of stress pulses with different prescribed peak deviator stress were then applied.

The first packet of stress pulses had a prescribed q_{peak} of 265 kPa, where q_{peak} denotes the peak deviatoric stress. A total of 40 cycles were applied. This prescribe q_{peak} value is higher than the corresponding q_{IS} of the corresponding monotonic tests (M-15-05), where q_{IS} is the deviator stress at onset of instability under monotonic loading of M-15-05 at q_{peak}. However, the effective stress ratio was less than η_{IS}. As shown in Figure 8. 3a, the ESP traced above that of M-15-05, and the prescribed q_{peak} was achieved. The overall location of the ESP moved left with each stress pulse, but at a rate that reduced with number of stress pulses. The stress-strain loops manifested were "tight". This implies instability is not governed by the magnitude of prescribe q_{peak} relative to q_{IS}. The effective stress ratio at instability, η_{IS} is represented by a dotted line in the q-p' space in Figure 8. 3a. This dotted line sometime referred to as the "instability line". In the context of this thesis, the instability line is only a graphical presentation of instability stress ratio, η_{IS} to indicate where ESP is crossing it. It does not comply that instability stress ratio, η_{IS} is independent of p'_0 and linear over a wide range of p'_0.

The second packet consisted of 5 stress pulses with a prescribed q_{peak} of 305 kPa. This higher q_{peak} led to higher rate of reduction in p', but the stress-strain loops were still "tight", and no instability was observed. It is pertinent to note that the highest stress ratio attained during these 5 load cycles was still less than η_{IS}.

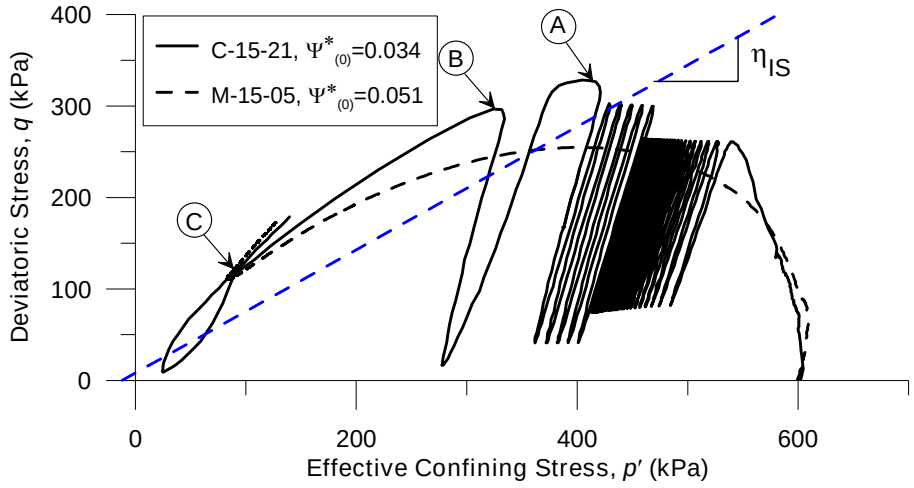

(a)

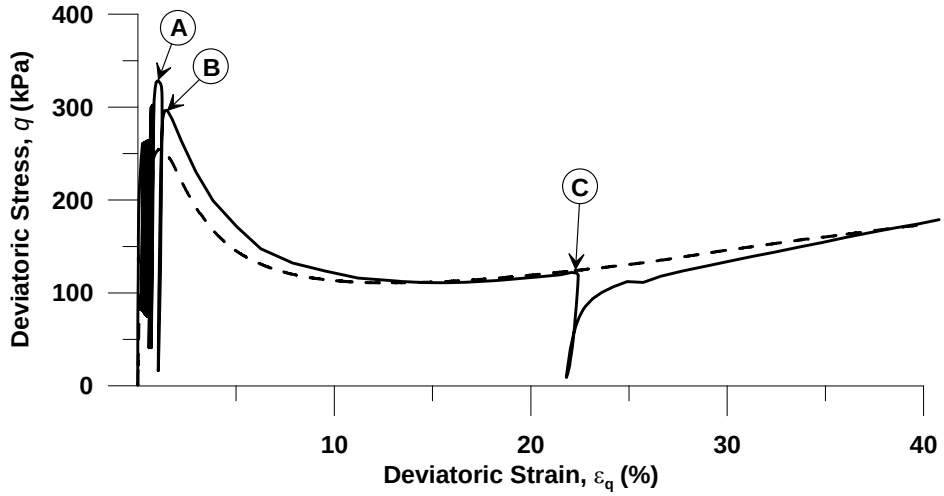

(b)

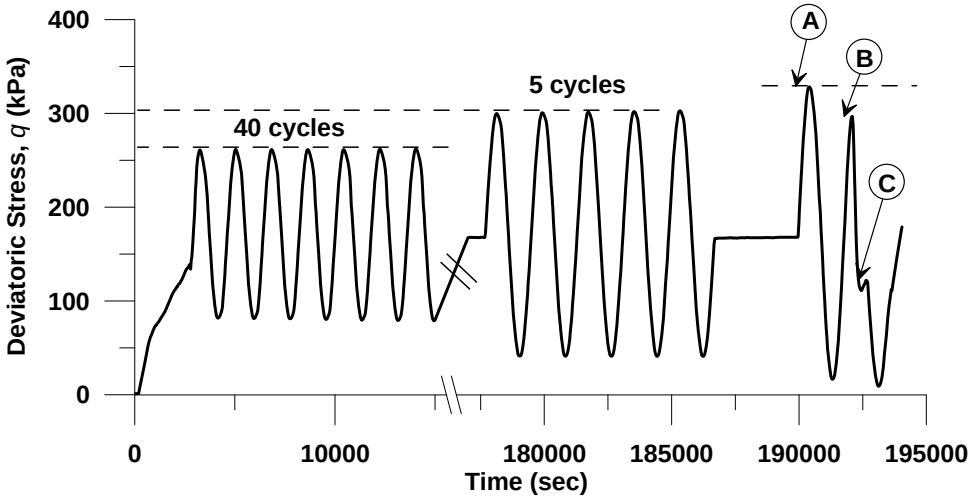

(c)

Figure 8. 3: Test pair M-15-05 and C-15-21 for 15% fines: a) ESP; b) q-ε_q response; c) stress-time plot.

The third packet of stress pulses had a prescribed q_{peak} of 330 kPa. In the first pulse, the prescribed q_{peak} was achieved at point "A" (of Figure 8. 3a&b) even though the ESP traced above that of M-15-05. At this q_{peak} value the stress ratio approached η_{IS}. The generation of pore water pressure "pushed" the ESP traced by the second pulse to point "B" which was located above the instability stress ratio line (see Figure 8. 3a&b). The prescribed q_{peak} could no longer be achieved. This implies instability is not governed by η relative to instability, η_{IS}. The ESP manifested during loading traced along a downward plummeting curve "BC" similar to that of M-15-05, although the curve traced by C-15-21 was located above that of monotonic loading. The deviatoric stress-strain curve of segment "BC" for cyclic and monotonic load were almost identical. For the next stress pulse beyond the point "C", the state of the specimen was beyond QSS. A higher q_{peak} can be developed as the responses of the specimen traced along the strain hardening leg of the corresponding monotonic test.

8.4.3 *Type A: Test pair M-15-04 for monotonic loading and C-15-20 for cyclic loading*

The equivalent granular void ratios, $e^*_{(0)}$ for C-15-20 and M-15-04 are 0.853 and 0.860 which lead to equivalent granular state parameter, $\psi^*_{(0)}$ of 0.038 and 0.045 respectively. The equivalent state parameters, $\psi^*_{(0)}$ are almost same and thus, their comparison is meaningful. Figure 8. 4a&b show comparison between ESPs and q-ε_q responses, whereas the cyclic load-time trace was plotted in Figure 8. 4c.

The specimen for the cyclic test was first sheared to a static deviator stress from which stress pulses were commenced. Three packets of stress pulses with different prescribed peak deviator stress were then applied.

The first packet of stress pulses had a prescribed q_{peak} of 225 kPa. A total of 10 cycles were applied. This time, the prescribed q_{peak} value is lower than the corresponding q_{IS} of the corresponding monotonic tests. The overall location of the ESP moved left with each stress pulse, but at a rate that reduced with number of stress pulses. The stress-strain loops manifested were "tight" which is similar to C-15-20.

The second packet consisted of 10 stress pulses with a prescribed q_{peak} of 265 kPa, identical to q_{IS}. This higher q_{peak} led to higher rate of reduction in p', but the stress-strain loops were still "tight", and no instability was observed. It is pertinent to note that the highest stress ratio attained during this 10 stress pulses were still less than $\eta_{IS.}$

The third packet of stress pulses had a prescribed q_{peak} of 310 kPa. In the first cycle, the prescribed q_{peak} was achieved at point "A" (of Figure 8. 4a&b) even though the ESP traced above that of M-15-04. At this q_{peak} value the stress ratio approached η_{IS}. The generation of pore water pressure "pushed" the ESP traced by the second pulses to point "B" which was located above the instability stress ratio line (see Figure 8. 4a&b). The prescribed q_{peak} could no longer be achieved. This again supports that instability is not governed by the magnitude of prescribed q_{peak} relative to q_{IS}, but rather related to effective stress ratio, η relative to η_{IS}. The ESP manifested during loading traced along a downward plummeting curve "BC" similar to that of M-15-04, although the curve traced by C-15-20 was located above that of monotonic loading. The deviatoric stress-strain curve of segment "BC" for cyclic and monotonic load were almost identical. For the next load cycle beyond point "C", the state of the specimen was beyond QSS. A higher q_{peak} can be developed as the responses of the specimen traced along the strain hardening leg of the corresponding monotonic test.

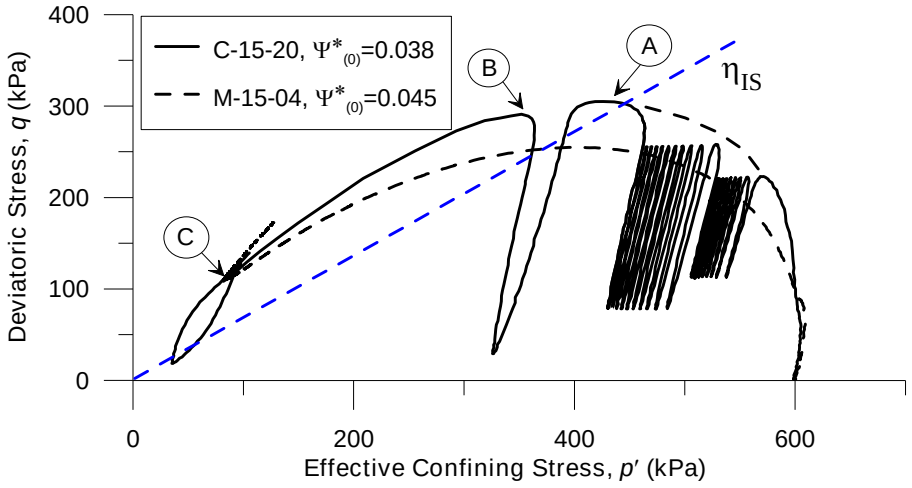

(a)

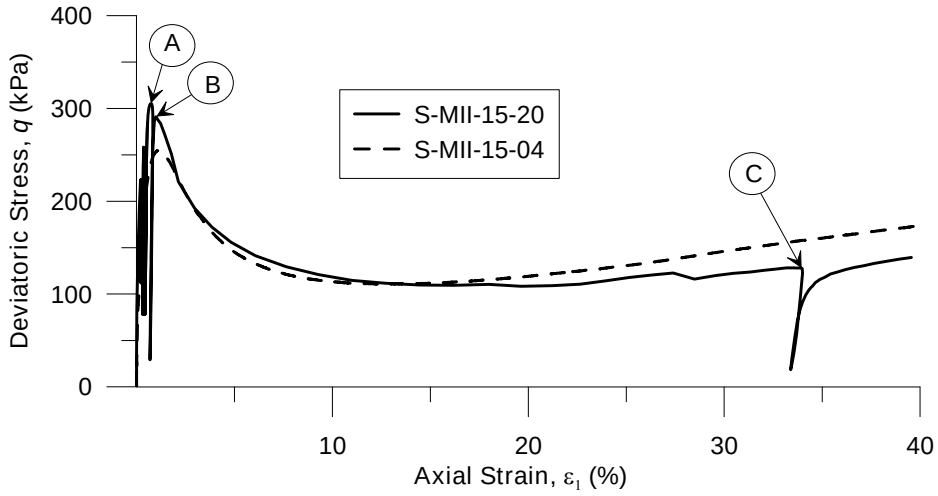

(b)

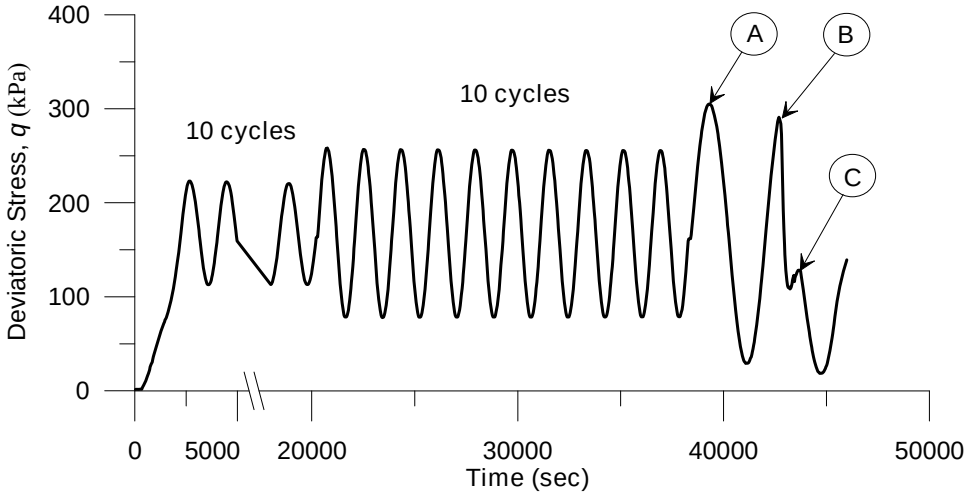

(c)

Figure 8. 4: Test pair M-15-04 and C-15-20 for 15% fines: (a) ESP; (b) q-ε_q response; (c) stress-time plot.

8.4.4 *Type A: Test pair M-20-02 for monotonic loading and C-20-20 for cyclic loading*

This section presents a comparison in between test pair M-20-02 for monotonic loading and C-20-20 for cyclic loading. Both tests have 20% fines content. The equivalent granular void ratios, $e^*_{(0)}$ for C-20-20 and M-20-02 are 0.868 and 0.874 which lead to equivalent granular state parameter, $\psi^*_{(0)}$ of 0.053 and 0.059 respectively. Thus, the equivalent state parameters, $\psi^*_{(0)}$ are almost same. The comparison in terms of ESP and q-ε_q responses is presented in Figure 8. 5a&b, whereas the cyclic load-time trace of the cyclic test was plotted in Figure 8. 5c.

The specimen for cyclic test C-20-20 was brought to a static deviator stress state; then five packets of stress pulses were applied sequentially. Note that part of the ESP in bringing the specimen to the static deviator stress state appears to be problematic as indicated by "-?-" in Figure 8. 5a. However, consistent pore pressure measurement was obtained prior to application of stress pulses.

The first packet had a peak deviator stress, q_{peak} of 195 kPa. This value is less than q_{IS} of the corresponding monotonic test. Furthermore, the effective stress ratio during this packet of stress pulses was always less than $\eta_{IS,}$ the instability stress ratio inferred from M-20-02. The ESP moved slowly to the left with stress pulses and the stress-strain loops (Figure 8. 5b) were "tight". There was no sign of instability.

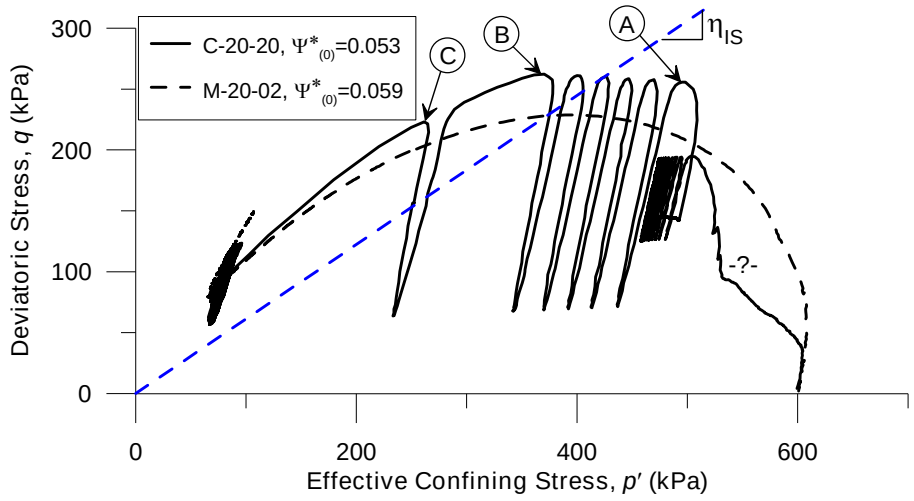

(a)

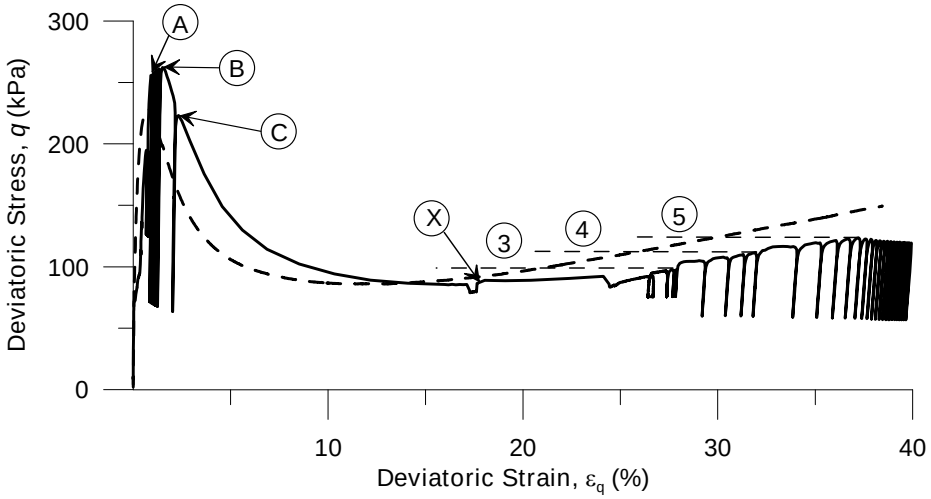

(b)

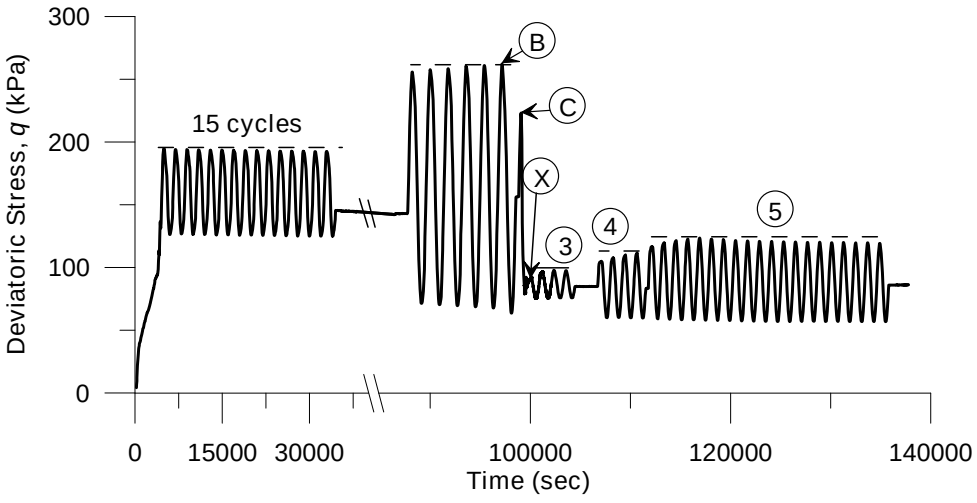

(c)

Figure 8. 5: Test pair M-20-02 and C-20-20 for 20% fines; (a) ESP, (b) q-ε_q response, (c) stress-time plot.

The second packet of stress pulses had a peak deviator stress of 255 kPa, which was higher than q_{IS} of the monotonic test. However, for the first 4 stress pulses of this packet, the effective stress ratio was less than η_{IS} and the prescribed q_{peak} could still be achieved. The cyclic stress-strain loops were also tight. However, the effective stress path moved left significantly with the next stress pulses. At the 5th pulses the ESP just crossed the instability line (as defined by η_{IS}). At the 6th pulses, the ESP was clearly above the instability line as indicated by point "B". Instability commenced as indicated the path "BC" which plummeted downward. This implies that instanility governed by η, relative to η_{IS}.

The 3rd packet of stress pulses was applied when the response reached "X" which corresponds to the condition of QSS in monotonic loading. The peak deviator stress in this packet of load cycles was 100 kPa. As indicated by point "X", the peak stress attained in first cycle of this packet was slightly below prescribed q_{peak}, but the prescribed q_{peak} was attained in subsequent stress pulses. This is associated with the strain hardening behaviour, although slight, of the corresponding monotonic tests.

The last two packets of stress pulses had a prescribed q_{peak} of 110 kPa for the 4th packet and 120 kPa for the 5th packet, i.e. of the prescribed peak deviator stress was of increasing value at a slight rate. The reason was to examine whether the post QSS strain hardening response of the corresponding monotonic tests could be observed. As evident from Figure 8. 5b&c, the first pulse of each packet could not attained the prescribed q_{peak} value, but the prescribed q_{peak} was attained in subsequent cycles. This clearly demonstrated that the slight strain hardening response of the corresponding monotonic test was reflected in the achievable q_{peak} in cyclic loading.

8.4.5 *Type B: significant strain softening to QSS followed by significant strain hardening*

Three pairs of tests that manifested "type B" behaviour are presented in this sub-section. In this type of behaviour shows a significant strain hardening behaviour observed after QSS though strain hardening was not rapid enough to mobilize a deviator stress higher than q_{IS} before end of test. First two comparisons are in between the monotonic and cyclic response of 0% fines content, i.e. host sand only, provide a benchmark for synthesizing the influence of fines content. The third comparison is in between monotonic and cyclic loading for sand with 15% fines. This gives a basis of justifying the effect of adding fines.

8.4.6 *Type B: Test pair M-00-08 for monotonic loading and C-00-20 for cyclic lading*

The comparison of effective stress path (ESP) and deviatoric stress-strain are presented in Figure 8. 6a&b, whereas the cyclic load-time trace was plotted in Fig. 8c. Both tests have 0% fines content. The equivalent granular void ratios, $e^*_{(0)}$ for C-00-20 and M-00-08 are 0.852 and 0.845 which lead to equivalent granular state parameter, $\psi^*_{(0)}$ of 0.037 and 0.030 respectively. The equivalent state parameters, $\psi^*_{(0)}$ are almost same and suitable for comparison.

The specimen for the cyclic test was first brought to a static deviator stress as indicated by point "A". Then two packets of stress pulses (of different prescribed peak deviator stress) were prescribed.

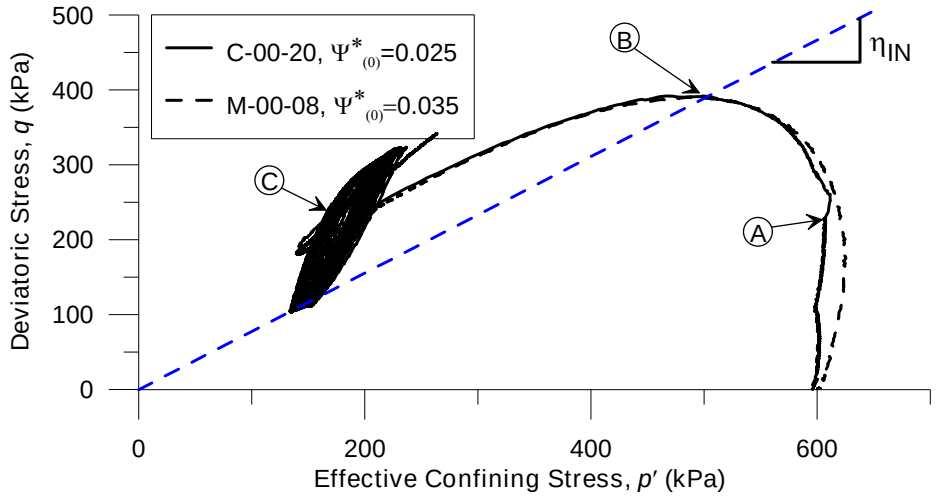

(a)

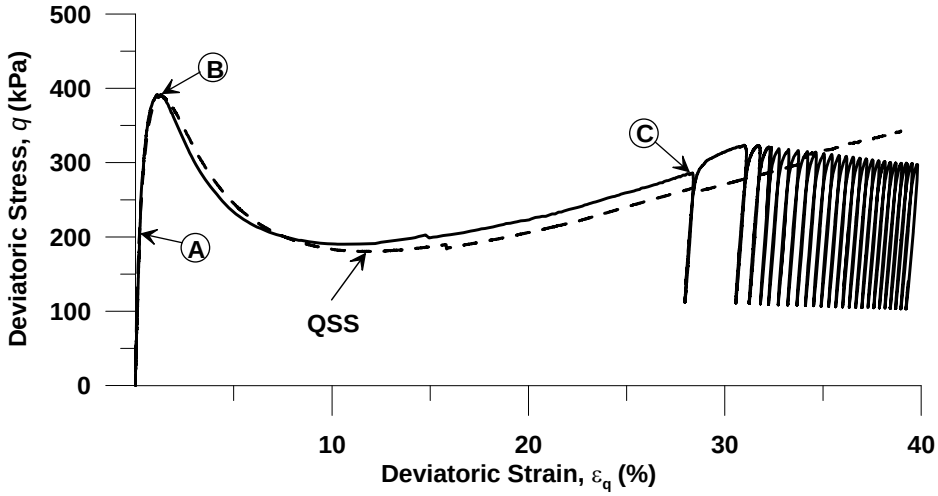

(b)

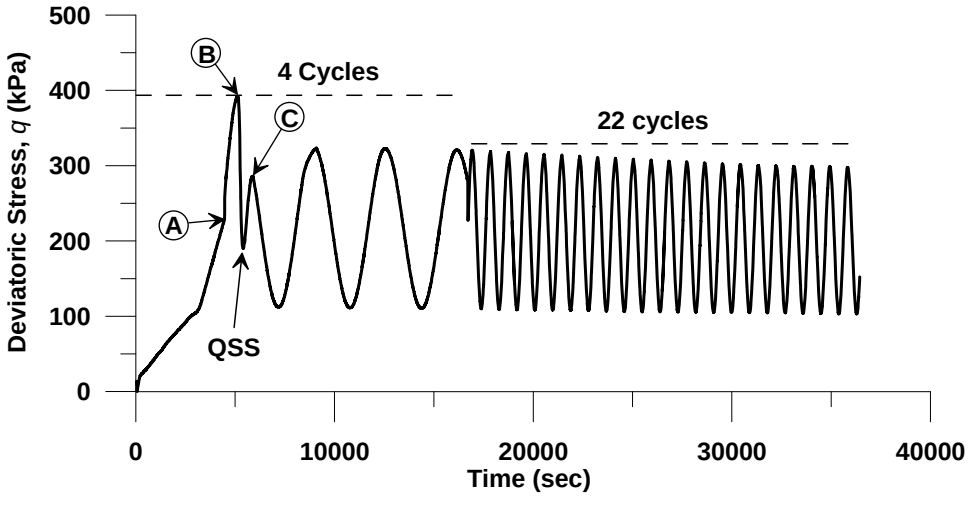

(c)

Figure 8. 6: Test pair M-00-08 and C-00-20 for host sand: a) ESP; b) q-ε_q response; c) stress-time plot

The first packet of stress pulses consisted of 4 pulses with a prescribed q_{peak} of 450 kPa. However, the highest deviator stress realised in the first pulse was at point "B" which has a deviator stress of ~395 kPa. The deviator stress then reduced during unloading and with the loading phase tracing out the strain hardening response in terms of both the ESP and q-ε_q responses, and as indicated by "ABC" in Figure 8. 6a&c. The peak deviator stress of the subsequent 3 pulses were located approximately on the post-QSS strain hardening leg of the monotonic test.

The second packet of stress pulses consisted of 22 pulses with a prescribed q_{peak} of 325 kPa. This peak deviator stress was achieved for all 22 pulses despite the first few cycles slightly "overshoot" the corresponding q-ε_q curves. This is not unexpected because loading rate for cyclic loading was at a rate considerably higher than that of monotonic loading, and that a slight rate effect was likely (Georgiannou et al. 2008; Hyodo et al. 1998; Mao and Fahey 2003). Note that the peak deviator stress appeared to drift slightly downwards with number of stress pulses. This is because the stress pulse prescription was based on load. The increase in cross-section area of the specimen led to a slight reduction in deviator stress achieved. It is also interesting to note that as the peak deviator stress was beneath the corresponding q-ε_q curve of monotonic testing, the stress-strain loop became "tighter".

8.4.7 *Type B: Test pair M-00-07 for monotonic loading and C-00-21 for cyclic loading*

The comparison of ESP and q-ε_q are presented in Figure 8. 7a&b, whereas the cyclic load-time trace was plotted in Figure 8. 7c. The equivalent granular void ratios, $e^*_{(0)}$ for C-00-21 and M-00-08 are 0.840 and 0.850 which lead to equivalent granular state parameter, $\psi^*_{(0)}$ of 0.025 and 0.035 respectively. The equivalent state parameters, $\psi^*_{(0)}$ are almost same and again suitable for comparison.

The specimen for the cyclic test was first sheared to a static deviatoric stress of q = 275 kPa. Then three different packets of stress pulses of different peak deviator stress were then sequentially applied.

The first packet of stress pulses consisted of 84 pulses with a prescribed peak deviator stress of 275 kPa. The ESP traced by this packet of stress pulses traced significantly below the instability line of the corresponding monotonic tests. There was minimal development of pore water pressure or deviatoric strain.

The second packet of stress pulses consisted of 12 pulses with a prescribe peak deviator stress of 405 kPa. For the first several pulses of this packet, the prescribed the ESP did not traced above the instability line (defined by η_{IS} of the corresponding monotonic test). The prescribed peak deviator stress could be developed. However, the development of pore water pressure was more significant compared to the first packet of 84 stress pulses. With further stress pulses, the ESP traced across the instability line and development of pore water pressure and deviatoric strain increased rapidly. At point "C" and "C1" (located above the instability line by a small extent), the prescribed peak deviator stress, q_{peak}, could not be developed as indicated by the

figure. The upper limit of the ESP response traced along a curve similar to, but located slightly higher than that of, the downward plummeting leg of the corresponding monotonic tests. Deviatoric strain also developed rapidly. With further development of strain, both the ESP traced beyond the corresponding QSS state of monotonic test M-00-07. The q_{peak} climbed back up again along the "upward bent" of the strain hardening leg of the corresponding monotonic tests. It is pertinent to note that when the prescribed deviator stress was located above the instability line, the responses, in terms of both ESP and q-ε_q, traced along a "upper limit" curve defined by monotonic loading.

The last packet of stress pulses consisted of 12 pulses with a prescribed peak deviator stress of 350 kPa. This brought the prescribed q_{peak} values to the deviator stress mobilized at the corresponding strain of the corresponding monotonic test. No sign of instability was observed as indicated by point "D" of Figure 8. 7b&c. The strain development with load cycles reduced. This is consistent with the prescribed q_{peak} value being located beneath the post-QSS strain hardening segment of the corresponding monotonic test.

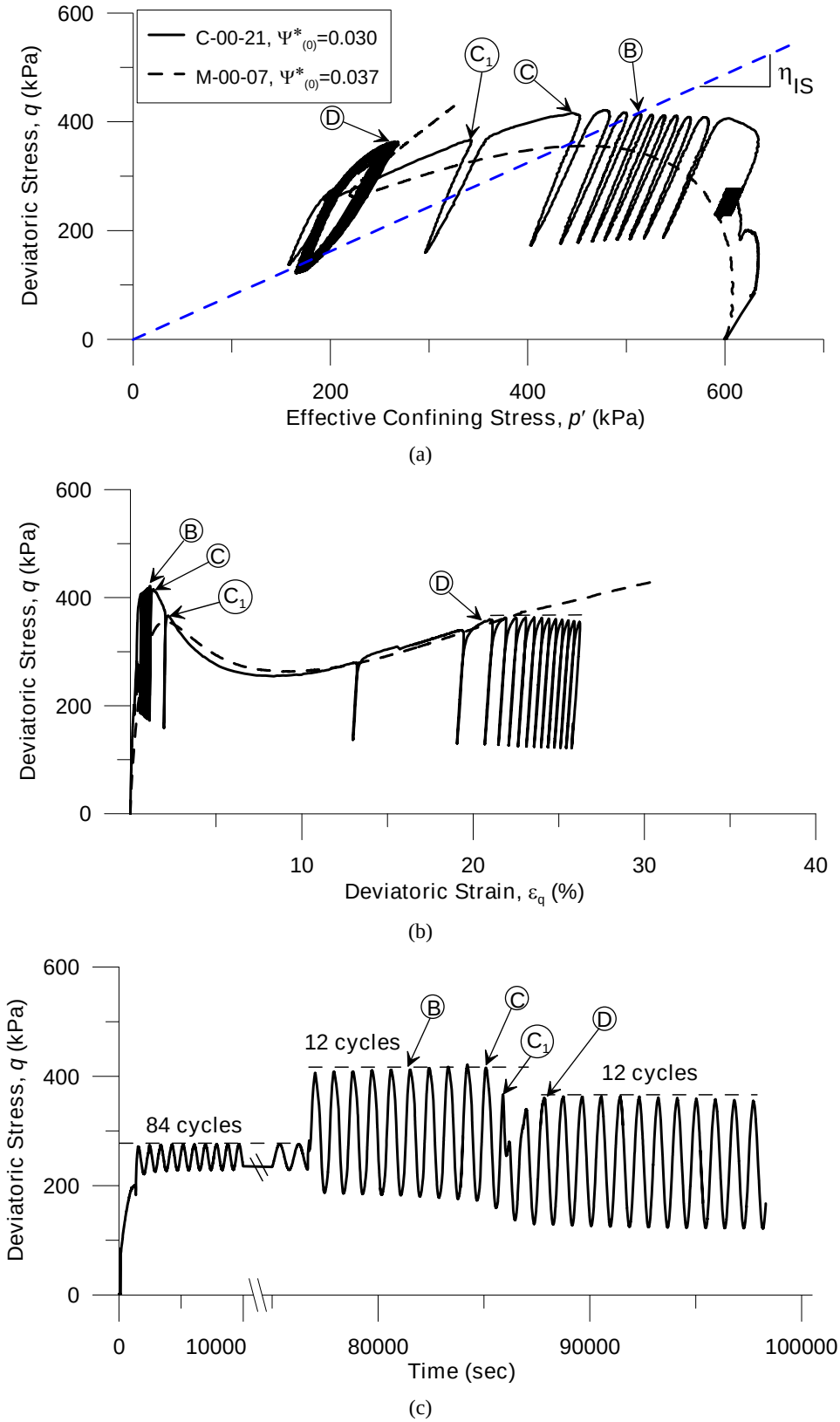

Figure 8. 7: **Test pair T-00-07 and C-00-21 for host sand: a) ESP; b) q-ε_q response; c) stress-time plot.**

8.4.8 *Type B: Test pair M-15-05 for monotonic loading and C-15-22 for cyclic loading.*

The comparison of ESP and q-ε_q responses is presented in Figure 8. 8a&b, whereas the cyclic load-time trace was plotted in Figure 8. 8c. Both tests have 15% fines content. The equivalent granular void ratios, $e^*_{(0)}$ for C-15-22 and M-15-05 are 0.862 and 0.886 which lead to equivalent granular state parameter, $\psi^*_{(0)}$ of 0.047 and 0.051 respectively. The equivalent state parameters, $\psi^*_{(0)}$ are almost same and suitable for comparison.

The specimen for the cyclic test was first sheared to a static shear stress of q = 75 kPa. Then four different packets of stress pulses of different prescribed peak deviator stresses were then sequentially applied.

The first packet of 81 stress pulses had a prescribed peak deviator stress of 100 kPa. This magnitude is significantly less than q_{IS} of the corresponding monotonic test. As shown in Figure 8. 8a, the overall location of the ESP moved left with each load cycle, but at a slow rate. The effective stress ratio during all 81 cycles was considerably less than η_{IS}. The stress-strain loops did not show any observable hysteresis. There was no indication of instability.

The second packet of 15 stress pulses had a prescribed q_{peak} of 300 kPa. This value, although higher than q_{IS} of the corresponding monotonic tests, can be developed with the first pulse as indicated by point "A" of Figure 8. 8a-c. At this stress state, the effective stress ratio was about close to η_{IS}. With the leftward movement (i.e. reduction in p') associated with stress pulses, the second pulse crossed the instability

line (i.e. achieving an effective stress ratio exceeding η_{IS}) and the prescribed q_{peak} could not be developed as indicated by point "B". The ESP moved along the monotonic path, traced along a curve indicated as "$BC_1C_2C_3$" in Figure 8. 8a. It first plummeted downwards and then bend upwards as shown in. It followed the upward bent because the deviatoric strain developed took the specimen pass the QSS point. This curve was of a shape similar to that of the corresponding monotonic test.

The third packet of 10 stress pulses had a prescribed q_{peak} of 225 kPa. This value was estimated from the deviator stress mobilized at point "D" of the corresponding monotonic test. The prescribed q_{peak} values could be developed in all 10 cycles. The development of ε_q with stress pulses was reducing. There was no sign of instability any more.

The last packet consisted of 3 stress pulses of increasing prescribed q_{peak} values of 240, 255, and 270 kPa. This increase in q_{peak} was estimated from the rate of post-QSS strain hardening of the corresponding monotonic test. The intention was to check whether an increasing q_{peak} value could be developed in line with the post-QSS strain hardening of the corresponding monotonic test. As evident from the Figure 8. 8b-c, these prescribed q_{peak} values could be developed and there was no sign of instability.

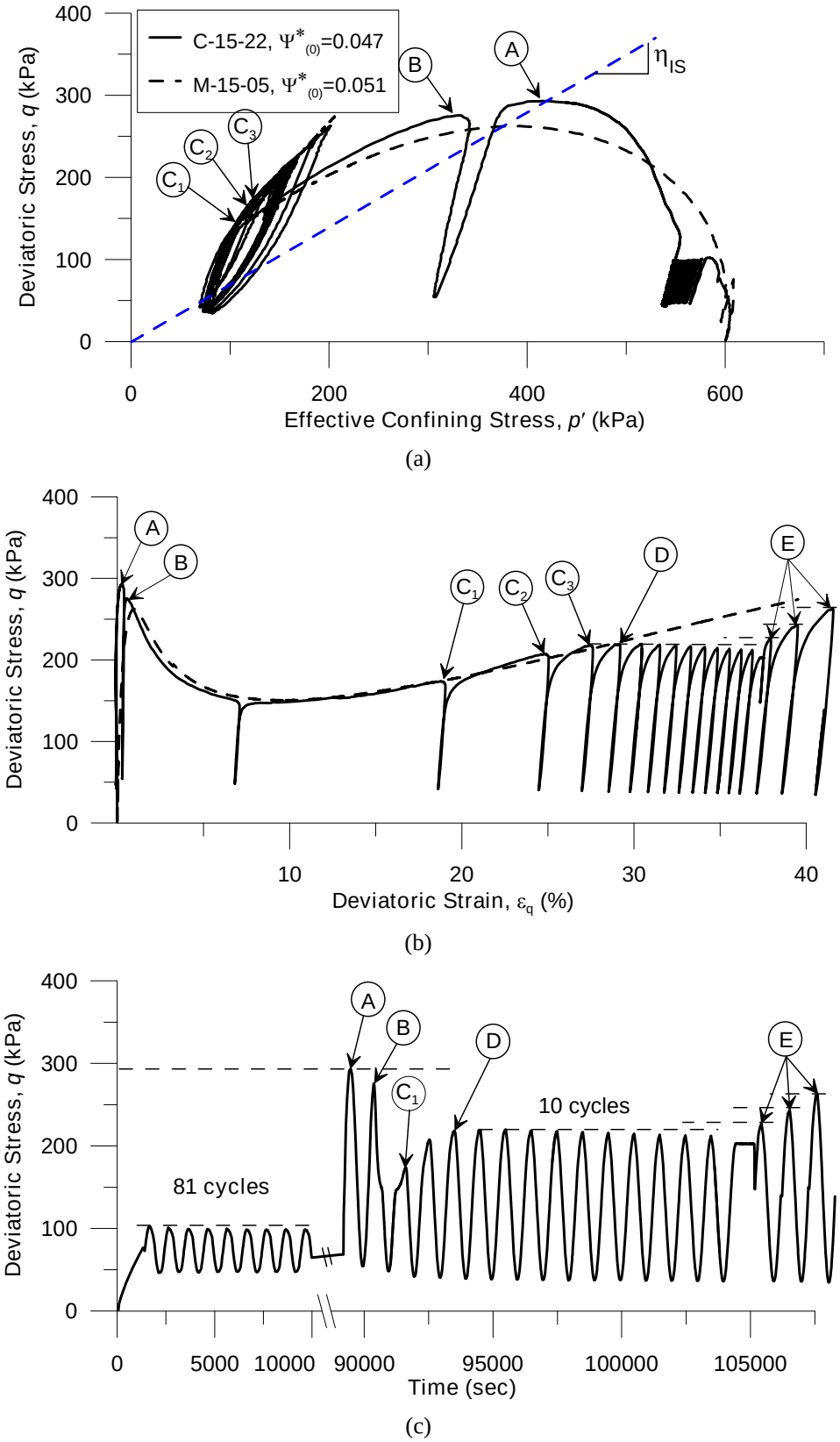

Figure 8. 8: **Test pair M-15-05 and C-15-22 for 15% fines: (a) ESP; (b) q-ε_q response; (c) stress-time plot.**

8.4.9 *Type C: slight strain softening to QSS followed by significant strain hardening*

Two pair of tests that manifested "type C" behaviour are presented in this section. In this type of behaviour shows a significant strain hardening after slight strain softening at QSS and the strain hardening was strong enough to mobilize a deviator stress higher than q_{IS} before end of test. First pair of comparisons between the monotonic and cyclic response of 0% fines content, i.e. host sand only, provide a benchmark for synthesizing the influence of fines content. Second pair presents comparison between sand with 15% fines.

8.4.10 *Type C: Test pair M-00-05 for monotonic loading and C-00-22 for cyclic loading.*

The comparison of ESP and q-ε_q is presented in Figure 8. 9a&b, whereas the cyclic load-time trace was plotted in Figure 8. 9c. The equivalent state parameters, $\psi^*_{(0)}$ are exactly same and thus suitable for comparison.

Six packet of stress pulses were applied to the test C-00-22. First packet of stress pulses denoted by 1 applied before QSS and slight strain soften was occurred during second packet of loading, denoted by 2. Other four packet of stress pulses were applied after QSS. Thus the responses of the two specimens can be compared over a significant domain. Test C-00-22 manifested less strain softening compared to M-00-05, however the extent of strain softening for both of these tests are still slight. Furthermore, the extent of strain hardening beyond QSS for both tests is significant.

As shown in Figure 8. 9c, six packets of stress pulses of increasing prescribed q_{peak} value were applied. The upper limit of the ESP traced during these 5 packets of stress

pulses traced closely along the ESP of the M-00-05. As evident from Figure 8. 9b, the prescribed deviator stress could be reached in all six packet. The prescribed q_{peak} value for the first pulse was above the "corresponding q-ε_q curve" of the corresponding monotonic test.

8.4.11 *Type C: Test pair M-15-07 for monotonic loading and C-15-23 for cyclic loading.*

The comparison is presented in Figure 8. 10a&b, whereas the cyclic load-time trace was plotted in Figure 8. 10c. Both tests have 15% fines content. The equivalent granular void ratios, $e^*_{(0)}$ for C-15-23 and M-15-07 are 0.822 and 0.819 which lead to equivalent granular state parameter, $\psi^*_{(0)}$ of 0.008 and 0.004 respectively. The equivalent state parameters, $\psi^*_{(0)}$ are almost same and suitable for comparison.

Stress pulses were applied to test C-15-23 after the specimen was sheared beyond QSS. Thus the responses of the two specimens can be compared over a significant domain. Test C-15-23 manifested more strain softening compared to M-15-07, but the extent of strain softening for this test is still slight. Furthermore, the extent of strain hardening beyond QSS for both tests is significant. As shown in Figure 8. 10c, five packets of stress pulses of increasing prescribed q_{peak} value were applied. The upper limit of the ESP traced during these 5 packets of stress pulses traced closely along the ESP of the M-15-07. As evident from Figure 8. 10b, the prescribed deviator stress could be realized, except the first pulse of the first packet as indicated by point "X". The prescribed q_{peak} value for the first pulse was below the "corresponding q-ε_q curve" of the corresponding monotonic test. With post-QSS strain hardening, the "corresponding q-ε_q curve" climbed upward and was above the prescribed q_{peak} .

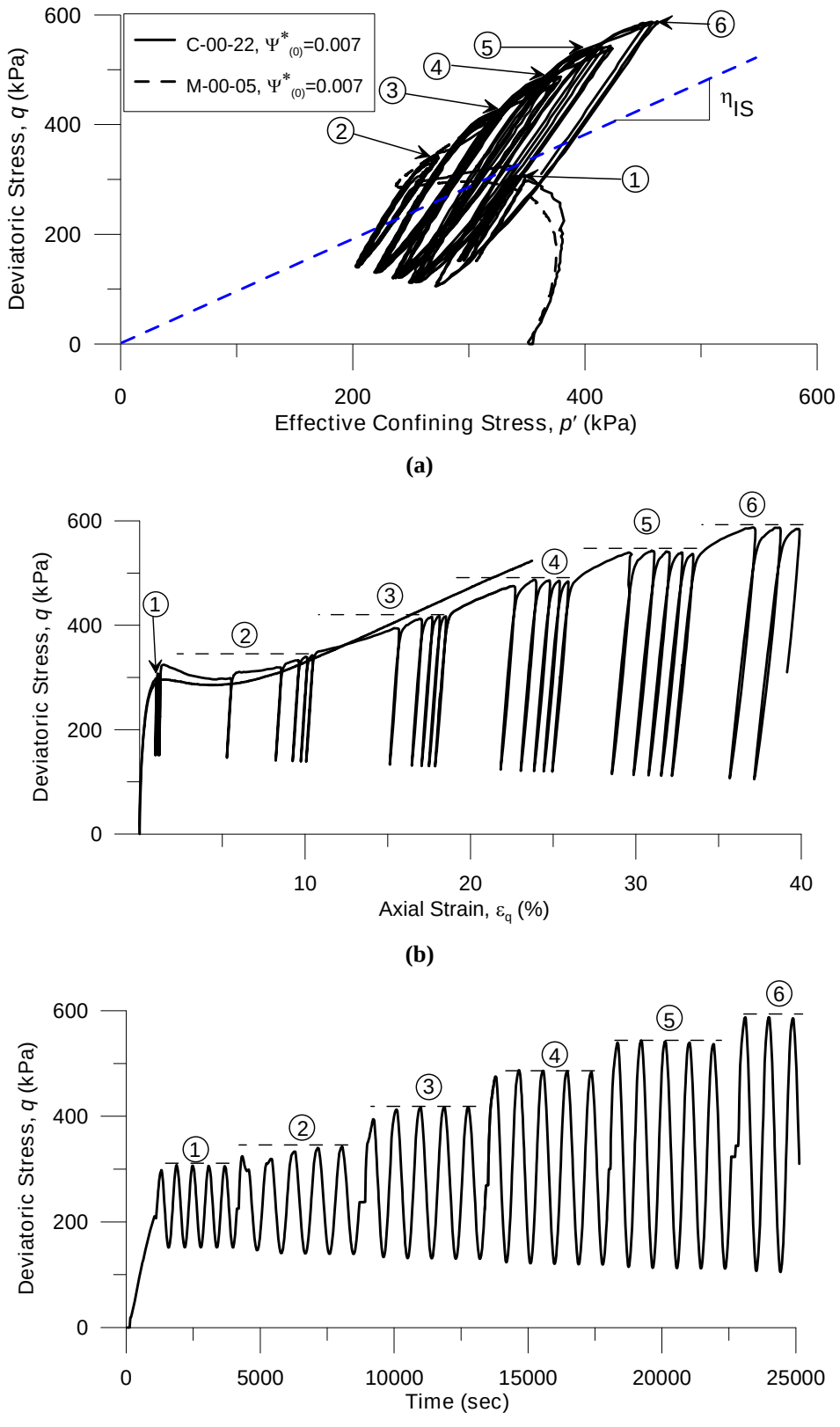

Figure 8. 9: **Test pair M-00-05 and C-00-22 for clean sand: a) ESP; b) q-ε_q response; c) stress-time plot.**

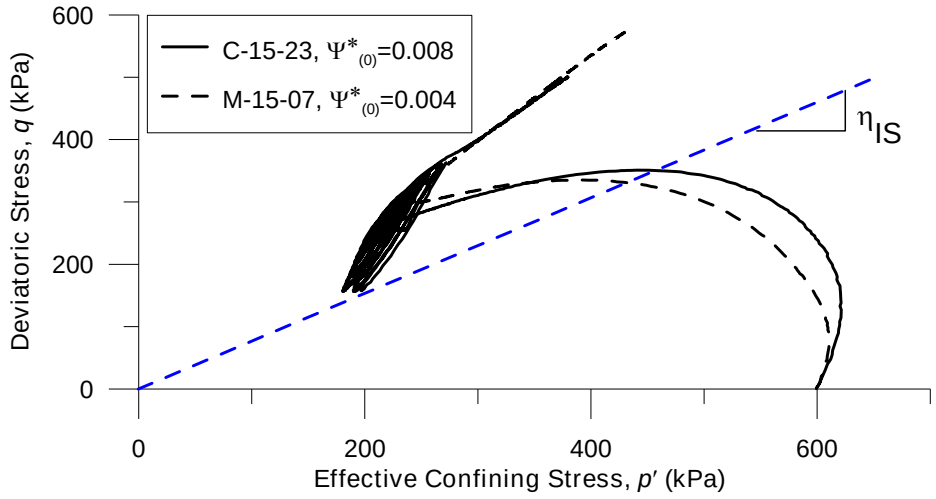

(a)

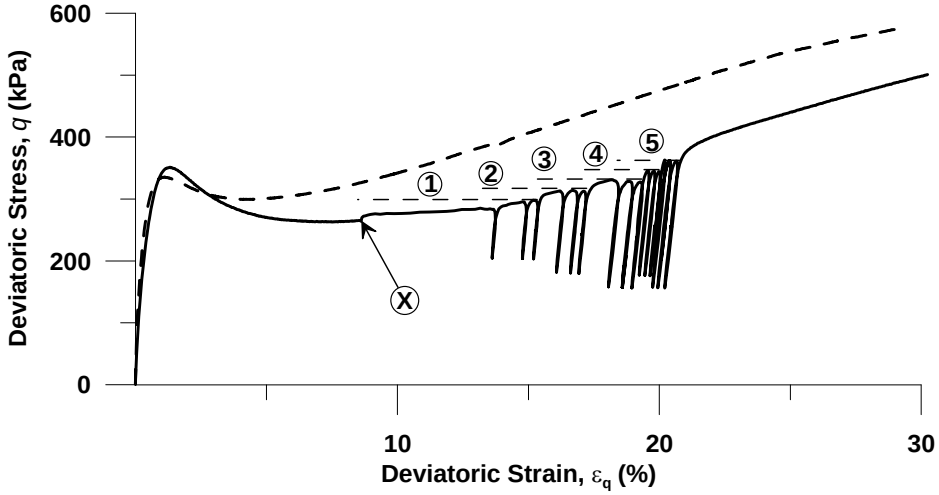

(b)

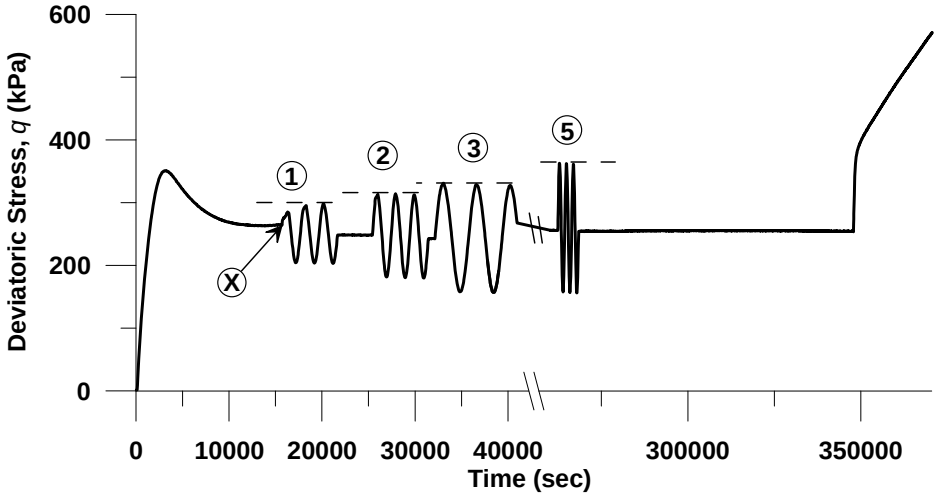

(c)

Figure 8. 10: Test pair M-15-07 and C-15-23 for 15% fines: a) ESP; b) q-ε_q response; c) stress-time plot.

8.4.12 *Synthesis of the Tests Results*

Eight pairs of tests are discussed, covering void ratio from 0.568 to 0.852, for sand with 0% to 20% fines content. A single set of rule can be used to correlate monotonic and cyclic loading behaviour for complete spectrum of post and pre-QSS strain hardening behavior irrespective of fines contents. The overall cyclic loading path is bounded by monotonic loading path. The cyclic instability before QSS is not governed by the magnitude of prescribed q_{peak} relative to q_{IS} for monotonic loading, but rather effective stress ratio, η relative to instability stress ratio, η_{IS}. The strain hardening behaviour after QSS is also bounded by the monotonic loading path of the corresponding test irrespective of fines contents.

8.5 EFFECT OF η RELATIVE TO η_{IS} ON CYCLIC INSTABILITY

It has been discussed in previous section that instability stress ratio is the onset triggering point both for monotonic and cyclic loading. As for cyclic loading, the effective stress ratio during pulses approached to the instability stress ratio with number of pulses, N and trigger instability when it reached to the instability stress ratio. However, the number of pulses, N required to trigger instability have a correspondence to the stress ratio, η at the prescribed peak deviatoric stress relative to the instability stress ratio, η_{IS}. Thus, an index is introduced as ratio between effective stress ratio, η at the prescribed peak deviatoric stress of cyclic loading and the instability stress ratio, η_{IS} of monotonic loading. It referred as "Instability Index" and can be written as

$$\varpi = \frac{\text{Effective stress ratio, } \eta}{\text{Instability effective stress ratio, } \eta_{IS}} \qquad \textbf{8. 1}$$

The instability index is a variable during testing; it increases with stress pulses as effective stress ratio changes with pulses. The growth of the ϖ with N give an indication on the effect of stress pulse on cyclic instability. However, the instability index at the first pulse, denoted by $\varpi_{(1)}$ here after, is an important parameter to get estimation on the number of pulses required to triggered cyclic instability.

8.5.1 ϖ - N Relationship for Clean Sand

The instability index, ϖ and number of cycles, N of each packet of cyclic pulses for C-00-21 is plotted in Figure 8. 11. It shows that instability index at first pulses, $\varpi_{(1)}$ also indicates whether a packet of stress pulses will approach to the cyclic instability or not. For example, in first packet of stress pulses, the initial $\varpi_{(1)}$ ($\approx$ 0.55) was not enough to approach instability stress ratio (1.0 at y-axis) with in 84 cycles; rather it became stable. On the other hand, in second packet of stress pulses, the initial $\varpi_{(1)}$ ($\approx$ 0.83) was large enough to reach instability stress ratio at 7^{th} pulses. It can be infer from Figure 8. 11 that any $\varpi_{(1)}$ higher than 0.83 may trigger cyclic instability with in less than 7 cycles and it could take more than 7 pulses if $\varpi_{(1)}$ is less than 0.83. On the other hand, $\varpi_{(1)}$ ($\approx$ 0.55) will not exhibit cyclic instability within 100 pulses (at least). The tests C-00-22 also showed similar behaviour as C-00-21 for clean sand.

8.5.2 ϖ - N Relationship for Sand with 15% Fines

The Figure 8. 12 shows the relation between instability index, ϖ and number of cycles, N of each packet of cyclic pulses for sand with 15% fines. Total three packet of stress pulses were applied on the sample before it reached to the cyclic instability. In the first packet of stress pulses, the initial instability index, $\varpi_{(1)}$ was 0.54 and it

may not be enough to approach cyclic instability within 100 cycles (Figure 8. 12). The initial instability parameter $\varpi_{(1)}$ was 0.67 for second packet of loading and ϖ -*N* plot shows that the curve bending upward to instability stress ratio, η_{IS} i.e. ϖ = 1.0. It indicates that increase in initial $\varpi_{(1)}$ decreases the required number of pulses to trigger cyclic instability. In third packet of stress pulses the ESP moves leftward in *q*-*p*′ space and effective stress ratio reached the instability stress ratio in first cycles.

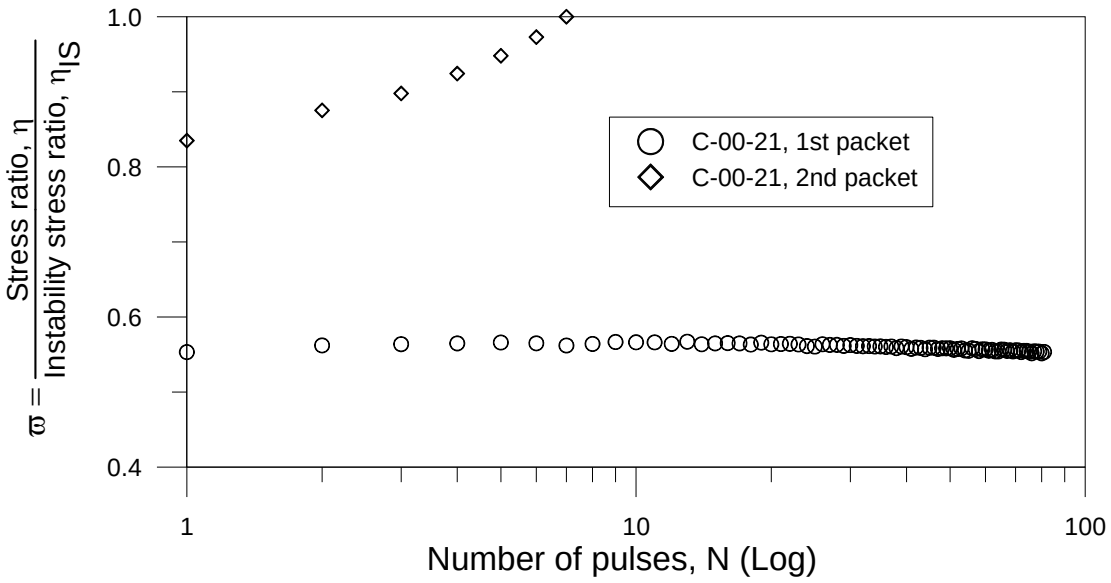

Figure 8. 11: Relation between instability index, ϖ and number of pulses, *N* for clean sand.

8.5.3 ϖ - *N Relationship for Sand with 20% Fines*

The instability index, ϖ and number of pulses, *N* for sand with 20% fines is plotted in Figure 8. 13. It shows that the concept of instability index as discussed is equally applicable for sand with 20% fines. A total two packets of stress pulses were applied to the sample. In first packet of stress pulses, the initial $\varpi_{(1)}$ (≈ 0.63) was not enough to approach instability stress ratio (1.0 at y-axis) with in 15 pulses; rather it shows a

stable trend. On the other hand the initial $\varpi_{(1)}$ (≈ 0.85) was large enough to reach instability stress ratio at 4th pulses.

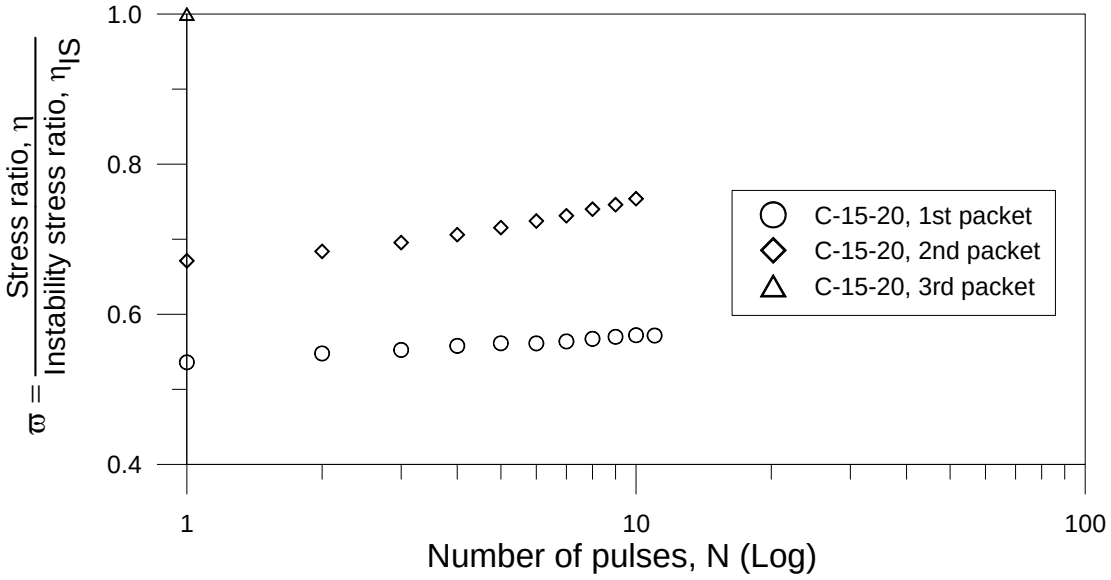

Figure 8. 12: Relation between instability index, ϖ and number of pulses, *N* for sand with 15% Fines.

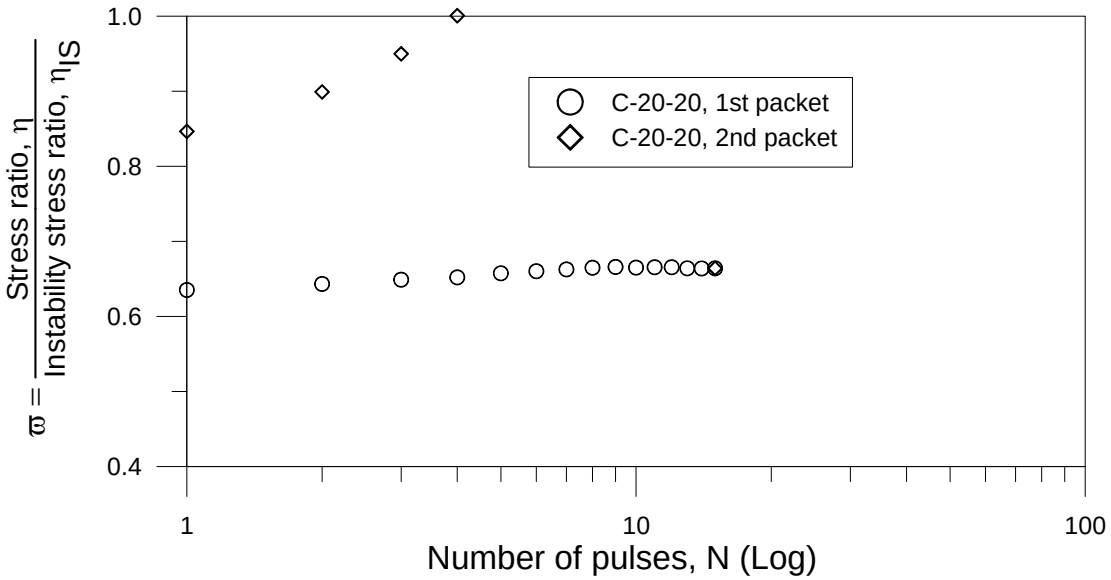

Figure 8. 13: Relation between instability index, ϖ and number of pulses, *N* sand with 20% Fines.

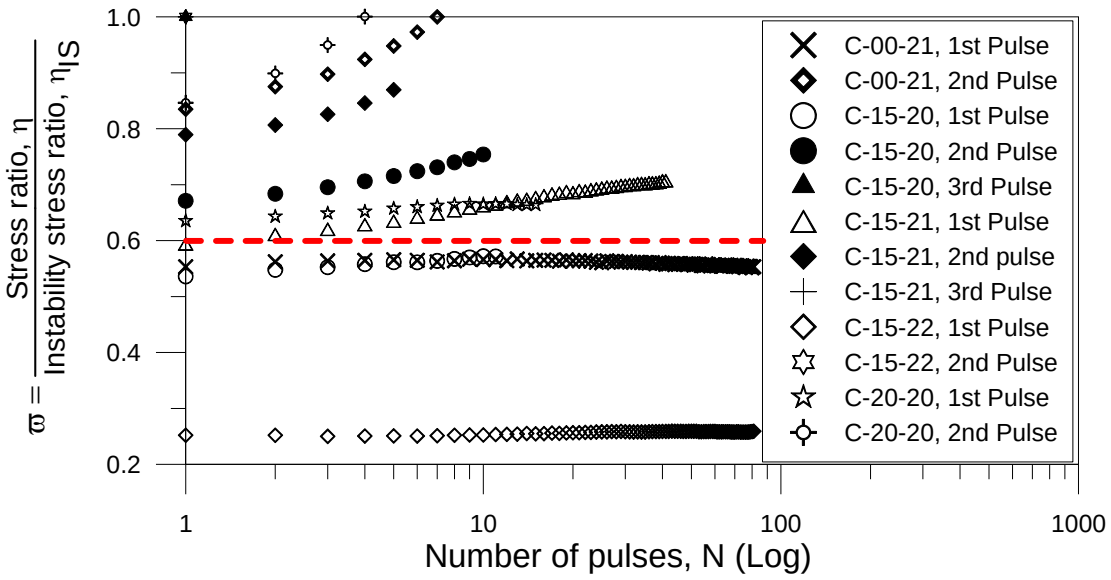

Figure 8. 14: Relation between instability index, ϖ and number pulses, *N* for sand with fines (f_c < TFC).

8.5.4 *Synthesis of the Results*

The Figure 8. 11 to Figure 8. 13 indicate that the instability index can be equally applicable for sand and sand with fines. Thus, all the data for sand and sand with up to 20% fines are plotted in Figure 8. 14. Their void ratio varies from 0.568 to 0.852. However, the range varies only from 0.819 to 0.874 in terms equivalent granular void ratio, *e**. The Figure 8. 14 supports the above finding i.e. the required number of pulses to trigger cyclic instability is less for higher initial instability index, $\varpi_{(1)}$ and it is independent of fines contents. There is also a region around $\varpi_{(1)} \approx 0.60$ in ϖ - *N* space which separates stable and non-stable region (at lest with in 100 cycles):

- $\varpi_{(1)} \leq 0.60$: the sample unlikely trigger cyclic instability with limited number of pulses (say 100 pulses).

- $\varpi_{(1)} > 0.60$: the sample will trigger cyclic instability with in limited number of pulses (100 pulses).

8.6 SUMMARY

This Chapter addresses the issues on the link between monotonic and cyclic loading behaviour with emphasis on cyclic instability and strain hardening behaviour after quasi steady state, QSS for a range of fines content (provided that f_c < TFC).

The test results showed that, for the complete spectrum of strain hardening behaviour, a single set of rules could be used to correlate monotonic and cyclic behaviour for a range of fines content. These rules are discussed below.

- The onset of instability in cyclic loading is not directly controlled by the magnitude of prescribed peak deviator stress, q_{peak} in cyclic loading relative to q_{IS}, the deviator stress at onset of strain softening for monotonic loading, but rather the development of an effective stress ratio exceeding η_{IS}, the instability stress ratio for monotonic loading.
- Once instability commenced, the ESP during the loading phase traced out a curve similar to, but located higher than, the ESP of a corresponding monotonic undrained test. The relationship between the cyclic-peak and cumulative ε_q traced along a curve similar to that of the corresponding monotonic shearing.
- For cyclic loading applied after shearing beyond the QSS point, the deviator stress that can be developed during cyclic loading is determined by the deviatoric stress-strain curve of the corresponding monotonic test. If the prescribed q_{peak} is less than the deviator stress mobilized at the corresponding ε_q of a corresponding monotonic test, the prescribed stress can be developed. Otherwise, the deviator stress developed during cyclic loading is bounded by

corresponding post-QSS strain hardening segment of a corresponding monotonic test.

- The minimum stress pulse required to trigger cyclic instability can be define by instability index, ϖ (the ratio of the effective stress, η at the peak of pulses to the instability stress ratio, η_{IS} corresponding monotonic loading). If initial instability index, $\varpi_{(1)} \leq 0.60$, then the sample unlikely trigger cyclic instability with limited number of pulses (say 100 pulses). If $\varpi_{(1)} > 0.60$, then the sample will trigger cyclic instability with in limited number of pulses.

CHAPTER 9

Conclusions and Recommendations for further Research

9.1 GENERAL

An experimental investigation on the effect of fines in sand-fines mixture under undrained axi-symmetric triaxial condition is presented in this thesis. Although the concept of equivalent granular void ratio, e^* may be used to model some of the effects of fines, the determination of its value is problematic because a parameter b was required in the calculation of e^* (from e). The parameter b represents the active fraction of fines in overall force structure of the sand-fines mixture and there was no prediction equation for b. To understand the physical attributes of b, the binary packing theory are examined in light of "fines-in-sand" model. This allowed in developing a physically reasonable and mathematically consistent, though semi-empirical equation for predicting b value (using only particles size ratio, χ and f_c as input parameter). The concept of a single equivalent granular steady state line, EG-SSL in e^*-log(p') space was introduced which was then used to define the equivalent granular state parameter, ψ^*. The e^* and ψ^* were used to modify a state dependent constitutive model and the model prediction was compared with experimental results for sand with fines, $f_c \leq$ 30%. The effect of fines types (in terms of plasticity and angularity) on the prediction equation of b was also examined with four different types of fines. The link between monotonic and cyclic loading behaviour for sand

with fines were also examined with emphasis on cyclic instability and strain hardening behaviour after quasi steady state, QSS for sand with up to 20% fines contents at same ψ^*.

9.2 CONCLUSIONS

The main results and conclusions drawn from this thesis are summarized below.

1. The steady state data points for sand with fines (≤ TFC) can be represented by a single trend line in e^*-log(p') space. This trend is called equivalent granular steady state line, EG-SSL. This EG-SSL line can be used to analyze the behaviour of sand with fines.

2. A study on binary packing theory in light of "fines-in-sand" revealed that b parameter can be expressed by a generalized functional relationship as $b = f(\chi, f_c)$. Thus, a prediction equation was developed. This function requires one calibrated parameter, m. A detail study shows that the m can be approximately assigned by a constant value of 0.30 for all data sets discussed in this thesis.

3. The concept of equivalent granular state parameter, ψ^* was proposed. It is found that the equivalent granular state parameter at the end of consolidation, $\psi^*_{(0)}$ is capable of predicting undrained behaviours (flow, non-flow, limited flow) for sand with fines provided $f_c \leq$ 30%. It is also capable of predicting undrained effective stress path, ESP and q-ε_q responses for sand with fines provided $f_c \leq$ TFC.

4. A state dependent constitutive model was modified in conjunction with ψ^* and e^*. Seven input parameters were needed in addition to four critical state input parameters. These seven parameters were obtained from drained tests. The model predictions were assessed with the followings.

   - The model prediction was compared with flow rule (drained test). The predictions were in good agreement with experimental results for sand with fines, $f_c \leq 25\%$.

   - The model predictions were compared with ESP and q-ε_q responses (undrained test) for flow, limited flow and non-flow behaviour. A good agreement was observed for sand with fines, $f_c \leq 30\%$.

   - The model predictions were also compared with published ESP and q-ε_q responses for undrained test (Bobei 2004). The predictions were also in good agreement with experimental results.

5. The effect of fines types (in terms of angularity and plasticity) on the prediction equation of b was also examined. It is found that fines types do not have significant effect on the prediction equation of b and equivalent granular void ratio, e^*. Hence, their effect on EG-SSL is negligible. However, fines angularity and plasticity have significant effect on the ESP and q-ε_q responses.

6. The link between monotonic and cyclic loading behaviour for sand with fines were also examined at same ψ^* with emphasis on cyclic instability and strain

hardening behaviour after quasi steady state, QSS for a range of fines contents (provided that f_c < TFC). They findings are

- It is found that the onset of instability in cyclic loading is related to the development of an effective stress ratio exceeding η_{IS}, the instability stress ratio for monotonic loading at same ψ^*.

- The minimum stress pulse required to trigger cyclic instability can be defined by instability index, ϖ (the ratio of the effective stress, η at the peak of pulses to the instability stress ratio, η_{IS} corresponding monotonic loading). It is found that at least $\varpi_{(1)}$ > 0.60 required to trigger cyclic instability.

- It is also found that cyclic loading path beyond the QSS is also bounded by monotonic path.

9.3 RECOMMENDATIONS FOR FUTURE RESEARCH

The experimental results for sand with fines presented in this thesis are in limited scope as it only discussed about "fines-in-sand" model. Thus, the following recommendations can be made for future research.

1. The experimentation and theoretical development of the thesis is limited to $f_c \leq$ TFC. It is not applicable for $f_c >$ TFC. Some published works show that inter-fine void ratio, e_f can be used in that case (Thevanayagam 1998; Thevanayagam 1999). As TFC is the transition between "fines-in-sand" to "sand-in-fines" model, thus theoretically equivalent granular void ratio, e^* and inter-fines void ratio, e_f equation (Equation 2.12 & 2.13) should merge smoothly at TFC. However, the Equation 2.12 and Equation 2.13 do not merge smoothly. Thus, the compatibility of these equations need further study.

2. The concept of equivalent granular void ratio, e^* considers soil consists of two components: sand and fines. Thus, force carrying hierarchy between sand and fines are considered in e^*. Some soil contains sand, silt and clay. Due to the size difference clay can be placed between the voids of silt particles and slit can be placed between the voids of sand. Thus, it is reasonable to consider a force carrying hierarchy among these three layers. A limited work is presented in Ni et al. (2006). However, this can be generalized for multiple force carrying hierarchy among multiple layers.

3. The equivalent granular void ratio, e^* is applicable if there is a gap between sand and fines gradation so that "fines-in-sand" model is valid. This concept

can be extended to large variety of particle size and distribution (sand-fines mixture).

4. A state dependent constitutive model was modified in conjunction of e^* and it was evaluated for sand with fines ($f_c \leq$ TFC). It could be interesting to modify a constitutive model in conjunction with inter-fines void ratio, e_f and to evaluate the model prediction with experimental results for $f_c >$ TFC. The comparison between these two models and model parameters might highlight some unknown attributes of the framework.

5. The link between monotonic and cyclic loading behaviour for sand with fines was examined with in a narrow range of ψ^*. It should be verified with a wide range of ψ^* for sand with fines, $f_c \leq$ TFC.

6. The instability index, $\varpi_{(1)}$ was introduced in Chapter 8. The number of cyclic required to trigger instability was decreasing with increasing instability index, $\varpi_{(1)}$. The value of instability index, $\varpi_{(1)}$ can be used estimate the number of cycle required to trigger cyclic instability for a prescribed stress pulse.